अंतरिक्ष भौतिकी प्रयोगशाला

SPL

Space Physics Laboratory

Scientific Accomplishments 2016-2017

Vikram Sarabhai Space Centre
Indian Space Research Organisation

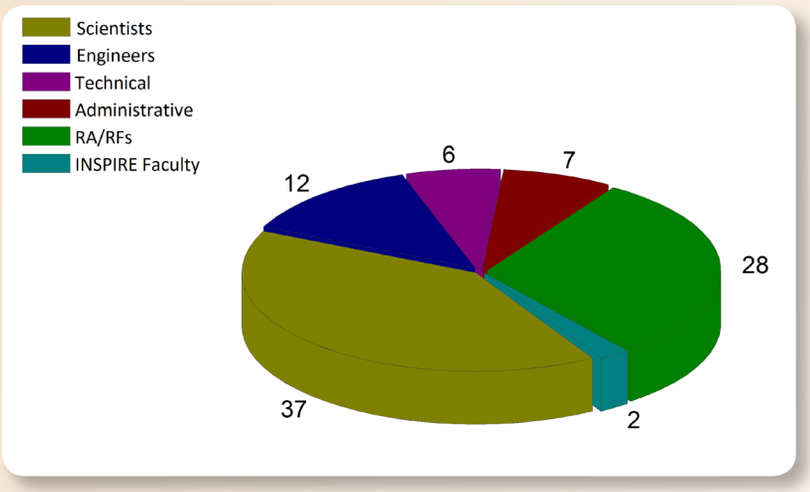

Human Resource

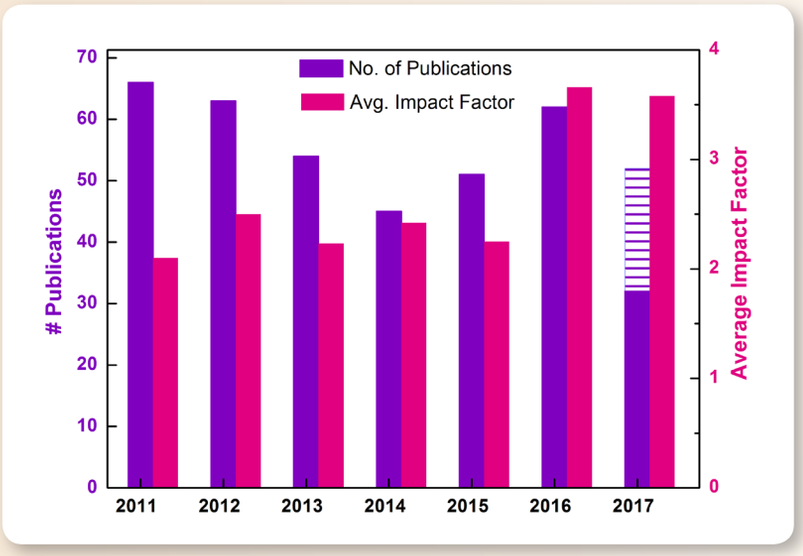

Publications

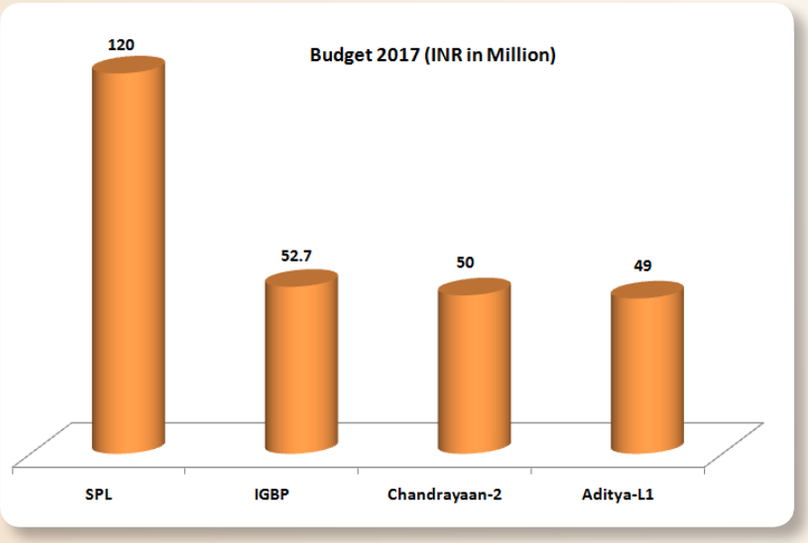

Budget

(₹ in Millions)

From the Director

Deriving its strength from the energy and drive of its people, the Space Physics Laboratory has emerged as one of the country's leading research centres in the area of Space Sciences. SPL's experimental and theoretical capabilities and modelling efforts continue to bring laurels, medals and honours to its scientists and young researchers.

Let me present the major accomplishments of SPL during the period 2016-2017, while also dwelling on the exciting challenges and opportunities that opened up for it.

The year saw rapid strides in all the research areas that SPL focused on namely, the Planetary sciences, Upper and Middle atmospheres and the Lower atmosphere.

The evolution of the coastal atmospheric boundary layer over Thumba was investigated based on long term observations using the Microwave Radiometer. Making use of the multi-year and multi-satellite (CloudSat, CALIPSO and CERES) observations, stratocumulus clouds over the subtropical oceans and their interaction with marine ABL were investigated and their short and long wave radiative impacts estimated.

The seasonal morphology of the vertical structure of coastal atmospheric boundary layer over Thumba was generated, which is being used as the mixing length scale in the COSMO model. Efforts were also made towards deriving the characteristics of the Indian summer monsoon onset during early onset years. Significant progress is achieved in the new initiative for the estimation of CO_2 fluxes over the Indian region using satellite and ground-based observations and atmospheric transport models.

The spatio-temporal variability of different trace gases (O_3, CO and CH_4) over Bay of Bengal during the summer monsoon period was simulated using WRF-Chem and validated against observations. The long term trend in CH_4 over Indian region was obtained based on satellite (SCIAMACHY) observations and compared against the values from global hotspots. Experimental facilities were set up for the study of carbonaceous aerosols over Indian region.

Quantitative assessment of the direct radiative forcing of composite aerosols as well as constituent species over the Indian sub-continent using a synergy of observations (ARFINetwork) and modelling was carried out. The observations of cloud-condensation nuclei (CCN) characteristics from the coastal environment of Thumba and from the high altitude site at Ponmudi have completed an annual cycle and the role of different air masses on the CCN characteristics was investigated. Aerosol observations were initiated from Eastern Himalayas (Tawang at 3 km AMSL) for the investigation of aerosol-cryosphere interaction and its impact on the state of Himalayan snow/glacier.

As in the past, the atmospheric modelling activity of SPL extended its support to all the PSLV and GSLV missions that took place from Sriharikota.

A new perspective of the Tropical Tropopause Layer (TTL) was established based on static stability criteria. The diurnal variability of global tropical tropopause and its role in stratospheric -tropospheric exchange processes were established. The research work on the frequency of occurrence of single and multi-layered clouds was yet another area that provided interesting insights.

The newly commissioned C-band polarimetric radar at TERLS Thumba, is being evaluated against disdrometer observations. The radar reflectivity and radial velocity from the radar are being assimilated into mesoscale weather models for thunderstorm prediction and capture of deep convective events.

Studies in the ionospheric region includes direct observational evidence for disturbance dynamo using INSWIM TEC measurements, gravity wave control of ESF through seeding based on long term ionosonde observations,

the role of wind shear in generation of F0.5 layer through simulations and observations as well as the horizontal extent of plasma bubbles and their drift using ground-based TEC and scintillation measurements. Measurements using the newly commissioned Fabry-Perot Doppler Spectrometer for thermospheric temperature and wind at Thumba, commenced in June 2017.

Discovery of a new population of suprathermal protons around the moon was made using the Chandrayaan-1 SARA/SWIM payload data. A one- dimensional photochemical model was developed for studying the electron density of the ionosphere of Titan.

Multi frequency GMRT observations have provided new insights into the surface and subsurface thermal structure of Venus.

Development of payloads such as CHACE-2, ChaSTE and RAMBHA on-board Chandrayaan-2 and the PAPA payload of Aditya-L1 mission is progressing well, to meet the targeted date of delivery.

Based on its merit, several science proposals from SPL have been selected for the forthcoming MOM-2 mission.

The High Vacuum Space Simulation Facility (HVSSF) has been augmented with low energy electron and ion sources and refurbished for the payload development activities. The facility was used for the characterisation of SPL payloads.

The technology and instrument development activities in SPL continues to support all the major payloads (Chandrayaan-2 and Aditya-L1) and ground based systems of the various experimental setup with in SPL and the networks (INSWIM, ARFI and NOBLE) of SPL, spread over India.

The realisation of a payload for the PSLV-C38 mission in a record time of two months, responding to an opportunity provided by the mission to fly a payload onboard, was a major challenge. The Ionization Density and Electric field Analyzer (IDEA) payload was designed, tested and flown onboard the Polar Satellite Launch Vehicle (PSLV -C38) on June 23, 2017. The experiment not only established the efficacy of the IDEA payload in giving simultaneous electron density and electric field measurements in the F region of the ionosphere, but also highlighted the potential of such short term opportunity missions in ISRO's forthcoming ventures.

Scientific activities and results from SPL figured several times in the'ISRO story of the week'.

SPL has actively participated in the 36th Indian Scientific Expedition to Antarctica and conducted scientific experiments in the area of polar atmospheric dynamics, atmospheric boundary layer, trace gases and aerosols.

Collaborations with national and international organisations continue with intense fervour resulting in pioneering research work and major scientific achievements.

The academic program of SPL continues to attract plenty of young researchers leading to the presence of a vibrant community of research scholars and research associates. In addition, SPL has been hosting INSPIRE faculties and national postdoctoral fellows of DST. SPL continues to support the summer research fellowship programs of the national science academies.

SPL organised a national level review meeting of ISRO- GBP projects, implemented by SPL,and attended by around 90 participants from all over India. SPL also hosted a week long Structured Training Programme on the topic of ''Challenges in Space Science and Exploration''. A day long brain storming meeting was organised to discuss and finalise potential experiments, viable on an extended PSLV-PS4 mission, where PS4 stage acts as an orbiting station.

The past year saw four Ph.D awardees and 48 publications with an average impact factor of 3.6, an impressive number in the area of Earth and Planetary Sciences. Eight SPL members bagged prestigious awards and honours. Four scientists received best paper/poster awards in national and international conferences.

Looking ahead, major missions are lined up one after the other, the Chandrayaan-2, Aditya-L1, MOM-2, the mission to Venus and so on. SPL is all poised and excited to face the challenges in each of these missions. As we continue on our path, SPL looks forward to a bright future.

It is with great pride and delight that I present this report.

राधिका रामचन्द्रन

राधिका रामचन्द्रन
Radhika Ramachandran

16 August 2017

Awards, Honours & Recognition

ANIL BHARDWAJ

- Infosys Prize in Physical Sciences, 2016.
- ISRO Outstanding Achievement Award, 2016.
- INSA Vainu Bappu Memorial Award, 2016.

SMITHA V THAMPI

- NASI-SCOPUS Young Scientist Award, NASI-Elsevier, 2017.

K. N. UMA

- ISRO Young Scientist Merit Award, 2016.
- Science and Engineering Research Board (SERB) Women Excellence Award, Department of Science and Technology, New Delhi, 2017.

M. B. DHANYA

- Young Research Award, Association of Asia Pacific Physical Societies, Division of Plasma Physics (AAPPS-DPP), under certificate of Laureate of Subrahmanyan Chandrasekhar Prize of Plasma Physics, 2016.

P. R. SUSEELA

- ISRO Annual Service Excellence Award, 2015.

SNEHA YADAV

- USRI-RCRS Young Scientist Award, Tirupati, India, 2017

VRINDA MUKUNDAN

- Fellowship from Royal Society, London to attend the Common Wealth Science Conference, Singapore, June 13 - 16, 2017.

MEGHA U BHATT

- DAAD scholarship for Research stay, Technical University Dortmund, Germany, October 16- December 15, 2017.

Academic Excellence

Best Paper/Poster Awards in Symposia/Conferences

VRINDA MUKUNDAN

- "Calculation of ion production rates and electron density profiles for the dayside ionosphere of Titan", 29th Kerala Science Congress, Kerala State Council for Science, Technology and Environment (KSCSTE), Mar Thoma College, Pathanamthitta; January 28-30, 2017 [Co-author: Anil Bhardwaj].

SIDDARTH SANKAR DAS

- "Distributions of ozone and water vapour in the UTLS over the Tibetan high" , Conclave of Young Scientists in Central and South Asian Region, The World Academy of Sciences' and 'Divecha Centre for Climate Change', IISc, Bangalore, December 5-7, 2016 [Co-authors: K. V. Suneeth and S. Aneesh].

ADITYA VAISHYA

- "Radiative Implications of Altitudinal Heterogeneity in Aerosol Properties in the Indo-Gangetic Plain", International Conference on Understanding & Predicting Climate change over the Asian Region (UPCAR - 2017), June 25-28, 2017, National Atmospheric Research Laboratory, Tirupati, India [Co-authors: Jayachandran V., Mukunda M. Gogoi and S. Suresh Babu].

MUKUNDA M GOGOI

- "Implication of Aerosols on the Photosynthetically Active Radiation Balance over North-East India", IASTA, Physical Research Laboratory, Ahmedabad, December 6-8, 2016 [Co-authors: T. Subba, B. Pathak and P. K. Bhuyan].

Ph.D. awarded

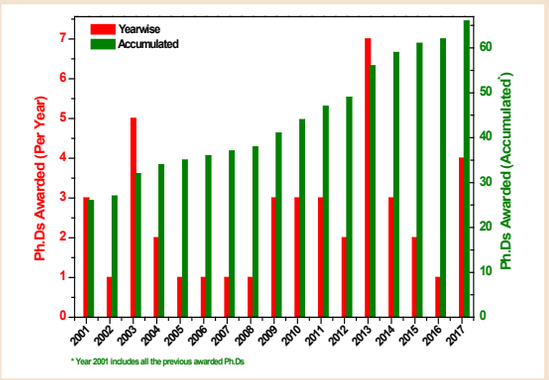

MADHAV HARIDAS M. K.

- "Dynamics of Equatorial and Low latitude Upper Atmosphere over Indian Region", Andhra University, Vishakhapatnam, September 2016 [Supervisor: Dr. G. Manju].

RENJU R.

- "Tropical Atmosphere Studies Using Ground Based Microwave Radiometer Profiler And Ancillary Sensors Over A Coastal Station Trivandrum", University of Kerala, Thiruvananthapuram, December, 2016 [Supervisors: Dr. K. Krishnamoorthy, Dr. C. Suresh Raju].

ARYASREE S.

- "Physico-Chemical Characteristics and Radiative Properties of Aerosols over Indian Coastal and Marine Environment" Cochin University of Science and Technology (CUSAT), Cochin, May, 2017 [Supervisor: Dr. Prabha R Nair].

MUHSIN M.

- "Characterisation of Thermal and Turbulent Structure in the Tropical Troposphere-Lower Stratosphere and Effect of Convective Clouds" Cochin University of Science and Technology (CUSAT), Cochin, August, 2017 [Supervisor: Dr. S. V. Sunilkumar].

'IDEA' for PSLV-PS4

The versatility as an in-situ probe, and potential as a satellite payload, of the indigenously developed 'Ionization Density and Electric Field (IDEA)' probe [a suit of three probes namely a Langmuir Probe, Magnetic field probe, and drift probe] flown onboard PSLV-C38 on a short mission was amply demonstrated, as it successfully measured the intended ionospheric parameters.

Research Work in Spotlight

ISRO Story of the Week

- The paper "Observation of Suprathermal Argon in the exosphere of Mars" by Anil Bhardwaj et al. published in Geophysical Research Letters (2017) made the "Story of the Week" at ISRO website on March 27, 2017 (http://isro.gov.in/observation-of-suprathermal-argon-mars-exosphere).

- The paper "New suprathermal proton population around the Moon:Observation by SARA on Chandrayaan-1" by M.B. Dhanya et al., published in Geophysical Research Letters (2017) made " The story of the Week" at ISRO website on June 27, 2017 (http://isro.gov.in/discovery-of-new-suprathermal-proton-population-around-moon-sara-onboard-chandrayaan-1).

Contents

SCIENTIFIC DISCIPLINES AND ACTIVITIES

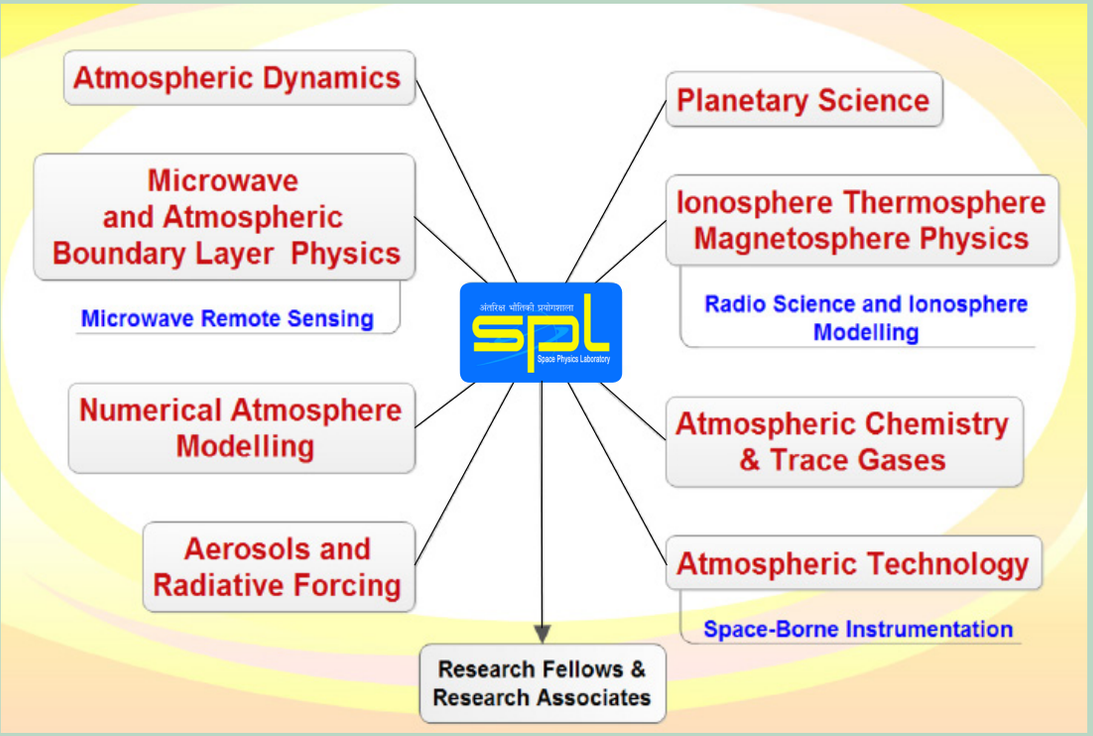

Microwave and Boundary Layer Physics

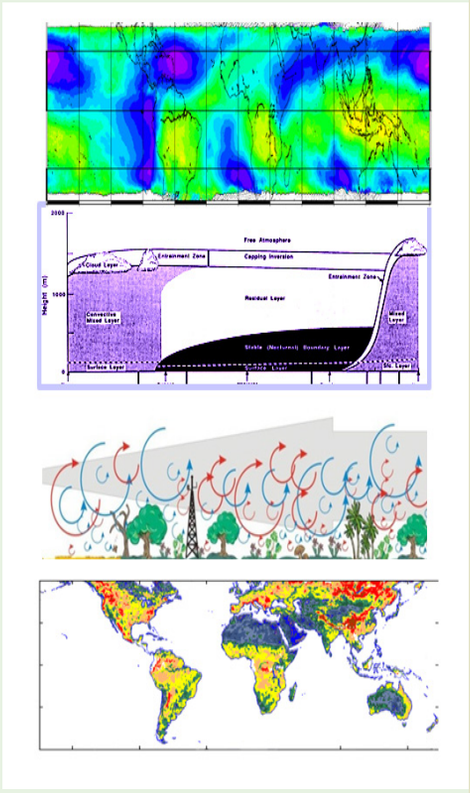

IGBP-NOBLE : Network of Observatories for Boundary Layer Experiments

The MBLP branch focuses on the surface characteristics, surface-air interaction and exchange processes, energy and radiation balance of the Earth-atmosphere system, structure and dynamics of atmospheric boundary layer (ABL) and its coupling with free-troposphere, clouds and the components of hydrological cycle and microwave remote sensing of the Earth and other planetary bodies. Main objectives are: (i) to improve the understanding and parameterization of the ABL processes including surface-air interaction processes, energy budget, turbulence, diurnal evolution of ABL, and the role of ABL processes in pollutant dispersal, cloud development and hydrological processes, (ii) improve the understanding on clouds and energetics of the Earth-atmosphere system, and (iii) spaceborne and ground-based microwave remote sensing of Earth's surface and atmosphere for deriving the surface properties, atmospheric water vapour, cloud characteristics and precipitation, including their potential impact on microwave propagation through the atmosphere. The NOBLE project of ISRO-GBP is aimed at characterising the ABL at a national canvas covering distinct climate and geographical zones.

Science Team

K. Rajeev
C. Suresh Raju
N. V. P. Kiran Kumar
Manoj Kumar Mishra
Nizy Mathew
M. Santosh

Research Associates/ Fellows

Tinu Antony
R. Renju
Ashok Kumar Gupta
Nithin Mohan
S. Lavanya
Edwin V Davis

Technical Support

Santosh Kumar Pandey
P. T. Lali
P. S. Ajeesh Kumar
P. P. Pramod
Neha Naik
Dinakar Prasad Vajja
P. Pradeepkumar

Atmospheric boundary layer characterization using microwave radiometer observations

Evolution of Coastal Atmospheric Boundary Layer (ABL) Structure

Boundary layer height (BLH) is one of the crucial parameters of ABL which plays a major role in the development of weather conditions and their feedback processes, and an important parameter in numerical weather prediction models. Conventional radiosonde profiles have limitations to study the rapid development and decay of the diurnal evolution of ABL due to significant time gaps in sampling interval. For the first time in the tropics, continuous soundings of temperature and humidity profiles observed using the ground-based Microwave Radiometer Profiler (MRP) with high temporal resolution have been used to investigate the continuous diurnal evolution of ABL height and its characteristics on seasonal mean basis over the coastal tropical station Thiruvananthapuram, (TVM; 8.5°N, 76.9°E).

Parcel method is used to determine BLH, in which the height of intersection of the actual virtual potential temperature (θ_v) profile with the dry-adiabatic ascent starting at near-surface θ_v is determined as the BLH. The temporal variation of the altitude structure of θ_v (Fig.1) shows that θ_v continuously increases with altitude during the night and morning hours (~23-08 IST), which characterizes the stable boundary layer conditions. The values of θ_v near surface are comparable to those at ~950 m during 12-16 IST, indicating the air parcel at surface can get well-mixed up to ~1 km altitude which represent the BLH during the convective daytime conditions. A strong capping inversion layer with virtual potential temperature lapse rate of >3 K/km prevails above the convective boundary layer. Response of the atmospheric mixing processes to the altitude variation of θ_v is well manifested in the diurnal evolution of water vapor mixing ratio (Fig.1 lower panel). Associated with the development of daytime convective ABL water vapor gets well mixed to the upper layers up to ~ 700 m to > 1 km during 12-18 IST. The diurnal variation

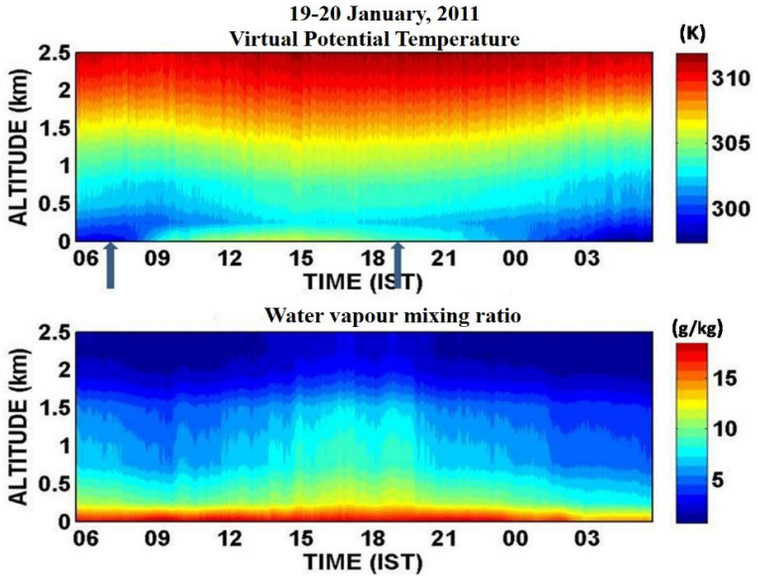

Figure 1: MRP derived virtual potential temperature (upper panel) and water vapor mixing ratio (lower panel) during 19-20 January, 2011 with arrows indicating time of sunrise and sunset over the region. Convective boundary layer develops after ~08 IST and its strength (upper altitude limit and temperature) increases between ~09 and ~15 IST [Renju et al., IEEE TGRS, 2017].

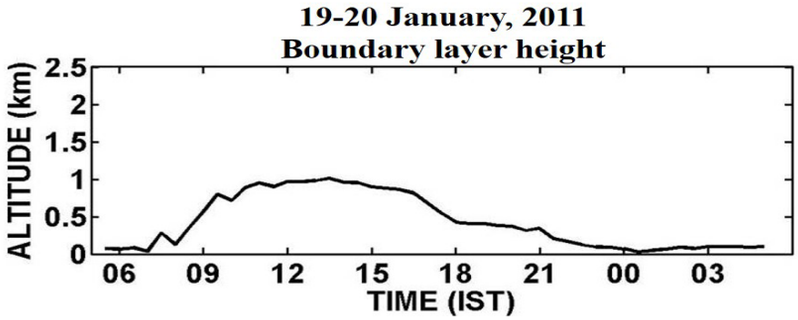

Figure 2: Diurnal variation of boundary layer height derived from MRP observations during 19-20 January, 2011 [Renju et al., IEEE TGRS, 2017].

of BLH (Fig.2) shows daytime convective ABL rapidly develops after ~09 IST when the BLH increases from <200 m altitude during the post-midnight and morning period to attain the maximum value of ~1000 m at 13-14 IST and systematically decreases after ~15 IST to ~500 m during 18-21 IST and to <200 m during the post-midnight period.

Validation of BLH derived from MRP observations

The BLH and its diurnal evolution derived from MRP are compared with the aerosol mixed layer height (MLH) derived from collocated dual-polarization MPL observations. The MLH showed a maximum extent up to ~1500 m which is higher than the BLH (~1000 m). This difference arises mainly due to the different physical processes governing the two tracers. The MRP derived BLH is also compared with that derived from the concurrent radiosonde measurements of temperature and humidity, following the θ_v gradient method, for 55 collocated radiosonde ascents. A mean absolute difference between two measurements is ~ 200 m which is attributed to the limitation of MRP vertical resolution,~ 100 m.

Multi-year monthly mean diurnal evolution of ABL

The continuous MRP observations (whenever fair weather conditions prevailed) during 2010-2013 are used to estimate the monthly mean diurnal variation of BLH by averaging the BLH values for the same location for the same months for all years using an equivalent-day analyses The contour map of the annual variation of the BLH diurnal variation (Fig. 3) during all months is characterized by a shallow (<200 m) ABL during the post-midnight and early morning and a rapid growth of convective ABL after 09 IST reaching the peak value before noon, which prevails until ~15 IST. The BLH gradually decreases from the afternoon peak value after ~15 IST. Subsequently the ABL gradually collapses into the nocturnal stable layer, which is quite shallow (<200 m). Around the noon time (12-15 IST) the vertical motion of thermals attains its maxima and the ABL depth remains somewhat similar (~700-1200 m). The maximum value of BLH occurs in the month of April (~1300 m). During the summer monsoon period (June-September), the development of convective ABL is weaker with daytime peak BLH in the range of 600-800 m. It is smaller during June-July when the region has maximum cloudiness.

Thermal Internal Boundary Layer (TIBL) and its seasonal mean variations

The seasonal variability in the diurnal evolution of the TIBL over the TVM is studied by equivalent day analysis of the time (at 5 min bin) -height variation of θ_v (Fig. 4) during all fair-weather days during the respective seasons except summer monsoon season. The winter period is characterized with the TIBL formation by 09-10 IST and its depth varies from ~200 m to ~600 m during the course of the day. This unstable TIBL lasts for ~9-10 hrs and diminishes by ~21 IST. The existence of TIBL is shorter during winter compared to the pre- and post-monsoon seasons. During the pre-monsoon period, due to longer days and high surface temperature, the formation of unstable layer is prolonged and TIBL persists for longer period ~12-13 hrs (Fig. 4 middle panel). During the post-monsoon period (Fig. 4 bottom panel) the TIBL formation is present for duration of ~12 hrs.

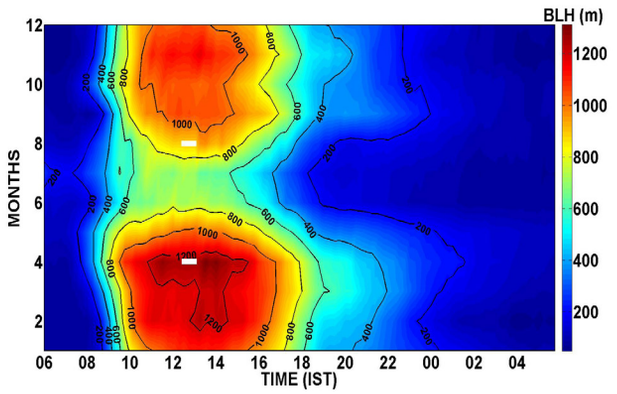

Figure 3: Annual cycle of the monthly mean diurnal variation of BLH derived from multi-year (2010-2013) MRP observations [Renju et al., IEEE TGRS, 2017]

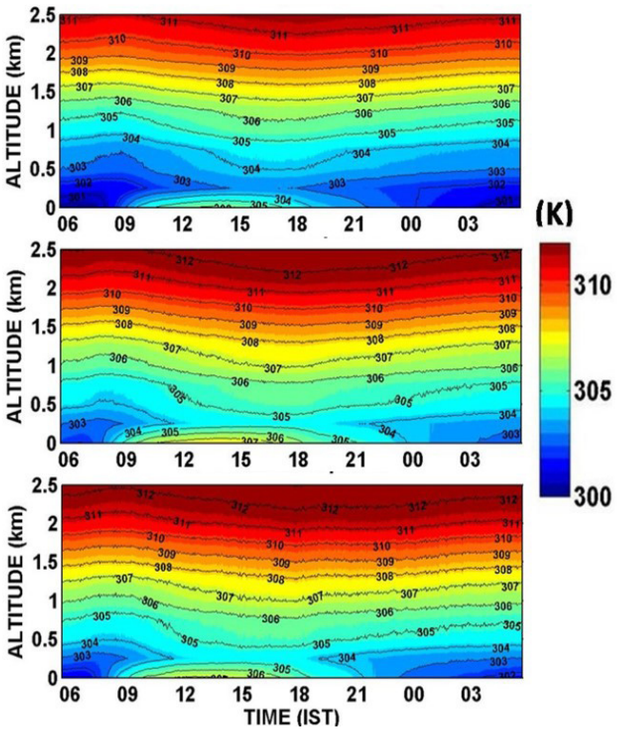

Figure 4: The seasonal mean diurnal variability of virtual potential temperature is shown for three consecutive years 2011-2013 for winter period (DJF) (Top panel), for pre-monsoon period (MAM),(Middle panel), for post-monsoon period (ON), (Bottom panel) with arrows indicating time of sunrise and sunset over the region for corresponding time [Renju et al., IEEE TGRS, 2017]

Stratocumulus clouds over subtropical oceans and their interaction with Marine ABL

Marine stratocumulus clouds (MSC), occurring under favourable conditions of large scale tropospheric subsidence associated with the descending limb of the Hadley cell, form the largest fraction of low-altitude clouds over some of the subtropical oceanic regions, especially the South Indian Ocean (SIO), the Northeastern Pacific (NEP), the Southeastern Pacific (SEP), and the Southeastern Atlantic (SEA). They play a pivotal role in regulating the energy balance and hydrological cycle of the Earth-atmosphere system and are tightly coupled with the marine atmospheric boundary layer (MABL) characteristics through radiative processes, thermodynamics and turbulence. During the Asian summer monsoon, they occur over the Mascarene high pressure belt (one of the key drivers of the monsoon circulation) over the South Indian Ocean and play a pivotal role in regulating the cold sea surface temperature (SST) over the area and hence might provide positive feedback to the maintenance of the high pressure belt. The main objectives of the present study are: (i) to investigate the seasonal mean characteristics and day-night changes of the low-altitude clouds at the major subtropical oceanic regions of considerable MSC occurrence, specifically focussing on the vertical distribution of these clouds, (ii) to quantify their short and longwave radiative impacts, and (iii) to delineate the physical processes responsible for the substantial day-night changes observed in their occurrence, including its coupling with the marine atmospheric boundary layer (MABL). Such observations are non-existent over the South Indian Ocean. This study has been carried out using multi-year (2006-2010) observations using CloudSat, CALIPSO and CERES.

Day-Night changes in the vertical distribution of MSCs

Based on satellite-based passive radiometric observations as well as earlier studies, the following regions of frequent MSC occurrence are identified: the South Indian Ocean (SIO: 20-35°S, 70-100°E), the Northeast Pacific (NEP: 15-35°N, 120-145°W), the Southeast Pacific (SEP: 5-25°S, 80-100°W) and the Southeast Atlantic (SEA: 10-30°S, 10°E-10°W). The analyses using the combined CloudSat and CALIPSO data (2B-GEOPROF-LIDAR) show a prominent annual cycle in MSC occurrence with most frequent occurrence during June-November over the SIO, June-August (JJA) over the NEP, September-November (SON) over the SEP and SEA regions. Hence, the present study mainly focuses on the above regions and seasons. The latitude-altitude sections of multi-year (2006-2010) seasonal mean vertical distribution of the frequency of occurrence of clouds (FC_ALT) and their respective day-night differences derived from the 2B-GEOPROF-LIDAR data over the NEP (during JJA) and the SEP, SEA and SIO (during SON) (Fig.5). All these regions are manifested by a significant band of low-altitude clouds, mostly confined to ≤2 km, with considerably enhanced nighttime occurrence. The occurrence of middle and high level clouds is less (less than 8-15% of cirrus occurrence) over most of these regions, indicating strong mid-tropospheric downdraft. The nighttime values of FC_ALT (40-65%) well exceed the daytime values (30-45%) at the altitude of maximum cloud occurrence (Hpc). As explained later, this diurnal variation is entwined with the diurnal variation of ABL through energy budget, thermodynamics and strengthening of boundary layer inversion. Unlike all the other regions, most of the SIO region is affected by convective clouds or convective outflow throughout the year (Fig. 6). Occurrence of low-altitude clouds and their nighttime enhancement are less prominent over the SIO compared to the other three regions.

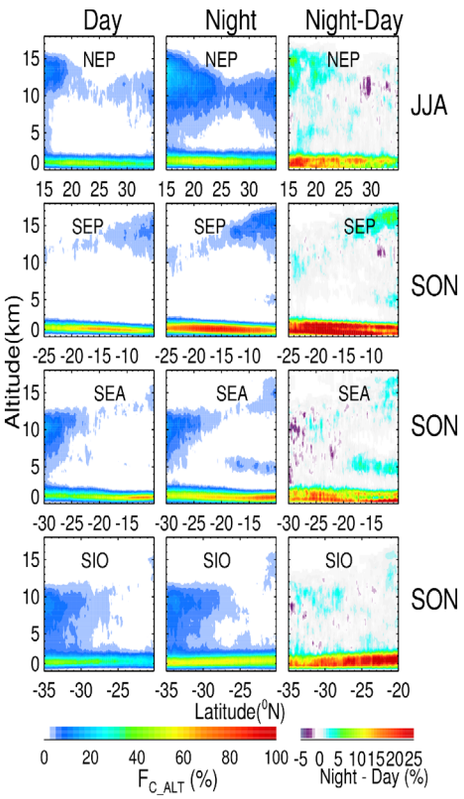

Figure 5: Latitude-altitude cross sections of multi-year (2006-2010) seasonal mean frequency of occurrence of clouds (FC_ALT) for daytime (left panel) and nighttime (middle panel) over the over the Northeast Pacific (NEP) during June-August (JJA) and the Southeast Pacific (SEP), the Southeast Atlantic (SEA) and the South Indian Ocean (SIO) during September-November (SON). The right panel shows the corresponding day-night differences in FC_ALT (night minus day) [Gupta et al., J. Atmos. Sol. Terr. Phys., 2017].

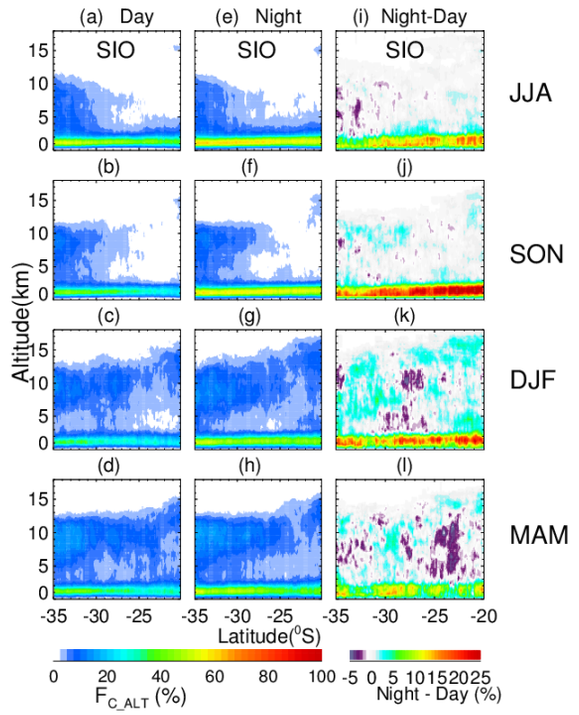

Figure 6: Same as Fig. 5, but for the South Indian Ocean (SIO) during June-August (JJA), September-November(SON), December-February (DJF) and March-May (MAM). [Gupta et al., J. Atmos. Sol. Terr. Phys., 2017].

Spatial variations of the altitude of maximum cloud occurrence

Clouds near the coastal regions are influenced by the thermodynamical processes associated with differential heating between the land and ocean and the associated changes in boundary layer. Coastal effect on the altitude of peak cloud occurrence (Hpc) and its day-night changes are investigated by considering the seasonal mean longitude variations in the vertical distribution of clouds. Figure 7 shows the seasonal mean F_{C_ALT} over two well separated longitude bands: one near the coastal region while the other is in the open ocean significantly away from the continental boundaries over the NEP region during JJA and over the SEP, SEA and SIO during SON. Over the SIO region, both the longitude sectors are in the open ocean away from the continents (as the occurrence of the low-altitude clouds is prominent only over the open ocean in this region). Over the NEP, the value of Hpc systematically increases from ~480-720 m near the coastal region (120-125°W) to ~960-1200 m between 135 and 140°W. The values of HPC over the SEP during SON increase westward from ~720-960 m at 70 -75°W to ~1200 at 90 - 95°W. Most of the above features observed over the SEP are seen at the SEA as well. The westward increase of Hpc observed in the above regions is persistent during both day and night. Over the SIO, the altitude of peak cloud occurrence is steady at ~1200 m. The above features indicate strong coupling among the variations in MABL, Hpc and F_{C_ALT}. Comparison of the earlier observations of MABL structure with the present observations suggests that the occurrence of marine low-altitude clouds peak below the MABL top.

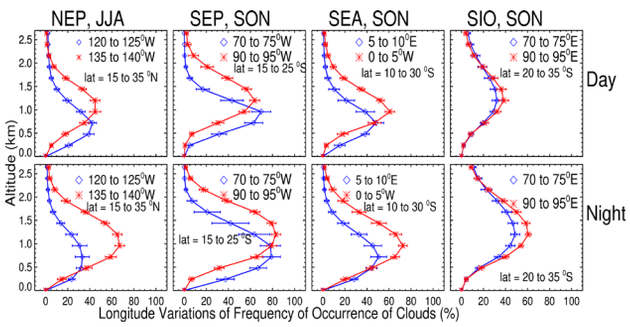

Figure 7: Seasonal mean F_{C_ALT} over two well separated longitude bands of 5° width for daytime and nighttime over the NEP, SEP, SEA and SIO. Geographical regions of averaging are indicated in the respective plots. [Gupta et al., J. Atmos. Sol. Terr. Phys., 2017].

Physical properties of MSCs

Probability distribution functions (PDFs) of the cloud base, top, and thickness during day and night over the four regions are depicted in Fig. 8. The PDFs of the cloud base altitude during day and night over the NEP, SEP and SEA regions have several similarities. During the nighttime, the most probable cloud base altitude is ≤ 480 m at these regions and the probability decreases exponentially for higher cloud base altitudes. In contrast, the cloud base altitudes during the daytime over the NEP, SEP and SEA regions show a distinct increase, with the most probable cloud base altitude of ~720 m. The most probable cloud base at SIO occurs at ~960 m during day and ~720 m during night, which is ~240 m higher than the corresponding values at the other regions. The PDFs of the cloud top altitude show a log-normal distribution with broad peaks appearing at 960-1440 m during both day and night over the NEP, SEP and SEA regions. On average, the nighttime values are larger than those during the daytime. In contrast, the cloud top altitudes at the SIO region during day and night are larger and peak at ~1700-1940 m.

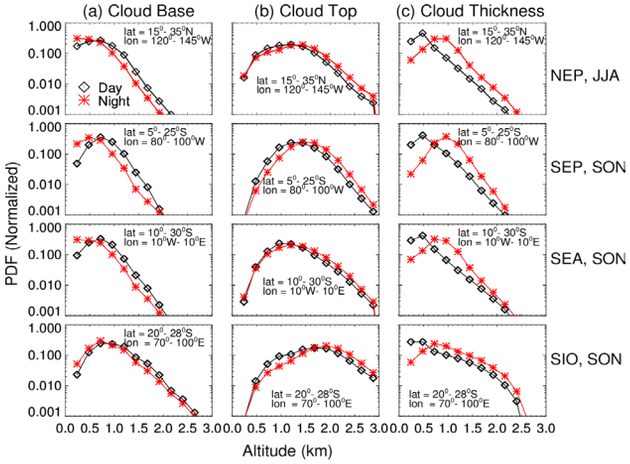

Figure 8: Multi-year (2006-2010) seasonal mean probability distribution functions (PDFs) of the cloud base and top altitudes and cloud thickness for low altitude clouds during the daytime and nighttime over the NEP (during JJA) and the SEP, SEA, and SIO (during SON). Latitude and longitude bands over which the averaging is done are indicated in the respective plots. [Gupta et al., J. Atmos. Sol. Terr. Phys., 2017].

The PDFs of the low-altitude cloud thickness show a monomodal distribution with mode thickness at ~480 m during the day and ~720-960 m during the night. Compared to the daytime, the nighttime increase in cloud thickness is by 300-370 m at the NEP, SEP and SEA, while it is the least (~200 m) at the SIO.

Shortwave and longwave radiative impact of MSCs

Diurnal variation of the low-altitude cloud occurrence and their dissipation are intertwined with their radiative impact. Changes in the occurrence and properties of these clouds can produce radiative effects and are investigated using CERES SYN1deg-M3Hour dataset. Figure 9 shows the seasonal mean diurnal variation of long and shortwave cloud radiative forcing (LWCRF and SWCRF) at top-of-atmosphere (TOA) over the MSC-dominated NEP (during June-August) and SEP, SEA and SIO (during September-November). Due to the low cloud top altitude, magnitude of the LWCRF is substantially smaller than the SWCRF. The seasonal mean LWCRF over SEP, SEA and SIO (about 13 Wm^{-2}) is larger than that over the NEP (about 10 Wm^{-2}). In all these regions, the LWCRF shows a broad peak during the post-midnight to morning period (01:30-07:00 LT) and a minimum around 16:30 LT. The nighttime peak values of LWCRF are comparable at SEP, SEA and SIO and are distinctly larger than that over the NEP. In contrast, the afternoon minimum values of LWCRF are almost comparable in all the regions. In all these regions, the SWCRF peaks around 10:30 LT, with comparable magnitudes over the NEP, SEP and SEA (-220 to -250 Wm^{-2}) and significantly smaller magnitude (-110 Wm^{-2}) over the SIO. This is because of the fewer daytime cloud occurrences over the SIO. Similarities and differences in the seasonal mean values of LWCRF and their diurnal variations at different regions are consistent with the regional variations and day-night differences of F_{C_ALT}.

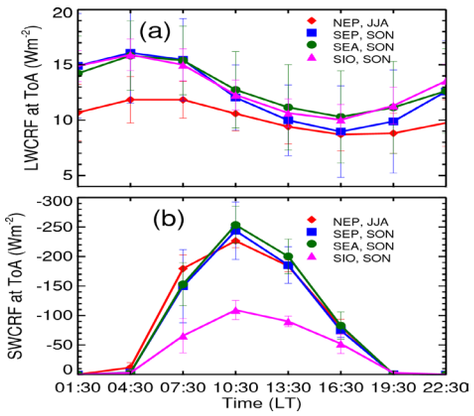

Figure 9: (a) Multi-year (2006-2010) seasonal mean diurnal variation of LWCRF averaged over the NEP (during JJA) and the SEP, SEA, and SIO (during SON). (b) Similar to (a) but for the seasonal mean daytime SWCRF. Vertical bars indicate the standard deviations. [Gupta et al., J. Atmos. Sol. Terr. Phys., 2017].

Physical mechanisms responsible for the strong day-night changes in MSC characteristics and their coupling with MABL

On the basis of the strong day-night changes in the occurrence and properties of MSCs, the following physical mechanisms responsible for their genesis and interaction with MABL have been ascertained. Emission of longwave radiation from the cloud top during night would enhance the cooling at the cloud capped MABL top. The resulting reduction in temperature at the MABL top will increase the instability (especially at the MABL top) and vertical mixing in the MABL during the nighttime. It would be more effective in supplying moisture from the surface layer to the cloud deck, leading to the thickening and frequent occurrence of low-altitude clouds during night. As the atmospheric temperature is expected to undergo less day-night variations in the free troposphere above the cloud capped MABL (which is manifested with mid-tropospheric subsidence and absence of clouds), the altitude region above the MABL top (with IR cooling by clouds) will continue to be stable during the nighttime as well. This will effectively trap moisture below the MABL top during night and increase cloud occurrence below this altitude. Thus, the longwave cloud radiative forcing, boundary layer mixing and cloud occurrence act as a chain of intertwined positive feedback loop. On the other hand, during the daytime, absorption of a fraction of the shortwave flux in the near-IR to mid-IR band by clouds will warm the cloud deck and partially offset the IR radiative cooling from the cloud top. This will increase the temperature at the cloud top layer and strengthen the temperature inversion at the MABL top, thereby increasing the stability of the daytime MABL. It will reduce the MABL turbulence and decrease moisture transport from surface layer to the MABL top, thereby potentially lifting the cloud base, as observed in the present study. Absorption of shortwave radiation at the cloud top and the resulting warming of this altitude region will also cause evaporation of droplets from the cloud top layer. The above factors might cause the thinning of clouds during the daytime. This is in conformity with the present observations which show a thinning of clouds due to lifting of cloud base and lowering of cloud top during the daytime without significantly altering Hpc. This also causes a reduction in cloud occurrence during the daytime.

Megha-Tropiques ScaRaB observations of aerosol radiative effect over the mineral dust dominated Arabian sea and the Atlantic ocean

Mineral dust originating from the desert regions constitutes an important fraction of the global aerosol system. Considerable uncertainty exists in the estimation of radiative effect of dust aerosols. During the Asian summer monsoon season (June – September), the Arabian Sea is covered by large-scale mineral dust plumes transported from the west Asian deserts. In contrast, the Atlantic Ocean experiences large-scale mineral dust transport from the Saharan region throughout the year. Direct observations of the radiative effect of these mineral dust plumes and their diurnal variations during summer over the Arabian

Sea are very limited. The main objective of this study is to provide direct observations of the diurnal variation of the instantaneous aerosol direct radiative effect (IADREE, as a function of SZA), diurnal mean aerosol direct radiative effect (ADREE) and diurnal mean aerosol direct radiative effect at TOA over the Arabian Sea during the Asian summer monsoon season and compare these with the corresponding parameters at the mineral dust dominated northern equatorial Atlantic Ocean during the same period. In the present study, SZA variation of the instantaneous aerosol radiative effect at TOA is estimated using the broadband shortwave fluxes (SWF) over oceanic regions during cloud-free conditions observed using MT-ScaRaB. Uniqueness of the low-inclination Megha-Tropiques satellite observations, which cover all local times over all regions in the tropics during the 51 days precession cycle of the satellite is utilized in this study, which is otherwise not possible using the long-term observations carried out using CERES onboard Sun-synchronous satellites. Estimates of the IADREE are carried out using the collocated observations of shortwave radiative fluxes at TOA under cloud-free conditions using MT-ScaRaB and aerosol optical depth (AOD) derived from MODIS data. Variation of AOD during daytime over the open ocean is neglected. These estimates of IADREE are also compared with those estimated from CERES data at 13:30 LT, the time at which CERES observations are carried out.

IADREE and its Solar Zenith Angle Variation

Figures 10(a,c) show the variation of the mean values of SWF, obtained using MT-ScaRaB during June-September 2012 and 2013 in the SZA range of 20°-35°, with the MODIS-derived AOD (collocated average within 1° latitude-longitude). All the values of SWF at AOD intervals of 0.1 are averaged. The vertical lines indicate the standard deviations. Figures 10(b,d) are similar to Fig. 10(a,c), but for CERES-derived SWF values. The SZA range of 20-35° is used here as most of the CERES observations are in this range of SZAs range. The slope of the best fit curve (which gives the IADREE at the above SZA) for CERES (-49 $Wm^{-2}\tau^{-1}$ in 2012 and – 52 $Wm^{-2}\tau^{-1}$ in 2013) and MT-ScaRaB (-50 $Wm^{-2}\tau^{-1}$ in 2012 and -41 $Wm^{-2}\tau^{-1}$ in 2013) are in agreement, within the uncertainty limit (±17%), despite being observed by different sensors. The year-to-year variability is also within the uncertainty limits.

Determination of the diurnal variation of IADREE requires that the radiative effect is estimated at different ranges of cos(SZA). This is because, to a first order, the airmass variation is a function of μ=cos(SZA) rather than the SZA. Though the MT-ScaRaB provides observations at all SZAs, the slope method cannot be applied to finer ranges of μ as the number of points at fine intervals of μ is rather less (especially at small values of μ when it increases rapidly with local time) and hence may not cover all ranges of AOD values with sufficient number of points. The difference method is better suited for the estimation of IADREE in this case. Variation of the seasonal mean SWF at TOA as a function of μ averaged for a low AOD (for 0<AOD<0.2) and high AOD (for 0.40<AOD<0.5)

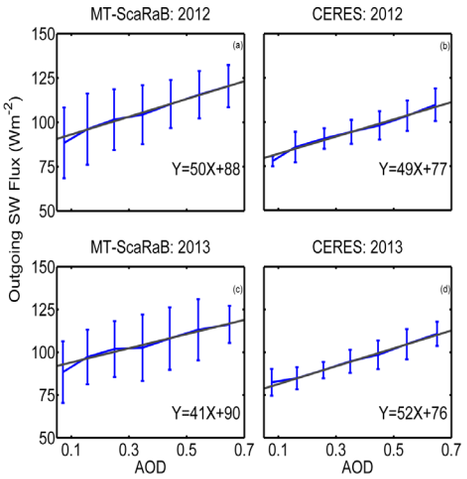

Figure 10 (a) Plot of MT-ScaRaB observed average clear sky upwelling shortwave fluxes during June-September of 2012 as a function of MODIS AOD at 550nm over the Arabian Sea region for solar zenith angle of 20°-35°. The line of best fit is also shown in panel along with the best fit equation. (b) Same as (a), but for CERES. (c, d) same as (a, b), respectively, but for June to September of 2013 [Mishra et al., IEEE Trans. Geosci. Rem. Sens., 2017].

conditions over the Arabian Sea and the Atlantic Ocean during the summer season of 2012, 2013 and 2014 are shown in Fig. 11 The corresponding mean values of AOD for the collocated points are also shown in Fig. 11. The values of SWF are averaged at different ranges of μ. The IADREE for a given value of μ is obtained by dividing the difference between the SWF value observed for high and low AOD conditions by the corresponding difference in the

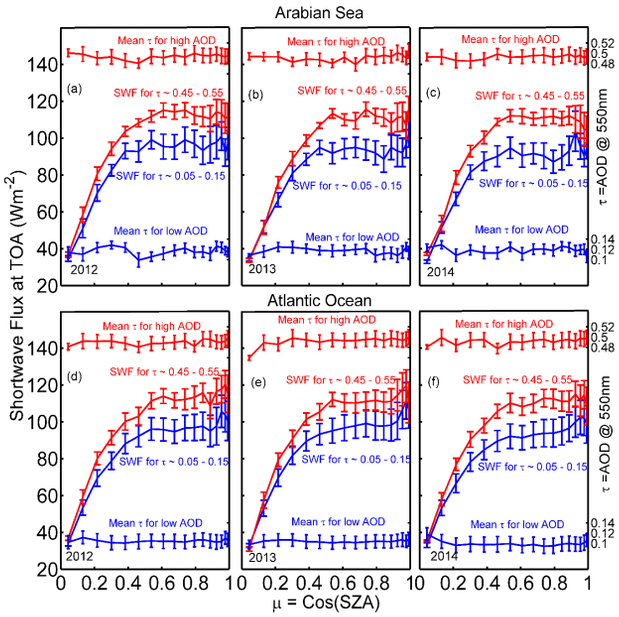

Figure 11: Diurnal variation of upwelling shortwave flux over the Arabian Sea (top panel: a-c) and Atlantic Ocean (bottom panel: d-f) during June-September of 2012 to 2014 obtained using MT-SCARAB for two different AOD bins centered at 0.1 and 0.5 by using collocated measurement of AOD at 550nm by MODIS . Standard error is shown as the vertical error bar. (IEEE Trans. Geosci. Rem. Sens., 2017).

AODs. The seasonal mean variations of the IADREE with μ during June-September of 2012-2014 over the Arabian Sea and the Atlantic Ocean are shown in Fig. 12. The IADREE systematically increases with μ and maximizes at ~0.6 to 0.8 (SZA ~53° - 36°) over both the Arabian Sea and the Atlantic Ocean. Structure of the variation of IADREE with μ is similar at the Arabian Sea and the Atlantic. However, the magnitudes of IADREE over the Arabian Sea are larger than those over the Atlantic by ~ 20%. This difference is more prominent at μ>0.5. The peak value of the IADREE over the Arabian Sea is -53 Wm-2τ-1 while that over the Atlantic is -40 $Wm^{-2}\tau^{-1}$. The values of the IADREE obtained using CERES over the Arabian Sea for 0.8<μ<0.90. These values are in agreement with those derived from MT-ScaRaB using the difference method.

Diurnal mean value of ADREE estimated by integrating the IADREE as a function of μ during June–September is -22.5±4.5 $Wm^{-2}\tau_{550}^{-1}$ and -18.5±3.6 $Wm^{-2}\tau_{550}^{-1}$ over the Arabian Sea and the equatorial Atlantic Ocean respectively. The smaller magnitude of the IADREE over the Atlantic Ocean compared to the Arabian Sea shows that the radiative impacts of the mineral dust transported to the Arabian Sea have larger cooling effect on the Earth-atmosphere system compared to that over the Atlantic. It may be noted that, the mineral dust transported over the Atlantic and the Arabian Sea have two different sources: the former is from the Saharan region while the latter is from the west Asian desert region of Arabia, Iran, and northwestern part of the Indian subcontinent. The observed variation in the IADREE also points to the distinct differences in the physical and radiative properties of the aerosols from these two regions.

Spatial variations of aerosol direct radiative effect (ADRE)

Long term (2000-2014) seasonal mean of MODIS-derived AOD (for June-September) data have been used to estimate the seasonal mean direct radiative effect caused by aerosols (dominated by mineral dust) over the Arabian Sea and the Atlantic Ocean by multiplying the observed AOD with the diurnal mean ADREE over the respective Oceans (Fig.13). The seasonal average of the diurnal mean ADRE at TOA over the Arabian Sea during June-September varies between -22 and -15 Wm^{-2} over the Arabian Sea at north of ~8°N. A rapid reduction in these values occurs towards the south of ~8°N, as a result of the substantially smaller aerosol loading over this region. The diurnal mean ADRE during this period over the equatorial Atlantic varies from -18 Wm^{-2} at the northwest African coast to -10 Wm^{-2} towards the West Atlantic Ocean. Compared to the Arabian Sea, the magnitude of the ADRE over the Atlantic is relatively smaller due to: (a) less value of ADREE over the Atlantic, and (b) lesser value of aerosol loading over the Atlantic compared to the northwest Arabian Sea during this period.

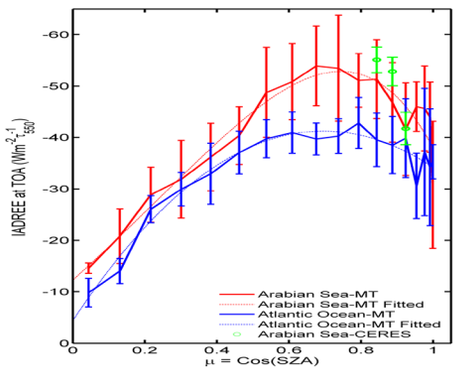

Figure 12: Mean diurnal variations of IADREE over Arabian Sea and Atlantic Ocean during June-September (averaged during 2012 to 2014) obtained from the upwelling SW fluxes using difference method. The 4 order best fit curves for the Arabian Sea and the Atlantic Ocean are also shown in the figure. Standard error is shown as the vertical error bar. The open circles indicate the corresponding values obtained for CERES observations for the same period [Mishra et al., IEEE Trans. Geosci. Rem. Sens., 2017].

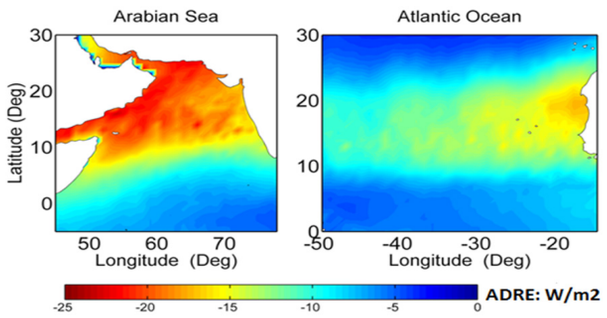

Figure 13: Spatial variations of the estimated seasonal mean ADRE over the Arabian Sea and the tropical Atlantic Ocean based on the seasonal mean AOD during June-September of 2000-2014 [Mishra et al., IEEE Trans. Geosci. Rem. Sens., 2017].

ABL Characteristics over a coastal location in Antarctica

Summertime ABL over coastal Antarctica is characterized by significant diurnal variability. Experimental observations were conducted to investigate the vertical structure of ABL and its variability over the Indian Antarctic station Bharati (68°S, 76°N, 48 m above mean sea level) during the Austral summer of 2016-2017. A total of 50 soundings from radiosonde along with surface meteorological observations were used to characterize the diurnal variation of ABL variability during the study period from 6th December, 2016 to 6th February, 2017. The observation period can be generally characterized as a calm and warm period. Radiosonde launches were conducted at 05:00 local time every alternate day. The campaign also had 4 intense observation periods (IOP) when radiosondes were launched at four hourly intervals for a period of one day each, to characterize the diurnal variability in the ABL and lower troposphere. Surface meteorological observations complemented the upper air observations. Data analysis is in progress.

Network of Observatories for Boundary Layer Experiments (NOBLE) Project

The ISRO-GBP-NOBLE project is aimed at investigating the atmospheric boundary layer characteristics and surface-air at distinct geographical and climate zones. Experimental exploration of the ABL parameters is mainly achieved through observations using tower-based fast-response micrometeorological sensors mounted at multiple levels. The project aims to establish long-term monthly mean variations of ABL parameters and energy fluxes and investigate the role of ABL in regional meteorology and associated feedback processes at different geographical locations representing typical geographic and climate conditions prevailing in the Indian region. Eight stations have been established under the IGBP-NOBLE project (Fig.14). During the reporting time, 32-m meteorological tower with 7 levels of instrumentation has been installed at TERLS, Thumba on 05 January 2017 (Fig. 15). Instrumented micrometeorological tower at Chellakkare, Bangalore (IISc) has been completed in June 2017. Data are being collected from these stations and analysis are in progress.

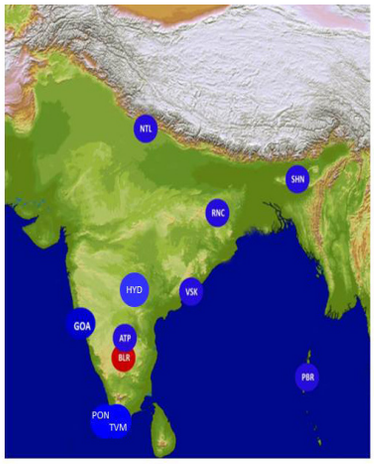

Figure 14: Locations of the network of NOBLE observatories as on June 2016. Red circle indicate the station under development.

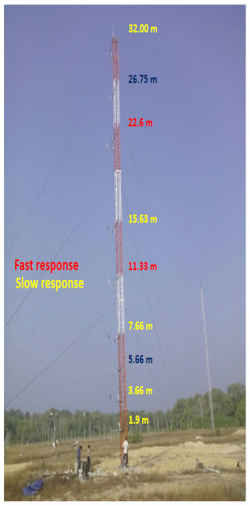

Figure 15: 32-m meteorological tower installed at TERLS.

Radio observation of Venus at meter wavelengths using the GMRT

The microwave observation of Venus from Earth in 1960s revealed basic information about Venus, such as its retrograde rotation and rotation period (243.1 days), the planetary radius is ~6052 km, etc. The two orbiter-based radars observations (Pioneer 10 and the Magellan mission) probed Venus surface in high spatial resolution at S band frequency (12.6 cm wavelength) in H-polarization. The Earth-based large aperture interferometric microwave observations at longer wavelength permit multi-frequency and multi-polarization radio observations of Venus at centimeter/decimeter wavelengths with reasonable spatial resolution. Here results of interferometric observations carried out at 3 different wavelengths 50 cm, 90 cm and 123 cm (or frequencies 606 MHz, 332.9 MHz and 239.9 MHz, respectively) using Giant Meter-wave Radio Telescope (GMRT) is reported.

GMRT Observations and data processing

The GMRT observations of Venus were carried out for six days between March 20 - 27, 2004. GMRT consists of 30 fully steerable parabolic dishes each of 45 m in diameter, 14 of which are located in a central array of ~1 km × 1 km extent and the other 16 in a Y-shaped array of extent 25 km. Two radio sources, 3C147 and 3C48 were used as primary flux calibrators at 60 6.0, 60 6.1 and 239.9 MHz and 3C48 was used for this purpose at 332.9 MHz. These primary flux calibrators were observed at the start and end of each observing session and their flux density values were obtained using Astronomical Image Processing System (AIPS) and Common Astronomy Software Applications (CASA) software. The another compact radio source 0318 + 164 was used as both the phase and bandpass calibrator, it was observed for ~5 minutes in every 30 min observation. The diameter of Venus was ~22.97 arc Sec. during the 6 days of observations. The Tb maps of Venus at 606.1 MHz is shown in Fig. 16, upper and lower panels, respectively. From the known solid angle subtended by Venus during these observations, its brightness temperature (Tb) is estimated from the observed values of its flux density using Rayleigh-Jeans law. The Tb of Venus in the wavelength range from 0.013 m (22.46 GHz) to 1.25 m (239.3 MHz), (Fig. 17) including the ones obtained by GMRT observations (Red color), indicate that Tb decreases with increasing wavelength beyond ~0.5 m, in contrast to the model which remains practically flat beyond ~0.06 m. The model Tb values agree very well with the observed values at shorter wavelengths (< 6 cm) increasing with the same in a log-linear manner and peaks at around 6 cm. The observations beyond 11 cm wavelength show a decreasing Tb values, but the model predicts the values of Tb at lower frequencies (or longer wavelengths) to be same as that at ~6 cm.

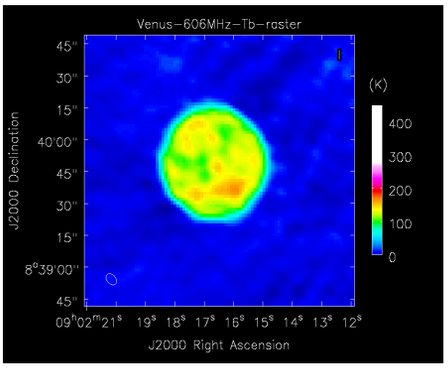

Figure 16: TB Image of Venus at 606.1 MHz [Nithin et al., Icarus,2017].

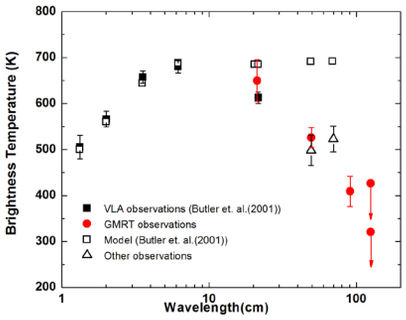

Figure 17: Plot of derived brightness temperature, Tb , versus wavelength. (■) shows measured values and (□) shows the model calculations by Butler et al. (2001) using the VLA. The T b value as obtained by Muhleman et al. (1973) is shown in (♦), that by Condon et al. (1973) is marked by (▲) and (•) shows values obtained using the GMRT (this work). Vertical lines show ±one rms values [Nithin et al., Icarus,2017].

At the GMRT observations frequencies, it can be assumed that the atmosphere is almost transparent. The possible mechanisms responsible for the reduction in Tb at radiowaves are: 1) the presence of selective wavelength absorbing ionosphere, 2) the variations in the dielectric constant or temperature of subsurface. In the case of Venus, the optical depth of its dense atmosphere at decimeter and meter wavelengths is much lower than unity and the observed emission is expected to be generated from its surface and subsurface with a certain depth. The reduction in Tb due to the atmosphere, ionosphere and the variation of surface dielectric values with decreasing frequencies are not expected to be significant. Radiative transfer (RT) model is an effective tool for computing thermal emission at GMRT frequencies by accounting for the detailed variation of temperature and dielectric properties with the depth of the terrain as well as with altitude of the atmosphere of Venus. Microwave RT model based analyses are progressing to explain the lower values of Tb at GMRT frequencies < 1 GHz where emission arises predominantly from a region further down the surface.

Development of ChaSTE Payload

"Chandra's Surface Thermophysical Experiment" - ChaSTE is a payload being developed at SPL for Chandrayaan-2 lander with the active involvement of different entities of VSSC. Main objective of ChaSTE payload is thermal characterization of the lunar regolith near the polar region (~70° latitude). ChaSTE is designed for deploying a thermal probe into the lunar regolith. The thermal probe consists of temperature sensors (RTDs) for temperature measurements and a heater for thermal conductivity measurements, attached to a low thermal conductivity cylindrical material. Design of the ChaSTE payload have been finalized considering that the probe should have sufficient strength for penetrating into the dense lunar regolith medium. Deployment mechanism for inserting the probe is designed such that it imparts minimum disturbances to regolith medium. The ChaSTE payload has four major modules: (1) Thermal measurement probe embedded with sensors and heaters, (2) Deployment mechanism for inserting the probe into the lunar regolith, (3) Electronic module for signal conditioning, control and payload interfacing and (4) Data mining and science extraction. The EM of the thermal probe and its material, deployment mechanism, and control systems has been designed and developed.

Considering the lunar environment, material used for making thermal probe should have very low thermal conductivity, easily machinable and sufficient strength for penetrating hard lunar soil. The thermal probe is made of CE-glass fabric laminated composites with the final cure schedule of 250 °C. This composites exhibits a thermal conductivity of ~0.4 to 0.5 $Wm^{-1}K^{-1}$ and density of ~1.5 g/cc and possesses good mechanical strength under wider temperature range (100-400 K). Several number of thermal probes made of this composite has been fabricated for test and characterization purpose.

The deployment and penetration mechanism to facilitate the penetration of the ChaSTE thermal probe into the Lunar regolith has been developed based on BLDC motor. The design includes the hold and release mechanism of the deployment on the deck of the Chandryaan-2 Lander. Method of direct pushing has been chosen for the deployment of thermal probe into lunar regolith owing to its simplicity and precision of penetration (depth and alignment). This method cause minimum disturbances to the lunar regolith medium. In this scheme the rotary motion of the ball screw is converted to linear motion of the nut. The probe attached to the guide moves linearly. The ball screw mounted on bearing is driven by motor. The mechanism of ChaSTE payload has been tested by integrating it with all the modules. It was able to deploy the probe in lunar simulant successfully. Figure 18 shows the setup for deployment characterization.

The onboard system for ChaSTE payload has two parts, probe electronics and processing electronics. The probe electronics is for exciting RTD sensors, acquiring analog voltages from the sensors and converting the acquired analog signals to digital signals by Analog to Digital Converter (ADC). 4-wire RTD configuration is chosen to achieve the required accuracy. The processing electronics is for acquiring digital signals from ADC and transferring the acquired data to Chandrayaan-2 Lander Craft using

Figure 18: Setup for characterization of deployment mechanism

serial CMOS interface. It also includes the circuit to drive motor for the probe deployment and to control the heater attached to the probe when receiving telecommands from the Lander Craft.

Different module of the ChaSTE payload are characterized and tested separately. In this respect, the penetration force required for penetration has been characterized by penetrating the thermal probe into the lunar simulant by using UTM (Universal Test Machine). It has been found that cone angle and diameter of the probe has large effect on the penetration force. The test was conducted for different levels of compactness and bulk density and the analysis are in progress.

Thermal characterization of Probe

A setup for thermal characterization of thermal probe has been designed and developed based on the heat transfer simulation of the thermal probe. The setup is capable of characterizing the thermal behavior of probe under different temperature and vacuum levels. The temperature control is achieved by pumping liquid nitrogen in the lunar simulant. The thermal probe embedded with sensors has been kept at the center of the cylindrical pot. The thermocouples are kept at different locations for monitoring the temperature. This setup is designed in such a way that its measurements will provide an assessment of uncertainties and heat flow paths in the thermal measurements by using ChaSTE thermal probe. Currently, different tests are being conducted for thorough thermal characterization of the ChasTE probe. Figure 19 shows the picture of test setup for thermal characterization of ChaSTE thermal probe.

The ground segment activity for the ChaSTE payload has been initiated. Under this a POC is being setup at SPL which will be capable of reception and processing the ChaSTE data. Programs for automated operations, preprocessing and reading the data, and conversion to PDS format are being developed.

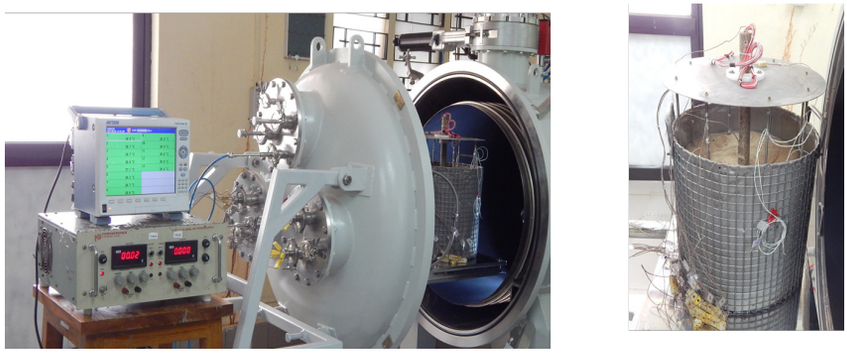

Figure 19: Experimental setup for thermal characterization of ChaSTE probe under different thermo-vacuum condition.

Future Projections

- Development and delivery of QM and FM models of ChaSTE payload.
- Setting up of the ChaSTE Ground Segment and analysis of data from lunar regolith.
- Analysis of polarized data from GMRT observation of Venus surface emission.
- Development of radiative transfer based surface parameter retrieval algorithm from the radiometric measurements of Martian surface.
- Investigation of deep convective cloud distribution and free tropospheric humidity from MT-SAPHIR data.
- Investigation of the diurnal and intra-seasonal variability of water vapour at different tropospheric layers using multi-year MRP observations.
- Development of UHF Wind Profiler
- Establishment of the NOBLE stations at Arid region and Gangetic plain.
- Experimental campaigns for addressing specific scientific issues, including the surface layer turbulent characteristics, diurnal development of ABL and pollutant dispersal.
- Day-night changes in the development of deep convective clouds and identification of the genesis mechanism.
- Investigation on the role of ABL on tropospheric dynamics, clouds, and precipitation.

Publication in Peer-Reviewed Journals

1. Mohan, N., Subhashis Roy, Govind Swarup, Divya Oberoi, Niruj Mohan Ramanujam, Suresh Raju C, Anil Bhardwaj , Radio observation of Venus at meter wavelengths using the GMRT, ICARUS, Vol. 297, 119–125, doi.org/10.1016/j.icarus.2017.06.026 (2017).
2. Renju, R., C. Suresh Raju, Manoj Kumar Mishra, Nizy Mathew, K. Rajeev and K. Krishna Moorthy, 'Atmospheric boundary layer characterization using ground-based microwave radiometric observations over a tropical coastal station', IEEE Transactions On Geoscience and Remote Sensing, doi: 10.1109/TGRS.2017.2735626 (2017).
3. Gupta, A. K., K. Rajeev, S. Sijikumar, Day-night changes in the altitude distribution, physical properties and radiative impact of low-altitude clouds over the stratocumulus-dominated subtropical oceans, Journal of Atmospheric and Solar-Terrestrial Physics 161, 118–126, doi: 10.1016/j.jastp.2017.06.021 (2017).
4. Mishra, M. K., Ashok Kumar Gupta, K. Rajeev, 'Space-borne Observations of the Diurnal Variation of Shortwave Aerosol Direct Radiative Effect at Top-of-Atmosphere over the Dust-dominated Arabian Sea and Atlantic Ocean', IEEE Transactions on Geoscience and Remote Sensing, 10.1109/TGRS.2017.2730758 (2017).

Publications in Proceedings

1. Suresh Raju C., et al., 'Development of Indigenous Mechanism for deploying thermal probe into Lunar Regolith', 10th National Symposium and Exhibition on Aerospace Related Mechanisms (ARMS -2016) Thiruvananthapuram, Kerala, India, 18-19 November 2016.
2. Tinu Antony, Suresh Raju, Nizy Mathew and Renju R., 'Microwave emissivity of arid regions of Australia', International Symposium on Antennas and Propagation, CUSAT, Cochin, 15-17 December 2016.
3. Renju R., Manoj Kumar Mishra, K. Rajeev, Suresh Raju C. and K. KrishnaMoorthy, Characterization of tropical convection using ground based Microwave Radiometric observations, International Symposium on Antennas and Propagation, CUSAT, Cochin, 15-17 December, 2016.

Conference/Symposium/Presentations

1. Renju R., Manoj Kumar Mishra, K. Rajeev, Suresh Raju C. and K. KrishnaMoorthy, Characterization of tropical convection using ground based Microwave Radiometric observations, International Symposium on Antennas and Propagation, CUSAT, Cochin,15-17 December, 2016.
2. Renju R. and Suresh Raju C., 'Characterization of tropical convection using ground based Microwave Radiometric observations', URSI, RCRS, Tirupathi, 01-04 March 2017.
3. Tinu Antony, Suresh Raju, Nizy Mathew and Renju R., Microwave emissivity of arid regions of Australia, International Symposium on Antennas and Propagation, CUSAT, Cochin, 15-17 December, 2016.
4. Suresh Raju C., et.al, 'Development of Indigenous Mechanism for deploying thermal probe into Lunar Regolith', 10th National Symposium and Exhibition on Aerospace Related Mechanisms (ARMS -2016), Thiruvananthapuram, Kerala, India, 18-19 November 2016.

Invited Lectures

K. Rajeev

1. Radiation Budget and Energy Transfer Between Earth and Atmosphere - with Focus on Vertical Coupling, Indian Geophysical Union Meeting, Indian Institute of Technology - Indian School of Mines, Dhanbad, 8-10 Nov. 2016.
2. Satellite Remote Sensing of Aerosols and Clouds, International Conference on Sensors and Small Satellite Technology for Disaster Management (SSTDM-2016), Amrita University, Kochi, 17 December 2016.
3. Climate of the Earth-Atmosphere System, ASMS, Thiruvananthapuram, 10 December 2016.
4. Lower Atmospheric Dynamics, First User Scientists Workshop on ST Wind Profiler Radar Applications, Advanced Centre for Atmospheric Radar Research, CUSAT, 9-10 February 2017.
5. Satellite Remote Sensing of Clouds – Past, Present and Future, UPCAR-2017, National Atmospheric Research Laboratory & SV University, Tirupati, 25-28 June 2017.

Suresh Raju C.

1. 'Detection of Deep Convective Clouds from MT-SAPHIR: New Methodology', URSI- RCRS-2017, Tirupati, India, 1-4 March 2017.
2. Microwave radiometry for Earth and planetary studies, Workshop on Remote sensing application and Sciences (RSAS-2016) Kolkota, 17 December 2016.

AEROSOLS CHEMISTRY AND TRACE GASES

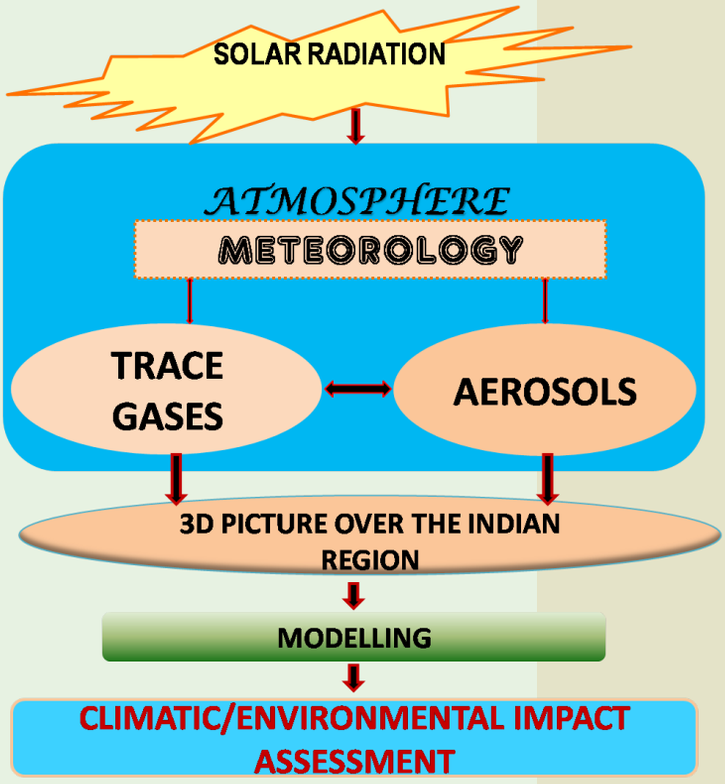

The increasing anthropogenic activities alter the chemical composition of earth's atmosphere by putting a variety of gases and particulate matter (aerosols) in to it. Even though they are minor species in terms of their mass/volume, they play key roles in the Geosphere-Biosphere system affecting the life forms and their living environment. The trace gases of environmental and climatic significance include O_3, CO_2, CH_4, N_2O, H_2O, CO, NO_2, SO_2, halogen species, CFCs, etc. ACTG branch focuses on the evolution of 3D distribution of these minor constituents over the Indian Land mass and surrounding oceanic environments making use of state-of-the art experimental facilities and satellite based data. The major facilities include on-line trace gas analysers, green house gas analysers (CO_2 and CH_4), aerosol samplers, Aerosol counter, ion chromatograph, gas chromatograph, ICP and balloon-borne ozone-sondes, etc. This branch is also involved in the polar research programme by conducting measurements of O_3, CO_2 and aerosol sampling at Antarctica. Recently steps have been taken to initiate modelling studies. The outcome of the research activities of this branch has applications in the areas of climate/weather research, air pollution assessment and control measures, environmental and health impact assessment, and design/development/validation of space-borne payloads for satellite remote sensing.

Science Team
Prabha R Nair
Sandhya K Nair
Prashant Hegde
Girach Imran Asatar
Revathy S Ajayakumar

Research Associates/ Fellows
Aryasree S
Kavitha M
Aswini AR

Technical Support
Anumod PG

Atmoshperic Trace Gases

Variations of surface O_3, CO and CH_4 over the Bay of Bengal during the summer-monsoon season and model simulations

The measurements of surface ozone (O_3), carbon monoxide (CO) and methane (CH_4) over the Bay of Bengal (BoB) were carried out during the summer-monsoon period of the year 2009, as part of the Continental Tropical Convergence Zone (CTCZ) experiment. O_3, CO and CH_4 mixing ratios varied in the ranges of 8–54 ppbv, 50–200 ppbv, and 1.57–2.15 ppmv, respectively during 16 July – 17 August 2009. The Weather Research and Forecasting model with Chemistry (WRF-Chem) version-3.5.1 was used to simulate meteorological and chemical fields during the campaign period. The model could simulate observed variations of O_3 and CO over the BoB during the summer monsoon season with an overestimation of absolute O_3 levels by 1.9 ppbv (i.e. ~6%) and absolute CO levels by 18 ppbv (i.e. ~16%).

An interesting phenomenon observed during the CTCZ experiment is the abrupt reduction in O_3 mixing ratios that accompanied the onset of heavy rainfall, despite the low solubility of O_3 in water. Figure 1 shows variations in O_3 (black circles) mixing ratios, surface temperature (orange curve), TRMM (Tropical Rainfall Measuring Mission) retrieved rainfall (thick grey vertical bars), and WRF-Chem-simulated vertical winds at pressure levels ranging from 950–750 hPa (coloured bars) during four such events on July 21, 26, and 28–29 and on August 10–11, 2009. While the first three low-O_3 events are not captured by WRF-Chem, the fourth event was reproduced.

The observed reduction in O_3 was associated with dynamics rather than wet scavenging. Airmasses undergoes downdrafts during heavy rainfall through air drag by the falling rain drops and in mesoscale subsidence that compensates convective updrafts. We suggest that, in the presence of O_3-poor airmass aloft, a downdraft would result in reductions in surface O_3 mixing ratios and an opposite scenario leading to O_3 enhancement could take place if downdrafts bring mid-tropospheric air, where typically O_3 is higher than at surface. The model-simulated meteorology shows occurrences of downdrafts at different pressure levels during the first three events on July 21, 26, and 28–29 (Fig.1a–c), which is further corroborated with measurements of air temperature aboard ship. Downdrafts of free tropospheric air could lead to a reduction in near-surface temperature and the air temperature measured aboard ship showed a sharp decrease of 2–4 °C, coinciding with the first three low-O_3 events (Fig.1a-c). Model-simulated vertical winds and variations in air temperature suggest that downdrafts did occur during the first three rainfall events. Since in situ measurements of O_3 vertical profiles are not available over the BoB during the study period, the observations taken at Thumba, Thiruvananthapuram, in the southern Indian region are used as a case study to investigate this hypothesis. The surface O_3 on July 15, 2011 at Thumba is observed to decline from 25 to 13 ppbv within 15–20 minutes, coinciding with the occurrence of intense rainfall (3.5–0.5 mm rain over a period of 5 minutes). The ozone profile has lower O_3 mixing ratios aloft (~22 ppbv at ~1 km) than near surface (~42 ppbv). With an O_3 distribution as observed in the present case study at Thumba, the downdraft during intense rainfall would have lead to the mixing of free-tropospheric air with near-surface air, or to the replacement of surface air with free-tropospheric O_3-poor air leading to reduced O_3 levels.

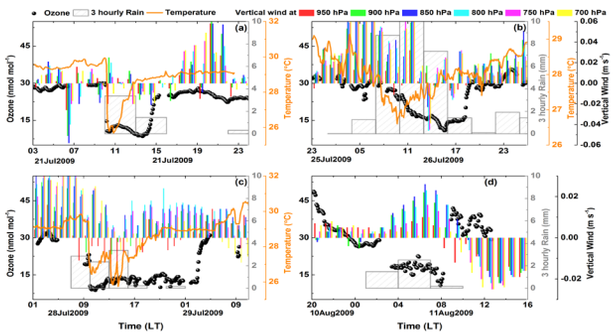

Figure 1: Surface O_3 (black dots) along with temperature (orange curve) and 3-hourly rainfall (grey vertical bar) during the four events of sharp decline in O_3 (a–d). Colours indicate the vertical wind as simulated by WRF-Chem [Girach et al., Atmos. Chem. Phys, 2017].

We have compared the in situ measurements of O_3, CO and CH_4 conducted during this study with a global reanalysis model, Monitoring Atmospheric Composition & Climate (MACC) to evaluate the global model fields in the BoB region. MACC model consists of ECMWFs' (European Center for Medium range Weather Forecasting) Integrated Forecast System (IFS) coupled with the MOZART (Model for OZone and Related chemical Tracers)-3 chemistry transport model.

The comparison of MACC reanalysis near the surface (at 1000 hPa) with in situ measurements (Fig. 2) shows that MACC reproduces the observed mixing ratios of O_3, CO and CH_4. The estimated mean biases for surface O_3, CO and CH_4 are 1.6 ppbv (5.3% of average in situ O_3, 29.7 ppbv), -2.6 ppbv (2.7% of average in situ CO, 96 ppbv) and 0.07 (4% of average in situ CH_4, 1.83 ppmv). The small magnitudes of mean biases show the capabilities of MACC reanalysis in reproducing the observed levels. However, it shows a limitation in capturing the variations. The squared correlation coefficients (R^2) between in situ observations and MACC reanalysis at 1000 hPa are 0.03, 0.13 and 0.25 for O_3, CO and CH_4, respectively.
This clearly shows that MACC reanalysis reproduces the observed mean concentration levels of O_3, CO and CH_4 over the BoB during summer monsoon with a small bias

of 2–5%. However, there is a limitation in reproducing observed variabilities of O_3 and CO. Variations in CH_4 are also well reproduced by MACC reanalysis.

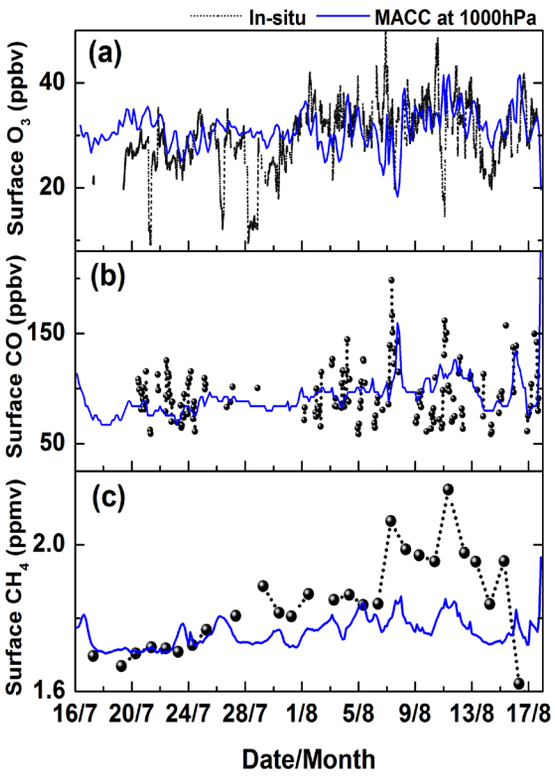

Figure 2: (a, b, c) A comparison of surface O_3, CO and CH_4 from in-situ measurements (black dots) with MACC reanalysis at 1000 hPa (blue line) along the cruise track over the BoB during the CTCZ experiment July -August 2009 [Girach et al., J. Earth Syst. Sci. 2017].

Unusual enchancement of troposheric and surface ozone over Himalayan region

Fig. 3a-e shows the Latitude–longitude map of ozone along the path of TES (Tropospheric Emission Spectrometer) spacecraft during 07–15 December 2008. Box shown in the figure represents the region near by the observational site, Nainital as marked by a star. Fig.3f-m represents Pressure-latitude map of TES ozone profiles outside/inside the box region during the satellite observations shown in 3a-e. It is to be noted that no satellite pass is available on December 7-11 during daytime and also no pass during night time over (or nearby) Nainital region. The enhancements in ozone mixing ratios are seen in the upper troposphere over higher latitude during 07–09 December 2008. This enhancement is due to intrusion of stratospheric ozone-rich air. It is interesting that the intrusion occurred on December 07 and 09 might have reached Nainital on December 11th showing the enhancement in the surface ozone values (Fig. 4).

The surface ozone over Nainital and Trivandrum; ozone mixing ratio at 300hPa from AIRS (Atmospheric Infrared Sounder) around Nainital region; and tropopause temperature around Nainital region during December 2008 are shown in Fig. 4. It is clearly evident from the figure that surface ozone is showing significant two fold enhancement, reaching ~58 ppbv on 11 and 12 December 2008, over Nainital whereas such variation is not observed over Trivandrum. In comparison to the surface ozone, ozone at 300 hPa averaged over Nainital region (29-30 °N and 79-80 °E) also shows enhancement. Absence of enhancement in surface ozone over Trivandrum points that this event has affected the surface ozone on regional scale but not the larger region. The increase in tropopause temperature is also seen during the ozone enhancement.

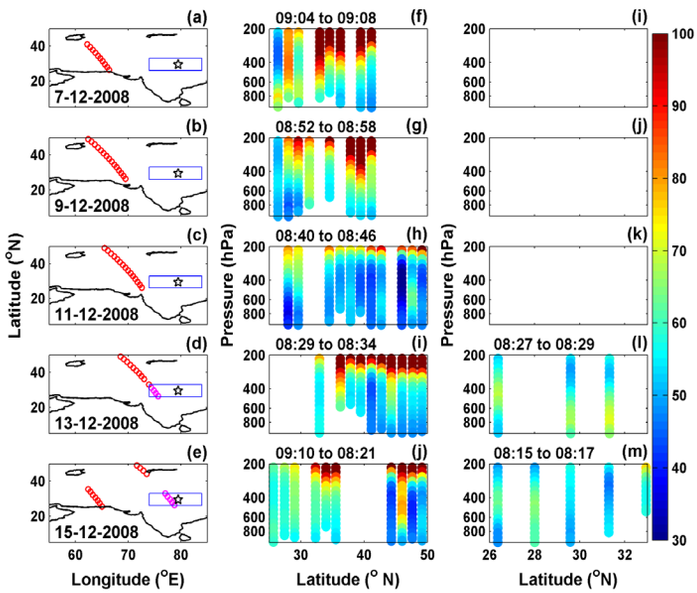

Figure 3: (a-e) latitude-longitude map of TES path during alternate days in 07–15 December 2008 and box (star) represents the part of Himalayan region (Nainital site). (f-j) Pressure-latitude map of TES ozone profiles during the observational period and (l-m) are the ozone profiles passing through the box region during 07–15 December 2008 [Phanikumar et al., Remote Sens. Environ. 2017].

Considering tropopause height of ~10 km on 9 December 2008, ozone-rich airmass took ~2 days to reach at Nainital altitude (~2km) and enhancement in surface ozone was observed on 11 December 2008. Based on this, we estimate mean descent rate of ozone to be ~ 4km day-1 in the troposphere. The stronger intrusion had occurred at higher latitudes (35–45 °N) compared to the Nainital latitude (29 °N) on 9 December and hence descent of ozone is not vertically straight but it has horizontal component which would lead to even faster descent rate than what is reported here. This descent rate is approximately 4 times higher than the value reported earlier.

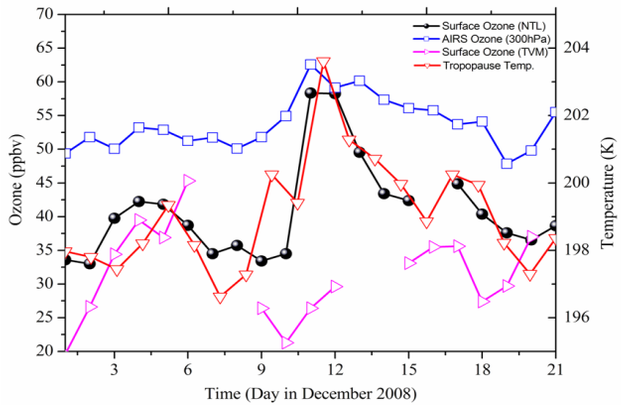

Figure 4: Temporal evolution of AIRS retrieved ozone at 300hPa (blue) averaged over Nainital region, daily surface ozone at Nainital (black), daytime surface ozone at Trivandrum (magenta) and tropopause temperature (red) over Nainital region during 01–21 December 2008 [Phanikumar et al., Remote Sens. Environ. 2017].

The high altitude site, like Nainital, is considered to be free from local pollution having good air quality conditions. As per the average surface ozone values in December month is around 30 ppbv or below over Nainital. In the present study, surface ozone values were ~58 ppb for two consecutive days. This points out that the air quality (considering ozone) can be poor occasionally over high altitude locations under such events of stratospheric intrusion of ozone into the lower troposphere.

SCIAMACHY observed changes in the column mixing ratio of methane over the Indian region during 2003-2009

The study deals the trends in the column averaged mixing ratio of methane (XCH_4) over the Indian region during 2003-2009 periods using the SCanning Imaging Absorption spectroMeter for Atmospheric CHartographY (SCIAMACHY) observations. Fig. 5 (a) shows a spatial map of XCH_4 over Indian region (5°- 40°N and 65°-100°E) as observed for the month of October 2004. Based on the observed regional differences in XCH_4 the Indian land mass is divided into five regions namely, Indo Gangetic Plain (IGP), Central India (CI), Thar, Northern part of Peninsular India (NPI) and Southern part of Peninsular India (SPI) as done in our earlier study (Kavitha and Nair, 2016a) and as marked on the map (Fig. 5 b).

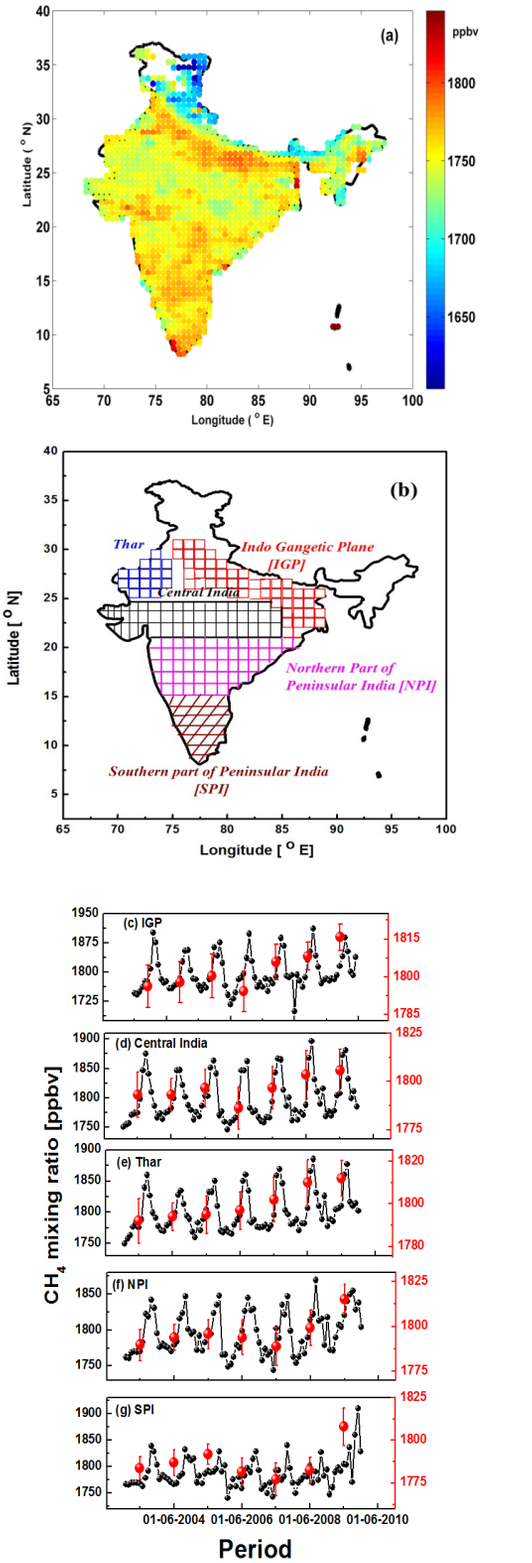

Figure 5: (a) Spatial map of XCH_4 over Indian region as observed by SCIAMACHY (October 2004) and (b) Study regions selected for the analysis: Indo Gangetic Plain (IGP), Central India (CI), Thar, Northern part of Peninsular India (NPI) and Southern part of Peninsular India (SPI). (c-g) Monthly and inter-annual variation of XCH4 (black and red circles, respectively) retrieved from SCIAMACHY for the study regions [Kavitha & Nair Atmos. Env. 2017].

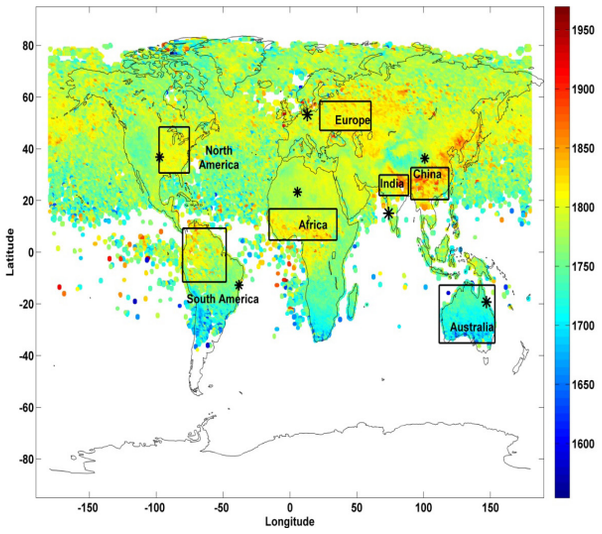

Figure 6a: Global distribution of SCIAMACHY-retrieved XCH_4 (for July 2004) with the rectangles representing the hotspots of XCH_4 over China, India, Europe, North America, Africa and South America along with Australia for this study [Kavitha & Nair Atmos. Env. 2017].

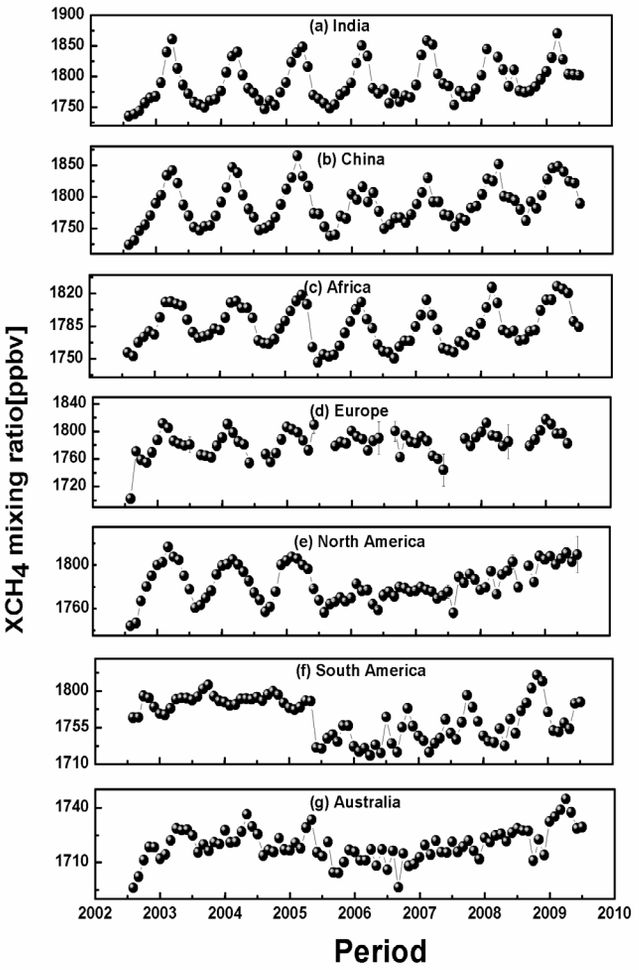

Figure 6b: Month to month variation and anomalies in the XCH_4 using SCIAMACHY measurement over (a) India, (b) China, (c) Africa, (d) Europe, (e) North America, (f) South America, and (g) Australia during 2003-2009 [Kavitha & Nair Atmos. Env. 2017].

The distinctly different seasonal variations in XCH_4 over these regions and their association with regional sources and meteorology are already reported (Kavitha and Nair 2016a). Regional differences in XCH_4 have been attributed to variation in emission from sources like livestock, rice cultivation, biomass burning and fossil fuel allied emission. Rice cultivation is found to be the main factor controlling the seasonal variation (of ~100 ppbv) in XCH_4 over the Indian region.

The monthly XCH_4 from 2003-2009 as obtained from SCIAMACHY for the five study regions are plotted in Fig. 5. The time series data over these regions are analyzed in terms of the variation in monthly and annual means (black circles and red circles, respectively). An overall increase in XCH_4 is seen in the monthly as well as yearly mean data. Except for the Southern Peninsular India (SPI), all other regions in India show an increasing trend in XCH_4 varying from 2.1 ppb to 3.5 ppb/year from 2003-2009. An increase of 2 to 4 fold increase (5.2 to 7.6 ppb/year) is observed after 2005 over all the regions compared to 2003-2005 after applying the bias correction before and after the sensor degradation. More or less similar trend observed in near-surface CH_4 (0.011 ppb/month) over Cape Rama, Goa, the only Indian CSIRO network station where long-term data is available. The inter-annual variation of XCH_4 over northern parts of India is closely linked with the rice cultivation. Except for IGP, all other regions show a rise in the livestock population during the 2003-2007 periods. Increase in CH_4 in Central India is found to be associated with the increased fossil fuel allied emissions (Oil and gas).

Comparison with global hotspots

A comparative study of the above discussed trends and those observed over global hotspot regions of CH_4 (Fig. 6a) was also carried out. Sharp peaks in XCH_4 are observed over India, China and Africa regions during Northern summer/monsoon months (July/August/September) (Fig. 6b). The seasonal amplitudes of XCH_4 are comparable over India and China and are associated with the emission of CH_4 from seasonally varying sources like agriculture, wetland emissions or biomass burning. Regional meteorology also plays role. The seasonal peaks do exist over Europe, but less pronounced. The peaks are evident in the North American region till 2006 after which this pattern disappears. Studies based on GOSAT observations of CH_4 over North America attributed the source of CH_4 to be anthropogenic like oil/gas mining, waste disposal, coal, livestock, and natural wetlands most of which are not seasonal. Over South America, a sudden dip seen in 2005 (attributed to retrieval issues associated with sensor degradation) followed by an increasing trend and a seasonal pattern.

Consistent seasonal patterns are not seen over the Southern hemispheric region of Australia, thus revealing more or less permanent sources of CH_4 over a year. Livestock is the single largest CH_4 sources over Australia contributing to ~50% of the emission and ~23% comes from coal and gas mining, both are more or less steady sources. However, a shifts in base line (seasonal minima) are observed over

Africa, China, South America and Australia from 2006 onwards. A decrease in the seasonal amplitude of XCH_4 is observed over most of the regions by 2006 and a build up afterward. The inter-annual trends are estimated based on the annual means for different periods. No significant trend is observed over most of the regions during 2003-2005 (except for India, China and Europe). But after 2005, a significant increase is observed with varying amplitudes. The increase in XCH_4 over most of the regions is higher (except over Australia), compared to those over Indian region. This analysis suggests that year-to-year variations, as well as regional patterns in XCH_4, are region dependent. The data of near-surface CH_4 mixing ratios available from ground observatories close to the study regions discussed above (and as marked by an asterisk (*) in Fig. 6a) were analyzed to see the trends in near-surface CH_4 and to compare with the mean XCH_4 estimated for a grid size of (2°-5°in latitude, 5°-15°in longitude) centered over these locations. The seasonal patterns of XCH_4 and near-surface CH_4 over selected locations over the globe showed that over most of the Northern hemispheric regions, the near-surface CH_4 is higher than XCH_4. Similarities, as well as differences, exist in the seasonal amplitudes and periods/duration of the peak, revealing in-homogeneities in the vertical distribution of CH_4. The differences are more pronounced over China, North America, Europe and African regions when seasonal peaks in XCH_4 correspond to a seasonal minimum in near-surface CH_4.

Analysis of ozonesonde profiles over Thumba: First-cut results

Detailed analysis of the balloon-based ozone profiles is being carried out to understand the variabilities in tropospheric Ozone. The average tropospheric ozone at is Thumba found to be 35±5.7 DU (maximum in March, 43.25 DU and minimum in October, 25.66 DU). The variations in tropospheric O_3 profile was found to be closely associated with changes in water content and temperature the detailed analysis of which is nearing completion. A comparison of total and tropospheric column ozone obtained by integration of ozonesonde profiles up to cold point tropopause with satellite based observations from Ozone Monitoring Instrument (OMI) shows more or less similar seasonal behaviour. But OMI retrieved tropospheric Ozone is found to be underestimate by 1 to 13DU.

Aerosol Chemistry

Carbonaceous and inorganic aerosols

The carbon component in the atmospheric aerosols has gained much attention recently because of their significant role in radiative effects, visibility reduction, health and climate effects. About ~20-70% of total suspended particulate matter is composed of carbonaceous matter in urban areas. Carbonaceous matter is mainly composed of organic carbon (OC) and elemental carbon (EC). They are emitted directly into the atmosphere as primary organic carbon (POC) mainly from biomass burning and fossil fuel combustion. Secondary organic carbon (SOC) forms through oxidation of gas phase volatile organic compounds and their subsequent conversion to particle phase. A major fraction (40-80%) of organic matter found in the atmosphere is water soluble. Water-soluble organic carbon (WSOC) plays a significant role in aerosol hygroscopicity and acts as CCN. Recent studies show that secondary organic aerosols are major part of WSOC. Over the Indian subcontinent, large spatio-temporal variability in different aerosol properties such as chemical composition, optical properties, mass concentration and radiative forcing have been reported by various groups based on land campaigns, field measurements, fixed location measurements and ship-borne experiments over oceanic regions. This work investigates the details of the chemical characteristics and sources of carbonaceous aerosols over the Thumba region (8.5°N, 76.9°E, 3 m asl) in India.

Aerosol samples collected over coastal location Thumba during September 2009 to March 2010 were investigated for concentrations of total carbon and nitrogen, elemental carbon, organic carbon, water-soluble organic carbon and ions (cations and anions) and their sources. Temporal variations of particulate chemical composition and the OC/EC ratio during the study period are shown in Fig. 7. On average, water-soluble components (30 $\mu g\ m^{-3}$) account for about 33% of total aerosol mass (92 ± 35 $\mu g\ m^{-3}$). Charge balance of the major ions revealed cation abundance over the region. Calcium was one of the abundant cation and Ca/Mg mass ratio centring around 3.6 ± 2.4 suggest that chemical composition of aerosols is dominated by calcareous dust which might have been transported form desert region surrounding the Arabian Sea. Sulphate was the major anion (6.1 ± 2.0 $\mu g\ m^{-3}$) and exhibits statistically significant positive correlation with NH_4^+ (R^2 = 0.76) indicating their dominant contribution from anthropogenic sources (e.g. $(NH_4)_2SO_4$). NO_3^- correlated to NH_4^+ and Ca^{2+} ($R^2 \geq 0.63$) suggesting that neutralization of NO_3^- might occur on the surface of the calcite particles to form $Ca(NO_3)_2$. NH_4^+ correlated to $nssSO_4$ with a molar ration of 1.01 ± 0.58. This indicates that the neutralization of H_2SO_4 occurred to form $(NH_4)_2SO_4$.

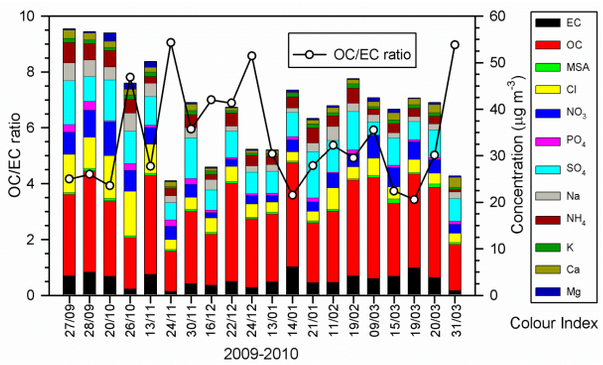

Figure 7: Temporal variations of particulate chemical composition and the organic carbon/elemental carbon (OC/EC) ratio during the entire sampling period [Hegde and Kawamura, Arch. Env. Cont. Tox. 2017].

Relatively high abundances of WSOC (range: 2.1 to 11.0 µg m^{-3}) account for 32% of water-soluble components and their significant positive correlation (R^2 = 0.58) with K^+ (range: 0.4 to 1.0 µg m^{-3}) provides an evidence for their large-scale contribution from biomass burning for the entire observation period. The temporal variations in the carbonaceous aerosols and air mass trajectories demonstrated that several pollutants with their precursor compounds are originated from north-western India and the surrounding oceanic regions.

No significant differences in day and night concentrations of marker compounds were noticed. Here it is noteworthy that, although local and or regional emissions are important in controlling the concentrations of carbonaceous aerosols over study area, the ambient meteorology indicates that their source strength seems to be weakened due to the dilution. This is mainly due to the mesoscale weather phenomenon common in coastal regions (i.e., sea breeze land breeze circulations). There are no significant local anthropogenic contributions over study region. Therefore, the datasets reported here could serve as a baseline observation of carbonaceous aerosols for a wider region in southern peninsular India, which could contribute to regional climate and air quality models. This would also point to adapting strict air quality measures to improve human health in addition to lower their climate forcing effects.

Carbonaceous and inorganic aerosols over a sub-urban site in peninsular India: First results

The aerosol samples were collected from a sub-urban site Ettimadai in Coimbatore using a high volume air sampler, operating at a set flow rate of 1.1 m^3 min^{-1}. Sampling period was approximately 6 h for each sample. Particulate matter less than 10 µm in diameter (PM_{10}) were collected on pre-combusted quartz microfiber filters. The samples collected in daytime (6:00-18:00 IST) as well as night-time (18:00-6:00 IST) in campaign mode during pre-monsoon, monsoon, post-monsoon and winter were subjected to chemical analysis using various techniques suiting to the composition like inorganic, carbonaceous, nitrogenous and their mass loading. For this the samples were extracted using appropriate techniques so that the individual components could be quantified with minimum uncertainty.

The order of abundance of chemical components on annual basis were SO_4^{2-} > OC > Ca^{2+} > HCO^{3-} > NO_3^- > NH_4^+ > EC > Na^+ > K^+ > Mg^{2+} > Cl^-. Average equivalent ratio of cations (sum of cations, µeq m^{-3}) to anions (sum of anions, µeq m^{-3}) was 1.2 ± 0.5 and showed a good correlation (R^2 = 0.89). Average PM_{10} concentration was found to be 41±21 µg m^{-3}. Mass concentration of PM_{10} was observed to be highest in winter and lowest during monsoon. About 76% of the PM_{10} could be analysed. The total carbonaceous aerosols and water soluble ionic species contributed to 31% and 45% of PM_{10} mass, respectively. Total carbonaceous aerosols (TCA=OM+EC) accounted for 31%, while water soluble inorganic ions constituted 45% of PM_{10} mass. OC contributed to 17% while EC 3% of PM_{10} mass. OC was the dominant species of TC contributing 84% and EC contributing 16% of TC. OC/EC exhibited an annual average of 5.7 ± 4.2. Average WSOC was 4.2 ± 2.9 µg m^{-3} and accounted for 60% of OC. The estimated average concentration for POC and SOC were 4 ± 2.5 µg m^{-3} and 3 ± 2.5 µg m^{-3} accounting for 56% and 44% of OC, respectively. Water Soluble Total Nitrogen (WSTN) and Water Soluble Organic Nitrogen (WSON) ranged from 0.2 to 6 µg m^{-3} (average 2 ± 1.5 µg m^{-3}) and 0.01 to 1.8 µg m^{-3} (average 0.7 ± 0.5 µg m^{-3}), respectively, during the study period. Water soluble total nitrogenous aerosols (WSTN) contributed to ~ 5% of PM_{10} mass. WSON contributed to ~34% of WSTN.

Large abundance of SO_4^{2-} and OC in PM_{10} along with good correlation of K^+ with OC, EC, POC, WSOC and SO_4^{2-} suggests biomass burning as a major source in this region. High SOC and OC/EC ratio shows the additional source for OC from secondary production which is significant during daytime. High concentration of Ca^{2+} and HCO^{3-} during daytime and their significant correlation suggests that windblown mineral dust adds to the mass loading during daytime. It was observed that PM_{10} mass concentration along with Ca^{2+}, HCO^{3-}, Mg^{2+} and OC maximises during evening hours when wind speed and temperature are highest that favours wind-blown mineral dust and secondary production of OC, respectively. This study region is influenced by biomass burning sources throughout the study period. However it is accompanied by mineral dust and secondary production during daytime which explains the observed high PM_{10} mass loading during daytime.

New Activities

Trace gas measurement at high altitude site Ponmudi

Trace gas measurement at high altitude site Ponmudi has been initiated. As part of this, a UV photometric Ozone analyzer and a NOx analyser have been installed there and data is being collected at regular intervals. Preliminary data analysis of surface ozone over Ponmudi shows a diurnal pattern different from that of Thumba. On most of the days O_3 showed a noon time low and night time enhancement and large fluctuations. This is different from that observed at Thumba, where O_3 depicts daytime high and night time low. Values of surface NOx is less as compared to that of Trivandrum. Strong anti-correlation between surface ozone and NOx which is observed at Trivandrum, is not seen at Ponmudi. Detailed analysis of data is going on.

Mini-Wide Range Aerosol Spectrometer (Mini-WRAS):

Aerosol number density-size distribution measurements are crucial in quantifying the radiative properties of aerosols and also in assessing the environmental/biological impacts. To investigate microphysics of aerosols and the inter-dependence of aerosol number density-size distribution and trace gases a 41-channel Aerosol spectrometer

(1371-MINI-WRAS) has been installed at Thumba. MINI-WRAS measures particles in the range of 10 nm to 32 µm in 41 channels. The ultrafine particles (nano sizer particles) in the range of 10 nm to 200 nm were measured in 10 channels. To cover the widest range of particle diameters, ranging from 10 nm to 35µm, the instrument combines two measurement methods: the electrical detection of ultrafine particles by means of a Faraday cup electrometer, and the optical detection of particles with diameters greater than approximately 200 nm by measuring the scattered light intensity so called optical measuring cell with laser (OPC). The combination of the above two measurement methods provides a particle size distribution in the range of 10 nm to 35µm in a total of 41 size classes. The smallest measuring interval is 60 seconds. The particle concentration range for the OPC, is in the range between 1 and 2,000,000 particles/l and the FCE between 3,000 and 1,000,000 particles/cm³. Data collection and analysis is in progress.

Aerosol sampling from Cochin, Chennai and Palghat

Initiated aerosol sampling at the industrial site Cochin for studies on organic aerosols on campaign mode covering different seasons. The analysis of samples for EC and OC has been started. At the eastern coastal location Chennai also, we have started aerosol sampling recently. Samples are being collected regularly on weekly basis. Few samples were also collected from Agali, Palghat.

Size Resolved Aerosol Sample collection: High Volume Air Sampler Integrated with Multistage Jet Cascade Impactor model HV-1000R integrated with AH-600 of M/s. Sibata Scientific Corp., Japan has been procured and installed at Thumba. It collects aerosols samples in 5 size ranges viz 1st stage: >7.0µm, 2nd stage: 3.3µm to 7.0µm, 3rd stage: 2.0µm to 3.3µm 4th stage: 1.1µm to 2.0µm and a backup filter for < 1.1µm. A typical mass concentration of aerosols measured at Thumba during premonsoon period (during 2016-17) in these size bins are 26.3±7.3, 13.6±7.8, 8.6±3.1, 8.0±1.0, 23.7±12.0 µg m^{-3}, respectively. The size resolved chemical composition is being analysed.

Inductively Coupled Plasma-Mass Spectrometer

Detection and quantification of metallic species and trace elements in the atmospheric aerosols is important in order to understand their impact (anthropogenic emissions) on the climate and health. Inductively Coupled Plasma Mass Spectrometer (ICP-MS; Quadrupole system) with a mass detection range from 4 to 290 amu and resolution of 0.4 amu analytical instrument is already setup. This state-of-the-art ICP-MS installed at SPL provides measurements of the metallic species and trace elements at ppb or ppt level. Argon is used as the plasma gas in ICP and considering its huge consumption (~18L/min), a suitable gas cylinder shed (which can host up to 60 cylinders) with an in built gas manifold system and purification panel was setup adjacent to the analytical system. Installation, commissioning of the ICP-MS equipment and training in the instrument operation, method development, and routine maintenance work has been completed. In order to inject liquid samples to the analytical instrument, solid aerosol samples have been extracted using an in house developed method. The best possible extraction of the heavy metals from the filters have been achieved using a mixture of acids ($HF+HNO_3+HClO_4$) in different combinations with variable pressure and temperature in a microwave digestion system equipped with thermoses made up of acid resistant high quality Teflon. The extracts were passed through 0.2 micron syringe filters to minimise the matrix effect. Spike recovery tests (~1ppb) for the selected trace elements using authentic stands (certified reference materials of NIST traceable) show excellent recovery of > 90%. Development of an ICP-MS analytical technique specifically for the quantification of the metallic species and trace elements have been made by developing and adopting the specific analytic protocol for aerosols that include tuning procedures, in order to adjust auxiliary and nebulizer flows to maximize counts at best stability. To cover a wide range of mass detection, method development and subsequent careful amendments were made using ^{7}Li, ^{60}Co, ^{115}In and ^{238}U calibration standards. Cleaning procedures for deteriorating moving parts of the system like sample introduction system that include nebulizer, spray chamber, peristaltic pump, plasma torch, ion extraction interface cones (sample, skimmer and extraction cones) are familiarised using 1M HNO_3 solution. Single mode interference removal has been achieved with helium gas supplement by adopting suitable spectral interference management technique like standard and KED mode of measurement. On a continuous mode of operation, the mass spectrometer was found have a dynamic range ~ 9 orders of magnitude with a background noise of ~1cps. The instrument was satisfactorily tested for natural elements like aluminum, silica, iron, lithium, beryllium, sodium, magnesium, barium, manganese, calcium that are present in ppm level and anthropogenic elements like phosphorus, potassium, titanium, vanadium, chromium, cobalt, copper, lead, zinc, nickel, arsenic, selenium, strontium, molybdenum, silver, cadmium, mercury, tin and antimony that are present in ppb level being quantified in the acid extracted aerosol filters.

Publications in Peer-Reviewed Journals

1. Girach, I. A., N. Ojha, Prabha R. Nair, A. Pozzer, Y. K. Tiwari, K. Ravi Kumar and J. Lelieveld, Variations in O3, CO, and CH_4 over the Bay of Bengal during the summer monsoon season: shipborne measurements and model simulations, Atmospheric Chemistry and Physics, 17, 257-275, doi: 10.5194/acp-17-257-2017 (2017).
2. Hegde, P., and Kawamura, K., Chemical constituents of carbon and nitrogen aerosols over Thumba region. Archives of Environmental Contamination and Toxicology, 1-18, doi: 10.1007/s00244-017-0426-5 (2017).

3. Phanikumar, D. V., K. Niranjan Kumar, S. Bhattacharjee, M. Naja, Girach I. A., Prabha R. Nair, and Shweta Kumari, Unusual enhancement in tropospheric and surface ozone due to orography induced gravity waves, Remote Sensing of Environment, doi: 10.1016/j.rse.2017.07.011 (2017).

4. Kavitha, M and Prabha R Nair, SCIAMACHY observed changes in the column mixing ratio of methane over the Indian region and a comparison with global scenario, Atmospheric Environment, doi: 10.1016/j.atmosenv.2017.07.044 (2017).

Presentation in Symposium/Conferences/Workshops

International

Kavitha, M., and Nair, P. R., "Spatio-temporal variation of methane over Indian region as observed by SCIAMACHY", European Research Course on Atmosphere (ERCA-2017), Grenoble, France, 20th January, 2017.

National

1. Aryasree, S and Prabha R Nair, Seasonal variation of aerosol radiative properties of aerosols over the coastal site Thiruvananthapuram and the marine environment of Bay of Bengal and Arabian Sea. UPCAR -2017, organised by NARL and SV University at Thirupati from 26-28 June, 2017.
2. Aryasree, S Prabha. R. Nair, Radiative properties of aerosols over the tropical coastal site Thiruvananthapuram based on collocated measurements of physical and chemical characteristics, IASTA, Ahmedabad, December IASTA bulletin vol. 22, ISSN 09714511, 2016.
3. Aryasree, S Prabha. R. Nair, Size characteristics and mass loading of aerosols over Arabian Sea and Bay of Bengal during premonsoon, IASTA, Ahmedabad, December 2016. IASTA bulletin vol. 22, ISSN 09714511, 2016.
4. Aswini, A R Prashant Hegde, Prabha R Nair, Carbonaceous and inorganic aerosols over a sub-urban site in peninsular India: temporal variability and source characteristics, UPCAR, organised by NARL and SV University at Thirupati from 26-28 June, 2017.
5. Aswini, A.R., Attended the winter school on "Atmospheric Aerosol Physics, Measurements, and Sampling Techniques" at IIT Madras during February 15-19, 2016.
6. Aswini, A.R., Hegde, P., and P. R. Nair, Carbonaceous and inorganic aerosols over a sub-urban site in peninsular India: Temporal variability and source characteristics IASTA bulletin vol. 22, ISSN 09714511, held at PRL from December 06-08, 2016.
7. Aswini, A.R., Participated and presented poster on "Carbonaceous and inorganic aerosols over a sub-urban site in peninsular India: temporal variability and source characteristics" at IASTA-2016 conference held by PRL from December 6-8, 2016.
8. Girach I. A. and Prabha R Nair, Seasonal variations of surface Ozone and Carbon monoxide over the Bay of Bengal: Synthesis of multi-campaign measurements, UPCAR -2017, organised by NARL and SV University at Thirupati from 26-28 June, 2017.
9. Girach I. A., N. Ojha, P. R. Nair, Y. K. Tiwari, K. Ravi Kumar, Variations of trace gases over the Bay of Bengal during the summer monsoon, TROPMET 2016 – National Symposium on Tropical Meteorology: Climate Change and Coastal Vulnerability, SOA University, Bhubneswar, 18-21 December 2016.
10. Girach I. A., Prabha R. Nair, K. V. Subrahmanyam, Koushik N., Shreedevi P. R., Mohammed Nazeer M., and Kiran Kumar N. V. P., "Surface ozone variation during summer season at Bharati station, Antarctica", "National Conference on Polar Science (NCPS)", National Centre for Antarctic and Ocean Research (NCAOR), Vasco-da-Gama, Goa. 16-17 May 2017.
11. Hegde, P., as expert panelist in technical session at the Workshop on "Need for Environment Pollution Monitoring Initiatives", International Science Festival held at National Physical Laboratory (NPL-New Delhi), on December 11, 2016.
12. Hegde, P., Aswini, A.R., and P. R. Nair, Chemical Characterisation of aerosol carbon and nitrogen isotopes at a site on the southwest coast of India. National Conference on Analytical Science and Technology (ANASAT 2015) held at Munnar during March 9-11, 2017. The Indian Society of Analytical Scientists (ISAS), Kerala Chapter conference proceedings, vol. 72, 48-50, 2017.
13. Nair, P. R. Girach I. A., Kavitha M., Revathy S. A., and Aryasree S., Systematic seasonal pattern of tropospheric trace species over Indian region, TROPMET 2016 – National Symposium on Tropical Meteorology: Climate Change and Coastal Vulnerability, SOA University, Bhuvaneshwar. 18-21 December 2016.

Deputations

Kavitha M., European Research Course on Atmosphere (ERCA-2017) at Grenoble, France, 11 January-9 February, 2017.

Invited lectures

1. Prabha R Nair, Remote sensing of atmospheric minor constituents, STP on Challenges in space science and exploration, STP lecture at VSSC, March 13-17, 2017.
2. Prabha R Nair, Atmospheric Trace gases: Spatio-temporal features over Indian region, UPCAR -2017, organised by NARL and SV University at Thirupati from 26-28 June, 2017.
3. Prabha R Nair, Atmospheric aerosols: physico-chemical characteristics, SRM University, Feb 22, 2017.

Aerosols & Radiative Forcing

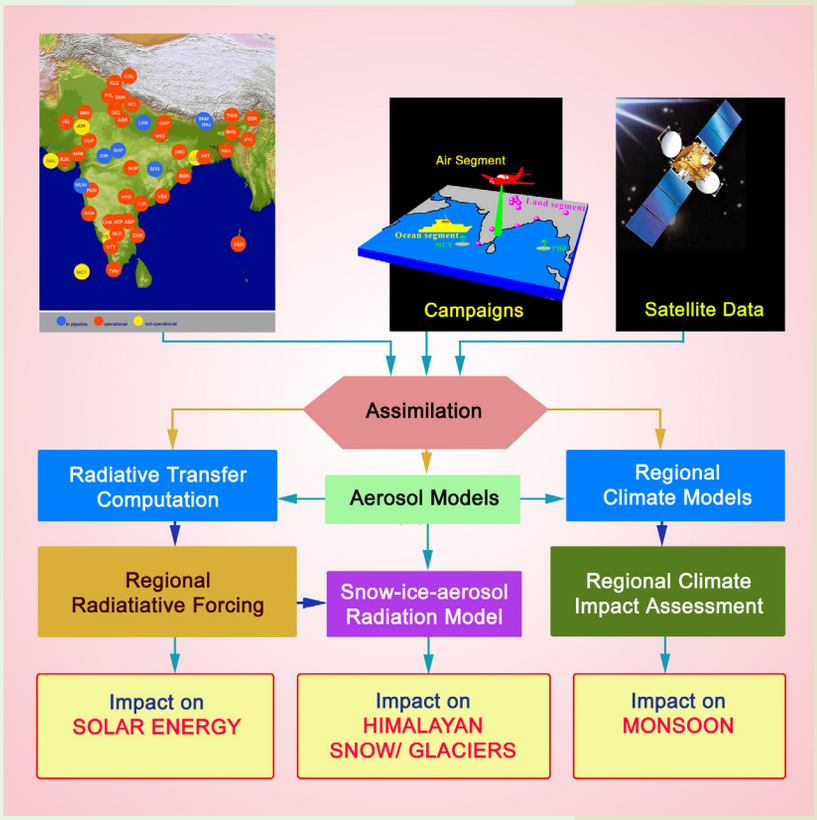

Aerosols and Radiative Forcing (A & RF) activities of SPL aim at the scientific understanding of the optical, microphysical, dynamical and radiative processes responsible for the climate impact of aerosols through aerosol-radiation, aerosol-cloud and aerosol-cryosphere interactions. The primary objectives include: (i) development of a primary aerosol database over the Indian subcontinent and adjoining Oceans by establishing and operating a network of aerosol observatories (ARFINET) under the ARFI Project of ISRO-GBP, (ii) conducting thematic multi-platform (ship, aircraft and high altitude balloon) field experiments addressing specific problems pertinent to the climate impact of aerosols, (iii) assimilation of ARFINET database with regional climate models for the assessment of potential climate impact, and (iv) investigations on aerosols over the remote Himalayan and Polar environments.

Science Team

S Suresh Babu
Mukunda M Gogoi
Vijayakumar S Nair
Sobhan Kumar Kompalli

INSPIRE Faculty

Aditya Vaishya

DST Post-Doctoral Fellow

Chandrakala Bharali

Research Fellows

Lakshmi N. B.
Jayachandran V.
Arun B. S.
Usha K. H.

Technical Team

Dinakar Prasad Vajja
Pramod P. P.
Ajeesh Kumar P. S.
Santosh Kumar Pandey

Direct radiative effects of aerosols over South Asia: Observations and modeling

The comprehensive and extensive compilation of the aerosol measurements over the Indian region has been carried out for the first time using the data collected from the 35 ground based observatories spread across the Indian region. It includes 27 aerosol observatories under the Aerosol Radiative Forcing over India (ARFINET) project of ISRO, 4 stations under theAerosol Robotic Network (AERONET) of NASA and 4 stations under the India Meteorological Department (IMD). These measurements were supplemented with GOCART model simulations to estimate the seasonal variations in direct radiative effects (DRE) due to constituents, total and anthropogenic aerosols. The estimation of aerosol DRE requires spectral variation of three major aerosol properties; (1) aerosol optical depth (AOD), (2) single scattering albedo (SSA) and (3) aerosol phase function or asymmetry parameter; in addition to the information on vertical profiles of atmospheric parameters (temperature, water vapor and ozone) and spectral surface albedo. The direct observation of AOD from the network of radiometers along with estimated values of SSA and phase functions from the GOCART simulations are used in this study. Extensive validation of the GOCART derived spectral steepness of AOD, SSA and asymmetry parameter are carried out with the radiometer measurements (AERONET and IMD) at distinct locations and are found to agree reasonably well both in terms of magnitude and seasonality.

Examination of the regional characteristics of AODs and their seasonality (over the Indian subcontinent) made using the radiometer network data (ARFINET, AERONET, IMD) supplemented with GOCART model simulations have revealed that most of the Indian regions experience high aerosol load throughout the year.. The annual mean value of regionally averaged AOD at 500 nm over Indian region is 0.45 ± 0.2. The annual mean values for different regions of Indian sub-continent such as: IGP, Eastern India, peninsular India and Western India are 0.63 ± 0.17, 0.58 ± 0.23, 0.43 ± 0.1 and 0.41 ± 0.1 respectively. The average fractional contribution of black carbon (BC), organic carbon (OC), sulfate, dust and sea salt to the total AOD for 35 network observatories during winter and spring seasons are shown in Fig.1. Considering the entire sub-continent, the BC aerosols contributed ~9.7 ± 1.5 % to total AOD during winter and 5.7 ± 1.8 % during spring season. The major contributor to the total AOD during winter is sulfate aerosols (44.8 ± 10.4 %), whereas mineral dust (48.7 ± 19.9 %) dominates during spring. The contribution of OC to the total AOD decreases from 21.4 ± 4 % in winter to 19 ± 6 % in spring. Regionally, the highest contribution of OC to the total is observed over the East India, where biomass burning activities are significant during winter and spring seasons. In general, AOD does not show significant seasonal variations over the Indian region. However aerosol chemical composition significantly changes with season. A systematic seasonal transformation of anthropogenic to natural aerosol system has been observed over the Indian region from winter to spring.

The regional variations of DRE due to composite aerosols (natural and anthropogenic) at the top of the atmosphere (TOA) and within the atmosphere are shown in Fig. 2 for winter and spring over various regions of the Indian subcontinent. The regional mean DREs for the entire Indian subcontinent at TOA, surface and atmosphere are −8.6 ± 3, −28.2 ± 12, and 19.6 ± 9 W m^{-2} respectively during winter and −6.8 ± 4, −33.7 ± 12 and 26.9 ± 9 W m^{-2} during spring. Compared to winter, higher warming occurs at the TOA and within the atmosphere during spring season.

This clearly indicates that the aerosol system over the Indian region is more absorptive during spring than winter and produces more warming in the atmosphere. Examining sub-regionally, the magnitudes of DRETOA and DREATM are higher over Eastern India and IGP followed by central and peninsular India. More than 25 W m^{-2} of solar radiation is being trapped in the atmosphere by the aerosols over East India, IGP and Central India during both the seasons.

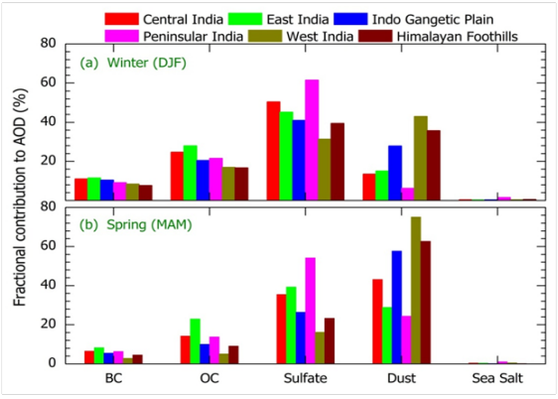

Figure 1: Fractional contribution of individual aerosol constituents to the aerosol optical depth (AOD) during winter (Dec-Feb) and spring (Mar-May) seasons at distinct regions of India [Nair et al., Clim. Dyn., 2016].

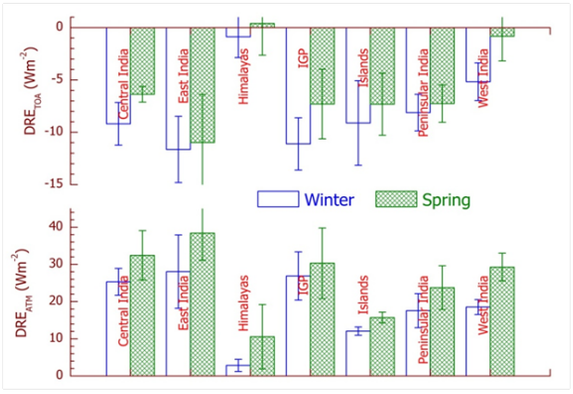

Figure 2: Direct radiative effects (DRE) due to composite aerosols at the top of the atmosphere (TOA) and within the atmosphere (ATM) over the distinct environments over the Indian subcontinent [Nair et al., Clim. Dyn., 2016].

It is interesting to note that, far away from the continental sources, the DREs over the oceans around India are not very low because of the transport of natural and anthropogenic aerosols from the landmasses to the oceans.

The diabatic heating rates estimated from the DREATM shows highest value of 1 K day^{-1} over the Eastern India and lowest value of 0.67 K day^{-1} over peninsular India during spring. Except at the Himalayan and Island stations, the heating rate values are higher than 0.5 K day^{-1} during spring and winter indicating the importance of diabatic heating of aerosols on regional climate.

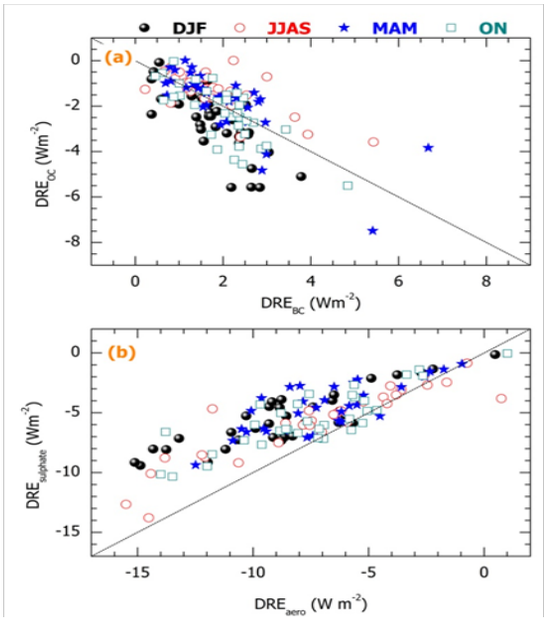

Figure 3: Scatter diagram of direct radiative effect (DRE) due to (a) black carbon and organic carbon and (b) sulfate aerosols and composite aerosols over the Indian region. Seasons are depicted with separate symbols [Nair et al., Clim. Dyn., 2016].

Figure 3 shows the scatter diagram of DRE at TOA due to BC versus OC and sulfate versus total aerosols during four seasons. The warming due to BC at the TOA is compensated fully or even slightly overwhelmed by the cooling due to OC at TOA, in all the seasons; with alarge variability. The sum of the DRE at TOA due to BC and OC is −0.13 ± 1 W m^{-2}, which indicates a small net cooling at TOA due to carbonaceous aerosols (BC + OC). This amounts to only less than 2% of the total aerosol DRE. It is interesting to note that the magnitude of the TOA effect due to these two species (OC and BC) are comparable, despite OC contributes twice as much to AOD as BC.Due to the compensation effect of DRE due to BC and OC at TOA, sulfate aerosols dominate (71%) the total aerosol DRE. This effect is stronger during summer monsoons and post-monsoon periods.

This clearly indicates that, to estimate an accurate DRE over India, sulfate measurements have to be constrained adequately with multi-platform measurements and modelling. It, thus, clearly emergesthat as far as the radiative perturbations are considered, BC–OC aerosol system have less forcing at TOA, than a less OC aerosol system or a no-OC or only BC aerosol system. Whereas the atmospheric radiative effect due to BC and OC are additive and internal mixture of BC and OC are more absorptive than their external mixture. In general, the low values of BC are associated with fossil fuel burning and high BC values are often seen during biomass burning events. On the backdrop of all these, it appears that fossil fuel aerosols (BC and OC) have more net warming effect (at TOA and in the atmosphere) than their biomass burning counterparts, which have net cooling (though very small) at the TOA. The BC and OC are mostly co-emitted and any mitigation of BC would result in reduction of OC also. Hence, an ideal mitigation strategy of decreasing BC alone would increase the cooling at TOA; whereas decrease in BC and OC together (realistic strategy) would result in decrease in cooling at TOA.

Radiative effects of absorbing aerosols over Northeastern India: Observations and model simulations

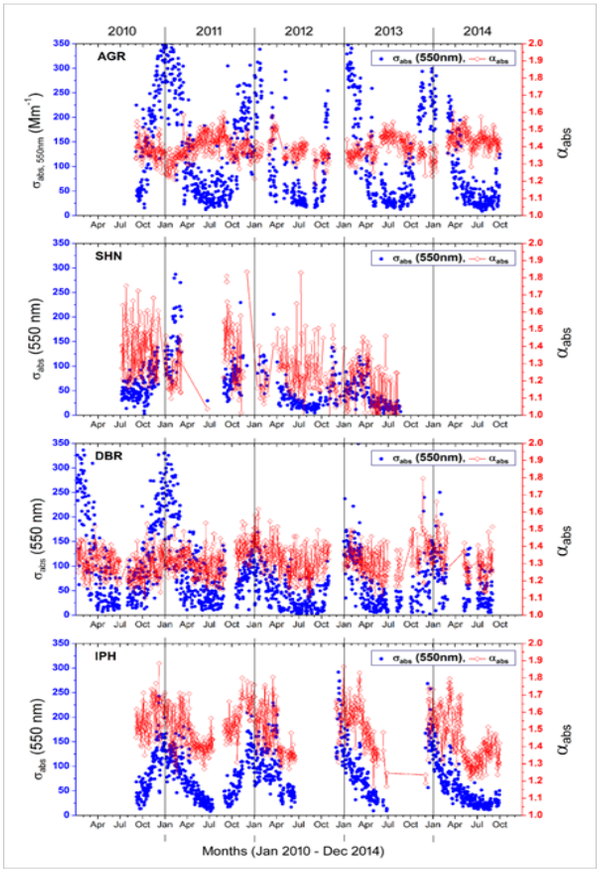

Figure 4: Time series of the daily mean values of aerosol spectral absorption coefficients (σabsin Mm^{-1}; shown by blue dots) at 550 nm, along with the daily mean values of absorption wavelength exponent (α_{abs}; shown by the open diamond symbols). αabswere derived from the slope of the linear least square fit between σabs obtained at 7-wavelengths of the aethalometer and λ in log-log scale for each set of measurements, following the equation $\sigma_{abs}=\beta\lambda^{-\alpha}$ [Gogoi et al., J. Geophys. Res., 2017].

Multi-year measurements of spectral properties of aerosol absorption are examined over four geographically distinct locations, Dibrugarh (DBR), Imphal (IPH), Shillong (SHN) and Agartala (AGR), of northeastern India (Fig.4). Results indicated significant spatio-temporal variation in aerosol absorption coefficients (σ_{abs}) with highest values in winter and lowest in monsoon.The spatio-temporal variations of α_{abs} gives a clear indication of different source processes acting on the spectral absorption properties of aerosols over different parts of the northeastern region.

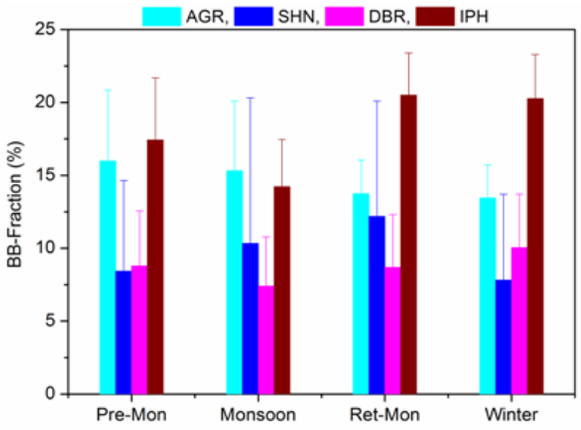

Figure 5: Seasonal variation of biomass burning fraction (BB, %) over the observational sites. The long term mean values are highest at IPH (~18.1 ± 4.2), followed by AGR (~ 14.8 ± 4.2), SHN (~ 9.9 ± 8.4) and DBR (~ 8.7 ± 3.7). For the estimation of BB-fraction, it is assumed that light absorption due to fossil fuel (FF) combustions varies inversely with wavelength (λ-1), while the spectral variation of aerosol absorption becomes much steeper when acted by biomass burning sources [Gogoi et al., J. Geophys. Res., 2017].

Figure 5 shows that the monthly mean values of biomass burning fraction (BB) over the four different locations.The western parts of the region, close to the outflow of Indo-Gangetic Plains, showed higher values of σ_{abs} and black carbon (BC) concentration—mostly associated with fossil fuel combustion. But, the eastern parts showed higher contributions from biomass-burning aerosols, as much as 20–25% to the total aerosol absorption, conspicuously during premonsoon season. This is attributed to a large number of burning activities over the Southeast Asian region, as depicted from Moderate Resolution Imaging Spectroradiometer fire count maps, whose spatial extent and magnitude peaks during March/April.

The ratio of column-integrated optical depths due to particulate organic matter and BC from GOCART (Fig. 6) showed good coincidence with the fire counts from satellite-based observations, indicating the increased vertical dispersion of absorbing aerosols, probably by the additional local convection due to higher fire radiative power caused by the intense biomass-burning activities. This indicates again the contrasting influence of fossil fuel emissions and biomass burning aerosols over north-eastern India, having gradient in τ_{pom}/τ_{BC} from west to east. As the OC/EC ratios are higher (~8) for biomass burning and lower (~2) for fossil fuel combustion, the above discussion hints to the significant contribution of biomass burning aerosols to total column abundance during the pre-monsoon season, during which columnar AOD also peaks. This suggests that pre-monsoon time aerosols are distributed to higher altitudes in the atmosphere and contributes to total columnar abundance, despite the surface concentrations are lower (than in winter).

In order to understand the model capability in reproducing the aerosol features having influence of distinct regional and seasonal source processes, the near surface BC mass concentrations for all the four observational sites were simulated using WRF-Chem model. At all the stations, model underperforms (Fig.7) by different magnitudes (RMS error is ~ 4 for AGR and < 2 for the other three stations), mainly during the winter. Interestingly, the BC values are overestimated in the pre-monsoon month March, having highest overestimation over the southeastern part, where the dominance of biomass burning aerosols are also high. There are several important factors that makes the simulation of BC over the south Asian regions very challenging. The use of annual average emission inventories, non-local boundary layer scheme leads to large uncertainty in the simulated values as the models tend to over-estimate the vertical transport even during the stable condition of the nocturnal boundary layer and during winter season leading to underestimation of the near surface concentrations. In addition, other possible causes include the poor representation of foggy conditions (thus

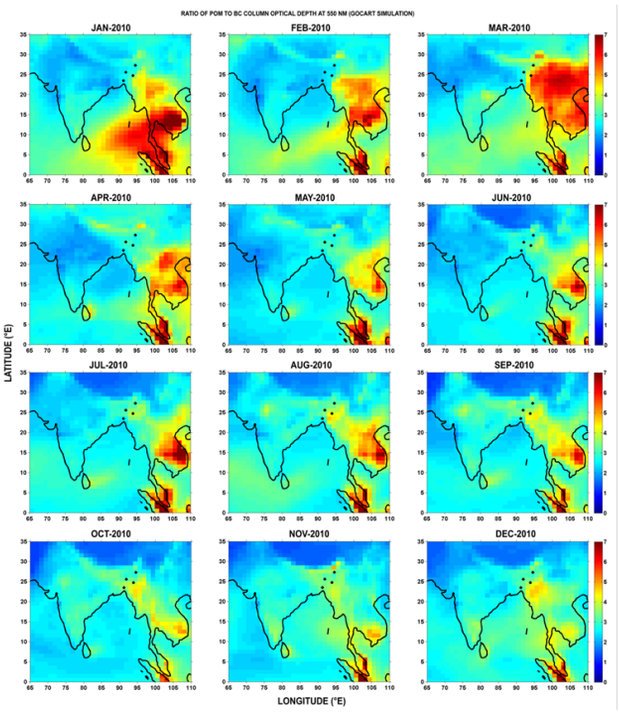

Figure 6: Spatial map of ratio of column integrated optical depths due to POM (particulate organic matter) and BC from GOCART model simulations for a representative year, 2010.In GOCART, POM is taken as 1.4 times the organic carbon mass. [Gogoi et al., J. Geophys. Res., 2017]

avoiding the aerosol hygroscopicity) in current models and missing or inadequate accounting of nitrate aerosols etc. These common problems and possible causes found in multiple models point out directions for future model improvements in this important region.

Having made a regional synthesis of BC and an estimate of the biomass burning fraction and its seasonality, we estimate the radiative forcing due to BC. Fig.8 shows the seasonal picture of the diurnally averaged ARF due to BC. Complying with the very high BC mass concentration at AGR, the forcing due to BC remained highest in the westernmost station during all the seasons and most conspicuously in winter. The surface forcing due to BC alone at AGR is as high as -30 Wm^{-2}, contributing > 45% to total forcing (-56.5 Wm^{-2}) due to composite aerosols; while the TOA forcing is 20 Wm^{-2}. The TOA forcing at the other stations is < 10 Wm^{-2} for all the seasons. The positive forcing at the TOA arises due to the absorption by black carbon in the atmosphere, which also leads to a net cooling effect (negative forcing) at the surface. BC contribution to total forcing is found to be highest (> 80%) in winter and retreating monsoon seasons at these locations. On the other hand at AGR, the atmospheric forcing is reported to be highest in winter (~ 56.2 Wm^{-2}) with BC contribution of ~88%. Thus significant contributions of absorbing aerosols to lower atmospheric warming is prevalent over this region, which needs further attention and detailed study to investigate their impact on monsoon and cloud dynamics. The highest atmospheric forcing due to BC at AGR during winter lead to a heating rate of as high as ~ 1.5 K day^{-1}, while the heating rate due to composite aerosols is 1.6 K day^{-1}.

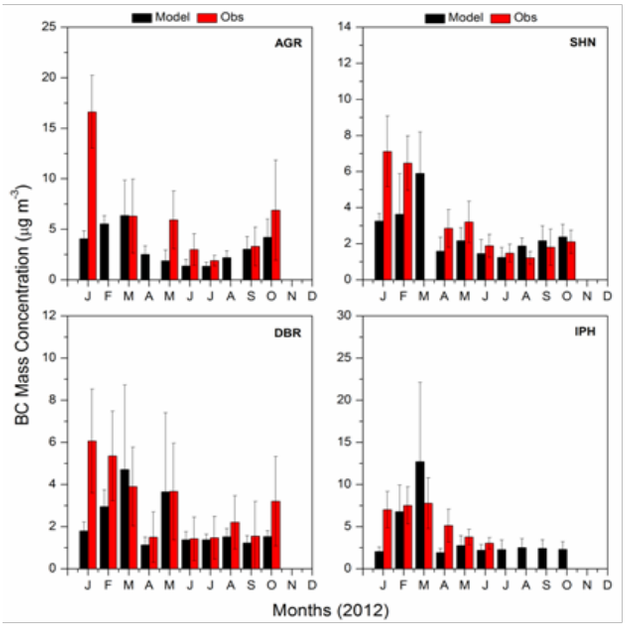

Figure 7: Monthly mean values of BC mass concentrations from experimental observation and WRF-Chem model simulation. The model simulation was carried out for the North-East Indian region (22-30°N, 88-98°E) centered at 27.4°N, 94.9°E with 60 grid points in both east-west and north-south directions (defined by Mercator projection). The horizontal grid resolution is 0.25° × 0.25°, having 30 vertical levels with the top layer at 50 hPa. The initial and lateral boundary conditions for meteorological parameters were obtained from NCEP Final analysis (FNL) available at spatial resolution of 1° × 1° for every six hours. Various other inputs to the model include the anthropogenic emission (e.g., CO_2, CH_4 and N_2O as well as some precursor gases from EDGAR on a 1° x 1° spatial grid), emission of trace gases from biomass burnings (obtained from NCAR Fire Inventory version 1), emissions of Gases and Aerosols from biogenic sources (using MEGAN). MOZCART (Model for Ozone and Related Chemical Tracers) combined with GOCART aerosol treatment was used for gas-phase chemistry [Gogoi et al., J. Geophys. Res., 2017].

The present study thus indicates that even a small region experiences distinct source impact on BC concentrations and model simulations vary by different magnitude from one location to another, mainly during the winter and pre-monsoon seasons. The present study also hints to the vertical distribution of absorbing aerosol, the lack of accurate quantification of which will always lead to the erroneous model simulations as well as biases in the BC radiative forcing estimations. That apart, the high resolution 3-dimensional study of BC is also essential for the accurate understanding of the aerosol influence on the Asian monsoon. Even though BC direct effect is the main driver of the surface cooling, the increased heating by BC decrease the low cloud cover, thus counteracts partially the direct effect.

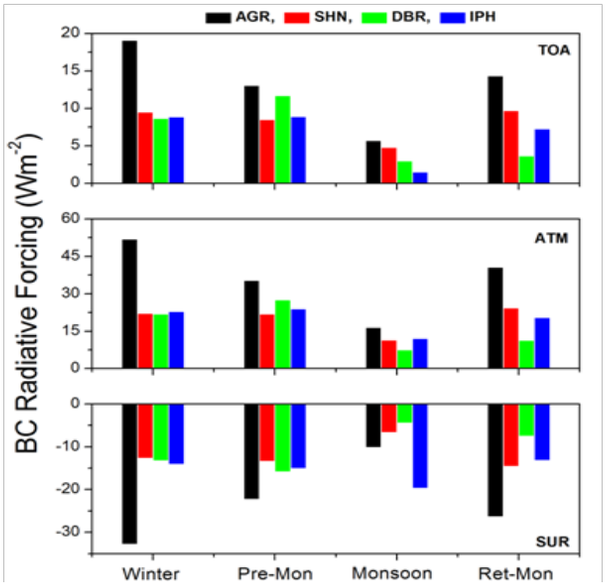

Figure 8: Radiative forcing due to BC (ARFBC) at the TOA, ATM and SUR over the four distinct locations of NE India at different seasons. The ARFBC represents the difference between the ARF foraerosols with and without the BC component. ARFBC has been estimated using Santa Barbara DISORT Atmospheric Radiative Transfer (SBDART) model; the inputs for which needed to represent the aerosolswere deduced from OPAC by constraining the values of spectral aerosol optical depths (AOD) and BC mass concentrations measured at each location [Gogoi et al., J. Geophys. Res., 2017].

Direct radiative forcing of aerosols over North-East India and adjoining areas: Satellite remote sensing

Twelve years of TOA CERES SW fluxes and MODIS AOD at 550 nm were analysed to assess the spatio-temporal distribution of aerosol optical and radiative properties in North-East India and adjoining areas (Fig.9). The selected locations in north-east India and the adjoining areas include: Dhaka (DAC), Agartala (AGR), Dhubri (DHB), Guwahati (GHY), Dibrugarh (DBR), Banmauk (BAN), Imphal (IPH), Aizwal (AZL) and Shillong (SHN).

In order to estimate the aerosol radiative forcing efficiency (ARFE) for each instantaneous values of ARF, the values of ARFins are plotted against corresponding daily mean AOD (Fig.10) and the slope of the least square fit between the two has been used as an indicator of forcing efficiency.

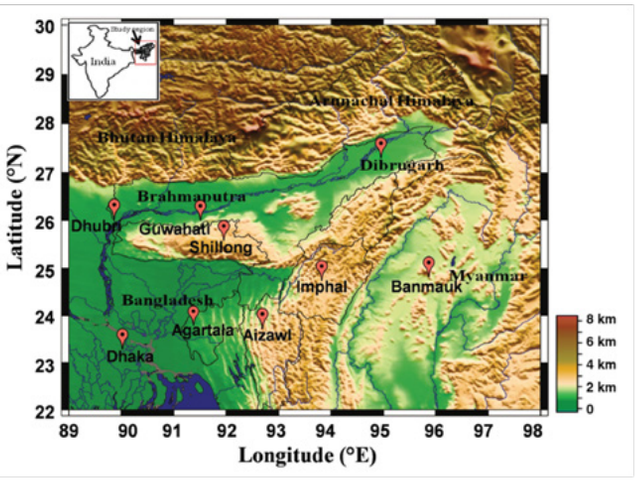

Figure 9: Map of North-East India and adjoining areas showing thetopography and the observation locations [Biswas et al., Int. J. Clim.,2017].

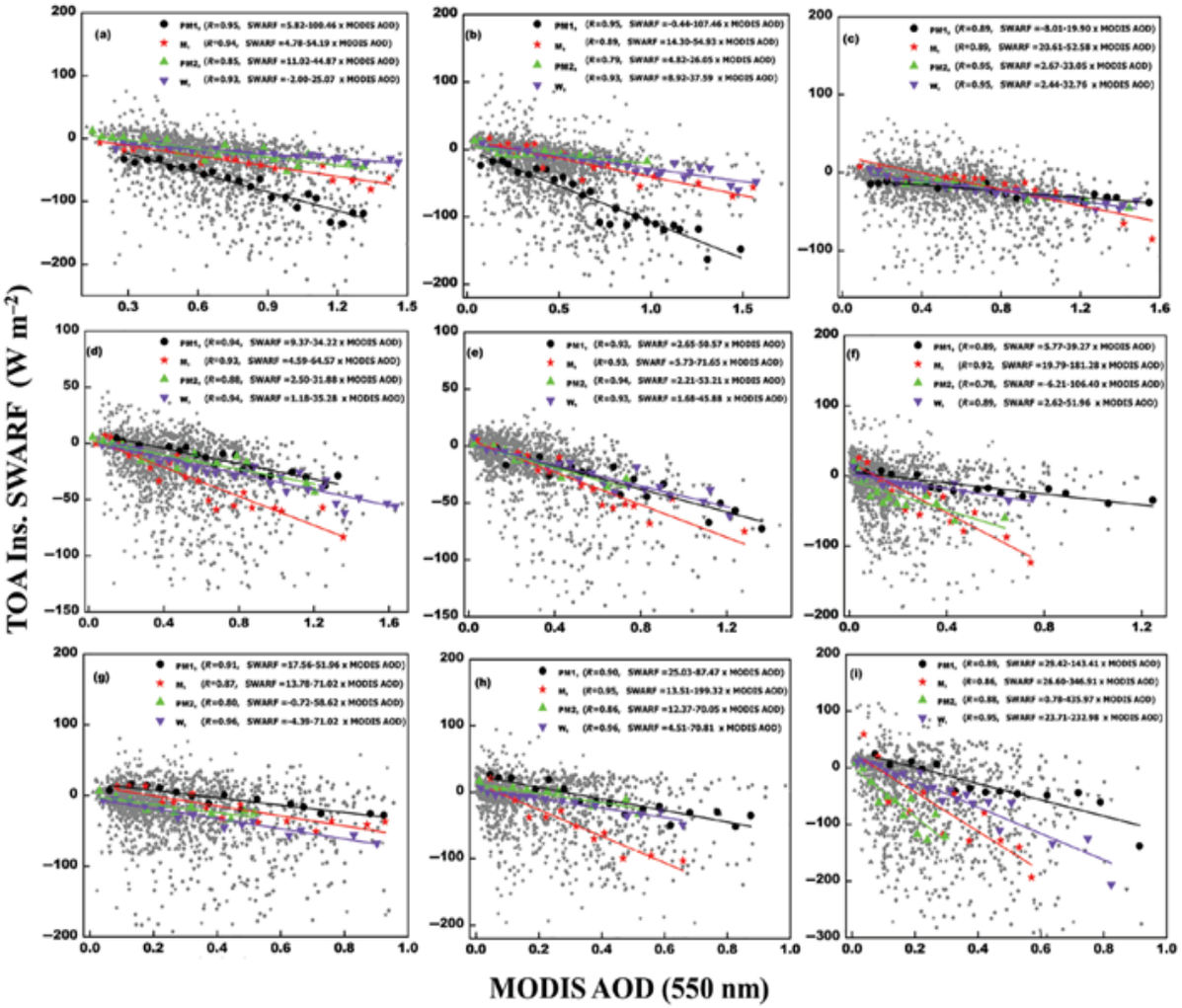

Figure 10.Instantaneous aerosol radiative forcing efficiency estimated by using median values instantaneous ARF (ARFins) against corresponding AOD for the period July 2002–December 2013 over North-East India and adjoining areas. Small gray star symbol represents the ARFins whereas large colored dots on each panel correspond to the median values. Different colors of the dots are representative of different seasons (Blue = MAM, Red = JJAS, Green = ON, and Pink = DJF). The linear regression line between ARFins and AOD for all data points is also shown for the stations (a) Dhaka, (b) Agartala, (c) Dhubri, (d) Guwahati,(e) Dibrugarh, (f) Banmauk, (g) Imphal, (h) Aizawl and (i) Shillong [Biswas et al., Int. J. Clim.,2017].

The results indicate that ARFE varies from its lowest value -34.49 $Wm^{-2}\tau^{-1}$ over DHB to its highest value -289.82 $Wm^{-2}\tau^{-1}$ in SHN. On a seasonal scale, forcing efficiency is higher in monsoon over all locations except DAC and AGR, where it is highest in pre-monsoon season.

There is a steep decrease in the TOA ARFins with AOD, at DAC and AGR, indicating the dominant effect of aerosols on TOA-ARF. However, ARFE becomes less negative if the surface reflectance increases for almost all the locations except DAC and AGA. As the AOD is more at these two places compared to the rest of the locations (being situated in the extended IGP) and are influenced by anthropogenic emissions from IGP apart from local sources, it is probable that aerosol contribution to ARF and hence to forcing efficiency is dominating over surface reflectance.

Quantification of carbonaceous aerosols in the Central Indo-Gangetic Plain: Fossil fuel vs Biomass sources

Based on the continuous measurement of aerosol spectral light absorption measurement at the ARFINET station Gorakhpur (26.75°N, 81.28°E, 85 m a.s.l.) in the central Indo-Gangetic Plains during August-2013 to July - 2015, quantification of the contribution of fossil fuel and biomass burning sources towards observed BC concentration is made.

In order to study and quantify the contributions from fossil fuels and biomass burning sources to BC, time series analysis of the BC was done along with that of Absorption Ångström exponent (α) and biomass burning percentage (BB%; defined as the ratio of BC from biomass burning sources to total BC). BC from the biomass burning sources is quantified assuming a two component BC model while α is calculated from the absorption coefficient assuming a power law dependency of absorption coefficient on wavelength λ. The daily variation of BC mass concentration (red circle), α (green triangle) and BB% (blue triangle), for the measurement period is shown in Fig.1. The daily averaged BC mass concentration varied from a low value of 1 μg m^{-3} to a high value of 51 μg m^{-3}. The general trend depicted by BC mass concentrations was that of an increase during post-monsoon and winter months and a gradual decrease in pre-monsoon months before attaining a low during monsoon months. Daily averaged α and BB% values varied between 1-2 and 4% - 60%, respectively, over the period of measurement and varied in tandem with the BC mass concentration.

Figure 12 shows the seasonally averaged BC mass concentration (black), source apportioned to emissions from fossil fuel (blue), and biomass burning (brown) sources. Winter season has highest BC mass concentration of ~ 19 μg m^{-3} with 14 μg m^{-3} from the fossil fuels sources and 5 μg m^{-3} from the biomass burning sources. Although post-monsoon season has nearly same BC mass concentration from biomass burning sources as winter season, its percentage contribution is higher. Monsoon season had lowest BC mass concentration of ~ 6 μg m^{-3} and also lowest contribution from biomass burning sources. Enhanced contribution from biomass burning sources to total BC mass concentration in winter and post-monsoon seasons can be due to high biomass burning activities during these seasons and advection of air masses from over the biomass burning regions before reaching the measurement site.

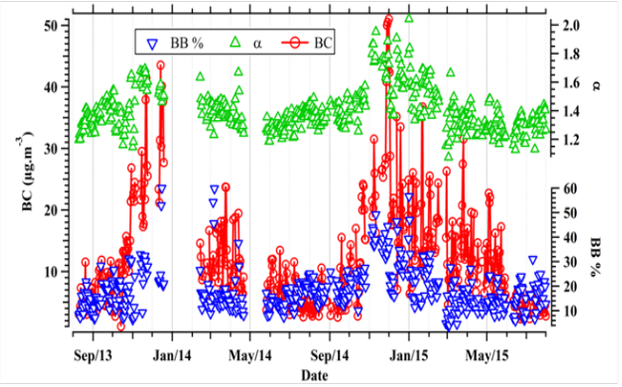

Figure 11: Daily averaged time series plot of BC mass concentration (red circle), α (green triangle), and BB% (blue triangle [Vaishya et al., Atmos. Res., 2017]).

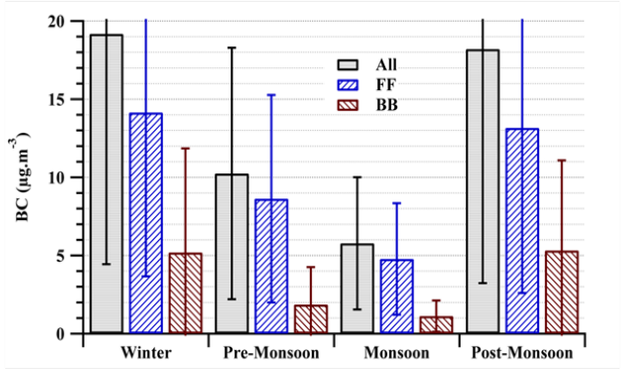

Figure 12: Seasonal quantification of BC mass concentration: all (black), from fossil fuel sources (blue), and from biomass burning sources (brown) [Vaishya et al., Atmos. Res., 2017].

It is concluded from the present study that aerosols from the biomass sources contribute ~ 28% during W and PoM seasons as against ~16% in pre-monsoon and monsoon seasons to the total black carbon aerosol content over the central IGP. Aerosols from the biomass sources in the winter and post-monsoon seasons contribute approximately twice to the total absorbing aerosol load as compared to that in the pre-monsoon and monsoon seasons due to change in source type of absorbing aerosols from fossil fuel to biomass burning and their relative source strength.

Springtime aerosol absorption over India: RAWEX Aircraft Experiment

The campaign mode measurements of the vertical distribution of the atmospheric aerosols were carried out in two phases using the instrumented aircraft (Beechcraft

B200) of National Remote Sensing Centre (NRSC), Hyderabad: (a) November–December 2012 (winter phase) and (b) April–May 2013 (spring phase). Seven base stations were selected to represent distinct regions of India: Central India (Hyderabad and Nagpur), Western India (Jaipur and Jodhpur), Indo-Gangetic Plain (Lucknow and Ranchi/Patna), and Himalayan foothills (Dehradun). In situ measurements of aerosol absorption at 781 nm were made using a photo acoustic soot spectrometer (PASS, Droplet measurements Technologies, USA) that was installed in the aircraft. Using PASS, the aerosol absorption is estimated by measuring the acoustic waves emanating from the aerosol sample while interacting with a laser beam using a high sensitive microphone.

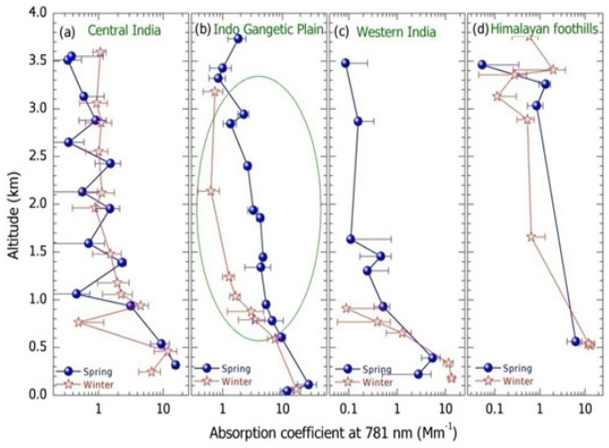

Figure 13: Vertical profiles of aerosol absorption coefficient measured over (a) Central India (Hyderabad, Nagpur), (b) Indo-Gangetic Plain (Lucknow, Patna/Ranchi), (c) Western India (Jaipur, Jodhpur), and (d) Himalayan foothill (Dehradun) during winter and spring seasons [Nair et al., Geophys. Res. Lett., 2016].

The mean vertical distribution of aerosol absorption coefficients obtained from the aircraft measurements for Central India, Indo-Gangetic Plain, Western India, and Himalayan foothills during the winter and spring seasons are shown in Fig. 13. Large seasonality is observed over the Indo-Gangetic Plain and Western India, whereas seasonal variations were insignificant for the Central India and Himalayan foothills. The absorbing aerosols are mostly confined to the lower altitudes (<1 km) during winter with very low values at altitudes above 1 km over most of the regions. In contrast, the aerosol concentration increases within lower free tropospheric altitudes by threefold to fivefold during the spring season over the Indo-Gangetic Plain and Western India. It is striking to note that the aerosol absorption over the Himalayan foothill regions is comparable in magnitude with the lower free troposphere and at the surface levels in both spring and winter seasons. In comparison with the Indo-Gangetic Plain and Central India, the magnitude of aerosol absorption is smaller over Western India, where there are far less industrial and biomass burning activities compared to the other parts of the country. However, it should be noted that the biomass burning activities associated with agriculture crop residue burning is significant over this region during the autumn (October–November) season.

Aerosol absorption optical depth (AAOD) is estimated by integrating the vertical profiles of aircraft-derived absorption coefficient up to 4 km. The AAOD at 781 nm wavelength has been extrapolated to the mid-visible wavelength (550 nm) using the power law function with a wavelength exponent (Angstrom exponent) equal to unity, assuming that the aerosol absorption is solely attributed to fossil fuel burning. We have considered this spectral extrapolation as the lower bound of the estimation since biomass burning and dust aerosols have much steeper spectral dependence (wavelength exponent > 2) than that from fossil fuel burning. Fig.14 depicts the AAOD estimated at 550 nm over different base stations during the winter and spring seasons and the AAOD retrieved using OMI/Aura. In general, (i) the AAOD values are high over the Indo-Gangetic Plain during winter and spring. (ii) The AAOD values remained comparable during both the seasons over the Indo-Gangetic Plain, despite the large seasonality in the vertical profiles of absorption coefficient. (iii) An increasing gradient toward the Indo-Gangetic Plain from south to north (latitudinal) and west to east (longitudinal) is also observed. The variations in the regional mean values of black carbon mass concentrations measured at different ARFINET stations and AAOD at 675 nm estimated from the AERONET observations at the Indo-Gangetic Plain, Western India, and Central India are shown in Fig.15. The mean AAODs over Lucknow derived from aircraft measurements were 0.029 and 0.04, respectively, for winter and spring seasons. The surface level BC mass concentration depicts an approximate twofold to threefold decrease from winter to spring, whereas columnar AAOD does not show a significant decrease toward spring. The AAOD values increased (from 0.020 ± 0.009 in winter to 0.048 ± 0.01 in spring over the Indo-Gangetic Plain) or remained constant (over west India) except for Central India. This finding clearly indicates the vertical heterogeneity and presence of elevated layers (possibly above 4 km) of absorbing aerosols during spring over the northern parts of India. The decrease in BC mass concentration at the surface from the winter to the spring season does not mean that the BC aerosols are removed from the atmosphere; rather, the black carbon is vertically redistributed and accumulated in the lower free troposphere. Advection of West Asian dust within the lower free troposphere also contributes to the observed high AAOD values during the spring season. In general, Fig.13 and Fig.15 indicate that the absorbing aerosol concentration increases above the boundary layer during the spring season. In contrast to the seasonal variations of surface and columnar aerosol absorption over the Indo-Gangetic Plain and West India, the BC mass concentration and columnar AAOD over Central India decreased from winter to spring, which is in line with the seasonal variation of the vertical profiles of absorption coefficient measured during the RAWEX aircraft experiment.

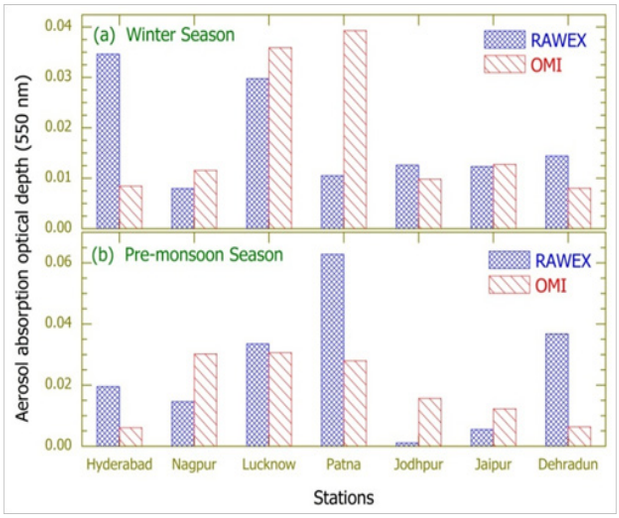

Figure 14: The aerosol absorption optical depth (AAOD) at 550 nm estimated from the vertical profiles of aerosol absorption coefficient measured over Hyderabad, Nagpur, Lucknow, Jodhpur, Jaipur, and Dehradun during spring and winter seasons. Simultaneous AAODs retrieved from OMI is also shown in the figure [Nair et al., Geophys. Res. Lett., 2016].

The spring time enhancement in elevated aerosol absorption over the Indo-Gangetic Plain has the potential to increase the atmospheric absorption of radiation at free tropospheric altitudes during spring. This enhancement leads to an increase in atmospheric direct radiative forcing (DRF atmosphere) over the region. It is found that aerosols absorb +24.9 Wm^{-2} over the Indo-Gangetic Plain during winter and +34.0 Wm^{-2} during spring. A similar pattern is observed over Western India, where atmospheric forcing was + 14.7 Wm^{-2} during winter and +19.8 Wm^{-2} during spring. Although the DRFatmosphere values at Central India (+24.6 Wm^{-2}) are comparable to that over the Indo-Gangetic Plain during winter, the Indo-Gangetic Plain experiences ~8 Wm^{-2} and ~14 Wm^{-2} more atmospheric warming during spring compared respectively to Central India and Western India. Atmospheric forcing over Central India also depicts increase from winter to spring season. This increase is in line with the inferences drawn from Fig.15. However, the availability of the solar radiation increases significantly during the spring season, which enhances aerosol absorption in the atmosphere by ~9 W m^{-2} from winter to spring even though the optical depth (AOD = 0.016) did not vary significantly. Additionally, the west Asian dust transport to North India will also contribute significantly to the spring time enhancement in atmospheric forcing. However, the relative contribution of BC and dust to the aerosol absorption is yet to be quantified. Although several studies addressed the direct effect of spring aerosols on Indian monsoon, it is rather unclear on the implication of the indirect and semidirect effect due to these aerosol layers. Hence, it is essential to conduct field experiments to resolve the uncertainties in the aerosol-monsoon interaction due to absorbing aerosols over the Indian region during the spring and summer monsoon seasons.

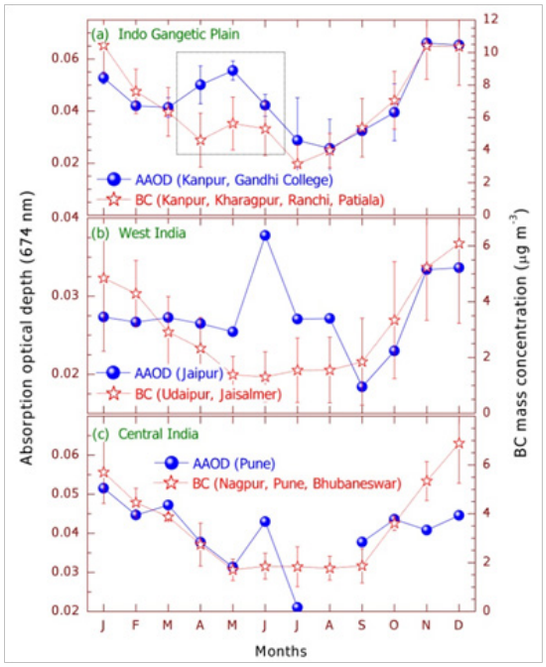

Figure 15: Mean variation of aerosol absorption optical depth at 674 nm estimated from AERONET measurements and BC mass concentration measured at ARFINET stations located at (a) Indo-Gangetic Plain, (b) west India, and (c) central India. The name of the station data used for estimating the regional mean is shown in the bracket [Nair et al., Geophys. Res. Lett., 2016].

CCN characteristics over a tropical coastal station during southwest monsoon: Observations and Closure studies

Due to large spatio-temporal variations in size distribution and chemical composition of aerosols across the Indian sub-continent, collocated measurements ofcloud condensation nuclei (CCN) and aerosol properties are essential for reducing the uncertainties in the assessment of aerosol-cloud interactions. For improving our understanding on the process of CCN activation, closure studies are also required to address the question regarding the dominance of size or chemistry, wherethe role of organic aerosols remain un-resolved for distinct aerosol systems. In the present study simultaneous observation of CCN and aerosol number concentration carried out from the southern coastal tip of peninsular India (Thiruvananthapuram: 8.5°N, 76.9°E, 3m amsl) are used to investigate the activation potential of the aerosol system and the uncertainties in the prediction of CCN concentration over the region. The measurements were carried out on campaign mode during summer monsoon period of 2013 (August and September) and 2014 (June to September). The CCN number concentrations were measured at five different supersaturations (0.2%, 0.4%, 0.6%, 0.8%, 1.0%) using a single column CCN counter at a time resolution of 1-Hz. The variation of CCN number concentration with supersaturation is parameterized based on Twomey's empirical relationship ($N_{CCN} = C\ SS^k$, where N_{CCN} represents number concentration of CCN and SS indicates the supersaturation values in percentage (%). The

C and k are constants estimated from the linear regression of the above relationship expressed in logarithmic scales. The slope of the CCN spectrum (k) represents the CCN activation potential of the aerosol system qualitatively. Activation ratio (AR) is the fractional contribution of CCN number concentration to total aerosol number concentration (CN), which is one of the most important information required for understanding the aerosol-cloud interactions and its radiative forcing.

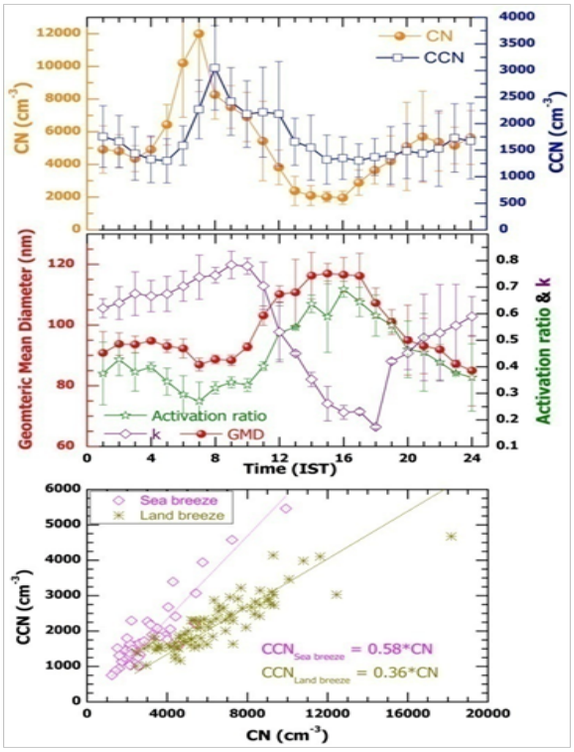

Figure 16: (i) diurnal pattern of mean CCN and total aerosol (CN) number concentration (top panel), (ii) activation ratio, slope of CCN spectrum (k) and geometric mean diameter (GMD) of the aerosol size distribution (middle panel) and (iii) scatter plot of CCN and CN concentration segregated for sea breeze and land breeze [Jayachandran et al., Atm. Env., 2017].

Figure 16 represent (i) diurnal pattern of mean CCN and total aerosol (CN) number concentration (top panel), (ii) activation ratio, slope of CCN spectrum (k) and geometric mean diameter (GMD) of the aerosol size distribution (middle panel) and (iii) scatter plot of CCN and CN concentrations segregated for sea breeze and land breeze. In contrast to CN concentration, CCN number concentration shows a weak diurnal variation with high values during early morning extending up to noon (2122 ± 476 cm-3) and low values during evening hours (1472 ± 160 cm-3). In contrast to CCN, a clear diurnal variation is observed for CN, k, AR and GMD. In general, diurnal variation of aerosol system over a coastal location is mostly associated with the boundary layer evolution and transition of local circulation from land breeze to sea breeze, which results in (i) decrease of aerosol concentration from 6586 ± 2239 cm^{-3} to 3355 ± 1287 cm^{-3} (ii) increase of aerosol GMD from 92±3 to 115±8 nm (iii) increase of CCN activation ratio from 0.37±0.05 to 0.62±0.08 and (iv) decrease of k value from 0.66±0.09 to 0.32±0.16. In general, there is a 42% change in CCN activation ratio for variation of 27 nm in aerosol GMD. The rate of change of activation ratio with respect to the change in GMD is about 1.5% nm-1. The mean activation ratio at 0.4% supersaturation is 0.58 ± 0.13 during sea breeze and 0.36 ± 0.09 during land breeze (Fig. 16c). During daytime, when sea breeze prevails, CCN activation ratio is higher than that of the land breeze regime (night and early morning time). The difference in the diurnal variation of k and CCN indicates that the effect of breeze change in CCN concentration is not significant since the number of CCN active aerosols in both the airmass is almost comparable. This implies that the contribution of marine aerosols to the CCN number concentration during sea breeze is comparable to the anthropogenic aerosols during land breeze which results in a weak diurnal variation in CCN and large diurnal variation in k values.

The Fig.17a shows the association of activation ratio with k value as a function of CCN number concentration. The present study shows an inverse relationship between k and activation ratio. It is seen that, low activation ratio and high k values are mostly associated with high CCN number concentration, which corresponds to the measurements during the early morning and nighttime. From the 'k' value we can infer the CCN activation efficiency qualitatively. Two extreme cases noted in Figure-17a are discussed in detail as Case 1 and Case 2. The Case 1 corresponds to a high activation ratio with low k value (during sea breeze time) and Case 2 represents an opposite situation (during the early morning hours). The aerosol number size distribution (NSD) corresponding to both cases are shown in Figure 17b. For Case 1, the total aerosol number concentration is 1613 cm-3 and the mode diameter is at ~150 nm. While in Case 2, the total aerosol number concentration is 14639 cm-3 and the mode diameter is at about 90 nm. It can be seen very clearly that the low k value and high activation ratio is mostly associated with a distribution having mode diameter higher than 100 nm (Case 1). Here the contribution of fine particles to the total aerosol number concentration is less. Figure 17c shows the variation of activation ratio with supersaturation for the two extreme cases discussed above. The effect of change in NSD can be seen in the magnitude of activation ratio and also in the rate of change of activation ratio with supersaturation. The mode diameter of the number-size distribution of the particles corresponding to Case 1 is beyond the critical activation diameter at a lower supersaturation range (0.2%). As shown in Case 1, 80% of the total aerosol particles get activated at 0.2% supersaturation itself, thus producing lower k values and higher activation ratios. In contrast, only 12% of the particles are activated at 0.2% supersaturation in Case 2. Even at 1 % supersaturation, only 38 % of the total particles are activated indicating the dominance of fine mode aerosols in the NSD. This large variation in CCN activation ratio over a 24 hour

period indicates the large differences in aerosol number size distribution and composition between marine and continental aerosol system.

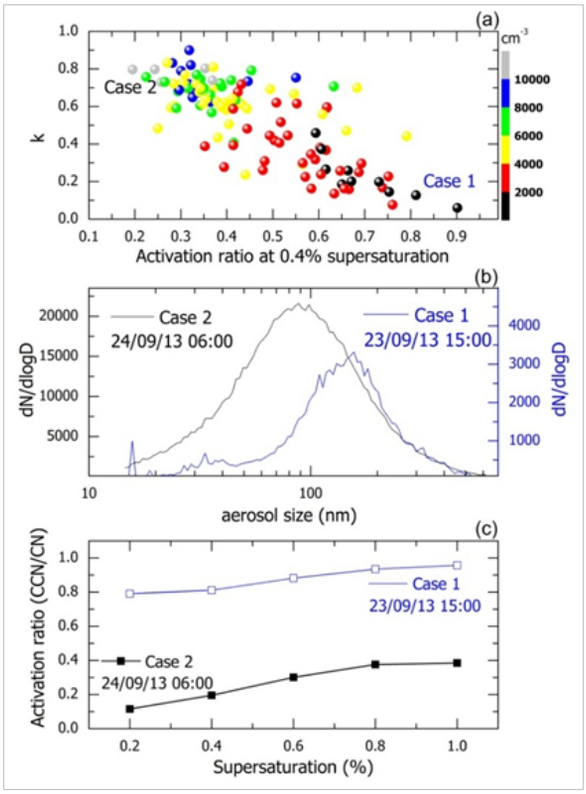

Figure 17: (a) Scatter plot of k values with CCN activation ratio at 0.4 % supersaturation. The color of the scatter indicates the CCN number concentration. (b) Aerosol number size distribution for two extreme cases marked on the top panel. (c) Variation of CCN activation ratio with supersaturation for the extreme cases marked on the top panel [Jayachandran et al., Atm. Env., 2017].

The CCN number concentration was estimated using the simultaneous and collocated measurements of aerosol NSD and with a prior knowledge on the mean chemical composition of aerosols over this site. It has been reported that the water soluble, organics, black carbon and mineral dust components constitute 44 %, 25 %, 5 % and 9 % respectively to the total aerosol mass during the monsoon season. Figure 18 shows the closure between the measured and predicted CCN number concentration at 0.2% and 0.6% supersaturation by assuming internal mixtures of (i) ammonium sulphate with organics and (ii) sea salt with organics for summer monsoon season. At low supersaturations (0.2%), sulphate with organics mixture significantly underestimates the CCN concentration whereas sea salt with organics slightly overestimates the CCN concentration (Fig.18a). In contrast to this, sulphate with organics predicts the CCN number concentration at higher supersaturation better than that of sea salt with organics as shown in Fig.18b. Large underestimation using sulphate with organics mixture at 0.2 % supersaturation clearly indicates the significance of highly soluble component like sea salt which cannot be neglected during the study period. In the absence of size segregated online chemistry and aerosol number size distribution, complete closure at a particular supersaturation need not be valid at other supersaturations. For example the sea salt with organics at lower supersaturations and sulphate with organics at higher supersaturations provide reasonable CCN closure over this region. In contrast, sea salt with organics at higher supersaturation and sulphate with organics at lower supersaturation fail to provide the satisfactory CCN closure.

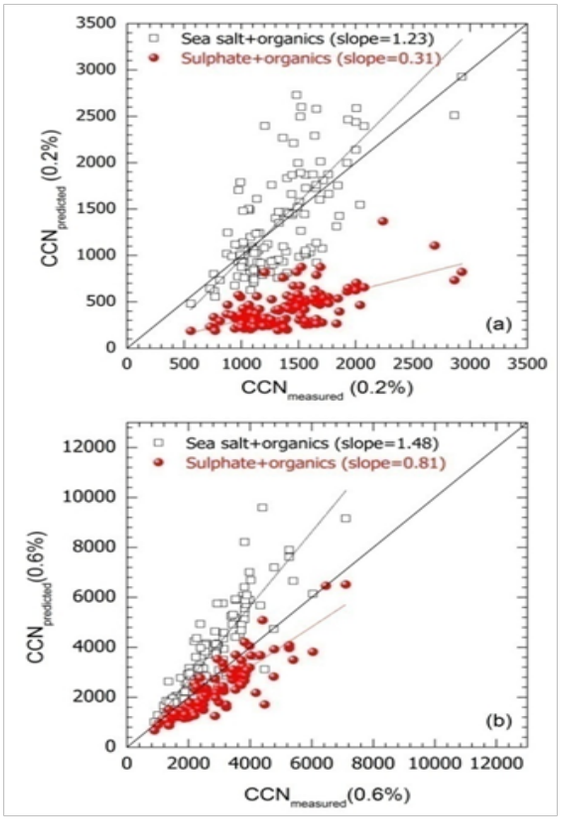

Figure 18: Scatter plot of predicted CCN concentration with measured values assuming internal mixture of ammonium sulphate and sea salt as soluble and organics as insoluble part for 0.2 and 0.6 % supersaturation [Jayachandran et al., Atm. Env., 2017].

This clearly indicates the importance of the online measurements of size segregated aerosol chemical composition along with the knowledge about water soluble organic carbon to predict the CCN number concentration and understand the CCN activity over a wide range of supersaturations at distinct environments over the Indian subcontinent.

Ongoing activities and future directions

Regional Climate Impact of Himalayan Aerosols

Light absorbing aerosols (such as BC and dust) show strongest radiative forcing over the highly reflecting surface such as glaciated terrain of Himalayas, and produce warming within the aerosol layer and the atmospheric region above the snow/glacier surface due to multiple aerosol – radiation interaction. This atmospheric heating

will subsequently increase the downward long-wave radiation to the surface, warming the surface. The southern slopes of Himalayas receives direct radiation from the sun and is directly exposed to the emissions from densely populated south Asian region including the Indo-Gangetic plains, while it experiences long-range transport of dust and carbonaceous aerosols from the Indian, West Asian and African deserts and south-eastern Europe. This makes Aerosol – Cryosphere – Radiation interactions all the more important over this region. Nevertheless, observational data on the physical and optical properties of Himalayan aerosols, as well as quantitative estimates of these aerosols in the snow-pack and glaciers are very limited. In this context, SPL has initiated aerosol observations from Himalayas by conducting periodic field campaigns and establishing chain aerosol observatories. During the reporting period, observations are initiated from Tawang (27°35′29″N, 91°52′53″E, 2916 m a.s.l.) in the eastern Himalayas.

Mixing state of Black carbon aerosols over distinct environments of India

Aerosol Black carbon (BC) plays an important role in the direct (through absorption of solar radiation) and indirect radiative forcing (by modifying the properties of clouds) of climate. However, the magnitude and sign of the net radiative effect is strongly dependent on the physical properties of the BC component of the particles, such as mass concentration, number size distribution and mixing state. Over the Indian region, information on mixing state of BC and its size distribution is not available. In this context, an experimental set up is being set up at different ARFINET locations to collect high temporal resolution data on BC mass size distribution, number concentration and mixing state which will be an important input for the assessment of climate impact of aerosols both through direct and indirect forcing.

Setting up of an experimental facility for Aerosol – Cloud Interaction studies

One of the largest sources of uncertainty in the assessment of aerosol effect on climate is the lack of understanding on the interaction of aerosols with clouds at various spatial and temporal scales. The ability of aerosols to act as cloud condensation nuclei varies significantly with aerosol composition and sizes. However, studies on the effect of different aerosol type on cloud microphysical properties over the Indian region are rather limited.In this context, a portable experimental set up for the concurrent measurements of aerosol size distribution, chemical composition, optical properties and mixing state with cloud condensation nuclei concentration will be made operational for generating region specific database. This will be an important input for the modelling community for the climate impact assessment.

Publications in Peer-Reviewed Journals

1. Gogoi, M. M., S. S. Babu, K. K. Moorthy, P. K. Bhuyan, B. Pathak, T. Subba, L. Chutia, S. S. Kundu, C. Bharali, A. Borgahain, A. Guha, B. K. De, B. Singh, M. Chin, Radiative effects of absorbing aerosols over Northeastern India: Observations and model simulations. Journal of Geophysical Research (Atmosphere), 122, doi:10.1002/2016JD025592 (2017).
2. Vaishya, A., P.R. Singh, S. Rastogi and S.S. Babu, Aerosol black carbon quantification in the central Indo-Gangetic plain: Seasonal heterogeneity and source apportionment, Atmospheric Research, 185, 13-21, doi:10.1016/j.atmosres.2016.10.001 (2017) .
3. Jayachandran V., V. S. Nair, S. S. Babu, CCN characteristics over a tropical coastal station during south-west monsoon: observations and closure studies, Atmospheric Environment, 10.1016/j.atmosenv.2017.06.012 (2017).
4. Babu, S.S., Aerosol Studies on and Around Antarctica, Proceedings of the Indian National Science Academy, 83, 441 -447, DOI: 10.16943/ptinsa/2017/48952 (2017).
5. K. R. Gopal, G. Balakrishnaiah, S.M. Arafath, K. R. O.Reddy, N. S. K. Reddy, S. P. Kumari, K. R. Kumar, T. C. Rao, T. L. Reddy, R.R. Reddy, S. N. Hussain, M. V. Reddy, S. S. Babu, P. M. Reddy, Measurements of scattering and absorption properties of surface aerosols at a semi-arid site, Anantapur, Atmospheric Research, 183, 84-93, doi.org/10.1016/j.atmosres.2016.08.016 (2017).
6. Reddy, K.R.O, G. Balakrishnaiah, K.R. Gopal, N.S.K. Reddy, T.C. Rao, T.L. Reddy, S. N. Hussain, M. V. Reddy, R.R. Reddy, S.S. Babu, Seasonal variation of near surface black carbon and satellite derived vertical distribution of aerosols over a semi-arid station in India, Atmospheric Research, 184, 77-87, doi.org/10.1016/j.atmosres.2016.09.003 (2017).
7. Biswas J., B. Pathak, F. Patadia, P. K. Bhuyan, M. M. Gogoi, S. S. Babu, Satellite-retrieved direct radiative forcing of aerosols over North-East India and adjoining areas: climatology and impact assessment, International Journal of Climatology, doi:10.1002/joc.5004 (2017).
8. Dhar, P., B. K. De, T. Banik, M. M. Gogoi, S. S. Babu and A. Guha, Atmospheric aerosol radiative forcing over a semi-continental location Tripura in North-East India: Model results and ground observations, Science of the Total Environment, http://dx.doi.org/10.1016/j.scitotenv.2016.11.200 (2017).

9. Li Z., K.M. Lau, V Ramanathan, G Wu, Y Ding, MG Manoj, J Liu, Y Qian, J Li, T Zhou, J Fan, D Rosenfeld, Y Ming, Y Wang, J Huang, B Wang, X Xu, S.S. Lee, M Cribb, F Zhang, X Yang, T Takemura, K Wang, X Xia, Y Yin, H Zhang, J Guo, PM Zhai, N Sugimoto, SS Babu, GP Brasseur, Aerosol and monsoon climate interactions over Asia, Reviews of Geophysics, 54, 866–929, doi:10.1002/2015RG000500.2016 (2016).

10. Preißler, J., G. Martucci, G. Saponaro, J. Ovadnevaite, A. Vaishya, P. Kolmonen, D. Ceburnis, L. Sogacheva, G. de Leeuw, and C. O'Dowd , Six years of surface remote sensing of stratiform warm clouds in marine and continental air over Mace Head, Ireland, J. Geophys. Res. Atmos., 121, 14,538–14,557, doi:10.1002/2016JD025360 (2016).

11. Nair, V. S., S. S. Babu, M. M. Gogoi, K. K. Moorthy, Large-scale enhancement in aerosol absorption in the lower free troposphere over continental India during spring, Geophysical. Research letters, 43, doi:10.1002/2016GL070669 (2016).

12. Nair, V. S., S. S. Babu, M. R. Manoj, K. K. Moorthy and M. Chin, Direct radiative effects of aerosols over South Asia from observations and modeling, Climate Dynamics, 1-18, doi:10.1007/s00382-016-3384-0 (2016).

13. Reddy, K R. O., Balakrishnaiah, G, Gopal, K R., Reddy, N. S. K., Rao, T. C., Reddy, T. L., Hussain, S.N., Reddy, M. V., Reddy, R. R., Boreddy, S.K.R., Babu, S.S., Long term (2007--2013) observations of columnar aerosol optical properties and retrieved size distributions over Anantapur, India using multi wavelength solar radiometer, Atmospheric Environment, 142, 238 -250, doi.org/10.1016/j.atmosenv.2016.07.047 (2016).

Invited Chapter in Book

1. S. K .Satheesh, S. Suresh Babu, B. Padmakumari, G Pandithurai and V. K. Soni, Variability of Atmospheric Aerosols over India, DOI 10.1007/978-981-10-2531-0-13, Observed Climate Variabilty and Change over the Indian region, M. N. Rajeevan and S. Nayak (Eds.) Springer.

Publications in proceedings

1. Gogoi, M. M., and S. S. Babu, Aerosol optical properties over the Svalbard region of Arctic: Ground-based measurements and Satellite Remote Sensing, Remote Sensing of the Atmosphere, Clouds, and Precipitation VI, Proc. of SPIE Vol. 9876 98761C-1, doi: 10.1117/15224081, 2016.

2. Singh P., Vaishya A., Rastogi S., 'Characteristics of black carbon aerosol and its association with different atmospheric parameters in the central IGP', Indian Aerosol Science and Technology Association (IASTA), IASTA - 2016 Conference Proceedings, Volume 22, pages 640-643, 6th -8th December, 2016.

3. Vaishya A., Kompalli S.K., Babu S. Suresh, 'Aerosol Humidograph Instrument for the Study of Aerosol Hygroscopic Properties.' Indian Aerosol Science and Technology Association (IASTA), IASTA - 2016 Conference Proceedings, Volume 22, pages 11-13, 6th -8th December, 2016.

4. Vaishya, A., Singh P.R., Rastogi S. and Babu S.S., Source apportionment of absorbing aerosols in the central Indo-Gangetic Plain, Proc. SPIE 9876, Remote Sensing of the Atmosphere, Clouds, and Precipitation VI, 98762F, doi:10.1117/15223580, 2016.

Presentation in Symposia/ Conferences/ Workshops

1. Vaishya A., Jayachandran V., Gogoi M. M. and Babu S. Suresh, 'Radiative Implications of Altitudinal Heterogeneity in Aerosol Properties in the Indo-Gangetic Plain', International Conference on Understanding & Predicting Climate change over the Asian Region (UPCAR - 2017), 25th - 28th June, 2017, National Atmospheric Research Laboratory, Tirupati, India.

2. Vaishya, A., Mukunda M Gogoi and S Suresh Babu, Regional and synoptic source influence on Arctic aerosols during spring, National Conference on Polar Science (NCPS-2017), NCAOR, Goa, 16-17 May, 2017

3. Arun B.S., Mukunda M. Gogoi, S. Suresh Babu, "Absorbing aerosols over the Himalayas: Importance and need of free-tropospheric measurements", Summer school on Antarctic climate variability and ice dynamics, NCAOR, GOA, 08-11 May 2017.

4. Gogoi M.M., Babu S. Suresh, Nair S. Vijayakumar, Vaishya A. 'Radiative implications of spring time aerosols in the Ny-Ålesund (Svalbard Island)', Podium presentation at the National Conference on Polar Sciences (NCPS-2017), 16th-17th May, 2017, Goa, India.

5. Gogoi M.M and S. Suresh Babu, An assessment on INSAT-3D Aerosol Optical Depth over India, National Symposium on Recent Advances in Remote Sensing and GIS with Special Emphasis on Mountain Ecosystems

& Annual Conventions of Indian Society of Remote Sensing & Indian Society of Geomatics, Dehradun (India), December 7 - 9, 2016.

6. Gogoi M.M, S Suresh Babu, AdityaVaishya, Vijayakumar S Nair, Radiative implications of spring time aerosols in the Ny-Alesund (Svalbard Island), National Conference on Polar Science (NCPS-2017), NCAOR, Goa, 16-17 May, 2017.
7. Singh P., Vaishya A., Rastogi S., 'Characteristics of black carbon aerosol and its association with different atmospheric parameters in the central IGP', Conference of the Indian Aerosol Science and Technology Association (IASTA -2016), Physical Research Laboratory, Ahmedabad, India, 6-8 December, 2016.
8. Vaishya A., Kompalli S.K., Babu S. Suresh, 'Aerosol Humidograph Instrument for the Study of Aerosol Hygroscopic Properties.' Conference of the Indian Aerosol Science and Technology Association (IASTA -2016), Physical Research Laboratory, Ahmedabad, India, 6 -8 December, 2016.
9. Subba, T., Binita Pathak, Mukunda M Gogoi, Pradip K Bhuyan, Implication of aerosols on the photosynthetically active radiation (PAR) balance over north-east India, Indian Science and Technology Association (IASTA-2016), PRL, Ahmedabad, 6 -8 December, 2016.

Conference/Symposium/Workshop

1. Vijayakumar S Nair, National workshop on Aerospace Systems Modelling and Simulations, Thiruvananthapuram, 9-10 December 2016.
2. Vijayakumar S Nair, National workshop on Space Applications for sustainable growth and advancement (SAGA 2017), Thiruvananthapuram, 19-20 May 2017.
3. Mukunda M Gogoi, National Conference on Polar Science (NCPS-2017), NCAOR, Goa, 16-17 May, 2017.

Invited Talk/ Lectures

1. S. Suresh Babu, Talk on "Aerosols and Regional Climate over India" workshop on Local and Remote influences on Rainfall over India (LORRI) at Divecha Centre for Climate Change, Indian Institute of Science, Bangalore, 18 -19 July 2016.
2. S. Suresh Babu, Talk on "Physics of Climate Change", Ozone day lecture at University College, Thiruvananthapuram on 23 September 2016.
3. S. Suresh Babu, Talk on "Aerosol Black Carbon over India: Observations and Modeling" International Brainstorming Meeting "Air Quality and Climate Change" 5-7, October, 2016, India Meteorological Department, New Delhi.
4. S. Suresh Babu, Talk on "Aerosols and South Asian Regional Climate", TWAS Young Scientists conference on Frontiers in Earth and Climate Sciences, Indian Institute of Science, Bangalore, 5 -7, December 2016.
5. S. Suresh Babu, Talk on "Aerosols and Regional Climate over Asian region" Understanding, Predicting and projecting Climate change over Asian Region(UPCAR), , Tirupati, India, 26-28 June 2017

Deputations

AdityaVaishya

- Deputation to Centre for Climate & Air Pollution Studies (C-CAPS), School of Physics, National University of Ireland Galway, Galway, Ireland for collaborative scientific work on the topic 'Quantification of influence of relative humidity and aerosol composition on the net aerosol radiative forcing' from 02 February-03 April, 2017.

Training Programme

1. Arun B.S., Training on Glacier studies and Remote sensing, Divecha Centre for Climate Change, IISc, Bengaluru, 19-30 June 2017.
2. Mukunda M Gogoi: Training on JAVA, at HRDD, VSSC, 20-22 December 2016.
3. Vijayakumar S Nair: Training on Certified ethical hacking, at HRDD, VSSC, 5-9 December 2016.

Numerical Atmosphere Modelling

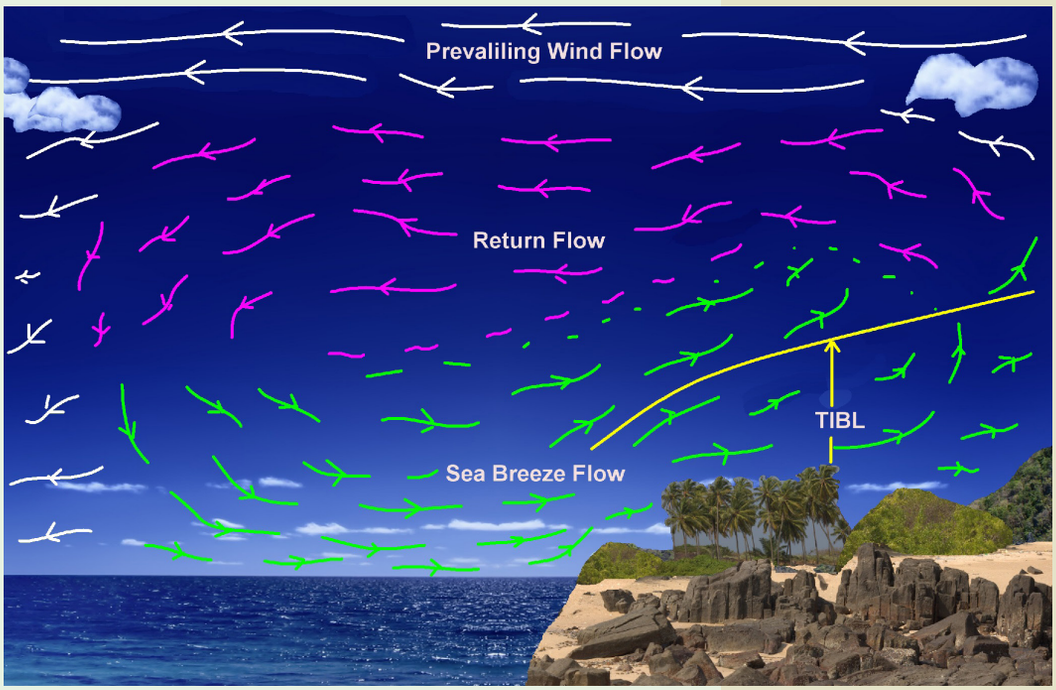

The atmospheric modelling activities in SPL began in a very humble and modest way in the early 1990s with development of a finite element two-dimensional atmospheric boundary layer (ABL) model and gradually spread its wings to the field of regional and global atmospheric/climate modelling through various numerical atmospheric models, such as: HRM, COSMO, WRF, RegCM, to name a few.

During the period of this report, the research and development activities pertaining to this branch were mostly focused on: (1) generation of seasonal morphology of the vertical structure of coastal atmospheric boundary layer over Thumba, which is being used as the mixing length scale in the COSMO model; (2) Deriving the characteristics of the Indian summer monsoon onset during early onset years; and (3) satellite and ground-based observations of CO_2 over the Indian region and how these are reflected in Lagrangian Particle Dispersion Model (LPDM). Beside these activities, this branch has been extending its continuous support to all the PSLV and GSLV missions by providing short-range weather predictions over Sriharikota through COSMO. In addition to these activities, the branch has also initiated a new program on the "Estimation of CO_2 fluxes through ground-based and space-borne platforms in conjunction with atmospheric transport models". As part of this new initiative, efforts are underway to establish a new experimental site of CO_2 measurements at the Kodaikanal Solar Observatory.

Science Team

Radhika Ramachandran
D. Bala Subrahamanyam
S. Sijikumar
K. N. Uma

Research Associates/ Fellows

T. J. Anurose[#]
S. Aneesh
K. Nalini
Freddy P. Paul
S. Roshny[$]

[#]Relieved in July 2016 and joined Goethe University as Postdoctoral Researcher
[$]Joined NAM Branch in February 2017

Atmospheric Boundary Layer Parametrization in COSMO Model

In continuation to the atmospheric modelling activities pertaining to the parametrization of atmospheric boundary layer (ABL), the master length scale was redefined in the default ABL parametrization scheme of COSMO model in 2015 – 2016. During the review period, we have prepared a detailed morphology of the vertical structure of coastal ABL over Thumba by making use balloon-borne meteorological database collected at Thumba.

Two-years morphology on the vertical structure of coastal ABL over Thumba

The coastal ABL is influenced by the presence of mesoscale sea breeze circulation, together with the local and synoptic weather, which directly or indirectly modulate the vertical thickness of ABL (z_{ABL}). Here, we investigate the challenges involved in the determination of the ABL heights, and discuss an objective method to define the vertical structure of coastal ABL. The study presents a two year morphology on the diurnal evolution of the vertical thickness of sea breeze flow (z_{SBF}) and z_{ABL} in association with the altitudes of lifting condensation level (z_{LCL}) over Thumba, a representative coastal station on the western coastline of the Indian sub-continent. The primary database for this study stems out of a multi-disciplinary field experiment, namely - the tropical tropopause dynamics (TTD), which was conceived under the Climate and Weather of Sun-Earth System (CAWSES) - INDIA program for addressing various aspects related with the troposphere-stratosphere interactions. As part of this field experiment, a total of eight balloon-borne GPS sondes are launched at three-hourly interval (typically at 0230, 0530, 0830, ..., and 2330 LT respectively) on daily basis for three consecutive days in each month since December 2010. For the present study, we have utilized a total of 516 sondes measurements spanning a period from January 2011 to December 2012. The study region is heterogeneous in nature with uneven terrain/plantations surrounding the western Ghats on one side of Thumba and the Arabian sea on the other side (Fig. 1).

The Indian sub-continent receives moist air flow from the adjoining oceanic regions during the south-west monsoon, which is also associated with frequent and intense rainfalls over a wide spatial domain. Fig. 2 shows the rainfall climatology for different months over Thiruvananthapuram for a period of 100 years spanning from 1901 to 2000. The rainfall pattern and their magnitudes for the year 2011 and 2012 were slightly different in comparison to the climatological features, particularly for the summer monsoon season. During the year 2011, the summer monsoon rainfall was mostly deficient, whereas the station experienced slightly excessive rainfall in the winter months. On the other hand, the year 2012 was mostly drought in nature as the rainfall for almost all the months were below the climatological values (Fig. 2).

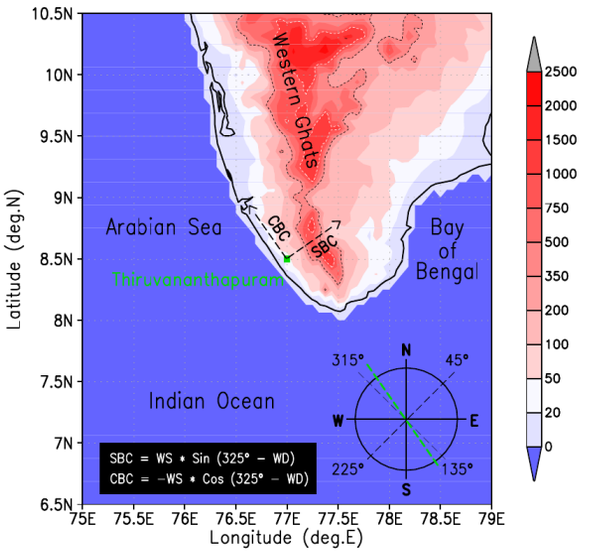

Figure 1: Location Map for the experimental site (Thiruvananthapuram) and its adjoining regions. The terrain heights are shown as the shaded contours. The geographical alignment of the Thiruvananthapuram coastline is shown through a straight line along 145° - 325° the encircled wind direction plot. Equations for sea breeze component (SBC) and coastal breeze component (CBC) are also provided within the figure [Anurose et al., Theor. Appl. Climatol., 2017].

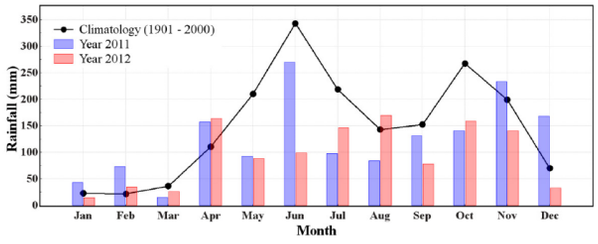

Figure 2: A hundred years climatology of monthly rainfall over Thiruvananthapuram for a period between 1901 to 2001, compared with the actual rainfall for the year 2011 and 2012. Courtesy: climatology database obtained from the India Meteorology Department (http://www.imd.gov.in/) [Anurose et al., Theor. Appl. Climatol., 2017].

Fig. 3 a(b), c(d), e(f) and g(h) depicts the monthly mean variations of near surface air temperature (AT), specific humidity (q), sea breeze component (SBC) and wind speed (WS) respectively, as a function of the local time for the year 2011(2012). The diurnal range of AT measurements was prominent (up to about 8° C) during the winter monsoon, whereas it was relatively weaker in the summer monsoon period. Thumba, being a coastal station, is always humid in nature and the amount of moisture is high in the surface layer ($q > 10\ g.kg^{-1}$). For a majority of the days, the site experienced a sea breeze flow in the daytime (inferred through the positive values of SBC, Fig. 3 e-f), whereas a land-breeze flow (having negative values of SBC) prevailed in the nighttime in both the years. The temporal width along the abscissa having the positive values of SBC

(shown in blue shades, Fig. 3 e-f) indicate the duration of sea breeze hours. A complete reversal of the winds from sea breeze to land-breeze and vice versa was prominent in the winter and pre-monsoon period.

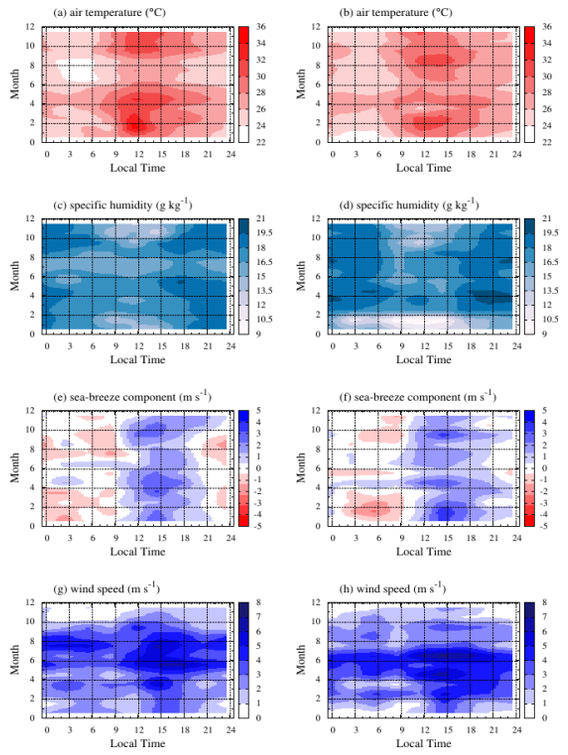

Figure 3: Left panel: Monthly mean variations in the near-surface (50-m altitude) (a) air temperature (in °C); (b); specific humidity (in g.kg^{-1}); (c) sea breeze component (in m s^{-1}); and (d) wind speed (in m s^{-1}) as a function of local time for the year 2011; Right panel: same as the left panel, but for 2012 [Anurose et al., Theor. Appl. Climatol., 2017].

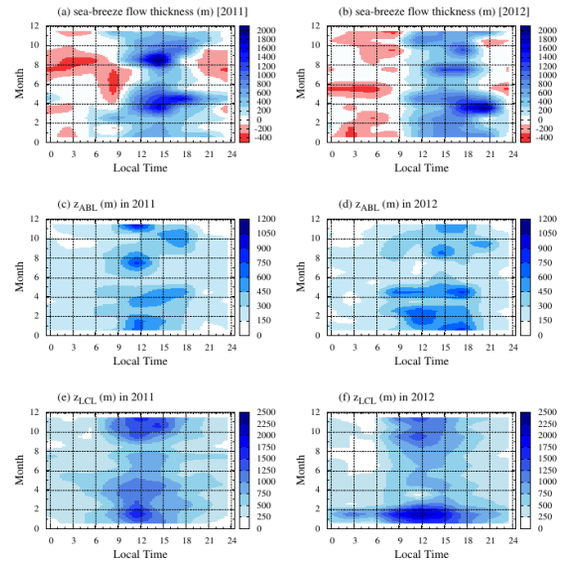

Figure 4: Left panel: Monthly mean variations in the (a) sea breeze flow thickness (in m); (c) z_{ABL} (in m); and (e) z_{LCL} (in m) as a function of local time for the year 2011; Right panel (b), (d) and (f): same as the left panel, but for 2012 [Anurose et al., Theor. Appl. Climatol., 2017]

The monthly patterns in the diurnal variations of coastal ABL in terms of sea breeze flow (z_{SBF}), together with z_{SBF} and z_{LCL} for two consecutive annual cycles of 2011 and 2012 is depicted in Fig. 4. The thickness of sea breeze flow is inferred from the vertical profiles of SBC, and the altitude corresponding to the first reversal in the magnitudes of SBC from positive (onshore flow) to negative (offshore flow) is marked as the top of the sea breeze flow. For accommodating the land-breeze flow together with the sea breeze flow, we have assigned a negative sign to the land-breeze flow thickness, which is shown in a different colored shades for discrimination from the daytime sea breeze flow. The vertical thickness of land-breeze flow is reasonably lower (< 450 m) than the daytime sea breeze flow. Among all the months, z_{SBF} peaks in April-May and September-October period, when the sea breeze flow is seen to extend from the surface to an altitude of about 2400 m. After attaining a maximum depth of the sea breeze flow typically by 15 LT, the flow sustains for a few more hours and gradually collapses after 20 to 21 LT through the intrusion of the land-breeze flow. In a broad sense, after the sunrise at about 0600 LT, as the turbulence activities grow in magnitudes, the ABL turns extremely unstable and its vertical thickness quantified as z_{ABL} also attains a peak. Subsequently after the sunset, the ABL experiences a stable stratification associated with low-level inversions, resulting in a shallow ABL during the nocturnal hours. For overcast conditions, the turbulent mixing extending from the surface to the z_{ABL} is confined only up to the cloud base as the intensity of mixing is not strong enough to overshoot the cloud base, in turn leading to a substantial reduction in the magnitudes of z_{ABL}. With a view to understanding the role of low-level clouds on the diurnal evolution of ABL and its feedback mechanism, the surface layer meteorological parameters are utilized for estimation of the altitude corresponding to the lifting condensation level (z_{LCL}). If the LCL is higher than the convective boundary layer height, clouds are not generated due to processes driven by the ABL. However, they can be formed due to large-scale dynamics. Similarly, under nocturnal stable conditions, vertical motions are inhibited and the relative location of LCL respect to the height of the stable boundary layer is irrelevant.

Fig. 5(a) depict the impact of variations in the surface layer moisture and total total index (TT) on the magnitudes of z_{LCL}, which include the whole database covering the daytime conditions between 0700 LT to 1900 LT. Mostly, the high values of q are associated with the stable conditions of ABL when the vertical thickness of ABL happens to be very shallow. Overall, the LCL altitudes show a rising behavior for drier atmosphere characterized by low values of q. With a view to examining the impact of convection on the altitudes of LCL, a scatter diagram is drawn between TT and z_{LCL} in Fig. 5(b). As per the meteorological convention, TT is a quantitative measure for the interpretation of the degree of convection. The atmospheric state represented with high values of TT is considered as prone to the convective activities, whereas low values of TT (< 40) are often associated with fair-weather conditions. In a majority of GPS sonde measurements shown in Fig. 5(b),

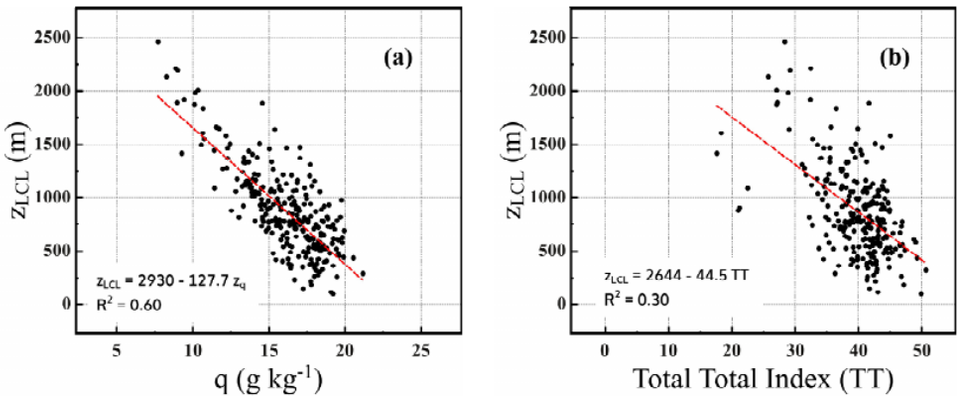

Figure 5: Scatter plot between (a) surface layer specific humidity (q) and z_{LCL}; (b) total total index (TT) and $z_{LC}L$ for daytime (unstable) conditions [Anurose et al., Theor. Appl. Climatol., 2017].

the lower atmosphere is characterized with high values of TT ranging from 40 to 50. Beyond a threshold value of TT (= 44), the atmospheric state becomes favorable for deep convection, and the magnitudes of z_{LCL} indicate low-level cloud base (< 800 m). Behavior of z_{LCL} with respect to the variations in the magnitudes of q and TT show appreciable anti-correlation. Following the anti-correlation plot, it is apparent that the low-level clouds are decoupled from ABL during winter (less humidity at surface and highest LCL), while in summer, a moisture low-level ABL leads to lower LCL.

Short-range weather predictions in support of PSLV/GSLV missions

The NAM branch of SPL is regularly extending its support to all the PSLV and GSLV missions carried out from Sriharikota by providing short-range weather predictions for SHAR region with the aid of COSMO model. This year, a revised scheme of initialization was adopted for operational applications which has helped in improving the forecast products from COSMO model for +24 to +48 h. As part of this new initialization approach, the initial conditions of COSMO model are extracted after spinning the model for a period of 24 h. During the review period, SPL has extended its support to all the operational launch campaigns of PSLV, GSLV and GSLV-Mk3.

New Initiatives

Satellite and ground-based measurements of CO_2 over the Indian region; its seasonal dependencies, spatial variability and model estimates

A new initiative is underway since January 2015 in the NAM branch to understand and investigate CO_2 emissions and transport in the Indian context through a network of in situ observations complemented by available satellite based observations and numerical modeling. As a first attempt we have demonstrated the distribution of Carbon dioxide (CO_2) concentration over the Indian subcontinent and the surrounding oceanic regions during 2009-2012, using measurements from satellites viz., Greenhouse gases Observation SATellite (GOSAT) and Atmospheric Infra-Red Sounder (AIRS), Carbon Tracker (CT) model simulations and flask measurements from two Indian stations Sinhagad (73.75ºE 18.36ºN) and Cape Rama (73.9ºE 15.1ºN). The concentration of CO_2 is observed to be maximum during pre-monsoon and shows a decreasing phase during post-monsoon season. In a regional scale, it is found that the Indo-Gangetic plain and the northern India have relatively higher concentrations compared to the other regions. The comparison between the CO_2 flask measurements over Sinhagad and Cape Rama with respect to that of GOSAT and CT clearly reveals that the differences in CO_2 are as high as 10 ppm between the ground and satellite based measurements. Further, we utilized the FLEXPART model to understand the source-receptor relationship over Cape Rama, Sinhagad and over the equatorial Indian Ocean to explain the observed features.

Presently installation of the National Institute of Environmental Studies (NIES) inverse model is in progress. The model will be used for understanding the contributions from different sources such as fossil fuel, biomass burning, forest fire etc. which can lead to an understanding the source apportionment of CO_2 over the Indian region.

Procurement and installation of CO_2 sensors at elevated levels at distinct sites in India

For understanding and quantifying the biosphere and anthropogenic contributions to the atmospheric rise of CO_2 by building a comprehensive carbon monitoring system for the Indian region, we plan to install masts equipped with Open Path CO_2 analyzers at distinct sites over India. The primary focus of this effort is to:

a) to study temporal and seasonal variability in CO_2 concentration and vertical fluxes

b) to compute the net ecosystem exchange (NEE) of CO_2

One such sensor is being installed at the IIA campus in Kodaikanal. A second one is being procured for installation at the Atmospheric research facility at Ponmudi. This

network of in-situ observations of CO_2, helps us to understand and investigate further, the CO_2 emissions and transport in the Indian context, when complemented by available space-based satellite observations and numerical modelling.

Work in Progress

As one of the new initiatives in the area of data assimilation, SPL has taken up the Advanced Regional Prediction System (ARPS) model for ingestion of land surface parameters extracted from the Indian satellites. With a view to investigating the efficacy of Indian sourced satellite observations in the ARPS model, the default surface and terrain features [i.e., United States Geological Survey (USGS)] are replaced with a similar database specifically prepared for the model domain throug the NRSC-BHUVAN (the Indian geo-portal) database of the National Remote Sensing Centre (NRSC) of ISRO. A special emphasis is paid towards preparation of land-sea mask, soil types, vegetation fraction, Normalized Difference Vegetation Index (NDVI) and similar datasets from the BHUVAN geoportal and make them compatible to the ARPS model. The ARPS model simulations with the USGS and NRSC-BHUVAN database are carried out to establish the role and effectiveness of the Indian satellite observations.

Future Projections

- Operationalization of "Open Path CO_2/H_2O Analyzer and Sonic Anemometer" at Kodaikanal Solar Observatory and Ponmudi
- Evaluation of COSMO model forecasts in assessment of ROANU cyclone trajectory and its temporal evolution over the Bay of Bengal
- Research mode operationalization of NIES (National Institute of Environmental Studies, Tsukuba, Japan) Eulerian atmospheric transport model for the Indian region
- Assessment of the COSMO and PALM model for the Large Eddy Simulations and its functional usage in addressing the problems pertaining to turbulence diffusion

Publications in Peer-Reviewed Journals

1. Anurose, T. J., D. B. Subrahamanyam and S. V. Sunilkumar, "Two years observations on the diurnal evolution of coastal atmospheric boundary layer features over Thiruvananthapuram (8.5° N, 76.9° E), India", Theoretical and Applied Climatology, doi: 10.1007/s00704-016-1955-y (2017).
2. Das, S. K., R. B. Golhait and K. N. Uma, "Clouds vertical properties over the Northern Hemisphere monsoon regions from CloudSat-CALIPSO measurements", Atmospheric Research, 183: 73-83, doi :10.1016/j.atmosres.2016.08.011 (2017).
3. Jyoti Bhate, Amit P. Kesarkar, Anandakumar Karipot, D. Bala Subrahamanyam, M. Rajasekhar, V. Sathiyamoorthy and C. M. Kishtawal, "A sea breeze induced thunderstorm over an inland station over Indian South Peninsula - A case study", Journal of Atmospheric and Solar-Terrestrial Physics, 148: 96-111, doi : 10.1016/j.jastp.2016.09.002), (2016).

Presentations in Symposia/Workshops/Conferences

International

1. Uma, K. N, M. V. Ratnam and S. B. Thampi., "Doppler Weather Radar and MST Radar observations of Tropical cyclone, XV workshop on technical and scientific aspects of MST Radar, National Institute of Polar Research, Japan, 26-31 May, 2017.

National

1. Aneesh S and S. Sijikumar., "Changes in the Indian Summer Monsoon Low Level Jet During Recent Decades", Frontiers in Earth and Climate Sciences: A Conclave of Young Scientists in Central and South Asian Region, IISc, Bengaluru, 5-7 December 2016.
2. Uma, K. N., Remote Sensing and its applications, NSSS college for Women, Trivandrum, 10 October, 2016.
3. Uma, K. N., "Tropical Mesoscale Convective Systems and its associated dynamics", Indian Institute of Science, Bengaluru, 01 July, 2016.

Invited Talks

1. Radhika Ramachandran, "Climate Modelling and Weather Forecasting for Drought", Water Management – Combating Climate Uncertainties, Directorate of Environment and Climate Change, Government of Kerala, Thiruvananthapuram, March 23, 2017.

2. Sijikumar S., "Remote sensing of Earth and other Planets: Indian Scenario", Seminar on Emerging Trends in Atmospheric and Climate Sciences, Department of Atmospheric Sciences, CUSAT, Cochin, May 3 – 4, 2017.

Public Outreach

1. Radhika Ramachandran

   Radio talk: "Space Exploration- Past, Present & Future"

   "**ബഹിരാകാശപര്യവേക്ഷണം – ഒരു എത്തിനോട്ടം**", All India Radio, Cochin, October, 2016.

Training Programme

1. Freddy P. Paul, Workshop on "Representation of physical processes in weather and climate models", INTROSPECT, IITM, Pune, February 13-16, 2017.
2. Uma, K. N., 81st Annual meeting of the Indian Academy of Sciences, Bengaluru, July 01-02, 2016.
3. Uma, K. N., Presentation skills and writing, VSSC, December 16, 2016.

Participation in Scientific Expedition:

1. Nalini, K., Pre-Antarctic Training, 2 Sept. 2016-28 Sept. 2016.
2. Nalini, K., 36th Indian Scientific Expedition to Antarctica, Dec 2016 to Mar 2017.

Atmospheric Dynamics Branch

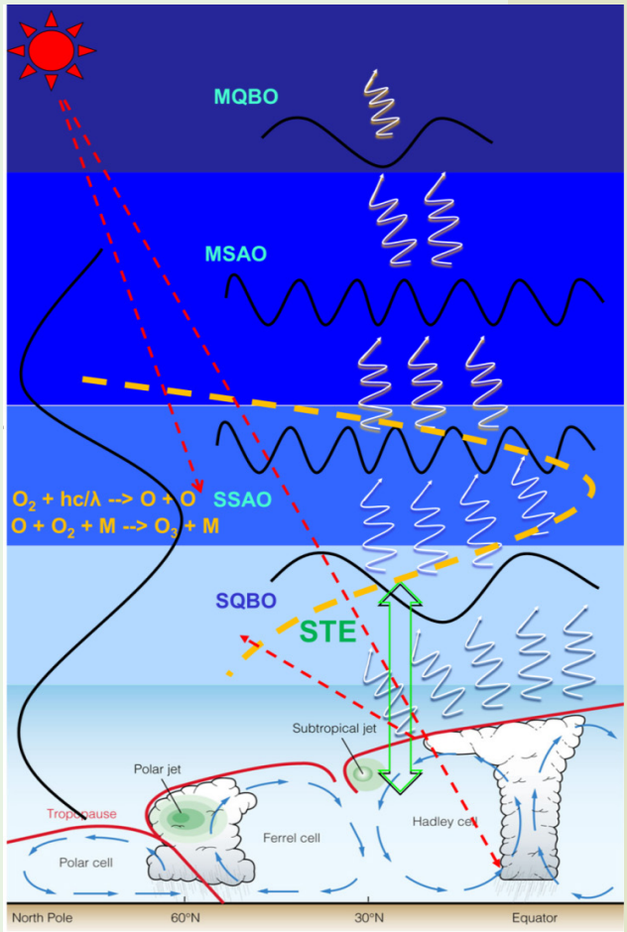

Space Physics Laboratory

The Atmospheric Dynamics Branch is carrying out front line research on various atmospheric processes responsible for altering the motion of the Earth's atmosphere, right from the ground to mesosphere-lower thermosphere. With this broad objective, the research activities are aimed at quantifying the spectra of atmospheric motion from gravity waves (few minutes) to solar cycle (11 years) using ground and space based observations and to quantify the various aspects of atmospheric waves such as source mechanism, propagation characteristics, role in atmosphere coupling, short and long-term variability and their representation or parameterization in global models. Apart from the studies on waves and oscillations, the branch focuses on the tropical tropopause dynamics and associated stratosphere-troposphere exchange processes, making use of simultaneous measurement of wind, temperature, ozone and water vapour. As part of SPL's Polar research program, the branch has carried out experimental campaigns at Bharati station in Antarctica, focusing on high latitude–low latitude coupling processes. Recently, the horizon is expanded by carring out the studies under the realms of cloud and climate dynamics, which is getting strengthened year after year.

Science Team

Geetha Ramkumar
Kishore Kumar K.
Sunilkumar S.V.
Siddarth Shankar Das
Venkata Subrahmanyam K.

Research Associates/ Fellows

Muhsin M.
Sneha Susan Mathew
Suneeth K.V.
Maria Emmanuel
Kousik N.
Satheesh Chandran

Technical Team

Mohan Kumar S.V.*
Shajahan M.
Manikantan Nair
Mohammad Nazeer M.

* Superannuated in August 2016

Middle Atmospheric Dynamics

A new perspective of Tropical Tropopause Layer (TTL) boundaries based on thermal and stability profiles

A new method is proposed to delineate the Tropical Tropopause Layer (TTL) based on static stability criteria. It is defined as the region extending from the level of minimum static stability (LMinS) to the level of maximum static stability (LMaxS) with a secondary minimum (LSM) in-between. The static stability and dynamic instability steadily increase from the base to the top of the TTL. Radiosonde data from three tropical stations (Singapore, Trivandrum and Gadanki) and COSMIC GPS RO data over the tropics during 2011-2014 are used for this investigation. This study demonstrates that, in terms of stability, the TTL is a composite of three sub-layers, viz., the bottom layer (BL)- the region between LMinS and LSM, the Middle Layer (ML)- the region between LSM and Cold point tropopause (CPT) and the Upper Layer (UL)- the region between CPT and LMaxS. Figure 1 shows the altitude profiles of temperature (T), lapse rate (γ), gradient of potential temperature (dθ/dz) and the brunt-Vaisala frequency (N^2) obtained from radiosonde data, along with the altitude profile of divergence of horizontal wind (D) derived from the vertical wind data obtained from MST radar at Gadanki on 27August 2013 at 02:30 IST (UT+05:30). The boundaries separating different regimes of the TTL identified from these profiles are marked in the respective panels. The CPT is located at 17.1 km with temperature 190.7 K. The lapse rate tropopause (LRT) is located at 16.95 km, 200 m below

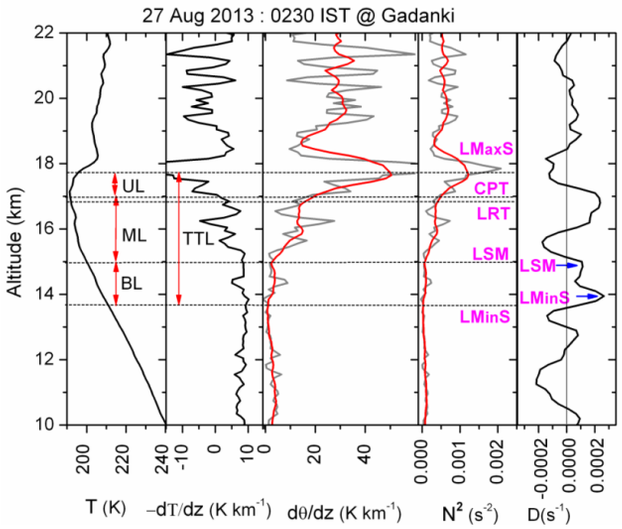

Figure 1: Profiles of temperature (T), temperature lapse rate (γ), potential temperature gradient (dθ/dz) and square of Brunt-väisälä frequency (N^2) derived from radiosonde observations over Gadanki on 27 August 2013 at 02:30 IST along with the divergence profile (D) derived from MST radar data. Red curve is the 9 point smoothed profile. The TTL parameters are indicated by arrow and labeled in each panel [Sunilkumar et al., J. Geophys. Res., 2017].

CPT. Minimum of dθ/dz is located at 13.6 km (taken as LMinS). A secondary minimum (LSM) is observed at 14.9 km. LMaxS is located at 17.65 km, 500 m above CPT. The thickness of TTL is 4 km with a depth of 1.3 km for BL, 2.2 km for ML and 0.5 km for UL. The altitude profile of D in Figure1 exhibits a primary positive peak at 13.95 km and a secondary positive peak at 14.95 km. These levels are found to be in good agreement with the level of LMinS and LSM, respectively, identified from the radiosonde profile. The secondary positive peak (between primary and CPT) is considered to be significant, if the value of D at secondary is greater than 20% of that at primary peak .It is clear that the static stability is very weak in the BL, moderate in the ML and strong in the UL.

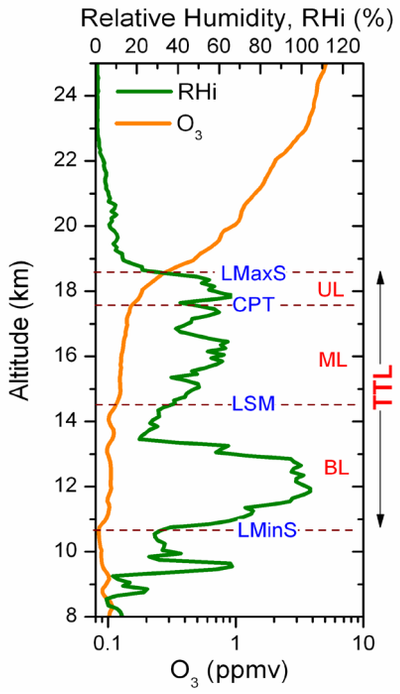

Figure 2: Altitude profiles of relative humidity with respect to ice (RHi) in the upper troposphere and lower stratosphere obtained from Cryogenic frost point hygrometer (CFH) along with the ozone mixing ratio obtained from ozonesonde over Trivandrum on 17 April 2014 [Sunilkumar et al., J. Geophys. Res., 2017].

Figure 2 shows the altitude profiles of relative humidity with respect to ice and ozone mixing ratio in the altitude region 8 to 25 km obtained from balloon-borne observations of cryogenic frost-point hygrometer (CFH) and ozonesonde on 17 April 2014 over Trivandrum. Both ozone and water vapour showed discernable changes across the different sub-layers of TTL. While the ozone clearly shows the marked departure from the tropospheric background value at LMinS, the water vapour mixing ratio reaches its stratospheric background value near LMaxS. The transition from the convectively dominated tropical upper troposphere to the radiatively dominated tropical lower stratosphere is well depicted in these profiles. The altitude gradients of these tracers across each sub-layers of TTL agree well with the expected variation in static

stability. Different dynamical processes in the upper troposphere and lower stratosphere region show significant variations in different layers of the TTL in terms of its occurrence and intensity. Figure 3 shows the altitude profiles of the frequency of turbulence (Ri< 0.25 and eddy diffusivity (K >0) estimated from radiosonde observations, the frequency of tropical cirrus obtained from CALIPSO observations, the mean water vapour mixing ratio obtained from MLS observations and the variance of ozone mixing ratio obtained from ozonesonde measurements along with the frequency of convective cloud tops inferred from IR brightness temperature of KALPANA-1. Occurrence of turbulence is maximum in the BL followed by a drastic decrease across the ML and becomes almost insignificant in the UL.

Similarly, the occurrence of tropical cirrus also is maximum in BL and decreases rapidly in the ML and almost insignificant close to the TTL-top (~18.7 km). Frequency of occurrence of thermal infrared brightness temperature less than 240 K at 5 K interval estimated over a region ±0.3° centered around the balloon launch locations are used to infer the frequency of occurrence of deep convective cloud tops (a measure of deep convection). This study showed that frequency of occurrence of deep convective cloud top is significantly high below the TTL-base and decreases exponentially from LMinS to LSM (2 to 0.5%). Even though, a few convective clouds penetrate the ML and cross the CPT; they seldom reach near TTL-top. Water vapour and variance of ozone mixing ratio shows marked variation across each sub-layers of the TTL. While the ozone variance begins to increase slowly in the BL, it shows an abrupt increase in the ML from LSM to CPT and an exponential increase in the UL.

Annual variation of the TTL boundaries (respective altitudes) over Trivandrum, Gadanki and Singapore along with the thickness of the TTL and their sub-layers are shown in Figure 4. At Trivandrum the TTL-base (the level of minimum stability) is around 12 km during winter and around 13 km in April and November, while the TTL-base over Gadanki is ~12.5 km during April -June and ~13 km during July-August. At Singapore, the mean level of the TTL- base is approximately at 12 km and the annual pattern is almost similar to that of Trivandrum. The annual variation of LSM altitude is relatively small (<1 km) for all the three stations. The annual pattern of TTL-top is similar to that of CPT, with a mean value of ~18.7 km, and a variation of ~1.5 km. In accordance with these variabilities, the thickness of the TTL as well as the thickness of BL, ML and UL also shows significant variabilities (shown as line graphs in the lower panels of Figure 4). In general, the TTL thickness shows a pronounced annual variation at Trivandrum and Gadanki. Over Trivandrum it showed a broad minimum (~5.5 km) during the April-November period and relatively larger values (~7 km) during the December-March period. Over Gadanki, a broad maximum in TTL thickness is observed during the November-May period (~7 km) and minimum values confining to July-August period (~5 km). Over Singapore, the variability of TTL thickness is relatively small (thickness is ~7 km during February-May and ~6 km during July-November periods). While the thickness of BL, ML and UL of TTL shows relatively large annual variation at Trivandrum, this variability is relatively small at Gadanki, and minimal variation at Singapore. Over Trivandrum and Gadanki, ML is relatively thin (~ 2 km) during the summer monsoon season and broad during the rest of the year. While the annual pattern of UL-

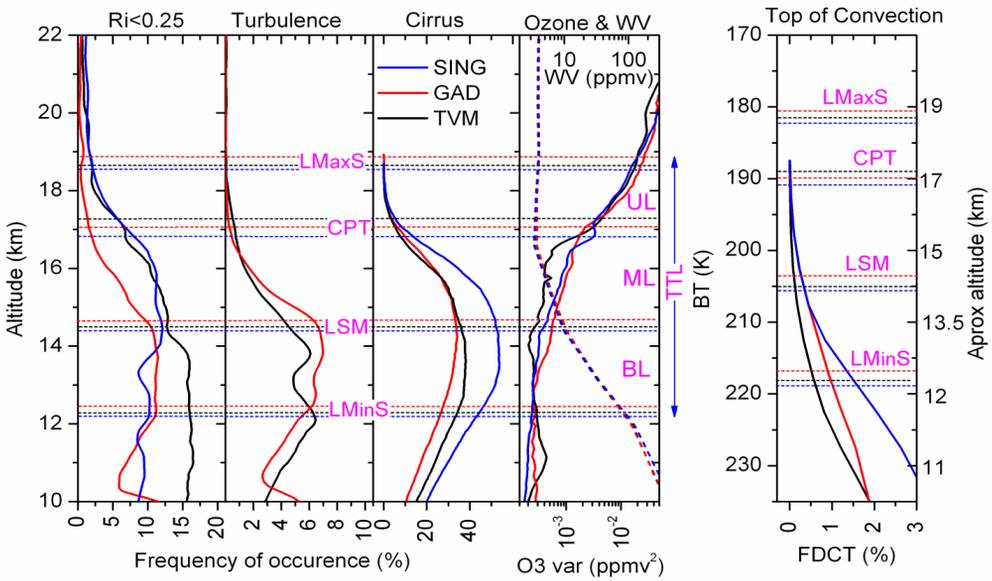

Figure 3: Altitude profile of frequency of instability from Ri< 0.25, frequency of turbulence parameters (K > 0) derived from radiosonde data, frequency of tropical cirrus derived from CALIPSO data, variance of ozone mixing ratio from ozonesonde data (continuous curve), water vapour mixing ratio (dashed curve) from MLS and frequency of deep convective cloud tops from IR brightness temperature of KALPANA-1 over Trivandrum, Gadanki and Singapore during the period December 2010-March 2014. Frequency of turbulence (in 2nd panel) is only for Trivandrum and Gadanki. The TTL boundaries are marked with dashed lines [Sunilkumar et al., J. Geophys. Res., 2017].

thickness at Trivandrum is almost similar to that of ML, the seasonal pattern of BL-thickness is minimum in April and November and maximum during December-February. At Gadanki, BL-thickness is minimum during April and July.

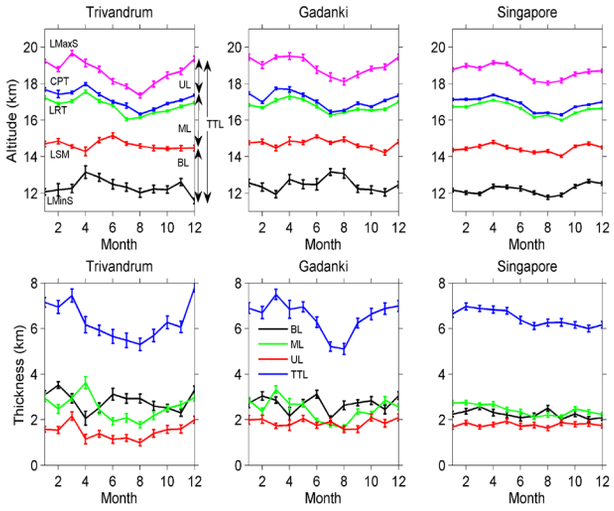

Figure 4: Mean annual variation of TTL boundaries (top panel) and thicknesses of TTL, BL, ML and UL (bottom panel) during December 2010 to March 2014 over Trivandrum and Gadanki. Vertical bars indicate the standard errors [Sunilkumar et al., J. Geophys. Res., 2017].

Spatial pattern of the TTL structure derived from GPS RO data depicts distinct features over the deep convective (DC) regions and over the regions where convection is less active (NC). In general, the levels of LMinS and LSM are located at a higher altitude over the DC regions (~12.5 km and ~ 15.5 km) compared to those over the other regions (11 km and ~12.5 km). The levels of CPT and LMaxS are located at a lower altitude (~ 16.7 km and ~18 km) over the DC regions and at a higher altitude over NC regions (~17.7 km and 19.75 km). This feature leads to a broader (thicker) BL and narrow (thin) ML and UL over the DC regions compared to the other regions. The mean thickness of TTL showed a decrease of ~2.5 km over the DC regions (~ 6 km) compared to the NC regions (~8.5 km).A major advantage of the new definition for the TTL detailed in the present study is that it can be locally defined and provides a definite criterion derivable from temperature profiles to characterize the TTL for delineating the thermal and dynamical processes in terms of tracer motion, transport and radiative effects. It can delineate the short time temporal variations of the TTL at a given location. Future studies may focus on these layers for better understanding of the stratosphere-troposphere exchange processes.

Diurnal variability of the global tropical tropopause

In recent years, there has been a growing interest to understand the dynamical characteristics of the tropopause, especially over the tropical region. The transport of water vapour from the tropical troposphere to the stratosphere is primarily controlled by the tropical cold-point tropopause (CPT) temperature. Minor change in the stratospheric water vapour may have significant effect on stratospheric chemistry and henceforth in the global radiation budget. Monitoring global tropopause structure, height and its variability can yield a better insight on the stratosphere-troposphere exchange (STE) and throw light on our understanding of climate change related issues. With the availability of the space borne GPS radio occultation (GPSRO) technique diurnal variability of the tropopause can be studied over the globe. Eight years (2007-2014) of temperature data from wet-profiles (which accounts for the water vapor in the troposphere) are used to study for the first time the global diurnal characteristics of tropopause. Height and temperature corresponding to CPT and lapse rate tropopause (LRT) are determined individually from each temperature profile. Finally, the global tropopause data is gridded in to 2.5 degree-latitude ×5 degree-longitude. Eight years of tropopause data sets are then divided in to four seasons viz., December-January-February (DJF), March-April-May (MAM), June-July-August (JJA) and September-October-November (SON). Figure 5 shows monthly mean diurnal anomaly of the CPT height (left) (hereafter CPT-H) and temperature (right) (hereafter CPT-T) as a function of time, averaged for different latitudinal belts (i.e. 20°-25°N, 15°-20°N, 10°-15°N, 5°-10°N, 5°S-5°N, 5°-10°S, 10°-15°S, 15°-20°S, 20°-25°S,). In y-axis, '0' indicate that the data is averaged between 0 and 3 LT and similarly other time markings in the y-axis corresponds to 3-hour averages. The diurnal mean is removed from every three hourly data for individual month (composite of seven years) to obtain the anomaly. The deep tropics (5°S-5°N) and 5°-10°N show a maximum and minimum CPT-H around 18-21 LT and 0-3 LT, respectively in all the seasons. As the latitude increases toward the north, i.e., between 10-15°N and 15-20°N, the CPT-H is observed to be maxima between 15-18 LT. At 20-25°N, a bimodal distribution is observed with one maximum between 12-15 LT which occurs during May-August and other between 18-21 LT during November-December. On the other hand, in the deep tropics and between 5°-10°N, the maximum CPT-T is observed between 6-9 LT. This feature is also observed at 10°-15°N but the amplitude is less compared to the other two latitude regions. A diurnal maximum in the CPT-T is observed between 18-21 LT as we move towards higher latitudes in the tropical region. In the Southern Hemisphere (SH), maximum amplitude in the CPT-H is observed between 18-21 LT during January-April, unlike the Northern Hemisphere (NH), where a consistent maximum is observed throughout the year. The CPT-H is minimum during 6-9 LT and the CPT-T is maximum during 6-12 LT from January to April. The analysis shows that the diurnal variability is very distinct between NH and SH. The distinct diurnal variability in the tropopause is in very close association with the convection that occurs over the land and ocean. It is well established that the maximum convection occurs during the afternoon hours over the land, whereas over the oceans, it occurs in the evening and late night. Generally, the tropopause height is controlled by atmospheric convections and thus, the maximum tropopause height is observed in the convective

zone. In the present analysis, the maximum tropopause height is observed during late evening, which indicates that there is a time lag between the maximum convection and tropopause height.

values of distributions, and the lower and upper edges of the box indicate the 25 and 75 percentiles, respectively. The maximum diurnal amplitudes in both CPT-H and CPT-T are observed over the deep tropics and gradually decrease

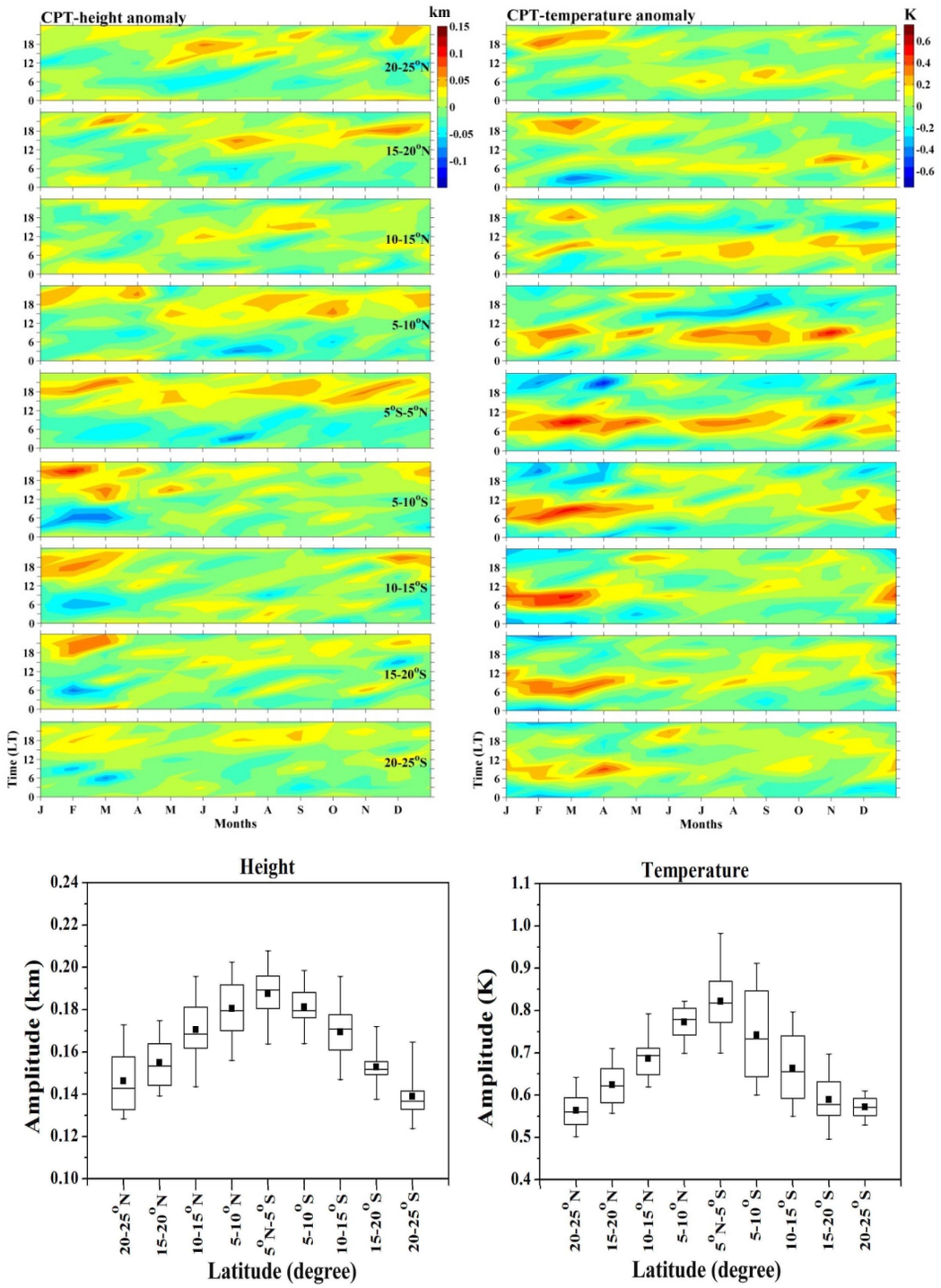

Figure6: Latitude variation of the diurnal CPT height (left), and temperature (right) amplitude [Suneeth et al., Climate Dynamics, 2017].

Figure 6 shows the box plot of the latitudinal variation of the diurnal amplitude of CPT-H and CPT-T. The diurnal amplitude is zonally averaged. The dots and horizontal bar indicate the mean and median, respectively. The upper and lower whiskers indicate the maximum and minimum

towards higher latitudes. The maximum (minimum) diurnal amplitude in CPT-H and CPT-T are found to be ~0.2 km (~0.13 km) and ~1 K (~0.5 K), respectively. Diurnal amplitude in the CPT-T over the SH is larger as that of the NH.

Cloud Dynamics

Distribution of the multi-layered clouds across the globe using CloudSat observations

Most of the studies on cloud dynamics emphasized the importance of cloud vertical structure on atmospheric circulations, including the effects of variations of cloud top and base heights, cloud-layer thicknesses, and the vertical distribution of multi-layered clouds as they significantly modify vertical and horizontal gradients in radiative and latent heat fluxes. There were studies in the past, which emphatically showed that the vertical gradients in the cloud distribution were more important to the circulation strength than horizontal gradients, which modifies the vertical radiative heating of the atmosphere. So, it becomes inevitable to establish the vertical distribution of clouds and to study their role in modifying the atmospheric circulation for a better understanding of cloud feedback mechanisms in totality. In this study, we use 4 years of (2007–2010) CloudSat and CALIPSO observations to study the distribution of multi-layered clouds and associated dynamics across the globe.

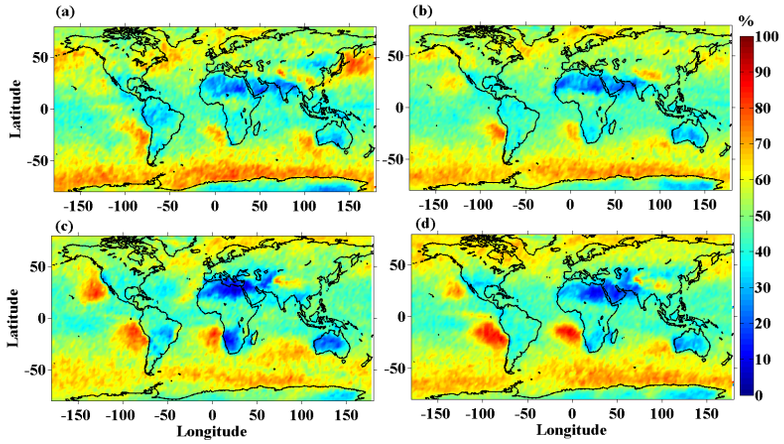

Figure 7: Four years mean seasonal variation of frequency of occurrence of single layer clouds during (a) DJF, (b) MAM, (c) JJA and (d) SON across the globe [Subrahmanyam and Kumar, Climate Dynamics, 2017].

Figure 7(a-d) shows the mean seasonal variation of frequency of occurrence of single layer clouds during DJF, MAM, JJA and SON over the globe respectively. The striking feature of this figure is the high frequency of occurrence of single layer clouds during all the seasons over Southern ocean. The single layer clouds are more or less uniformly distributed over the entire longitudinal belt over 60-70° S and the frequency of occurance ranges from 60-70% with minimal seasonal variations over this region. However, figure 7(a) and (c) reveal that the frequency of occurrence of single layered clouds over Southern ocean is relatively high during Austral summer as compared to winter. Apart from Southern and Northern hemispheric high latitudes, high fraction of single layer clouds also occur over the South Pacific Ocean near west coast of South America (~ at 20^0-30^0 S latitudinal belt) and over South Atlantic Ocean near west coast of South Africa. These two cloud regimes show pronounced seasonal variation with maximum occurrence during SON (~80%) and minimum during MAM (~60%). An additional patch of high fraction of single layered clouds occurs over North Pacific Ocean near west coast of North America (~ at 20^0-30^0 N latitudinal belt), which shows maximum during JJA and minimum during DJF. On the other hand, very low frequency of occurrence of one-layer clouds can be noticed from figure 7 (a-d) over North and South Africa, Middle-East and Australia over the 20-30^0 latitude belt in both the NH and SH . Even though the low frequency of occurrence of single-layered clouds is observed over the same geographical locations during all the seasons, they exhibit pronounced seasonal variation in magnitude with very low fractions during JJA in both the hemispheres. However, it is very interesting to note the couplet of low and high fraction of single-layer clouds over the descending branch of the Hadley cell, which is more prominently seen during JJA over the west coast of South Africa and South America. It is expected to be cloud free zone over the descending branch of the Hadley cell. Over the land, the driest regions are found over the descending branches of Hadley Cell. However, over the oceanic regions of Hadley Cell descending branch, due to availability of moisture in the lower levels, single layer clouds can form as observed in figure 7.

Figure 8(a-d) shows the distribution of two-layered clouds during the DJF, MAM, JJA and SON seasons. One interesting inference that can be drawn from figures 7 and 8 is that the frequency of occurrence of single layered cloud is high over oceans, whereas in the case of two-layered cloud it is high over land, especially over the low latitude-equatorial belt. One can notice the migration of Inter Tropical Convergence Zone (ITCZ) from South to North and back during DJF to SON. Over the equatorial region, the high frequency of occurrence of two–layer clouds (~40%) is observed over South America, Central Africa and Indonesian regions during all the seasons with maximum during DJF and minimum during JJA over the 50^0 S to 50^0 N latitudes. The locations of relatively high frequency of occurrence of two layered clouds over the equatorial regions more or less coincide with the ascending limbs of the Walker circulation. During JJA, there is an increase in the frequency of occurrence of two-layered clouds over the Indian sub-continent and surrounding oceans, which

persist during SON also. The signature of descending branch of Hadley cell is more pronounced in multi-layered clouds. Abundance of deep convective clouds are formed during the Indian summer monsoon period and produces large amount of cirrus clouds, which are formed from the anvil of deep convective clouds and spread by the tropical easterly jet. Moreover, during this season, the monsoon low level jet brings moisture from the adjacent oceans to the Indian sub-continent thus aiding the formation of clouds. The prevailing dynamics during this season is dominated by low level jet in the lower troposphere and tropical easterly jet in the upper troposphere. It is believed that the shears associated with these jets play a vital role in the formation of multi-layered clouds by smearing the clouds. During the Austral summer also relatively high frequency of occurrence in these clouds are observed over ITCZ, especially over land regions viz., South America, Central Africa and Indonesia. These regions again coincide with the ascending limbs of Walker circulation as discussed in the case of two-layered clouds. Further, the frequency of occurrence of three-, four- and five-layered clouds is estimated. The distribution of these clouds are found to be similar to two-layered cloud structures, which exhibits the equatorial maxima during almost all the seasons and pronounced maximum during JJA over the Indian sub-continent.

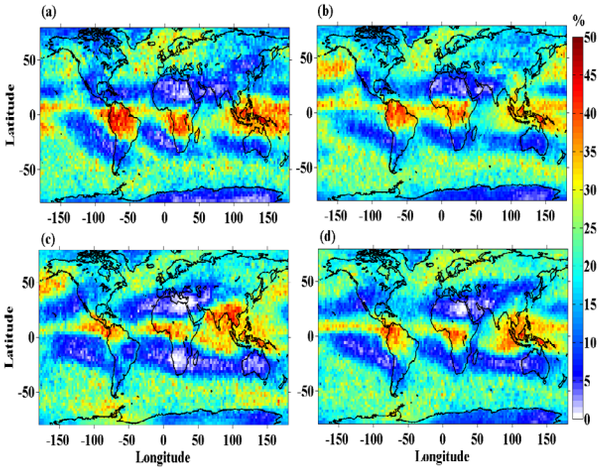

Figure 8: Same as figure 7 but for two-layer clouds [Subrahmanyam and Kumar, Climate Dynamics, 2017].

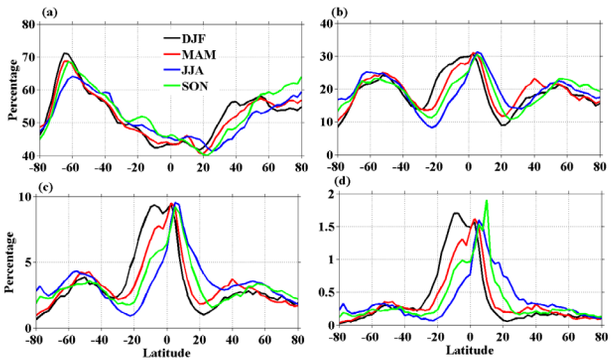

Figure 9: The latitudinal and seasonal distribution of zonal mean frequency of occurrence of (a) single, (b) double, (c) triple and (d) four-layer clouds [Subrahmanyam and Kumar, Climate Dynamics, 2017].

After constructing the distribution of one-, two-, three-, four- and five-layered clouds across the globe, an effort is made to further quantify the occurrence of multi-layer clouds in terms of zonal mean frequency of occurrence. Figure 9 (a-d) shows the zonal mean frequency of occurrence of one-, two-, three- and four-layered clouds respectively. Form this figure, it can be noted that the single layer cloud distribution exhibits two peaks, one over Southern Hemispheric high latitudes and another over Northern Hemispheric high latitudes coinciding with the ascending limb of Polar Cell. The minimum in frequency of occurrence of one-layered clouds is observed over the Tropics as shown in figure 9(a) during all the seasons. The zonal mean latitudinal distribution of two-layered clouds depicted in figure 9(b) reveals three peaks. Two peaks are found over the same region as in the case of single layered cloud distribution shown in figure 9(a). However, there is an additional peak over the equator in the two-layered cloud distribution, which can be attributed to the presence of ascending limbs of Walker circulation over these regions. The four-year zonal mean latitudinal distributions of three-layered clouds are shown in figure 9(c), which is very similar to figure 9(b) except for magnitudes. The SH exhibits pronounced seasonal variation in three-layered cloud distribution as compared to the NH. Figure 9(d) depicts the zonal mean four-layered cloud distribution, which also exhibits similar variations as two and three cloud layers. The zonal mean five-layered cloud distribution was also estimated (not shown), which shows preferential peak over the tropical latitude. The occurrence of five-layered cloud is more over 0-20^0 S latitude during DJF and MAM seasons, while it is more over 0-20^{0}N latitudes during JJA and SON periods. Thus the present study constructed the global distribution of vertically resolved multi-layer clouds and brought about the role of large-scale dynamics in controlling their distribution, for the first time.

Ongoing Activities

Regional Features of Hadley Cell

Most of the recent studies on the Hadley Circulation (HC) have quantified its rate of expansion using several zonally averaged metrics such as meridional Mass Stream Function (MSF), Tropopause, Outgoing Long wave Radiation (OLR), Subtropical Jet etc. However, as tropical heating is closely tied to land-sea distribution, the expansion rate is envisaged to vary from region to region. In this regard, a study is carried out to obtain the regional features of HC width from three objectively defined tropopause-based metrics for the first time, using eight years of COSMIC GPS-RO temperature profiles. Definitions of two of the existing tropopause-based metrics, viz. meridional gradient of tropopause (TpGr) and tropospheric bulk static stability (BSS), are extended to determine the zonally resolved HC widths. In addition, a third metric is proposed, which is based on the pronounced amplitude of annual oscillation of the tropopause (TpAO) height over the subtropical region. The reliability of the tropopause-based metrics in delineating the zonally resolved HC width is established by comparing it with the annual cycle of the zonal mean

HC width obtained from the MSF metric estimated from the ERA-I reanalysis dataset. Regional features of the total width of the HC and their relationship to the location and movement of the Inter-Tropical Convergence Zone (ITCZ), whose locations are also derived from the specific humidity observations of the COSMIC GPS-RO data, are studied. It is envisaged that the present results will have potential applications in investigating the zonally resolved trends in HC expansion.

Polar atmospheric dynamics

In order to study the thermal and dynamical structure of the middle atmosphere over Polar Regions and also to look into the possible dynamical connection between the Polar middle atmosphere and the low latitude counterpart, balloon borne experiments were conducted as part of 34th and 35th Indian Scientific Expedition to Antarctica (ISEA) during 2014-2015 and 2015-2016. As continuation to these, balloon borne Radiosonde/ Ozonesonde observations were conducted for vertical profiling of atmospheric thermodynamic parameters, in 36th ISEA also during 21 November 2016 to 14 February 2017. Total of 50 radiosonde launches were conducted, including 7 ozonesonde launches. Studies on characterizing atmospheric gravity and planetary waves prevailing over Bharati (69^{o}S, 76^{o}E), Antarctica, making use of these observations from 34th, 35th and 36th ISEA are going on. Gravity waves are characterized in terms of vertical and horizontal propagation characteristics, intrinsic frequency, kinetic and potential energy densities. Signatures of upward propagating waves in lower troposphere and downward propagating waves in the lower stratosphere are observed. The vertical wavelengths of GWs are found to be around 4-5 km in lower troposphere and stratosphere. Detailed studies are in progress.

New Initiatives

Ceilometer installation at Thumba

As a part of Integrated Lidar System project, a Ceilometer is successfully installed at Thumba on 9th August 2016. The Ceilometre is working round the clock since August 2016 and providing the cloud based altitude up to three layers, which will be used to get the cloud statistics . The central objective of the Ceilometer observations is to establish the cloud statistics over the observational site for cloud research applications as well as for scheduling of the Rayleigh lidar system, which will be procured in near future. Figure 10(a) shows a photograph of Ceilometer instrument installed at Thumba. Figure 10 (b) shows the backscattered profile on 20th August 2016 derived from Ceilometer measurements. It is noticed that the ceilometer observations show noise above 6 km during the noon hours. However, this noise does not hamper the efforts in delineating the cloud base and top altitudes.

Evaluation of C-band Polarimetric DWR at TERLS, Thumba- Preliminary results

Recently, a C-band polarimetric DWR was installed and commissioned at Thumba for weather monitoring and research. The DWR operates in the frequency range of 5.6 to 5.65 GHz with a peak transmitting power of 250 kW at 0.004 % duty ratio and employs state of the art technology

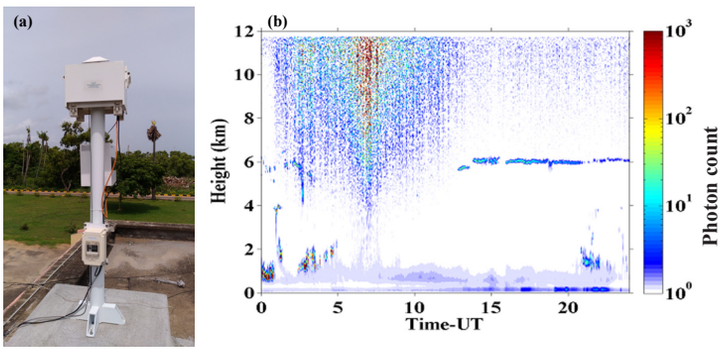

Figure 10: (a) Ceilometer instrument installed at Thumba (b) Backscattered profile on 20-08-2016 from Ceilometer at Thumba.

Gravity wave Saturation Theory

After successfully developing methodologies and algorithms for space based gravity wave studies, an initiative has been taken for testing existing gravity wave saturation theories as suggested by the SAC of SPL. Recent lidar observations of high temporal and vertical height resolution of middle atmospheric temperature are used for the study. After routine characterization of gravity waves, a two-dimensional spectrum has been computed to obtain the vertical wavenumber and frequency spectra simultaneously. The saturation spectra estimated from theory are then fitted to the observed spectrum. The similarities and discrepancies between the theoretical and observed spectrum are being interpreted by employing the existing gravity wave saturation theories. A detailed analysis of the vertical wavenumber spectrum of gravity waves is under progress.

for both transmitter and receiver system. The C-band DWR provides the observation of reflectivity, radial velocity and spectrum width as base products. Further, it provides polarimetric products differential reflectivity (Zdr), differential phase shift (dp) and correlation coefficient (ρ_{hv}). We have carried out an observational campaign to validate the C-band DWR products in November and December 2016. During the campaign period, C-band DWR observed the convective cloud system on 1st and

5th December 2016. Before the commencement of the campaign, the C-DWR has been calibrated using a metallic sphere and the appropriate corrections were made to the radar constant. To validate the rainfall measurement of C-DWR, which is one of its important derived products, the Disdrometer measured rain rate at NCESS-Trivandrum are used. Qualitatively, the spatial patterns of reflectivity observed by C-Band DWR and GPM-PR show a good agreement. However, the quantitative comparison with rain gauges around the radar region is currently underway.

Future Projections

- Realization of Integrated Lidar System
- Testing of Gravity wave parameterization schemes in middle atmospheric models
- A campaign to study the diurnal characteristics of thermal structure, ozone and water vapour associated with tropical cyclones
- Vertical structure of latent heating for various types of clouds
- Characterizing the vertical structure of precipitating convective clouds using C-band Polarimetric DWR observations at TERLS
- Seasonal and Diurnal variation of Tropical Tropopause Layer (TTL)
- Effect of deep convection on the thermal structure of troposphere and lower stratosphere and TTL
- Diurnal variation of tropospheric water vapour: In situ (radiosondes) & satellite measurements
- In situ observation (FPH) of water vapour in the UTLS region: Seasonal variations and comparison with satellite and re-analysis dataset

Publications in Peer-Reviewed Journals

1. Anirban Guha, Kumarjit Saha, Barin K De, K. V. Subrahmanyam, Shreedevi P. R., Space weather effects on lower ionosphere: First investigation from Bharati station during 34th Indian scientific expedition to Antarctica, Advances in Space Research, doi:10.1016/j.asr.2017.02.004 (2017).
2. Anurose, T. J., D. B. Subrahamanyam and S. V. Sunilkumar, "Two years observations on the diurnal evolution of coastal atmospheric boundary layer features over Thiruvananthapuram (8.5° N, 76.9° E), India", Theoretical and Applied Climatology, doi: 10.1007/s00704-016-1955-y (2017).
3. Mehta S, M VenkatRatnam, S.V. Sunilkumar, Rao, D.N., B.V. Krishna Murthy, Diurnal variability of the Atmospheric layer height over a tropical station in the Indian Monsoon region, Atmos. Chem. Phys., 17, 531–549, doi: 10.5194/acp-17-531-201 (2017).
4. Selvaraj, D., A. K. Patra, S. Sathishkumar, K. Kishore Kumar, and D. Narayana Rao , On the governing dynamics of the VHF radar echoes from the mesosphere and collision dominated lower E region over Gadanki (13.5°N, 79.2°E), doi: 10.1002/2016JA023297 (2016).
5. Subrahmanyam, K.V., Karanam Kishore Kumar, CloudSat observations of Multi-layered clouds across the globe, Climate Dynamics, 49:327-341, doi:10.1007/s00382-016-3345-7 (2017).
6. Suneeth, K.V., Siddarth Shankar Das, and S. K. Das, Diurnal variability of the global tropical tropopause: results inferred from COSMIC observations, Climate Dynamics, 1-16, doi : 10.1007/s00382-016-3512-x. 10.1007/s00382-016-3512 (2017).
7. Sunilkumar S V, Muhsin M, VenkatRatnam, K Parameswaran, B V Krishna Murthy, Maria Emmanuel, Boundaries of Tropical Tropopause Layer (TTL): A new perspective based on thermal and stability profiles, Journal of Geophysical Research, 122, 741-754, doi:10.1002/2016JD025217 (2017).
8. Venkateswara Rao,N., M. Venkat Ratnam, C. Vedavathi, T. Tsuda, B. V. Krishna Murthy, S. Sathishkumar, S. Gurubaran, K. Kishore Kumar, K. V. Subrahmanyam, and S. VijayaBhaskaraRao,Solar cycle modulation of the quasi-two day wave in the low-latitude mesosphere and lower thermosphere, Journal of Atmospheric and Solar–Terrestrial Physics 152 ,20–29, doi:10.1016/j.jastp.2016.11.005 (2017).

Presentations in Symposia/workshops/conference

International

1. Das, S.S., M. V. Ratnam, K. N. Uma, A. K. Patra, S. Aneesh, K. V. Subrahmanyam, I.A.Girach, K. K. Kumar and G. Ramkumar,"How, where and when the 'stratospheric intrusion' take place during the passage of tropical cyclone: Results inferred from Indian MST Radar and satellite observations", 15thInternational Workshop on Technical and Scientific Aspect of MST Radar held at National Institute of Polar Research, Tachikawa, Tokyo, Japan during 26-31 May 2017.

2. Das, S.S., K.V.Suneeth, M.V. Ratnam,"Role of Tropical easterly jet (TEJ) in stratospheric-troposphere exchange: Observations inferred from Indian MST Radar", 15thInternational Workshop on Technical and Scientific Aspect of MST Radar held at National Institute of Polar Research, Tachikawa, Tokyo, Japan during 26-31 May 2017.

3. Kumar, K.K., "Long-term Observations of Low-Latitude Middle Atmospheric Dynamics using multi-platform observations", 9th work shop on Long-Term Changes and Trends in the Atmosphere, Kühlungsborn, Germany, 19-23 September 2016.

4. Kumar, K.K., "Equatorial and Low-Latitude Mesosphere Lower Thermosphere Wind System: The Atmospheric Beaches", 9th work shop on Long-Term Changes and Trends in the Atmosphere, Kühlungsborn, Germany, 19-23 September 2016.

5. Maria Emmanuel, Sunilkumar. S .V, Muhsin .M, B. Suneel Kumar, N. Nagendra, Geetha Ramkumar, Rajeev. K. 'Tropical lower stratospheric water vapour over India- a seasonal picture from in situ and satellite observations', 3rdInternational RCRS-URSI,Tirupati, 01-04 March 2017.

6. Kumar, K.K., K.V. Subrahmanyam, Geetha Ramkumar Meteor radar observations of quasi two day waves in the mesosphere lower thermosphere over low and equatorial latitude, 3rdInternational RCRS-URSI, Tirupathi, 1-4 March, 2017

7. Subrahmanyam, K. V. and Karanam Kishore Kumar, "New insights into the convective system characteristics over the Indian summer monsoon region using space based passive and active remote sensing techniques", 3rdInternational RCRS-URSI, Tirupathi, 1-4 March, 2017.

National

1. Das, S.S., and K. V. Suneeth, "Distribution of ozone and water vapour in the UTLS region over the Tibetan high", Frontiers in Earth and Climate Sciences : A conference of Young Scientists in Central & South Asian Region, Indian Institute of Sciences (IISc), Bangalore, 5-7 December 2016.

2. Koushik N, GeethaRamkumar., Subrahmanyam K.V., Kumar K.K., Girach Imran., M Santosh., K Nalini., Mohammed Nazeer., P. Shreedevi., "Characteristics of Gravity and Planetary Waves over Bharati(69S, 76E), Antarctica from Balloon borne Radiosonde Observations", National Conference on Polar Sciences, NCAOR, Goa, 16-17 May 2017.

3. Maria Emmanuel, S V Sunilkumar, M. Venkat Ratnam, M Muhsin, Diurnal evolution of tropospheric water vapour over Indian Peninsula, National Symposium on Tropical Meteorology Climate change and coastal vulnerability, TROPMET-2016, Bhuwaneshwar, 18-21 December 2016.

Invited Talks

1. Siddarth Shankar Das, National Institute of Wind Energy, Chennai 18th and 19th International Training Course on "Wind Turbine Technology and Application" held during August 18, 2016 and February 6, 2017.

Deputations

K. Kishore Kumar

9th work shop on Long-Term Changes and Trends in the Atmosphere, Kühlungsborn, Germany, 19-23 September 2016.

Siddarth Shankar Das

15th International Workshop on Technical and Scientific Aspect of MST Radar held at National Institute of Polar Research, Tachikawa, Tokyo, Japan, 26-31 May 2017.

Training Programme

1. Maria Emmanuel, SMART training on "Satellite Scatterometry with special emphasis on ScatSat-1," SAC, Ahmedabad, 23-25 November 2016.

2. Satheesh Chandran P R, SMART training on "INSAT-3DR: Observations to applications," SAC, Ahmedabad, 07-10 March 2017.

Ionosphere Thermosphere Magnetosphere Physics

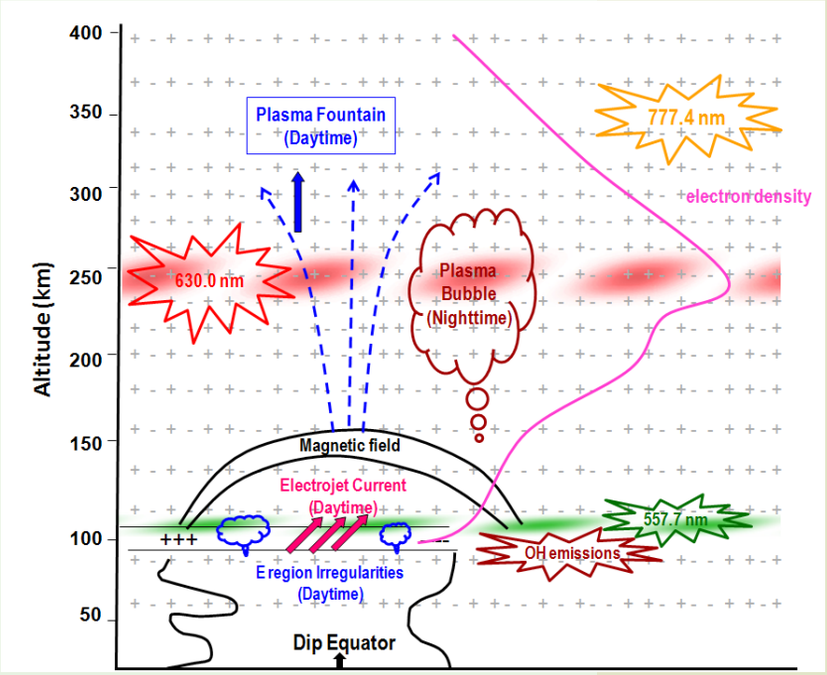

The aim of Ionosphere Thermosphere Magentosphere Physics (ITMP) branch is to investigate the terrestrial upper atmosphere in context of its energetics and dynamics vis-à-vis the vertical and lateral coupling this region has with the magnetosphere above and lower atmosphere below it; and make use of these studies to provide better input for technological applications wherever possible. ITMP aims at extending these studies to other solar system bodies as well.

Science Team

Tarun Kumar Pant
Raj Kumar Chaudhary
Manju G.
Smitha V. Thampi
Vineeth C.
Md. Mossarraf Hossain
Mridula N.

Inspire Faculty

Ms. Sneha Yadav

Research Fellows

Shreedevi P. R.
Ajesh A.
Aswathy R. P.
Harikrishanan V.#
Krishnaprasad C.

Technical Team

Mohan Kumar S. V.*
Sreelatha P.
Pradeepkumar P.
Shajahan M.
Anumod P. G.
Manikantan Nair N.
Mohammad Nazeer M.
Uttam S. Purthy
Rosmy John
Satheesh Kumar B

* Superannuated in August 2016

Relieved in July 2017

Observational evidence for Disturbance Dynamo on the daytime low latitude ionosphere: A case study based on the June 28, 2013 Space Weather Event

In the studies of the low-latitude ionospheric response to geomagnetic storms, the Prompt Penetration Electric Field (PPEF) is usually inferred using IMF Bz or IEFy data, and has clear signatures in the ground magnetic field data. In contrast, the identification of Disturbance Dynamo Electric Field (DDEF) is mostly based on inferences from the ionospheric observations and modeling. The major challenge in identifying the DDEF from ionospheric observations lies in delineating the effects of DDEF from those due to composition changes. A case of the westward disturbance dynamo (DD) electric field, influencing the daytime equatorial and low-latitude ionosphere, during a geomagnetic storm that occurred on 28–29 June 2013 (minimum Dst ~-130 nT) is studied. The GPS total electron content (TEC) observations from a network of stations in the Indian equatorial, low and middle latitude regions along with the radio beacon TEC, ionosonde, and magnetic field observations are used to study the storm time behavior of the ionosphere.

As seen from Figure 1a-e, there was hardly any change in the TEC over Shimla and Delhi and Trivandrum from the quiet-day mean behavior on 28 June 2013. The TEC over Bhopal (anomaly crest region) showed only a marginal increase (close to the standard deviation) in the afternoon hours. However, on 29 June 2013, the TEC over the stations Shimla, Delhi and Bhopal remained substantially low from morning till evening (Fig.1f-j). This negative ionospheric storm effect seen over the low and middle latitudes is basically due to the presence of a westward DDEF.

The degree to which the EIA was affected by the storm time DD electric fields was further understood from the latitude variation of TEC, provided by the LEO beacon based observations shown in Figure 2. The presence of an EIA crest on 28 June was clear from the satellite passes that commenced at 14:09 IST and 15:21 IST, respectively (Figure2a). In contrast, on 29 June 2013, the EIA was completely suppressed as evident from the TEC variation at 14:39 IST, 15:05 IST and 16:15 IST (Fig.2b). The TEC showed a maximum over equator that decreased towards northern low- latitudes, which is a direct evidence for the presence of westward DD electric field.

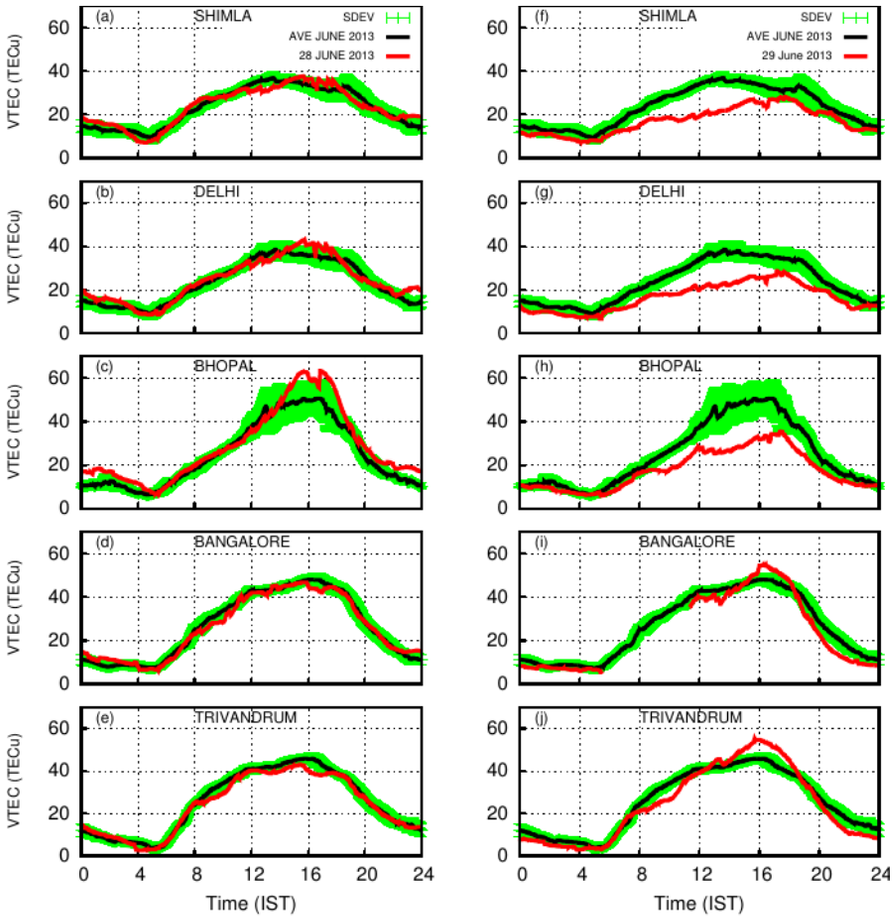

Figure 1: TEC variation at the GPS stations during 28 June 2013 and 29 June 2013 (red curves) in the left and right panels respectively. The black line represents the mean quiet day variation of TEC for Ap < 4 days along with the standard deviation shown in green [Thampi et al ., J. Geophys. Res., 2016].

This study shows that in case of the daytime zonal electric fields becoming westward during the late main phase to recovery phase of a storm from the morning hours, the ionization fountain can completely cease and the latitude variation of TEC can be completely altered. Further, this study provides a clear example of the effect of storm-time neutral dynamical forcing on the low latitude plasma density distribution.

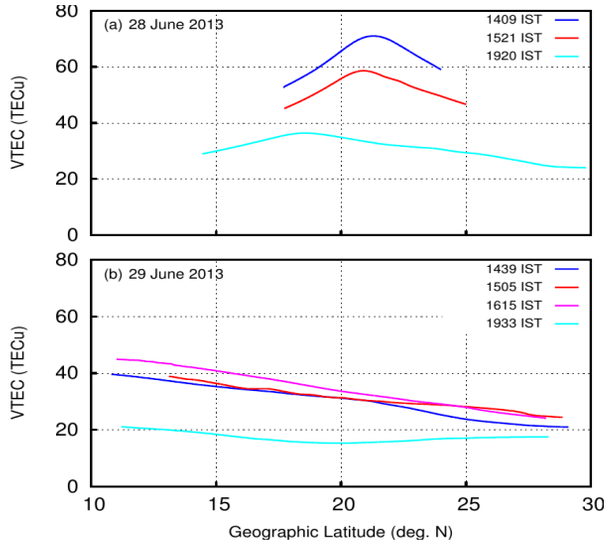

Figure 2: The latitudinal variation in TEC as observed by LEO beacon receiver at Trivandrum, for different local times on 28 and 29 June 2013. The absolute TEC variations are estimated from the single station observations of relative phase using the method described in Thampi et al (2014) [Thampi et al., J. Geophys. Res., 2016].

Gravity wave control on ESF day to day variability: an empirical model approach

The gravity wave control on the day-to-day variability of occurrence of Equatorial Spread F (ESF) is studied using ionosonde data for the Autumnal Equinox season for the years 2000-2008 at magnetic equatorial location. During low solar activity period, the amplitude of the seed perturbations, is a very critical parameter which decides, whether or not ESF would occur on a given day. It had been shown that the requisite seed perturbation at a particular altitude (which forms a threshold curve) showed solar activity and seasonal dependence.

The altitude variation of the requisite seed perturbations is examined for autumnal equinox of solar cycle 23. Based on the above solar cycle variability (Fig.3), an empirical model is developed wherein the threshold curve for autumnal equinox (ae) season of any year may be delineated provided the solar flux index (F10.7) is known. The exponential relation obtained between Seed and h'F of each year is of the general form, Seed = y0 + A exp(R0 x h'F). It is seen that y0, A and Ro are directly modulated by solar flux and empirical relationships are established between these parameters and F10.7. Thus for any given solar flux and h'F, the exponential threshold curve for ESF occurrence can be simulated using the above model derived values. The years 2001 (high solar activity, annual mean F10.7 flux being ~150), 2004 (moderate solar activity, annual mean F10.7 flux being 105) and 1995 (low solar activity, annual mean F10.7 flux being 80) are chosen for testing the validity of the above empirical model expression. The mean F10.7 flux for ae of 2001, 2004, and 1995 are 210.3, 105.8 and 73 respectively. These values are substituted in the model expression and the requisite seed perturbations are derived for varying altitudes. The empirical model curves so derived for ae 2001 (top panel), 2004 (middle panel) and 1995 (bottom panel) are shown in Fig.4. Overall, 95.6% success is achieved in predicting ESF occurrence/non occurrence using the present model, considering the three years together.

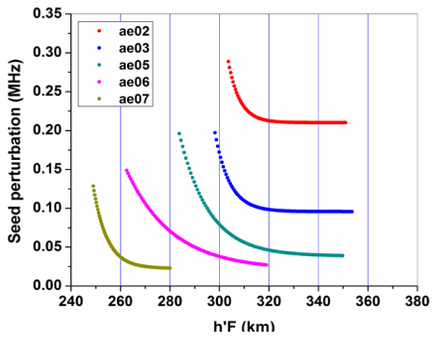

Figure 3: Solar cycle variation of the threshold curves for ESF occurrence for different years of solar cycle 23 [Aswathy and Manju, J. Geophys. Res., 2017].

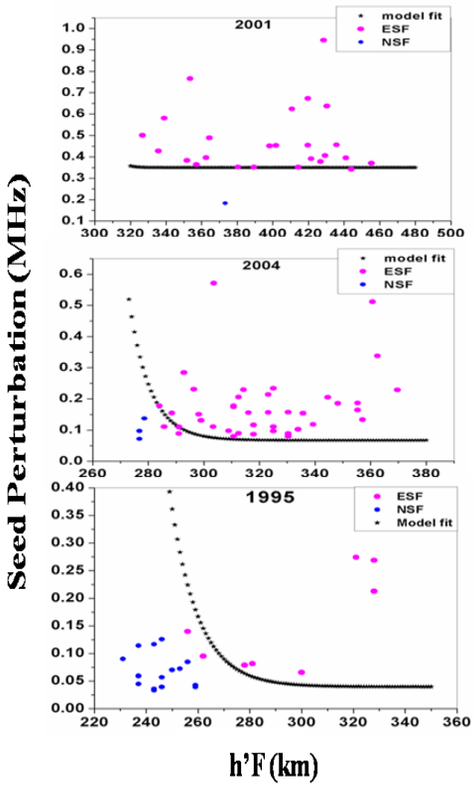

Figure 4: The empirical model curves so derived for ae 2001 (top panel), 2004 (middle panel) and 1995 (bottom panel) [Aswathy and Manju, J. Geophys. Res., 2017].

This model has the potential to be used to predict the occurrence of ESF, if the base height of ionosphere is in the electrodynamically controlled region. This study is thus extremely important from the point of view of predicting communication and navigation outages due to ESF occurrence.

Solar activity variations of nocturnal thermospheric meridional winds over Indian longitude sector

A comprehensive analysis of nocturnal thermospheric meridional wind pattern encompassing two solar cycles is accomplished in the Indian longitude sector. Significant difference is seen in winds between high (HSA) and low solar activity (LSA) epochs, with less equatorward winds during pre midnight hours for high solar activity years (Fig.5). The solar flux relationship of mean winds during pre midnight hours is established. An integrated approach using the existing observational techniques, models as well as satellite based inputs are employed to understand the underlying causative mechanisms behind the observed solar activity responses of thermospheric winds.

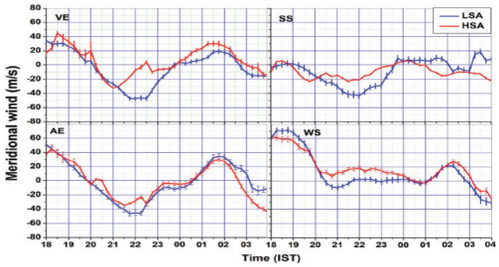

Figure 5: Mean temporal evolution of thermospheric meridinal winds during two solar activity epochs for Autumnal equinox, Vernal equinox, Summer solstice and Winter solstice [Madhav et al., J.Atmost. Sol. Terr. Phys., 2016].

The ion drag imparted by the increased magnitude of electron density and a stronger EIA, during post sunset hours of HSA years is having the major say in the reduction of equatorward meridional winds (Fig.6).

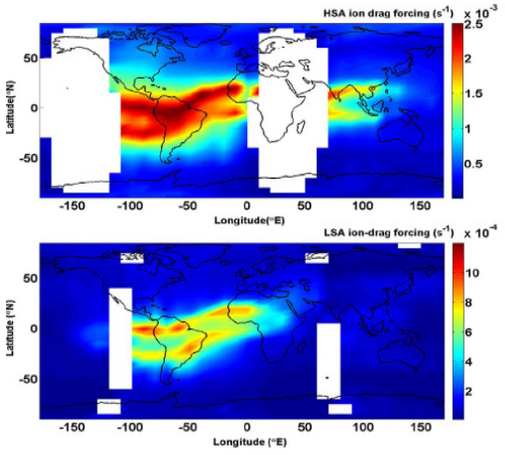

Fig. 5. Ion-drag force estimated for HSA and LSA during 2200 h for AE.

Figure 6: Ion drag force estimated for HSA and LSA for Autumnal Equinox [Madhav et al., J.Atmost. Sol. Terr. Phys., 2016].

During post-midnight period, the MTM effects become dominant and hence the ion drag effects and consequent effects on winds are not clearly evident. By around 0200–0300 IST, the MTM effects diminish, but by then the EIA is also inhibited and so the ion drag effects on winds becomes less significant. The study highlights the need to improve the existing models incorporating the effects of physical processes like MTM and ion drag effects.

The impact of St. Patrick's Day storm of 17 March 2015 over the Indian longitudes using 2D TEC maps: New insights

The 2D (lat. x long.) total electron content (TEC) maps have been generated by using the ionospheric correction data transmitted by the Indian Satellite Based Augmentation System(SBAS)-GAGAN. The advantage of this unique technique is the fact that by using a single SBAS-enabled receiver, the information over the entire region served by SBAS can be obtained irrespective of the location of the receiver. This makes it a novel, powerful and cost-effective way for ionospheric and space weather related studies. These 2D maps have been employed, for the first time, to investigate the effect of the most talked about space weather event of the current solar cycle i.e., the St. Patrick's Day geomagnetic storm that triggered on 17 March 2015, on the equatorial and low-latitude region of the Indian longitudes. These 2D TEC maps for 16 March (Quiet day) and 17 March 2015 (Storm day), as shown in figure 7, having a large latitudinal (5° S-45° N) and longitudinal (55°-110° E) coverage, show the complete reversal in the longitudinal structure/pattern of EIA during the recovery phase of the storm as compared to the quiet day. It was observed that even a separation of few degrees in longitude (~15°) could experience significantly different forcing.

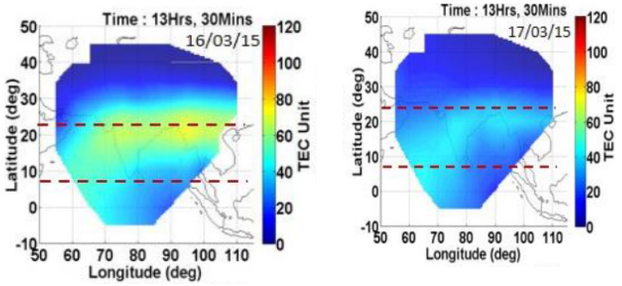

Figure 7: The 2D TEC images for 16 (Quiet day) and 17 March 2015 (Storm day) during evening (1320 UT) sector. The colour code represents the TEC values. Each plot has a maximum latitudinal and longitudinal extent of ~5° S to 45° N and ~55° to 110 ° E [Yadav et al., Space Weather, 2016].

SBAS-derived TEC maps: a new tool to forecast the spatial maps of maximum probable scintillation index over India

Understanding L-band scintillation with a goal to be able to forecast is considered as an extremely important task as it affects the accuracy and reliability of satellite-based navigation services. The strength of the scintillation on

any given day forms one of the crucial elements to be a part of any scintillation forecasting scheme. An attempt has been made to forecast the strength of scintillation using the background ionospheric electron density distribution. The scintillation forecast maps, such as the one for April 26, 2012 exhibited in figure 8, have been generated as early as 19:30 LT using SBAS platform and the already established relationship between the dusk time TEC and the maximum probable scintillation intensity (S4max). The superposition of actual S4 measurements, obtained from the GAGAN network of receivers, on the forecasted S4 max map shows that the actual measurements are less than the predicted S4 max except on very few occasions. This simple technique has the potential to predict the 2D maps of maximum probable scintillation index for the whole night which, with more refinements, could evolve into a viable forecast or forewarning system.

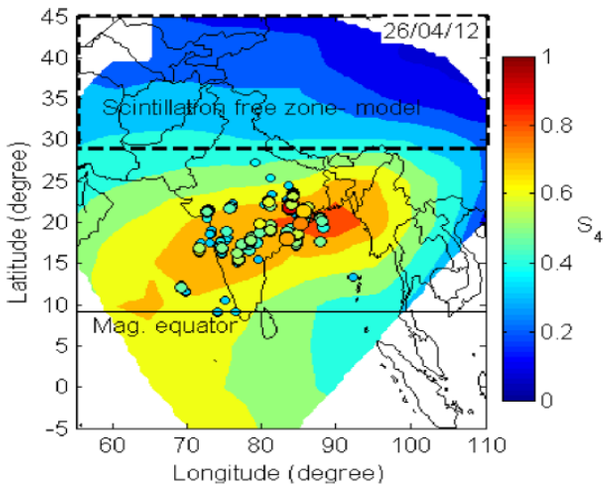

Figure 8: Comparison of forecasted scintillation strength with actual measurements of the S4 index on April 26, 2012.The circles denote the S4 measurements at different ionospheric pierce points (IPPs) observed by ground stations. The color code inside circles depicts the strength of measured scintillation—S4 index. The dashed rectangular region represents the scintillation-free zone [Sunda et al., GPS Solutions, 2017].

A numerical simulation study on the role of horizontal wind shears in the generation of F0.5 layers over the dip equatorial location of Thiruvananthapuram

Additional stratifications that are formed near the base of the F1 region and do not exhibit significant downward descent are referred to as the F0.5 layers. They are a class of Intermediate layers formed in the transition or valley region between E and F layers.

A numerical simulation is carried out to estimate the rate of convergence of ionization required to produce a F0.5 layer with peak plasma frequency (foF0.5) of 3.2 MHz from three different background layer densities, over Thiruvananthapuram (8.5°N; 77°E; dip latitude ~ 0.5°N), a dip equatorial station in India. Further the simulation study is extended to understand the convergences required by considering the seasonal mean peak F0.5 layer frequencies also.

In the current simulation study, first the convergence required to generate a layer of given electron density from a background ionosphere without layer is estimated assuming that this convergence is caused by a meridional wind shear over the dip equator with gravity waves as the source of these wind shears. Further perturbation amplitude in velocities which are capable of producing the meridional wind shears required to form the layer are estimated. One possible mechanism by which this convergence can be produced is by a horizontal shear in the meridional wind. The corresponding shears required to generate the layer with the above convergence conditions are estimated. It is found that gravity waves are capable of generating wind shears, leading to the pooling of ionization and the generation of the layer over the dip equator. Meridional winds with the gravity wave induced wind shear is numerically estimated and the ion convergence provided by gravity waves of different horizontal wavelengths are calculated and plotted in Fig.9. Finally, the short scale gravity waves of periods around 3–23 min have been inferred to be more efficient in generating the wind shear when compared to large scale horizontal waves leading to the generation of F0.5 layer.

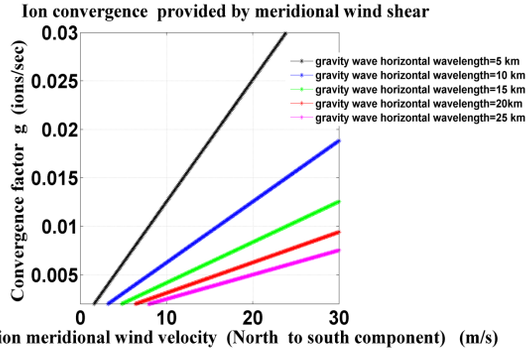

Figure 9: Shows the convergences produced by different perturbation velocities of gravity. waves of five horizontal wavelengths as marked in the figure [Mridula and Pant, J.Atmost. Sol. Terr. Phys., 2017].

A study on the evolution of plasma bubbles using the single station-multisatellite and multistation- single satellite techniques.

The characteristics of plasma bubble-induced ionospheric irregularities were analyzed by estimating the drift velocity of plasma bubbles, their percentage of occurrence, seasonal/LT distributions, and east-west spatial width using multifrequency Global Navigation Satellite Systems (GNSS) receiver systems at Trivandrum, Bangalore, Hyderabad, Delhi, and Hanle. Two techniques, namely, single station - multisatellite and multistation-single satellite observations, were used in the analysis by tracking two geostationary Indian satellites GSAT-8 (PRN 127) and GSAT-10 (PRN 128) for the year 2014. These techniques

are depicted in figure 10. In addition, GNSS receiver data from a recently commissioned near-equatorial station at Changanacherry, Kerala, were used to evaluate 15 plasma bubble events during the period of 29 October 2015 to 31 October 2016. For most of the scintillation events, the values of S4 index lie within the range of 0.2–0.29 for Trivandrum and Bangalore and 0.5–0.59 for equatorial crest station Hyderabad. The number of occurrence of scintillation event was highest during 21:00–21:59 LT for Trivandrum, Hyderabad, and Delhi. For near-equatorial station Changanacherry, the maximum probable LT of occurrence is 22:00–22:59, and 21:00–22:59 for Bangalore. Most of the scintillation/plasma bubble evolution events occurred with drift velocities lying in the range of 120–140 m/s for Trivandrum, Changanacherry, and Hyderabad. For Bangalore, and Delhi, the most probable ranges of drift velocity were 120–160 m/s and 80–100 m/s, respectively. Based on the distributions of east- west width, it is understood that the highest probable value of east-west width for Trivandrum, and Changanacherry, would lie within the range of 100–150 km. However, this parameter would preferably be well within the range of 150–200 km for Hyderabad and Bangalore, and 100–200 km for Delhi.

The drift velocities of irregularities/plasma bubble calculated by both methods at near-equatorial region were of the same order. For single station-multisatellite technique, the IPPs were approximately oriented along east-west direction, which offered an ideal geometry for determining the drift velocity along east-west direction and east-west width of the plasma bubble. But for the multistation-single satellite case, the IPPs were separated along east-west direction and latitudinally also. Since, the single station-multisatellite method has low values of uncertainties compared to multistation-single satellite case, we concluded that the first technique (single station-multisatellite) is superior to the second one (multistation-single satellite) to evaluate bulk motion of plasma bubbles.

Studies and Programmes in Progress

Study of the Venus atmosphere and ionosphere using the radio occultation experiments with the Akatsuki spacecraft

Radio Occultation experiments to study the Venus atmosphere and ionosphere was conducted at the ISRO Deep Space Network, Byllalu using the Akatsuki spacecraft. A listening test was performed on 6-7 January 2017 to assess the quality of the signal received, which was found to be good. The Radio Occultation experiment was performed on 21 March 2017. The data processing is being performed to retrieve the vertical profiles of the Electron density in the ionosphere and the Temperature and Pressure in the neutral atmosphere. The Akatsuki spacecraft offers a unique opportunity to study the low-lattitude regions of the Venus, since it is the first to have an equatorial orbit.

Development of an in-house refractive bending model from first principles to calculate the Doppler shift of an X-band radio signal travelling through a planetary atmosphere and ionosphere

The interaction of radio waves with free electrons in the ionosphere and the molecules in the neutral atmosphere introduces a phase shift in the signal. An attempt has been made to quantify the Doppler shift in the X band signal (8.4 GHz), which is being used for Deep Space communications, due to the planetary atmosphere and ionosphere. Radio Occultation studies have yielded profiles of the neutral atmospheric and ionospheric composition to determine the vertical profiles of refractivity. These are aided by experimental measurements of refractivity by the major constituents of the atmosphere . The model would be used to reduce error in X-band signals, and also to highlight finer details in the signal spectrum, which would provide

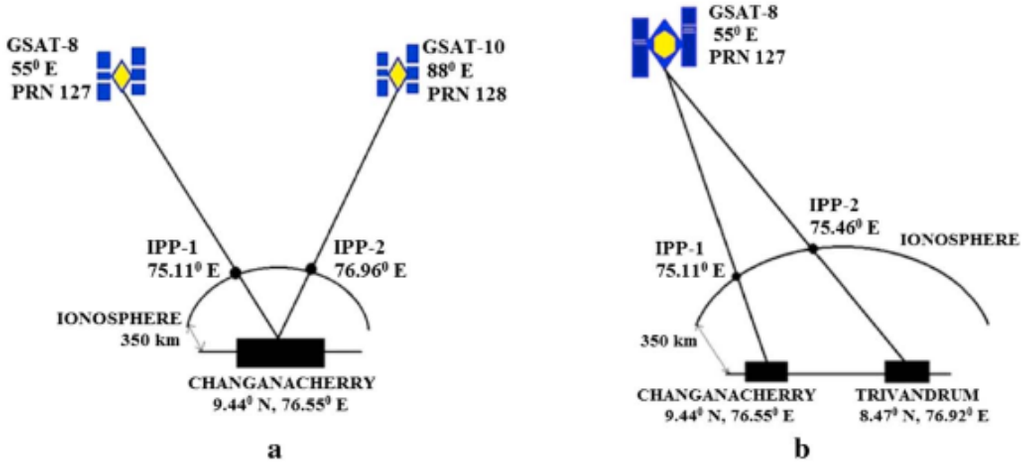

Figure 10. Schematic diagrams of (a) single station-multisatellite and (b) multistation-single satellite observational techniques [Unikrishnan et al., J. Geophys. Res., 2017].

information on the dynamics of the atmosphere. The public domain data available from the MGS mission to Mars is being used to validate the model.

Radio Anatomy of Moon Bound Hyper Atmosphere (RAMBHA) onboard Chandrayaan-2 Lander

RAMBHA is a comprehensive package of two scientific experiments proposed for the forthcoming Chandrayaan2 Lander, to achieve a better understanding of the lunar plasma environment. The two RAMBHA experiments are (i) a Langmuir probe (LP) for in situ measurements of ambient electrons, ions, densities and their temperatures, (ii) a Dual Frequency Radio Science (DFRS) experiment. Both experiments are being developed presently at VSSC, ISAC and ISTRAC. The basic operational parameters and the mechanical/ electrical system aspects related to RAMBHA-LP have been discussed earlier. The RAMBH-LP payload consists of the mechanical module and the electronics module.

The designs of the mechanical/Electronics systems and design reviews/interface meetings have been completed. The mechanical fabrication of EM and QM probes is also completed. The FM realization is underway. The Engineering Model has undergone various developmental testing towards assessing system behavior. The tests conducted include (a) System level deployment test in ambient, (b) Boom structural survivability test, (c) Insulation measurement between LP and Hinge adaptor, (d) Probe current measurement, (e) Trials for cable routing through Boom. For the electronics system, the PCB fabrication is ongoing. EM onboard software is in final stage. QM/FM realization is on-going expected to be completed soon so that the designer level tests on RAMBHA could be done.

Ionization Density and Electric field Analyzer (IDEA) Payload onboard PSLV-C38

Electron density and electric field are the two most important parameters in the ionospheric F region (peak altitude 300-350 km) which play a key role in modulating all the major physical processes in the equatorial and low latitude ionosphere. An experiment using the Ionization Density and Electric field Analyzer (IDEA) payload was proposed onboard the Polar Satellite Launch Vehicle (PSLV) C38 with the objective of measuring electron density and electric field in a polar orbit around the earth at 350 km and flown on June 23, 2017. The overall mission lifetime was just about one day. The measurements not only established the efficacy of IDEA payload in giving simultaneous electron density and electric field measurements in the F region of the ionosphere, but also highlighted the potential of such short term opportunity missions in ISRO's forthcoming ventures.

The IDEA payload consists of the Electron density and Neutral Wind (ENWi) and LP payloads which have been flown earlier during Sooryagrahan Campaign in 2010. In the present experiment the measurements of electron density and electric field were made in F region, according to the dynamic range of the expected currents in the two payloads that were worked out earlier. The changes were incorporated in the electronics to cover the proposed dynamic range (Table 1).

ENWi Probe

Ne	Current
1000/cc	207pA
$1.4x10^6$/cc	360nA

Langmuir Probe

Ne	Current
1000/cc	271nA
$1.4x10^6$/cc	417μA

The electronics was designed to detect the current range of 150pA-400nA in two of its inputs, which connected to the ENWi sensor during mission, and in the range of 250nA-450μA in the input connected to the LP sensor. These were tested in lab using standard variable current sources as well as in vacuum chamber using ion (ENWi) and electron (LP) sources (Fig.11 top and bottom panels respectively).

In general, simultaneous electron density, irregularities and electric field measurements will provide information on the generation and evolution of ionospheric phenomena like Equatorial Ionization Anomaly (EIA) and Equatorial Spread F (ESF) which are important in view of their adverse effects on communication/navigation systems. Further, multiple experiments with the IDEA payload configuration can lead to the fine tuning of the payload parameters for a future polar orbiting satellite mission.

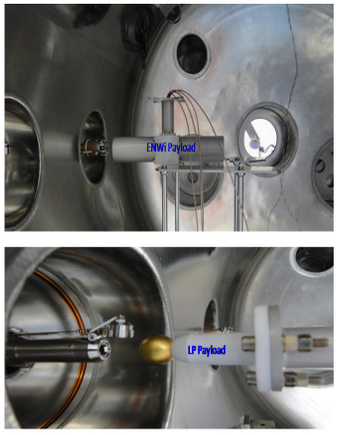

Figure 11: IDEA payload test set up at HVSSF chamber.

Optical modeling of Doppler Asymmetric Spatial Heterodyne Spectrometer (DASH) for thermospheric winds and temperature measurement

A photometric model of the DASH has been developed using the optical design software - TracePro. DASH is modified version of SHS, which is known to be a compact, high performance optical spectrometer similar to Fourier transform spectrometer (FTS) but it provides several crucial advantages compared to FTS and Fabry-Pérot interferometer.

This model will be translated into a ground based DASH system for terrestrial thermospheric winds and temperature measurements. DASH will be capable of measuring the Doppler shift in the thermospheric 630 nm emissions that will be used for retrieving the thermospheric winds, and the temperature information will be extracted from the line shape. This model involves simulation of all the optical components and the extensive ray tracings to optimize the design parameters, which will be implemented in the DASH hardware design. Outputs from this model are optical interferograms, which contain the line shape and the Doppler information of the 630 nm airglow emissions. These interferograms are visualized using the Zemax software. The thermospheric airglow observation design layout of the tuned DASH is shown (Fig. 12). This design includes the entry optics for allowing the sky light to let into the system. With this design, field of view of DASH is 8 degree. The parallel sky-light at multiple-wavelength that comes within 8° field of view are let into the entrance optics. Filtered light of wavelength 630 nm goes through the Interferometer and produces the multi-fringe interferogram of non-zero spatial frequency that is recorded using the CCD. Simulated 630 nm airglow Interferogram obtained is shown in Fig. 13. Fourier analysis of these Interferograms will yield the line spectrum as well as the Doppler information.

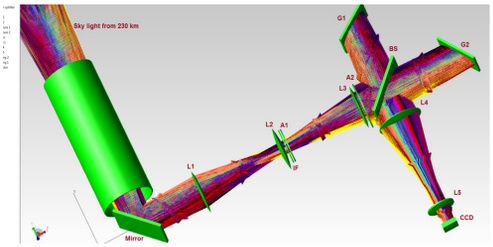

Figure 12:Airglow observation design layout of the tuned DASH.

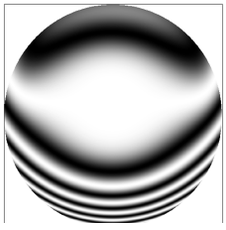

Figure 13: Simulated 630 nm airglow Interference pattern.

New experiments

Doppler imaging Fabry-Perot Interferometer for thermospheric winds and temperature measurements

It is known th at retrieval of thermospheric winds and temperature is crucial to understanding how these parameters drive the electric fields and chemistry that ultimately control the Earth's Thermosphere-iononsphere system. In this context, for comprehensive understanding of several un-answered problems, especially from the equatorial region, development of a Doppler imaging Fabry-Perot Interferometer (FPI) with the capability of thermospheric winds and temperature measurements was undertaken. Development of this FPI has been completed. The system has been commissioned recently at TERLS and is operational now. Central to this system is a 10 cm clear aperture etalon with a 1.5 cm air gap [FSR ~ 0.13 Å; FWHM ~ 0.013 Å]. Other crucial optics used in this system is a telecentric lens system that matches the etendue telecentrically with the a narrow-band interference filter [CW 630nm, FWHM 4 Å]. It samples the thermospheric OI 6300 Å nightglow emission at four cardinal directions (45° elevation angle) and the zenith to measure the wind-induced Doppler shifts, which then are used to retrieve the winds. Fig. 14 shows first results of the thermospheric winds and temperature measurements over Thumba on 18.06.2017 using this FPI.

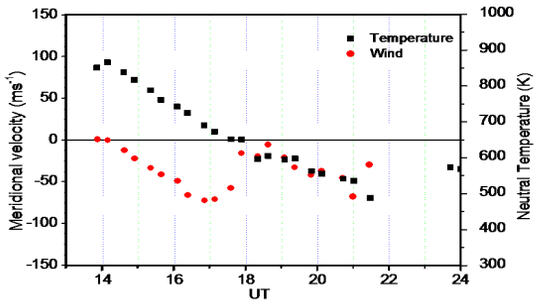

Figure 14: First spectrometeric measurements on the nighttime thermospheric winds and temperature over Thumba on 18.06.2017.

High resolution scanning Grating Monochromator

For their detailed investigations of Mesosphere-Lower Thermosphere-Ionosphere (MLTI) obtaining high resolution spectral information of the airglow emissions at wide wavelength range are crucial. In this context, development of a 2-meter focal-length scanning high resolution grating spectrometer was undertaken. Development of this spectrometer has now been completed. The system has been installed recently and is operational now. This spectrometer currently has resolution ~ 0.033 - 0.043 Å. It provides wide wavelength coverage (185-860 nm) with the use of two diffraction gratings of 1800 grooves/mm and 2400 grooves/mm.

Future Projections

Two of the important immediate goals of ITMP are to (a) complete the development of the flight model of the proposed RAMBHA payload in time for Chandrayaan-2 mission, (b) develop, install and commission the proposed AAVTAR. Apart from these, efforts are on to launch the next phase of activity under the INSWIM program. In this program, ground based optical and radio experiments will become operational in a network mode. A laboratory for the atmosphere ionosphere studies from Antarctica

has been proposed to be established in coming years. This laboratory will house among others, the ionospheric thermospheric experiments like the ionosonde and optical spectro/photometers and facilitate measurements round-the-year. We also envisage that the new Spatial Heterodyne Spectrometer and the Multiwavelength Alltime Airglow Photometer, being developed in-house, will soon be field tested and operational. These new experimental capabilities will be used to strengthen and facilitate measurements to understand various aspects of the atmosphere-ionosphere, magnetosphere-ionosphere and Sun-Earth coupling processes.

Publications in Peer-Reviewed Journals

1. Aswathy R. P. and G. Manju, Gravity wave control on ESF day to day variability: an empirical approach, Journal of Geophysical Research (Space Physics), doi:10.1002/ 2017JA023983 (2017).
2. Madhav Haridas, M. K., G. Manju, and T. Arunamani, Solar activity variations of nocturnal thermospheric meridional winds over Indian longitude sector, Journal of Atmospheric and Solar Terrestrial Physics, 147, 21–27, doi:10.1016/j.jastp.2016.06.010 (2016).
3. Thampi, S. V., P. R. Shreedevi, R. K. Choudhary, T. K. Pant, D. Chakrabarty, S. Sunda,S. Mukherjee, and A. Bhardwaj, Direct observational evidence for disturbance dynamo on the daytime low-latitude ionosphere: A case study based on the 28 June 2013 space weather event, Journal of Geophysical Research (Space Physics), 121, doi:10.1002/2016JA023037 (2016).
4. Mridula N., Tarun Kumar Pant., On the role of horizontal wind shears in the generation of F0.5 layers over the dip equatorial location of Thiruvananthapuram: A numerical simulation study, Journal of Atmospheric and Solar Terrestrial Physics, doi:10.1016/j.jastp.2017.02.005 (2017).
5. Unnikrishnan, K., H. Sreekumar, R. K. Choudhary, V. M. Ashna, K. M. Ambili, P. R. Shreedevi, and P. B. Rao, A study on the evolution of plasma bubbles using the single station-multisatellite and multistation-single satellite techniques; Journal of Geophysical Research (Space Physics), 122, 3678–3688, doi:10.1002/2016JA023503 (2016).
6. Bhardwaj, A., T. K. Pant, R. K. Choudhary, D. Nandy, and P. K. Manoharan, Space Weather Research: Indian Perspective, Space Weather, 14, doi:10.1002/2016SW001521 (2016).
7. Sneha Yadav, R. Sridharan, Surendra Sunda, Tarun K. Pant: Further refinements to the Spatio temporal forecast model for L-band scintillation based on comparison with C/NOFS observations: Forecast model for L-band scintillation. Journal of Geophysical Research (Space Physics), 04/2017; doi:10.1002/2017JA023869 (2017).
8. Surendra Sunda, Sneha Yadav, R. Sridharan, M. S. Bagiya, P. V. Khekale, Pan Singh, S. V. Satish, SBAS-derived TEC maps: a new tool to forecast the spatial mapsof maximum probable scintillation index over India, GPS Solutions, doi: 10.1007/s10291-017-0625-6 (2017).
9. Sneha Yadav, R. Sridharan, Surendra Sunda, Impact of the 17 March 2015- St. Patrick's Day storm on the evolutionary pattern of equatorial ionization anomaly over the Indian longitudes using high resolution spatio-temporal TEC maps -New insights, Space Weather,14, doi:10.1002/2016SW001408 (2016).
10. Deepak K. Karan, Duggirala Pallamraju, Kedar A. Phadke, Tatiparti Vijayalakshmi, Tarun K. Pant, Shyamoli Mukherjee: Electrodynamic influence on the diurnal behaviour of neutral daytime airglow emissions. Annales Geophysicae 11/2016; 34(11):1019-1030, doi:10.5194/angeo-34-1019-2016 (2016).

Technical/Scientific reports

1. Mridula N and Tarun Kumar Pant, Mean And Extreme Bounds Of Atmospheric Temperature For The Altitude Of 60 km To 1000 km Over SHAR Region, SPL-SR-01-2017, June 2017.
2. Ratan Singh Bisht, Nitesh Thapa, Anshul Kumar Porwal, Limb Viewing Hyper Spectral Imager (LiVHySI) onboard YOUTHSAT-01 : Observations and Results, SAC, Ahmedabad, [contributions from Tarun Kumar Pant, SPL, VSSC], October 2016.

Presentations in Symposia/Workshops/Conferences

1. Aswathy R. P. and G. Manju, Gravity wave control on ESF day to day variability :An empirical approach 29th Kerala Science Congress, Pathanamthitta, Kerala, January 28-30, 2017.
2. Aswathy R.P. and G. Manju, Gravity wave control on ESF day to day variability, URSI-RCRS, Tirupathi, Andhra Pradesh, March 1-4, 2017.

3. Tarun Kumar Pant and Mridula N, Layering of Ionosphere, URSI-RCRS, Tirupathi, Andhra Pradesh, March 1-4, 2017.

4. C. Vineeth, N. Mridula, K. K. Kumar and T. K. Pant Meteoric Activity and Counter Electrojet: An intriguing Connection, URSI-RCRS, Tirupathi, Andhra Pradesh, March 1-4, 2017.

5. Sneha Yadav, S. Sunda, and R. Sridharan, "The impact of the 17 March 2015- St. Patrick's Day storm on the evolutionary pattern of Equatorial Ionization Anomaly over the Indian longitudes using high resolution spatio-temporal TEC maps – New insights", 3rd URSI-Regional Conference on Radio Science (URSI-RCRS-2015), Tirupati, India, 1-4 March 2017.

6. Sneha Yadav, R. K. Choudhary,Tarun K. Pant, and S. Sunda, "Impact of sudden stratospheric warming event of 2009 on the low-latitude ionosphere of the Indian zone", 3rdURSI-Regional Conference on Radio Science (URSI-RCRS-2015), Tirupati, India, 1-4 March 2017.

7. C. Vineeth and G. Manju, First User Scientists Workshop on ST Wind Profiler Radar Applications, Advanced Centre for Atmospheric Radar Research, CUSAT, Kochi, 9-10 February 2017.

8. Ajesh A and Aswathy R. P., Seminar GNSS Aids and Applications, Institute of Radio Physics and Electronics, University of Calcutta, 23 September, 2016.

9. Mridula N., attended National Workshop on Space Applications for Sustainable Growth and Advancement (SAGA), held at Thiruvananthapuram, 19-20 May, 2017.

10. Ajesh A., International School on Space Science, (by SCOSTEP/ ISWI, at Smt. Kasturbai Walchand College, Sangli, Maharashtra, 7-17 November 2016.

Invited Talks and Public Outreach

Dr. T. K. Pant

1. "Space Research : Perspective from SPL-ISRO", 1st INSPIRE Workshop International Satellite Program in Research and Education, National Central University, Taiwan (Invited Talk through Skype), 21 July, 2016.

2. "SENSE: Payloads from SPL, "Satellite for Near Earth Space", Physical Research Laboratory, Ahmedabad, 30 August, 2016.

3. "GNSS Aids and Applications: Ionosphere/Atmosphere Perspective, GNSS Aids and Applications", Institute of Radio Physics and Electronics, University of Calcutta, 23-24 September, 2016.

4. "Sun Earth Connections: Emerging Perspective", DST's IMPRESS program, Indian Intitute of Geomagnetism, Mumbai, 22-24 February, 2017.

Dr. C. Vineeth

1. "Remote Sensing of Earth's Near Space: Techniques and Challenges", V. V. College of Science and Technology, Kanjikkode, Palakkad, 13 January 2017.

2. Convenor, Functional Committee for Resource Material Generation, World Space Week 2016, VSSC.

3. Member, Functional Committee for Printing and Publications, World Space Week 2016, VSSC.

4. Focal Person, Lecture at School, World Space Week 2016, VSSC.

Training Programme

1. Dr Manju G and Dr. Smitha V Thampi, Structured Training Prgram : "Challenges in Space Science & Exploration", SPL, VSSC, 13-17 March, 2017.

2. Dr. Smitha V Thampi, First National Finite Element Developers/FEAST users meet, VSSC, 12 December 2016.

3. Dr. C. Vineeth, HRDD training on "Certified Ethical Hacking", VSSC, 5-9 December 2016.

Planetary Science Branch

The Planetary Science Branch (PSB) of SPL is carrying out front line research on various planetary science aspects using theoretical/modeling approaches, ground-based as well asspace-based telescopic observations, and experiments on planetary missions. Planetary science branch plays lead role in planetary exploration by actively participating in developing scientific payloads for the space and planetary missions of ISRO as well as analysis and interpretation of the scientific data. The research and development activities of PSB is categorised under four major themes. These themes are (a) interaction of solar radiation with planetary atmospheres and the processes initiated through this interaction, (b) solar wind and its interaction with different planets and planetary objects, (c) planetary neutral atmospheres through in-situ observations , and (d) planetary surface and sub-surface characteristics including the mineralogy and thermal aspects. These themes have, in the past, necessitated the development of experiments like Sub-keV Atom Reflecting Analyzer (SARA) and Mars Exospheric Neutral Composition Analyzer (MENCA) onboard ISRO's Chandrayaan-1 and Mars Orbiter Mission (MOM) that have led to path breaking results. Presently, experiments like PAPA are being developed for ISRO's forthcoming Chandrayaan-2 and Aditya-L1 missions.

The High Vacuum Space Simulation Facility (HVSSF) of SPL, which is catering to the development, testing and calibration of scientific payloads developed within VSSC as well from outside ISRO, is getting augmented as per the developmental needs of scientific payloads. In addition, a clean room facility is setup at SPL for the payload development. The overall research activities under the four broad scientific themes are described in the following sections

Scientific Faculty
Anil Bhardwaj*
Satheesh Thampi R.
Vipin Kumar Yadav
Dhanya M. B.
Abhishek J.K

Research Fellows
Vrinda Mukundan
Govind G Nampoothiri

Research Associates
Megha Bhatt

Other Contributors
Smitha V Thampi#

Technical Team
Sreelatha P
Pradeepkumar P
Tirtha Pratim Das
Neha Naik
Dinakar Prasad Vajja
Rosmy John
P G Anumod
Aneesh A N

* Took charge as Director, PRL in March 2017
\# Faculty, ITMP, SPL

Interaction of solar radiation with planetary atmospheres

A photochemical model for the dayside ionosphere of Titan

Photoionization of the gases N_2 and CH_4 in the atmosphere of the Saturnian moon Titan initiates a complex chain of chemical reactions, causing the production of heavy hydrocarbon and nitrogen bearing molecules, radicals, ions, along with a suit of free electrons. We have developed a one dimensional photochemical model to understand the complex chemistry scheme in the ionosphere of Titan and to calculate the density profiles of major ions and electrons, which are generated as a by-product of the chemistry on the dayside ionospheric region. An energy deposition model is also developed, which describes the absorption of solar UV radiation using Beer Lambert law. The attenuated solar flux, thus obtained is used for calculating photoelectron production rate, which is subsequently used in the calculation of steady state photoelectron flux by employing an Analytical Yield Spectrum (AYS) approach. AYS for N_2 available in the literature is combined with the AYS of CH_4, which has been developed using Monte Carlo technique (Bhardwaj and Mukundan, Planet. Space. Sci., 2015) to obtain the composite yield spectrum which is subsequently used in the calculation of photoelectron flux. Primary production rate of major primary ions, like N_2^+, N^+, CH_4^+, CH_3^+, etc. due to photon and photoelectron impact are calculated. The ion production rate is used as input to a photochemical model which includes ion-neutral chemistry. The production and destruction reactions of various ions are taken in the model to calculate the number density of different ionic species and electron. We concentrated on the T40 flyby of Cassini orbiter and used the in-situ measurements from instruments onboard Cassini as input to the model.

It has been found that the model calculated electron density is higher than the observation by a factor of 2 to 3 around the peak when compared to the observations made by the instruments onboard Cassini mission viz. the Ion Neutral Mass Spectrometer (INMS) and Langmuir Probe (LP) (Fig.1). We studied the impact of different model parameters, viz. Photoelectron flux, ion production rates, electron temperature, dissociative recombination rate coefficients, neutral densities of minor species, and solar flux on the calculated electron density to understand the possible reasons for this discrepancy.

Recent studies have suggested that the overestimation of plasma density is likely related due to the overproduction of suprathermal electrons by the models. We studied the impact of the exaggerated photoelectron fluxes on plasma density calculations and could find that decreasing the photoelectron flux by the suggested amount decreases the electron density only by 10 to 20%. This shows that exaggerated photoelectron fluxes may not be an important factor in causing aberrance in the modeled electron density. Our model shows that plasma densities are very sensitive to electron temperature and any improvement in this parameter can help in the betterment of ion and electron density calculations. The use of different available density profiles of minor neutral species HCN and NH_3 have noticeable impact on the calculated densities of the major ions $HCNH^+$, $C_2H_5^+$, and CH_5^+; however, the overall impact on electron density is not appreciable (< 20 %) due to the coupled chemistry between these three ions. Even though increasing the dissociative recombination rate coefficients of the ions $C_2H_5^+$, and CH_5^+ by a factor of 10 reduces the difference between modeled and observed densities of the major ions, the modeled electron density is still higher than the observation by ~60% at the peak. We show that the use of different solar flux models (HEUVAC, SEE and S2K) can cause only about 15% change on the modeled electron densities.

The Cassini observed density profiles are consistent with model calculations when we varied the parameters which influence the loss of ions and electrons, viz. electron temperature and dissociative electron recombination rate coefficients. This shows that even though the over-estimation in the production parameters, namely photoelectron flux and primary production rate of N2+, may contribute towards the disagreement between the modeled and observed plasma density profiles to some extent, a more significant role is played by the loss processes. It is probable that some important chemical reactions are missing that may account for the additional loss of ions and electrons.

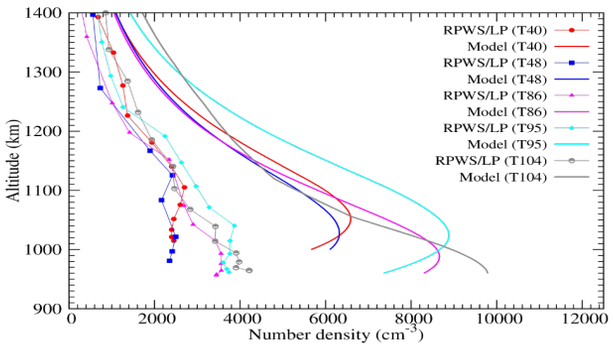

Figure 1: Modeled and measured electron density profile for the dayside ionosphere of Titan for the Cassini flybys T40, T48, T86, T95 and T104. Symbols show the electron density measured by the Langmuir Probe onboard the Cassini orbiter during these flybys and the solid lines are the modeled profiles for the corresponding flybys [Vrinda and Bhardwaj et al. Icarus, 2017].

Solar wind and its interaction with planets and planetary bodies

Science results from the SARA experiment onboard Chandrayaan-1

Discovery of a new population of Suprathermal protons around Moon

A new population of suprathermal protons (H^+) has been observed around the Moon by the Solar Wind Monitor (SWIM)/SARA. The observations were made when the Moon was located outside Earth's bowshock. The

observed protons are found to have energy of about 1.5 to 3 times that of solar wind. The energy-time spectrogram for such an event observed in orbit 1915 on 15 April 2009 (~13:29 to 15:27 UT) is shown in Fig.2a. In this orbit, SWIM had observations on both dayside and in the lunar plasma wake region (night side of the Moon). The strong signal seen around 15.0 h UT (marked as 'A') corresponds to solar wind observations on the dayside. The signal 'B' with energies comparable to that of solar wind corresponds to the protons in the near-wake region. The population marked as 'C' observed across the terminator to the night side of the Moon, with energies as high as 2.5 to 3 times that of solar wind (>1800 eV) is the new population of ions. The velocity distribution of the protons is in the plane defined by the component of ion velocity parallel to the convective electric field (VE), and the velocity component perpendicular to both the convective electric field (Ec) as well as the interplanetary magnetic field (BIMF) constitutes a partial ring shaped distribution (Fig.2b). The mass analysis suggests m/q=1. The component of the ion velocity parallel to the BIMF (VB) is as large as 200 km s−1 (Fig.2c), suggesting that the ions are of nonthermal origin. The pitch angle distribution of the ions indicates that the ions have their dominant velocity component perpendicular to BIMF (Fig.2d). Thus, the observed ions are protons of non-thermal origin (suprathermal protons) which travel under BIMF and Ec. To investigate the origin of these protons, the trajectories of the ions are constructed using a backtracing model. The trajectories (Figs.3a–3f) show that the observed ions pass through the minimum height of the cycloid at altitudes >500 km above the dayside lunar surface, indicating a high-altitude source. This is further seen from the plot of the speed of these ions as a function of the altitude above the dayside lunar surface (Fig.3g), where the velocity minimum suggest an extended source located at altitude >500 km. Similar events have been observed in several other orbits of Chandrayaan-1.

In order to explain the observed suprathermal protons, several possible sources are considered, which include ionization of ionization of backscattered lunar energetic neutral hydrogen atoms, ionization of lunar exospheric hydrogen, inner source pickup ions, interstellar pickup ions, ionization of neutral solar wind, and solar wind H^+ reflected from Earth's bow shock. The comparison of the observed flux (density) with that expected from these sources and the velocity distribution suggests that an

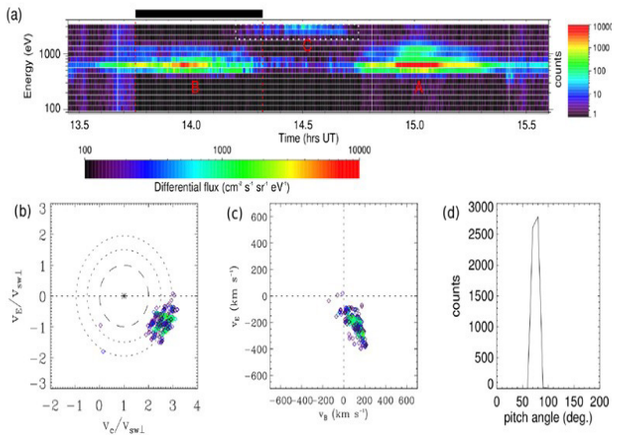

Figure 2: (a) Energy-time spectrogram from SWIM observations in orbit 1915 on 15 April 2009 during ~13:30–15:30 UT. The black filled box on the top of the panel indicates the time interval when SWIM made observations in the lunar wake. The red dotted vertical lines mark wake entry and exit timings. The high-energy signals (>1800 eV) across the terminator to the wake (signal marked as 'C') are enclosed within the white rectangle. (b) The velocity distribution of the population 'C' in the Vc-VE plane normalized with the solar wind velocity component perpendicular to BIMF (Vsw⊥) for the high-energy event ('C'). Vc is the ion velocity component perpendicular to both the convective electric field (Ec)and the interplanetary magnetic field(BIMF), and VE is the ion velocity parallel to Ec. The value of Vsw⊥ (~260 km s-1) is averaged over the time interval of the high-energy event. The dashed inner circle is centered at (+1, 0) indicated by an asterisk with unit radius and represents the distribution expected for zero initial velocity ions of m/q = 1. The two dashed inner and outer circles centered at (1, 0), and passing through the data points with radius = 1.5 and 1.9, respectively, represent the boundaries of the ring-shaped distribution. (c) Velocity distribution in the VB-VE plane, where VB is the component of ion velocity parallel to BIMF. (d) Pitch angle distribution of the ions [Dhanya et al., Geophys. Res. Let., 2017].

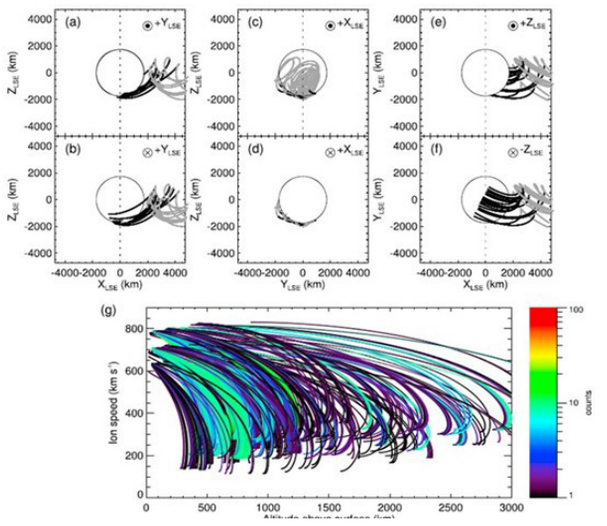

Figure 3: Trajectories of the suprathermal protons during the backtracing projected in different planes in aberrated Lunar Centric Solar Ecliptic (aLSE) coordinates. In aLSE coordinates, the x axis is antiparallel to the solar wind velocity (Vsw), the z axis is towards the ecliptic north, and the y axis completes the right-handed coordinate system. (a) XaLSE-ZaLSE plane as viewed from +YaLSE, (b) XaLSE-ZaLSE plane as viewed from −YaLSE, (c) YaLSE -ZaLSE plane as viewed from +XaLSE, (d) YaLSE-ZaLSE plane as viewed from −XaLSE, (e) XaLSE-YaLSE plane as viewed from +ZaLSE, and (f) XaLSE-YaLSE plane as viewed from −ZaLSE. In each panel, the black curves indicate the first part of the trajectories (before the first velocity minimum) as backtraced from the observed location. The remaining part of the trajectory is shown in grey. (g) Ion speed during backtracing as a function of altitude above the dayside lunar surface. The velocity profile is shown only up to the first velocity minimum (first part of the trajectories during backtracing). The color bar indicates the particle counts observed in a given energy and direction bin of SWIM that are backtraced [Dhanya et al., Geophys. Res. Let., 2017].

additional source is required to explain the population. This indicates that our knowledge about Moon is still limited and calls for further exploration. These observations are also important to understand the environment of any non-magnetized body without atmosphere in our solar system as well as exoplanetary systems.

First observation of Energetic Neutral Atoms from the Lunar Night side Surface

SARA observed for the first time, the energetic neutral atoms that originate from the lunar night side surface (Fig.4). Figs. 4(a)-(d) show that ENAs are not confined to the lunar dayside surface, and there is a substantial amount of ENAs from just beyond the terminator, which are seen forming a wide ring structure parallel to the terminator. Two distinct hydrogen ENAs are observed with distributions parallel to the terminator. The spectral shape, and the intensity

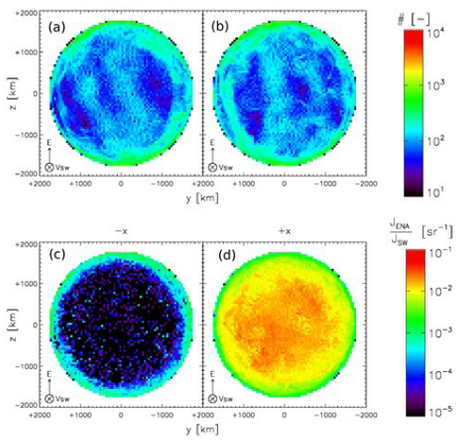

Figure 4: Projections of lunar ENA observations in the y-z plane of a coordinate system where the origin of the system is at the center of the Moon, the x direction points toward the Sun, i.e., antiparallel to the solar wind velocity (-Vsw), the z axis is along the convective electric field of solar wind (E), and the y axis completes the right-hand system. (a) Number of observations as viewed along the −x hemisphere (lunar night side), (b) Number of observations as viewed along the +x hemisphere (lunar dayside), (c) Differential ENA flux divided by the divided by the number of observations and the solar wind flux (sr-1) as viewed along the −x hemisphere (lunar night side), (d) Differential ENA flux divided by the divided by the number of observations and the solar wind flux (sr-1) as viewed along the +x hemisphere (lunar dayside) [Vorburger et al., Geophys. Res. Let., 2016].

indicate that these particles originate from the bulk solar wind flow. The first distribution reaches ~6° into the night side, and is explained by the kinetic temperature of the solar wind protons. The second distribution reaches up to 30° beyond the terminator with a maximum at solar zenith angle of ~102°, and this population has been identified as due to acceleration of solar wind protons by the ambipolar electric field and by the negatively charged lunar night side surface. This study not only showed the surface interaction of solar wind accessing the near wake region, but also provided the first observations indicative of the solar zenith angle dependence of the positive dayside surface potentials

Solar wind interaction with the Mercury

Both the Moon and Mercury possess surface bound exosphere. However, Mercury is a magnetized planet, which makes the interaction of solar wind with Mercury a unique scenario. Based on the knowledge of the solar wind scattering from the Moon, the scenario of similar process happening at Mercury is investigated.

The solar wind plasma precipitation on Mercury happens through (1) dayside open field lines referred to as cusp; (2) closed field lines connected to the plasma sheet referred to as aurora; (3) dayside closed field lines referred to as nose; and (4) the 'direct precipitation' where the high solar wind dynamic pressure pushes the magnetopause below the Hermean (Mercury) surface. The empirical angular scattering function and the energy spectrum derived for the ENAs and for the protons scattered from the Moon based on the SARA observations are used for a range of incident plasma parameters since the solar wind conditions at Mercury are different from that of the Moon. From these, the differential fluxes of hydrogen ENAs and the protons from Mercury are estimated for the different plasma precipitation conditions happening on Mercury. The results are shown in Fig. 5.

Results suggest that surface-scattering is a strong source of ENAs at Mercury (up to ~10^8 cm^{-2} s^{-1}). Surface scattered protons are also found to be significant with high fluxes up to ~10^7 cm^{-2} s^{-1}. The significant ENA flux will be very useful for remote-sensing of the plasma conditions at the surface. The scattered protons are important for wave generation and the filling in of the loss cone of mirroring and quasi-trapped populations. These results are important to interpret the measurements by the upcoming Bepicolumbo mission to the Mercury.

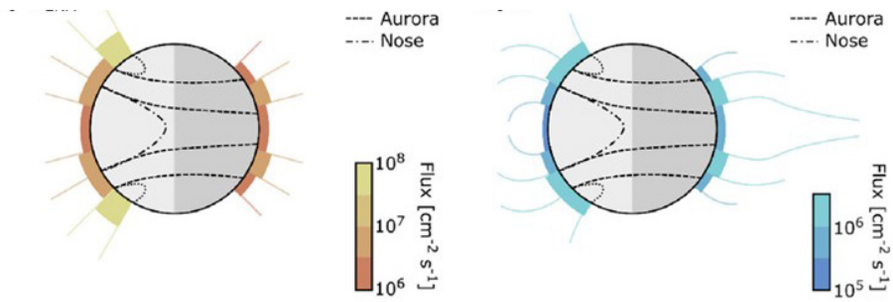

Figure 5: Illustration of the expected flux of (1) hydrogen ENA (HENA), and (b) H+ scattered from the surface of Mercury. The dotted, dashed and dash dotted curves enclose different regions of plasma precipitation onto the Hermean surface. The direction of the Sun is towards the left hand side in each panel of the figure [Lue et al., Icarus, 2017].

Plasma Analyzer Package for Aditya (PAPA) onboard the Aditya-L1 mission

The developmental activities of Plasma Analyser package for Aditya (PAPA) for the upcoming Aditya-L1 mission is in full pace. The Preliminary Design Review (PDR) of PAPA payload has been completed and accordingly major action items given by the committee are being pursued vigorously for the timely completion of the payload. Engineering model of PAPA subsystems like Front End Electronics (FEE), High Voltage Programmable Power Supply (HVPPS) and PAPA Processing Unit (PPU) are in progress. The time of flight (ToF) design has been completed and the proto model fabrication is in progress. The Engineering Model (EM) of the Electrostatic Analyser section (ESA) of the PAPA payload has been thoroughly characterized for its energy and angular responses. The standard 18mm (active detector area) MCP was used as the detector. The entire testing and characterization of ESA was carried out in the High Vacuum Space Simulation Facility(HVSSF) of SPL. The data were acquired using the laboratory data acquisition system. Prior to the ESA testing, complete characterization of MCP detectors (six numbers) were carried out for choosing the optimum detector for ESA. The salient features of the detectors as well as the ESA testing and characterization are described in the subsequent sections.

Pulse Height Analysis of Micro Channel Plates

Micro Channel Plates (MCPs) are highly sensitive charged particle detectors, which are being planned to use as the detector for PAPA payload. Their operation principle is based on electron avalanche generated between two ends of a semiconducting glass tube, which are maintained at a potential difference of about 2000V. The electron avalanche, being highly dependent on the number of electrons generated at each successive levels of collisions, can yield a range of gain values.

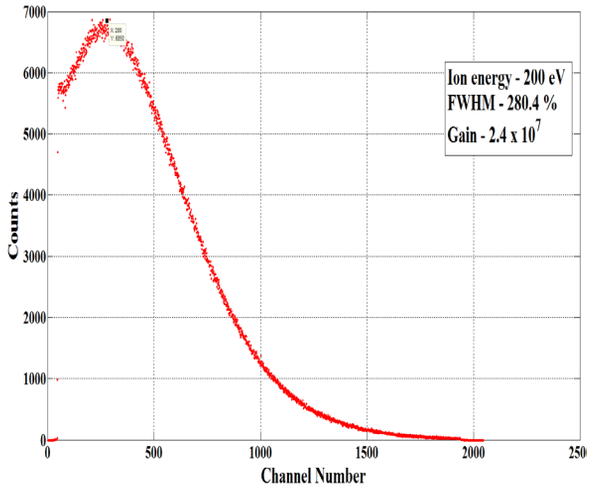

Figure 6: Plot of Pulse Height Distribution of MCP for ion energy of 200 eV when biasedat a voltage of 1800V.

In order to accurately count the number of particles, it is essential to calculate the gain and the FWHM values of the gain distribution. This was carried out for four good quality MCPs and corresponding results compared and given below. It is observed that all the four MCPs shows a gain of ~ 10^7 when they were biased at a voltage range of 1800-2000 V. Fig. 6 shows a typical Pulse Height Distribution (PHD) curve of 18 mm MCP for incoming ions of 200 eV energy when it was biased at 1800 volts. The pulse height distributions are sufficiently narrow, which indicates the consistency of MCPs.The pulse height distribution matches with the pattern given by the manufacturer in the range of 1700-1900V. The gain values also match with the manufacturer specified values. Table 1 summarises the values of gain obtained for four MCP detectors based on their characterisation.From the above set of experiments, MCP-2 was chosen as the optimum detector to be used for ESA. The major characteristicsof MCP-2 are listed below in Table 2.

Table 1: Normal Gain of the MCP at 2000 V voltage

MCP Serial number	Nominal gain
MCP-2	10^7
MCP-4	10^7
MCP-5	10^7
MCP-6	10^7

Table 2: Characteristics of MCP-2

Parameter	Value
Resistance (ohm)	570 (Ohm)
Dark Count	Less than 5 counts/sec/cm^2
Gain	10^7
Ideal Working Voltage	1700 -1900 V

Testing and Calibration of Electrostatic Analyser (ESA) of PAPA payload

Energy Angle calibration

The ESA part of PAPA payload was tested for energy filtering and angular filtering properties using singly charged positive ions of He, Ar and Xe.Fig. 7 shows the energy response of ESA for He ions at different energies. The energy resolution of ESA for He ions at 100 eV is shown in Fig.8. Apart from energy resolution, various other quantifiable parameters such as analyser constant, angular resolutions etc. were determined and compared with the simulated results. Fig.9 shows the comparison of theoretical and experimental analyzer constant for ESA and shows better matching. Fig.10 shows the angular response of ESA for He ions at 100 eV energy. The results matches well with simulations and thus validate the performance of the ESA.

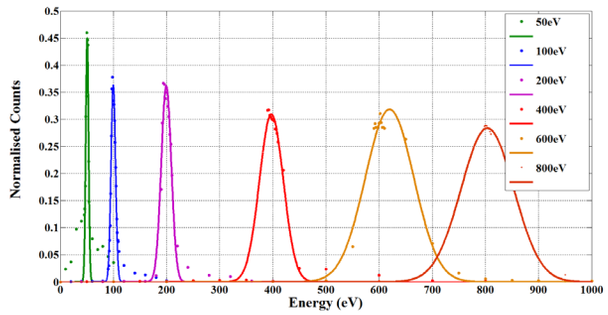

Figure 7: Response of ESA for different energies of He ions.

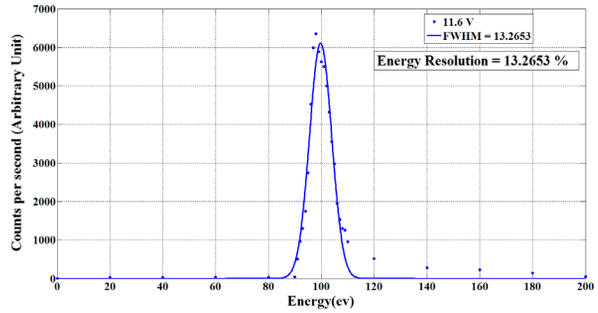

Figure 8: Energy resolution testing for He ions at 100eV.

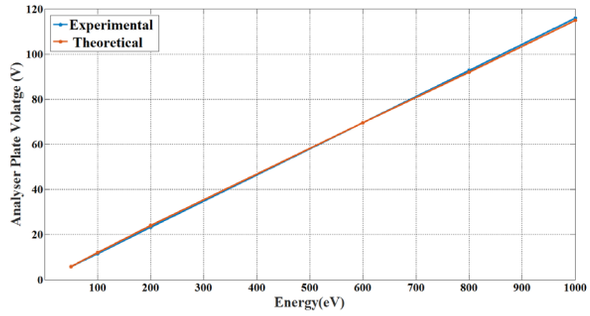

Figure 9: Experimentally determined Analyser constant andsimulation results at different energies.

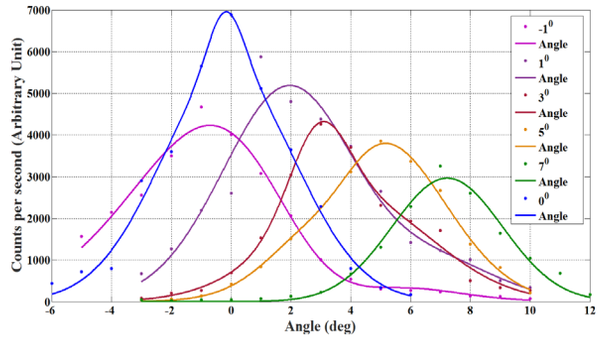

Figure 10: Angular response of ESA for He Ions at 100 eV energy.

Solar plasma waves studies with magnetic field measurements at L1 point:

As a prelude to analyse the data expected to come from the magnetic field experiment onboard Aditya-L1 spacecraft, an attempt has been made to detect the long period plasma (Alfven) waves at L1 point using the interplanetary magnetic field (IMF) data from WIND and ACE spacecraft's. On analysing the magnetic field data from fluxgate magnetometers (FGM) onboard WIND and ACE, it is observed that distinguished pattern as observed on January 10, 2015, was initiated on January 09, 2015 and lasted till January 11, 2015 as shown in Fig.11.

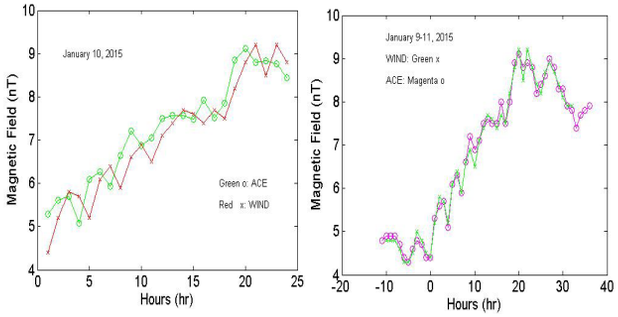

Figure 11: IMF on January 10, 2015 as measured by WIND and ACE [Vipin, U.J.Phys. Appl. 2016].

The possible cause of this could be the plasma (Alfven) waves emanating from the Sun. The correlation between the proton velocity and the magnetic field comes out to be 0.66 for WIND and 0.74 for ACE spacecraft. For Alfven waves, there is an exact correlation between the magnetic field and the velocity of ions which are stick to the magnetic field lines. This good correlation is another evidence of the presence of Alfven waves at L1 point.

Estimation of the electric potential developed on a spacecraft

Spacecraft potential is the amount of charge acquired by a spacecraft when it is passing through a plasma environment in space and this charging effect can have serious consequences on the sensitive electronic equipments onboard a spacecraft that need to be maintained within specified voltage levels, deviations from which may eventually lead to system failures. Hence, it is important to estimate the spacecraft charging while designing a spacecraft in the initial stages as well as measure it during its operation. Prior to design a spacecraft, it is prudent to simulate the space environment and the charging of spacecraft on ground using numerical programmes. An effort has been initiated by me to precisely model the spacecraft-plasma interactions and estimate the subsequent charging with a computer program, SPIS (Spacecraft Plasma Interaction System). Subsequent to it the plan is to compare the simulation outcomes with laboratory experiments.

Study of planetary neutral atmospheres/ exospheres

Mars Exospheric Neutral Composition Analyzer (MENCA) onboard Indian Mars Orbiter Mission (MOM)

The Mars Neutral Composition Analyzer (MENCA) aboard the Indian Mars Orbiter Mission (MOM) is a neutral mass spectrometer, which provides the in-situ measurement of the low latitude neutral exosphere of Mars. MENCA consist of an ionizer to ionizer the incoming neutral species, and subsequent mass analysis and a detector system consisting of channel electron multiplier and Faraday Cup.

Science Results from MENCA onboard MOM

Suprathermal Argon in the Exosphere of Mars

The altitude profiles of Argon-40 (Ar), which is a minor constituent in the Martian exosphere, are studied using MENCA observations. The observations correspond to four orbits during December, 2014 (Martian Solar Longitude (Ls) period of 250°-257°, when MOM was closest to Mars (MOM's periapsis was the lowest). The upper limit of Ar number density corresponding to this period is ~ 5×10^{5} cm^{-3} (~250 km), and the typical scale height is ~16 km, corresponding to an exospheric temperature of ~275 K. However, on two orbits, the scale height over this altitude region is found to increase significantly making the effective temperature > 400 K. Fig.12 shows the mean trend of the altitude variation of the number density of Ar, derived from two typical orbits each. The scale height derived from mean trend of observations during December 10 and 13 is ~16 km, which translates to an exospheric temperature of 275 K that is consistent with the previous estimates. However, if we consider the mean trend of altitude variation derived from the exponential fits for the other two orbits, a mean scale height of 26 km is obtained (Fig.13, blue line). In this case, the corresponding exospheric temperature is above 400 K, indicating the presence of a suprathermal population of argon atoms on these days.

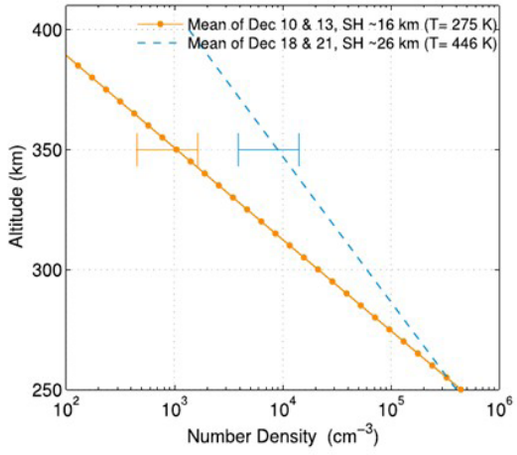

Figure 12: Mean trend of the altitude variation of the number density of Ar, derived from two typical orbits each. The error bars represent the mean uncertainty level. SH is the scale height, and T is the exospheric temperature derived from scale height [Bhardwaj et al., Geophys. Res. Lett., 2017].

The Neutral Gas and Ion Mass Spectrometer observations on the Mars Atmosphere and Volatile Evolution mission also indicate that a change in scale height in Ar and CO_2 densities occurs near the upper exosphere (around 230–260 km). These observations confirm significant suprathermal CO_2 and Ar populations in the Martian exosphere. Significant wave-like perturbations are observed but only on certain days when suprathermal population is seen. Pickup ion-induced heating is discussed as the other viable source.

MENCA Payload Operation Centre (POC) at SPL

The MENCA Operation Centre in SPL is the nodal point for the MENCA operation, data reception and the monitoring of the health of MENCA. The MENCA data is received regularly at the POC from the Indian Space Science Data Center (ISSDC). Housekeeping (HK) data files are received and processed regularly and quick look plots of the relevant HK parameters are generated for assessing the health of MENCA.

The pipeline for MENCA data archival as per the international Planetary Data System (PDS) standards has been jointly developed by SPL and SAC, which was successfully installed and functional at ISSDC. The pipeline has been generating the data sets required Long Term Archive (LTA) of MENCA data, which is meant for release to general public. The first of data sets around Mars from Mars Orbiter Mission (MOM) has been successfully released to public on 24-09-2016. The various activities towards release of the second year data sets of MOM to public are also in progress.

New Initiatives

New initiatives are being made to understand the solarwind and its dynamics using existing data from missions like SOHO, WIND, ACE etc. to study the following specific scientific objectives

- To trace the origin of the shape of the solar wind electron velocity distribution functions (EVDFs) and to study its evolution from solar coronal heights to large radial distances from the Sun, which yields information about the physical processes associated with the acceleration region.
- To study of the role of suprathermal electrons on the EVDFs will give insights in to the physical mechanisms behind solar wind particle acceleration.
- The study of the nature of solar wind EVDFs during solar transient events such as solar flares. This will give more insights into the dynamics happening in the solar wind during the transient events and it will help to study

about the possibilities of energy transport mechanisms from radiative events to particles.

- Composition of Jupiter Irregular Satellites:Three Jovian irregular satellites; Himalia (JVI), Elara (JVII), and Carme (JXI), using the SpeX instrument onthe NASA IRTF are being studied to identify spectrally dominant minerals.This could provide us with insights into a narrow time window when our Solar System was forming.Initial modeling results of Himalia and Elara suggest a very reduced environment with negligible amount of Fe3+ present on these bodies. Also phyllosilicates are present in each case indicate the past aqueous alteration in the parent body(s) of these irregular satellites.
- Compositional studies of Mare Moscoviense using Chandrayaan-1 VIS-NIR data:Spectral and elemental maps of mare Moscoviense, derived using the Moon Mineralogy Mapper (M3) and Infrared Spectrometer-2 (SIR-2) data-sets. A total of five distinct spectral units from the basin floor based on the spectral properties have been identified. Detailed analysis of the entire Moscoviense basin indicates that the concentrations of orthopyroxene, olivine, and Mg-rich spinel, named as OOS rock family are widespread and dominant at the western and southern side of the middle ring of the basin with one isolated area found on the northern side of the peak ring.

Augmentation and refurbishment of High Vacuum Space Simulation Facility

Major steps have been taken to attain necessary capabilities for the testing and calibration of a suit of instruments, currently under development, in SPL's High Vacuum Space Simulation Facility (HVSSF). An ion source based on the principle of Electron Cyclotron Resonance (ECR), which can supply mono charged positive ions with energies in the range of 1keV-30keV, and an electron source which can generate continuous as well as controlled bursts of electrons are being procured. Both the electron and ion sources are equipped with beam steering and focussing capabilities. A mu-metal shield which ensures a magnetic interference free region inside the vacuum chamber is also being procured. The shield was designed to accommodate the vacuum pumping ports, viewing ports, Job manipulator and the charged particle beam entry mechanisms. Further, to understand the effect of UV photons on solar wind measuring instruments a UV source is being procured. This will help to characterise the effectiveness of the UV suppression system and ebanol-C coating employed in the PAPA payload. The detector characterisation chain is well established and its capability has been demonstrated by the successful energy-angle calibration of PAPA ESA bench model. Several automation modules which can control instrument biasing, instrument rotation and count measurements have been created and demonstrated.

To ensure safe operation of sensitive instruments, antistatic tables have been deployed in the payload assembly room. Fig. 13 shows the photograph of the refurbished HVSSF lab. HVSSF is currently being utilized for the testing and calibration of the payloads such as PAPA onboard Aditya-L1, CHACE-2 onboard Chandrayaan-2 and IDEA on PSLV C38. Apart from these, payloads developed outside ISRO such as the METEOR smoke particle detector of VIT are also being tested and calibrated in the facility.

Figure 13: Photograph of the refurbished HVSSF lab.

Future Projections

Immediate Goals

The analysis of SARA data to investigate the transport of solar wind scattered from the dayside lunar magnetic anomalies to near lunar plasma wake region, and the presence solar wind protons reflected from the Earth's of bow shock in near lunar environment is progressing. Analysis of NIR spectral data from Chandrayaan-1 mission integrated with other lunar mission's data-sets will be continued to characterize spectral units from the mare regions.The spectral characteristics of swirls will be identified in the NIR wavelength region and its association to the magnetic anomalies will be studied in detail. Regarding PAPA, the immediate goals include testing and Calibration of the Time of Flight (TOF) Section of PAPA payload, characterising the UV response of the PAPA payload and testing the efficiency of UV trap and ebanol-C coating. Testing and characterisation of flight model of CHACE-2 payload to be flown aboard Chandrayan-2 will also be pursued in fast track mode.

Long Term Goals

Development of plasma analyzersfor the upcoming planetary missions (Mars Orbiter Mission-2 and Venus). Studies of plasma environment of planets Mars and Venus using available mission data.Continuation of Mineral and morphological studies of Mars surface using MOM-MCC and MRO datasets. Development of Plasma Wave Detectors (PWD) and Energetic Neutral Atom (ENA) detectors.

Publications in Peer-Reviewed Journals

1. Anil Bhardwaj, Smitha V. Thampi, Tirtha Pratim Das, M.B. Dhanya, Neha Naik, Dinakar Prasad Vajja, P. Pradeepkumar, P. Sreelatha, Abhishek J.K., R. Satheesh Thampi, Vipin K. Yadav, B. Sundar, Amarnath Nandi, G. Padma Padmanabhan and A.V. Aliyas, "Observation of Suprathermal Argon in the Exosphere of Mars", Geophysical Research Letters, 44, 2088 – 2095; doi:10.1002/2016GL072001 (2017).
2. M. B. Dhanya, A. Bhardwaj, Y. Futaana, S. Barabash, M. Wieser, M. Holmström, and P. Wurz, "New suprathermal proton population around the Moon: Observation by SARA on Chandrayaan-1", Geophysical. Research Letters, 44, doi:10.1002/2017GL072605 (2017).
3. Vorburger, A., P. Wurz, S. Barabash, Y. Futaana, M. Wieser, A. Bhardwaj, M.B. Dhanya, K. Asamura, "Transport of solar wind plasma onto the lunar nightside surface", Geophysical Research Letters, 43, 10, 586-10,594, doi:10.1002/2016GL071094 (2016).
4. Lue C, Y. Futaana, S. Barabash, M. Wieser, A. Bhardwaj, P. Wurz, K. Asamura, Solar wind scattering from the surface of Mercury: Lessons from the Moon, Icarus, 296, 39 – 48; doi: 10.1016/j.icarus.2017.05.019 (2016).
5. Anil Bhardwaj, Tarun Kumar Pant, R.K. Choudhary, Dibyendu Nandy, P.K. Manoharan, "Space Weather Research -Indian Perspective, Reprise of 2001 Space Weather Monograph", Space Weather, 14, 1082-1094; doi:10.1002 /2016SW001521 (2016).
6. Vipin K. Yadav, "Plasma Waves in the Sun"; Universal Journal of Physics and Applications; 10 (6), 193-197; doi:10.13189/ujpa.2016.100603 (2016).
7. Prakash Chauhan, Anil Bhardwaj, P. Senthil Kumar, Prabhjot Kaur, and N. Bhandari, "Understanding our celestial neighbours: An Indian perspective in planetary sciences and exploration", Proceedings of Indian National Science Academy, 82 (3), 403-423, doi:10.16943/ptinsa/2016/48457 (2016).
8. Smitha V. Thampi, P.R. Shreedevi, R.K. Choudhary, Tarun Kumar Pant, D. Chakrabarty, S. Sunda, S. Mukherjee and Anil Bhardwaj, "Direct observational evidence for Disturbance Dynamo on the daytime low latitude ionosphere: A case study based on the 3 June 28, 2013 Space Weather Event", Journal of Geophysical Research, 121, 10,064 -10,074, doi:10.1002/2016JA023037 (2016).
9. R.K. Choudhary, K.M. Ambili, Siddhartha Choudhary, M.B. Dhanya and Anil Bhardwaj, "On the origin of the ionosphere at the Moon using results from Chandrayaan-1 S-Band Radio Occultation Experiment and a photochemical model", Geophysical Research Letters, 43, 10,025-10,033; doi:10.1002/2016GL070612 (2016).
10. Vrinda Mukundan, Anil Bhardwaj, "Dayside ionosphere of Titan: Impact on calculated plasma densities due to variations in the model parameters"; ICARUS, 229, 222-239, doi:10.1016/j.icarus. 2017.07.022 (2017).

Publications in Proceedings

1. Rasul Muthu A., Vipin K. Yadav and Shefin Shoukath, "Solar plasma wave studies at L1 point with magnetic field measurements from magnetometers"; Proceedings of International Conference on Advanced Communication, Control and Computing Technologies (ICACCCT-2016); May 25-27, 2016; Syed Ammal Engineering College, Ramanathpuram, Tamil Nadu. Page: 298-302; IEEE: CFP 1521T-ART; ISBN: 978-1-4673–9545-8; doi:10.1109/ ICACCCT.2016.7831650.

Scientific/Technical Report

1. PAPA-Modes of operation, on-board Data Processing requirements; PAPA-SPL-VSSC-AP-02-2016, September 2016.
2. Preliminary Design Review Document for the Plasma Analyser Package for Aditya (PAPA) Payload of Aditya-L1 Mission; PDR-PAPA-SPL-VSSC-01, November 2016.

Presentations in Symposia/Workshops/Conferences/Seminars

International

1. Megha Bhatt, Vishnu Reddy, Karsten Schindler, Ed Cloutis, Anil Bhardwaj, Lucille L. Corre and Paul Mann; "Spectral similarities between Jupiter irregular satellite Himalia and main belt c-type asteroids"; Lunar and Planetary Science Conference (LPSC); March 20-24, 2017, The Woodlands, Texas, USA.
2. Megha Bhatt, Urs Mall, Christian Wöhler, Anil Bhardwaj, Arne Grumpe, Daniela Rommel; "Spectral characterization of mare Serenitatis using Chandrayaan-1 data"; Lunar and Planetary Science Conference (LPSC); March 20-24, 2017, The Woodlands, Texas, USA.
3. Megha Bhatt, Christian Wöhler, Arne Grumpe, Daniela Rommel, Anil Bhardwaj, Urs Mall; "Study of mare Moscoviense using VIS-NIR spectrometers on-board Chandrayaan-1"; 41st COSPAR Scientific Assembly, 2016.
4. M. B. Dhanya, Anil Bhardwaj, Yoshifumi Futaana, Stas Barabash, Martin Wieser, Mats Holmstrom, Peter Wurz, and Abhinaw Alok, "Protons in the Near-Lunar Plasma Wake from SWIM/SARA on Chandrayaan-1", Joint 13th Asia Pacific Physics Conference and Australian Institute of Physics Congress (APPC-AIP), December 4-8, 2016; Brisbane Convention and Exhibition Centre, Brisbane, Australia.
5. Raksha J. Jathanna, Vipin K. Yadav, Surekha Kamath and Anil Bhardwaj, "Estimation of the charging effects on a Spacecraft", The 3rd Conference on Astrophysics and Space Science (APSS-2017); January 3-5, 2017, Bangkok, Thailand.
6. Vipin K. Yadav, Neha Gugar and Anil Bhardwaj, "Alfven wave detection at first Lagrangian point with magnetic field measurements"; 3rd URSI Regional Conference in Radio Science (URSI RCRS-2017); March 01–04, 2017; Tirupati, Andhra Pradesh, India.
7. Audrey Vorburger, Peter Wurz, Stas Barabash, Martin Wieser, Yoshifumi Futaana, Anil Bhardwaj, M.B. Dhanya, and Kazushi Asamura, "The Moon observed in Energetic Neutral Atoms: Review of the Scientific Findings from SARA/CENA on board Chandrayaan-1", EGU General Assembly, April 23-18, 2017; Vienna, Austria.
8. Vrinda Mukundan and Anil Bhardwaj, "Photochemical modeling of the ionosphere of the Saturnian moon Titan"; Common Wealth Science Conference 2017, June 13 - 16, 2017, Singapore.

National

1. Vrinda Mukundan and Anil Bhardwaj, "Calculation of ion production rates and electron density profiles for the dayside ionosphere of Titan"; 29th Kerala Science Congress, organized by Kerala State Council for Science, Technology and Environment (KSCSTE) jointly with KFRI; Mar Thoma College, Pathanamthitta, Kerala 28–30 January, 2017.
2. Vrinda Mukundan, TIFR School on Advances in Atomic Collisions (TISAAC); Homi Bhabha Center for Science Education (HBCSE), Mumbai, March 6-18, 2017.
3. Vipin K. Yadav, "Science from magnetometer"; First Workshop: Science with Aditya-L1 Mission; B.M. Birla Auditorium, Jaipur, Rajasthan, March 06, 2017.
4. Satheesh Thampi and PAPA team, "Science Objectives of PAPA payload on board Aditya-L1mission" XXXV Meeting of Astronomical Society of India (ASI-2017); B.M. Birla Auditorium, Jaipur, Rajasthan, March 06–10, 2017.
5. Vipin K. Yadav and Anil Bhardwaj, "Solar Plasma (Alfven) wave observation at L-1 point with the magnetic field measurements"; XXXV Meeting of Astronomical Society of India (ASI-2017); B.M. Birla Auditorium, Jaipur, Rajasthan, March 06–10, 2017.
6. Govind. G. Nampoothiri, R. Satheesh Thampi and Anil Bhardwaj, Nature of solar wind suprathermal electrons during different class of solar flare events in the ascending phase of 24th Solar Cycle, XXXV Meeting of Astronomical Society of India (ASI-2017); B.M. Birla Auditorium, Jaipur, Rajasthan, March 06–10, 2017.

Deputations

1. Megha Bhatt; Scientific discussions on the spectral characterization of lunar mare regions using Chandrayaan-1 data; Max Planck Institute for Solar System Research, Goettingen, Germany, July 16–30, 2016.

2. M.B. Dhanya; Joint 13th Asia Pacific Physics Conference and Australian Institute of Physics Congress (APPC-AIP); Brisbane Convention and Exhibition Centre, Brisbane, Australia; December 4-8, 2016.
3. Anil Bhardwaj; Science Week Lecture, University of Mauritius, Mauritius, September 28, 2016.
4. Anil Bhardwaj; Frontiers in Theoretical and Applied Physics (FTAPS-2017), American University of Sharjah (AUS), Sharjah, UAE, February 22, 2017.
5. Vrinda Mukundan; Common Wealth Science Conference by the Royal Society, London, Singapore, June 13–17, 2017.

Invited Talks

Anil Bhardwaj

1. "Solar-Planetary-Moon Connection", IIA-ISAC National Symposium on Exoplanets, Kodaikanal Observatory, Kodaikanal, Tamilnadu; October 7-8, 2016.
2. India to Mars: The Indian Mars Orbiter Mission (MOM), TWAS Young Scientists Conference on "Frontiers in Earth, Climate and Ocean Sciences", Indian Institute of Science (IISc), Bangalore, December 6, 2016.
3. "Solar System and Planetary Exploration", Lecture at The Bangalore Science Forum, in National Science College, Basavanagudi, Bangalore; January 18, 2017.

Vipin K. Yadav

1. "Plasma Waves in the Universe", Indian Institute of Geomagnetism (IIG); Navi Mumbai, Maharashtra, March 10, 2017.
2. "Plasma Instrumentation and Waves in Universe", Institute for Plasma Research (IPR); Gandhinagar, Gujarat, April 12, 2017

Megha U. Bhatt

"Spectral Analysis of Mare Moscoviense and Mare Serenitatis using VIS-NIR Spectrometers on-board Chandrayaan-1", Space Application Centre, Ahmedabad, Gujarat, July 11, 2016.

Public Outreach

Anil Bhardwaj

1. "Moon eliciting man's curiosity since time immemorial", Talk at All India Radio, Trivandrum, in context of First Human Landing on Moon; July 22, 2016.
2. "Indian MOM", Invited Lecture at NCETE-16, Lourdes Matha College of Science and Technology, Kuttichal, Trivandrum, August 9, 2016.
3. "Indian MOM", Fresher's Day Lecture, Indian Institute of Space Science and Technology (IIST), Trivandrum; August 10, 2016.
4. Interaction with about 400 students from Rural Schools World Space Week celebrations, Dr. Srinivasan Auditorium, VSSC, October 5, 2016.
5. "Planetary Science: My work, talk at Felicitation program and seminar at Kerala Academy of Sciences, Trivandrum, December 23, 2016.
6. "Solar System", National Seminar on Trends in Theoretical Physics, Department of Physics, University College, Trivandrum, January 13, 2017.

M.B. Dhanya

1. Member, Functional Committee for Resource Material Generation, World Space Week 2016, VSSC.
2. Member, Functional Committee for Printing and Publications, World Space Week 2016, VSSC.

Distinguished Talks / Colloquiums

1. "India to Mars: The Mars Orbiter Mission (MOM)", Science Week Lecture, University of Mauritius, Mauritius, September 28, 2016.
2. "MOM and SARA: Mars and Moon, Institute Lecture at Indian Institute of Technology, Kanpur, November 7, 2016.
3. INSA Vainu Bappu Memorial Medal Lecture, INSA Annual Meeting, NISER, Bhubaneswar, December 29, 2016.
4. "A New View on Solar Wind - Moon Interaction from SARA/Chandrayaan-1", Frontiers in Theoretical and Applied Physics (FTAPS-2017), American University of Sharjah (AUS), Sharjah, UAE, February 22, 2017.

Convening of Scientific Sessions

Anil Bhardwaj

Chairman, Editorial Committee, Centre Hindi Seminar, VSSC, July 19-20, 2016.

Satheesh Thampi

1. Chairman, Sub-committee, SPL day lecture, 17th March, 2017.
2. Member, Organising committee, Structured Training Programme (STP-2017); SPL, VSSC, March 13-17, 2017.

Vipin K. Yadav

1. Member, Sub-committee, Structured Training Programme (STP-2017); SPL, VSSC, March 13-17, 2017.
2. Member, Editorial Committee, Centre Hindi Seminar, VSSC, July, 2017.

M B Dhanya

Member, Sub-committee, [Assigning Projects to team members, preparing Questionnaire, and arranging for evaluation of project presentation]; Structural Training Program (STP-2017); SPL, VSSC, March 13-17, 2017.

Training Programme

1. Vipin K. Yadav; Structured Training Program – 2016: "Sensor Payload Data Processing and Value Addition for Strategic Applications", ADRIN, Secunderabad, Telangana, November 21-26, 2016.
2. Vipin K. Yadav; Structured Training Program – 2017: "Challenges in Space Science and Exploration"; SPL / VSSC, Thiruvananthapuram, Kerala, March 13-17, 2017.
3. M.B. Dhanya and Vipin K. Yadav; VSSC in-house Training "Certified Ethical Hacking"; June 12-16, 2017.

Atmosphere Technology Division
Spaceborne Instrumentation Section

Atmosphere Technology Division (ATD) focuses on the development of satellite, rocket- and balloon-borne scientific payloads and ground-based systems for insitu probing and remote sensing of the Earth's atmosphere and space environment and planetary atmospheres. ATD is also responsible for augmentation and maintenance of the ongoing experimental systems, providing technical support to the scientific activities of SPL and development of common technical facilities. It works in close coordination with the scientific branches of SPL and provides technical expertise for realization of the scientific ideas. The Space Borne Instrumentation Section (SBIS) provides design, development and testing support for the scientific payloads of SPL.

Engineers

Mohan Kumar S.V.*
K. Rajeev
P Sreelatha
P. Pradeepkumar
Tirtha Pratim Das
M. Shajahan
Dinakar Prasad Vajja
Neha Naik
N. Manikantan Nair
P. P. Pramod
M. Mohammed Nazeer
P. S. Ajeeshkumar
Rosmy John
P. T. Lali

Technical Team

G. S. Asoka Kumar
Uttam S Purty
P. G. Anumod
B. Satheesh Kumar
A. N. Aneesh

* Superannuated in August 2016

Development of Payloads onboard Chandrayaan-2

Development of CHandra's Atmospheric Composition Explorer-2 (CHACE-2)

CHandra's Atmospheric Composition Explorer-2 (CHACE-2) is a quadrupole neutral mass spectrometer based instrument scheduled to fly onboard Chandrayaan-2 and is meant for studying the lunar neutral exosphere from 100 km circular polar orbit. Table 1 presents the specifications of the CHACE-2 instrument.It has the heritage of CHACE-1 onboard Chandrayaan-1 and MENCA onboard MOM-1, but with improved features. Summary of the development and characterisation are provided below.

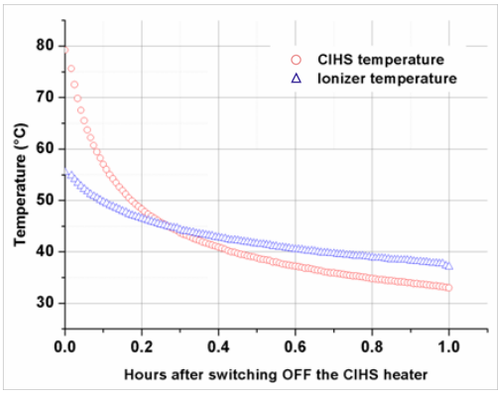

Figure 2: Temperature evolution of the CIHS and the CHACE-2 ionizer wall when the CIHS heater is switched OFF.

Mass range	1 to 300 amu (programmable through telecommand), with 1 amu mass resolution
Ionization technique	Electron impact ionization
Sensors	Quadrupole Mass Analyser (QMA) for relative abundance measurement and Bayard-Alpert (B/A) gauge for total pressure measurement
Detectors	Faraday Cup and Channel Electron Multiplier (CEM)
Mass budget	4.15 kg (including the power module)
Power Budget	30 W raw power for nominal operations

Thermal experiments

CHACE-2 features a heater shroud surrounding the ionizer section of the CHACE-2 sensor called the CHACE-2 Ionizer Heater Shroud (CIHS), equipped with a 5 W heater, in order to keep the sensor warm. This will facilitate accelerated removal of the adsorbed volatiles, while the payload is switched OFF. Experiments were performed to characterize the radiative heat transfer from the CIHS to the wall of the ionizer of the CHACE-2 sensor. Figures 1 and 2 show the temperature evolution of the CIHS and the ionizer wall, when the CIHS heater is switched ON and OFF respectively at a pressure level of 5×10^{-6} Torr. In steady state, an increase of the ionizer wall temperature by ~30°C has been recorded. The thermal time constants for heating and cooling of the ionizer wall are observed as 1.1 hours and 0.3 hour, respectively.

Study on the CHACE-2 system noise

The system noise of CHACE-2, which limits its detection threshold, was characterized using the sensor inserted in Ultra High vacuum of 10^{-9} Torr at the UHV laboratory of SPL. The ionizer of the sensor is switched OFF and hence the dark current data represent the system noise.The system noise in the mass spectrum is characterised by measuring the dark current observed at different scan rates and are subjected to statistical analysis (Fig.3), which revealed a normal distribution of noise with mean around zero and standard deviation varying with the scan rate. Figure 4 shows that the noise floor systematically increases with mass scan rate.The dark current representing the system noise follows Normal distribution, with mean zero and standard deviation as a function of the integration time (determined by the mass scan rate in points per second). The sensitivity of the detector system is ~10 A/Torr, which indicates that the minimum detectable partial pressure is less than 10^{-14} Torr. This complies with the sensitivity requirement for detecting the lunar exospheric species at an altitude of 100 km.

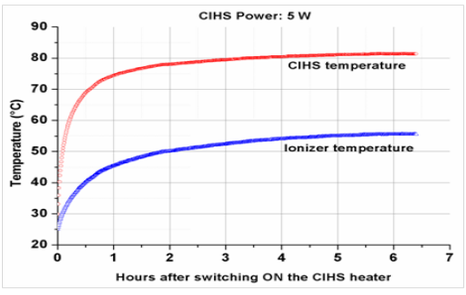

Figure 1: Temperature evolution of the CIHS and the CHACE-2 ionizer wall when the CIHS heater is switched ON.

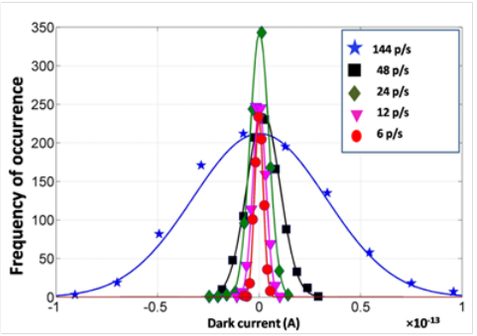

Figure 3: Frequency distribution of the noise data for different scan rates.

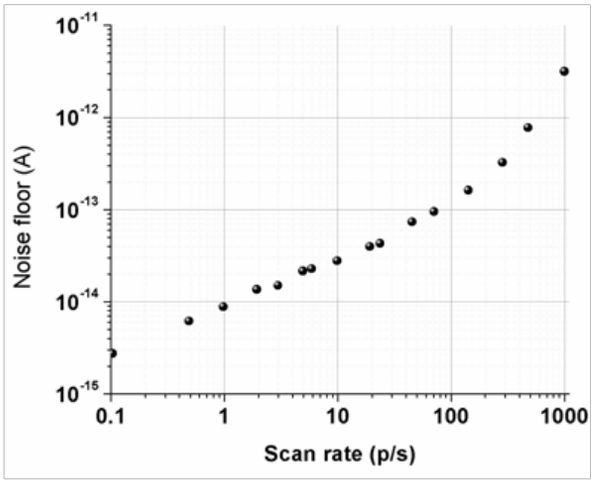

Figure 4: Variation of the noise floor with the mass scan rate.

Throughput versus mass resolution optimization in quadrupole mass spectrometer

In a quadrupole mass spectrometer, the mass resolution is determined by the intersection of the operating line (bias curve) of the quadrupole mass analyser with the Paul stability regions, obtained by solving the Mathieu's differential equation. The slope of the bias curve in the Paul stability plane controls the mass resolution of a quadrupole mass filter, which, in turn, can be changed by varying the DC and RF voltages applied at the quadrupole rods. The mass resolution affects the throughput of the quadrupole mass filter; better mass resolution (sharper mass peak) decreases the throughput. An experiment is conducted at the UHV laboratory, SPL where the mass spectra of the residual gases were acquired at a stabilized pressure of 5×10^{-7}Torr at different mass resolutions. The experiment was conducted with a CEM detector bias voltage of 1400 V, focus voltage of -20 V and ion energy of 4.5 eV. It is observed that for a variation of the mass resolution from 112 to 16 (corresponding variation of Δm is from 0.25 amu to 1.77 amu), the throughput increases by a factor of ~40 (Fig.5).

In order to probe the trace constituents of a planetary upper atmosphere or exosphere, it is often desirable to have higher throughput of the mass filter, when the mass resolution is not an essential requirement. This improves the signal strength of a peak. This technique of optimization between mass resolution and throughput will be useful for probing planetary exospheres, especially for extending the range of the radial profiling of the constituents.

Channel Electron Multiplier (CEM) Gain

An experiment was conducted to study the dependence of the gain of the Channel Electron Multiplier (CEM) detector on the mass (m) of the incident ions and the bias voltage (V) of the CEM. The mass-dependent gain of the CEM de-emphasizes the signals corresponding to the heavier species and emphasizes the ones for the lighter species. The main objective of this experiment was to derive the mass-dependent gain profile of the CEM, which will be a divisive correction factor towards restoring the correct relative abundances of the different species detected by the mass spectrometer.Ultra high vacuum of $\sim8\times10^{-9}$Torr is achieved in the vacuum chamber. First, the mass spectrum obtained after disabling the CEM so the only functional detector is the Faraday Cup detector which has no internal

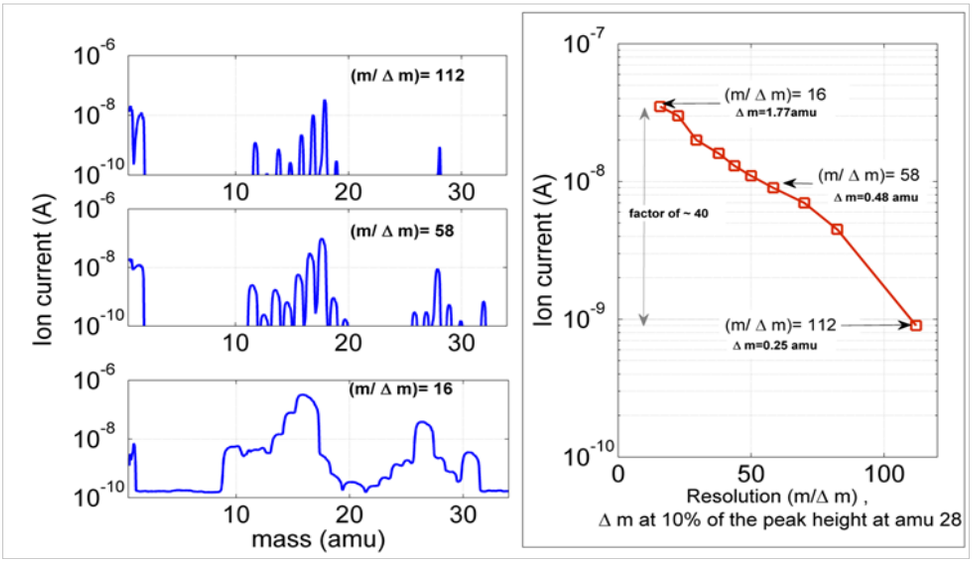

Figure 5: (Left panel) Mass spectra of the residual gases acquired at a stabilized pressure of 5×10^{-7}Torr at three different mass resolutions of the quadrupole mass filter, with idential detector bias voltage, ion injection energy and other parameters (m= 28 amu and Δm is the peak width at 10% of the peak height). (Right panel) Variation of the ion current with mass resolution for amu=28.

gain. This was followed by mass spectrum determination after enabling CEM. The strengths of the peaks obtained using only Faraday Cup and the CEM-Faraday Cup combination were compared in order to compute the CEM gain at different mass bins. Only the peaks whose

respective signal strengths are stabilised are used for the comparison and gain calculation.

Variation of the gain (G) with ion mass (m) for different bias voltages (Fig.6) show that the CEM gain consistently decreases with the increasing ion mass.

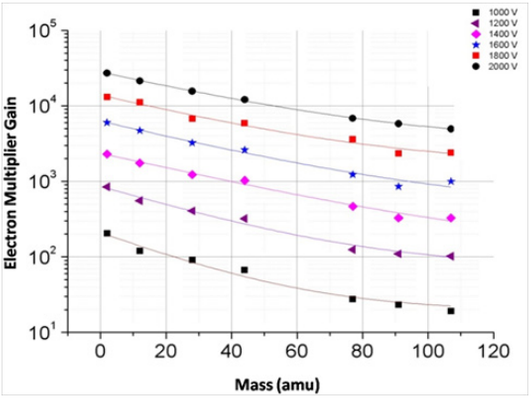

Figure 6: Variation of CEM gain with ion mass for different bias voltages.

Development of Onboard Electronics of CHACE-2 (OSCOT)

Engineering version of the Onboard System for CHACE-2 Operation Telecommand-Telemetry (OSCOT) has been developed and tested. The FPGA-based OSCOT card incorporates all necessary circuits for flawlessly controlling and interfacing the mass spectrometer sensor with various spacecraft systems like BDH, TM, OBT and TC through MIL-STD-1553 interface. The OSCOT is assembled and tested successfully meeting all the project requirements. The following are the major challenges and milestones achieved in this activity.

a) The requirement of telecommand based program upload has been implemented and tested. The onboard program can be uploaded byte by byte or in bulk.

b) The 'telecommand based onboard program switching on the fly' has been successfully implemented and tested. This requirement demands the onboard processor to fetch the next instruction from the newly selected memory and not from the current program memory, which it normally does within 42ns. This TC based program switching also was implemented and tested in a precise manner.

c) All interfaces like MIL-STD-1553, SPI, UART and 8/16 bit parallel bus were tested.

d) This system has two masters (Microprocessor and the Mil-Std-1553 controller) asynchronously controlling and sharing the common resources with proper handshaking having a priority based response time of a few microseconds.

e) The system requires the interfacing of the devices with multiple bus widths of 8 and 16 bits.

A detailed characterization of the telecommands along with the instrument response had been carried out in the laboratory environment. This has helped to finalize the packet structure of the telecommands for the mission.

The FPGA code for the OSCOT card has been fully developed and implemented and is ready for satellite interface test. The CHACE-2 onboard firmware had been implemented and programmed in to the EEPROM of OSCOT. The qualification and flight models (QM and FM) of the OSCOT card circuit design, PCB design and fabrication had been completed.

CHACE-2 Onboard Software, CISDAT

Entire operation of CHACE-2 is based on the onboard software called CISDAT (CHACE-2 Integrated Software for Data Acquisition, Telemetry and Telecommand) residing in the onboard memory. Structure chart of CISDAT is shown in Fig.7. The software has been developed in assembly language for 8051S microcontroller core embedded in FPGA. The CISDAT comprises of several modules, which communicate with one another in order to realize the total functionality of the software.Various processes of the CISDAT are: (i) read initializations and default configuration from PROM, send the codes directly to the PCCU, (ii) read commands from PROM, modify and store the same in RAM and send the commands from RAM to the PCCU, (iii) acquire data from the PCCU and verify the data and store the same in RAM, (iv) update BDH descriptor after acquiring 1Kbytes to transfer though 1553B, (v) process telecommand by modifying configuration accordingly, (vi) read configuration from PROM/EEPROM (if flag is set), modify and store configuration in RAM and send the same from RAM to the PCCU, and (vii) update TM descriptor after accessing TM sub-addresses to transfer through 1553B.The programming sequence of CISDAT is as follows (Fig.7): (i) Initialization of 8051S controller, (ii) Initialization of 1553B controller, (iii) Initialization of PCCU, (iv) Load ARM Memory. The data acquisition has the following steps: (i) Start Sweep, (ii) Get Sweep Data, (iii) Get Operating Status, (iv) Process Telecommand if received, (v) Load Operating Parameters. Software Design Details Document (SDD) is generated and software development (EM) has been completed. Integrated testing of the software with the hardware and checkout system is in progress.

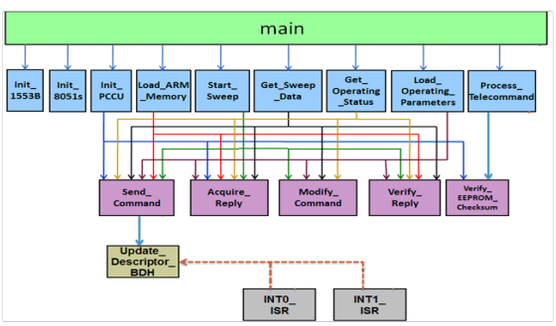

Figure 7: Structure Chart of the CISDAT.

CHACE-2 Checkout System Development

An integrated CHACE-2 checkout system (Fig.8) is being developed on a PXIe system using LabVIEW, to test all the interfaces on ground. The hardware of the CHACE-2 checkout system is a PXIe based system with a 1553 interface card and a multichannel DAQ card. The 1553 interface card is programmed for the BDH and digital TM interfaces as per the requirements of the payload, which involves precise timings for various data transfers and onboard activities. The BDH data is acquired as per an onboard data ready flag status which is probed at precise time intervals. The digital TM data is acquired from both main and redundant channels alternatively at prefixed durations. The checkout system also sends an onboard timer for synchronization of the onboard system with the clock signals. All these operations are time tagged and is programmed to function synchronously in a specific sequence. However, the telecommands are configured as user defined events and are sent asynchronously. The TC selection and servicing is configured in such a way that it does not affect the normal operation of the data acquisition on the same 1553 bus. The BDH data separation, processing and plotting module to generate online plots of the data acquired from the payload is also integrated with the other modules in the same LabVIEW program. The analog and digital DAQ card is used to acquire the analog TM data and to generate pulse commands for the DC-DC converter and reset pulse for the payload. A separate LabVIEW program has been made for this purpose. All the data are displayed on separate windows.

which showed that the probe resistance and the outputs are identical in the two cases. The laboratory-based test setup is shown in Fig.9. The probe performance was also evaluated in hot test at 70˚C and cold test at -50˚C.

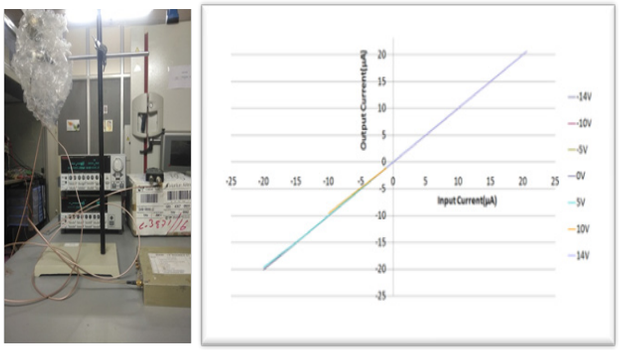

Figure 9: Test setup and output transfer curves for different bias potentials.

RAMBHA-LP Checkout System Development

The checkout system hardware for RAMBHA-LP includes the Spacecraft Simulator of Rambha (SiSoR), a multiport RS232 extender card and a USB based analog DAQ. The system block diagram is shown in Fig. 10. The SiSOR PCB fabricated through ECAD, VSSC is being populated with components. The checkout software for analog telemetry has been developed in LabVIEW. The software for BDH acquisition and TC in LabVIEW are also initiated.

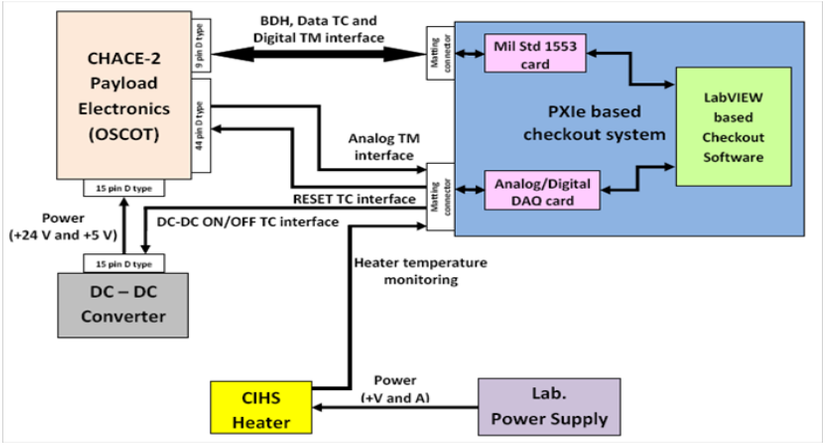

Figure 8: Block diagram of Checkout system for CHACE-2 Payload.

RAMBHA Langmuir Probe payload onboard Chandrayaan-2 Lander

The engineering model of RAMBHA Langmuir Probe (LP) fabricated by MVIT/ VSSC has been tested in the laboratory by providing low current input signals as well as varying bias voltages using a calibrated set of instruments. The output from the probe is measured through the newly developed front end electronics. These tests were done before and after coating the probe with Titanium Nitride,

ChaSTE Payload of Chandrayaan-2 Mission

Chandra's Surface Thermo physical Experiment (ChaSTE) is one of the payloads of Chandrayaan-2 Lander. ChaSTE is developed jointly by Space Physics Laboratory in collaboration with other entities of VSSC (MVIT, PCM, STR, AERO, PRSO, SR, AVN) and Physical Research Laboratory (PRL). Main objective of the experiment is insitu measurements of temperature variations and thermal conductivity within 100 mm of the lunar surface

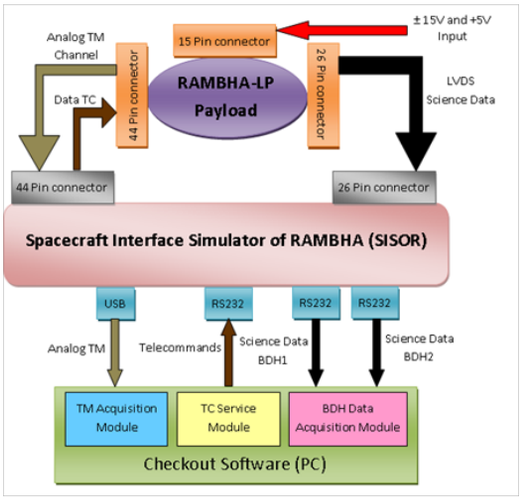

Figure 10: Block diagram of Checkout system for RAMBHA LP Payload.

(regolith). The probe consists of 10 temperature sensors (RTDs) mounted at different locations along the length of the probe. Also a heater is attached to the probe for thermal conductivity measurements. Besides the thermal probe, the payload consists of an electronics module for signal conditioning, control and payload interfacing and a deployment mechanism for inserting the probe into the lunar regolith.

ChaSTE Onboard Electronics

Functional requirements of the front-end electronics are: (i) excitation of RTD sensors, (ii) acquisition of analog voltages of the RTDs, motor current and probe heater current, and (iii) digitization of the analog voltages. Functional requirements of the processing electronicsare (i) Power ON and OFF interfaces, (ii) deployment motor (BLDC) drive for probe deployment, (iii) penetration motor (BLDC) drive for probe insertion into lunar soil,

Figure 11: Engineering model of ChaSTE Payload undergoing functional tests.

(iv) acquisition of digitized analog voltages from front-end electronics card, (v) data transfer to lander-craft in serial CMOS interface (BDH), (vi) probe heater drive for active mode of payload operation, (vii) reception and execution of telecommands for motor and heater drive operations, and (viii) generation of telemetry for motor drive and probe insertion status.Onboard electronics (EM) and the integrated test (EM) of electronics with deployment mechanism, penetration mechanisms and probe sensors have been completed. Processing electronics PCB (QM) design and fabrication has been completed. The integrated engineering model of ChaSTE payload has been tested (Fig.11) and was found to satisfy all the functional requirements.

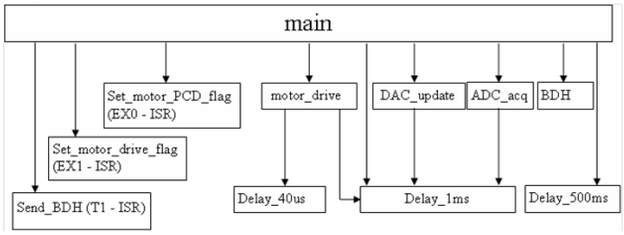

Figure 12: Structure Chart of Onboard Software of the ChaSTE Payload.

ChaSTE Checkout Software

The checkout software is interfaced to the checkout hardware for testing various interfaces of the onboard electronics of the ChaSTE payload. The objectives of the software are generation of various TCs for the operations of the payload, acquisition and display of the Telemetry (TM) status, and science data (BDH) and the archival of the data in proper format. The program is developed in Visual Basic. The software GUI contains sub-panels for the display of TC, TM and BDH data. The required TCs can be issued by clicking the buttons on the TC sub-panel. The various TM data are displayed in tabular format in the respective sub panel. The BDH sub-panel displays the science data in graphical as well as tabular formats after converting into engineering units. Also, provision is given to acquire and save the redundant BDH data. Development of the checkout software (EM) has been completed.

IDEA payload for PSLV-C38

The Ionozation Density and Electric Field Analyzer (IDEA) payload has been developed and successfully flown on PSLV-C38. This is a modified version of the ENWi-LP payloads successfully flown in sounding rockets during Sooryagrahan-2010 campaign. With the sensor probes remaining the same, the electronics has been fine tuned to cater to the enhanced current measurement range. The payload electronics also makes use of space grade components in line with the requirements of the packages for PSLV. Detailed lab-based functional tests were carried using standard low current sources for input. The checkout system is developed as a LabVIEW based system using a multichannel USB data acquisition card. This was used for

acquiring and logging the data during all the ground tests. The block diagram of the test setup is shown in Fig. 13.

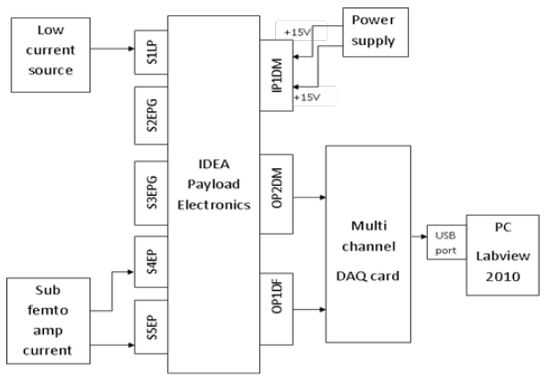

Figure 13: Block diagram of laboratory test set up for IDEA payload.

The payload, which includes the two sensors ENWi and LP, and the complete electronic systems were tested and qualified by QDTE, VSSC, as per the standard test procedures for PSLV packages. The environmental tests include thermal, vibration, thermo-vacuum and EMI tests. The response of the electronics was monitored during each of these tests. Plots of the data obtained from each sensor for varying current range, after the environmental tests, (Fig.14) indicate that the payload health is normal after the tests. Based on above analysis, the payload was recommended for PSLV flight.

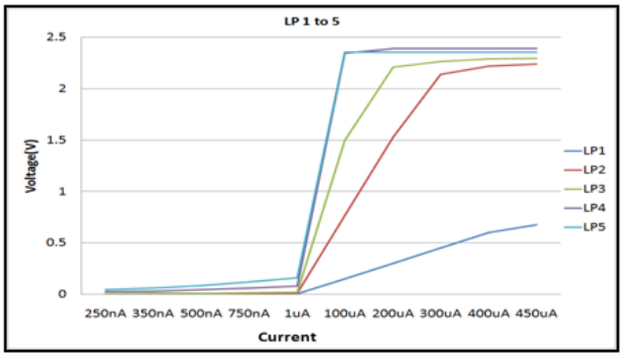

Figure14(a): Gain channels of LP for current varying from 250nA to 450uA.

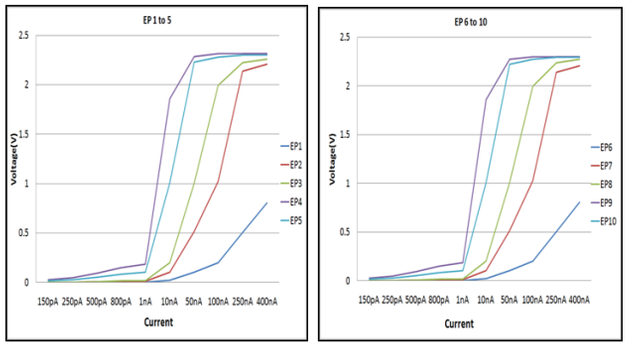

Figure14(b): Gain channels of ENWi 1 and 2 for current varying from 150pA to 400nA.

Characterisation of the sensor probes

In order to understand the response of the probes, a test setup (Fig.15) was made in the HVSSF, SPL with the probes mounted inside the chamber one by one and connected to IDEA electronics kept outside the chamber. The low energy ion source has been used for ENWi characterisation and the electron source for LP characterisation. It is seen that both the probes respond to the changes in emission/ electron current.

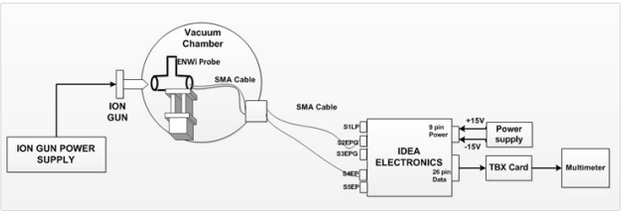

Figure 15(a): Block diagram of test setup for characterization of ENWi probe with ion source.

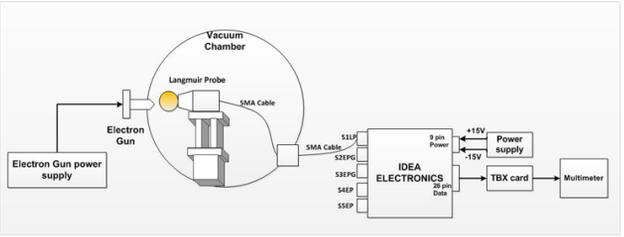

Figure15(b): Block Diagram of test setup for characterization of LP with electron source.

SOUnding Rocket EXperiment (SOUREX)

The SOUREX programme envisages scientific payloads to be flown onboard Rohini sounding rockets for ionospheric studies. Flight model of the ENWi-LP payload for measurement of electron density and E-region winds has been tested and qualified for flight after GATE level environmental tests. The standby hardware is realized and is presently undergoing tests. A picture of the three components of the realized payload is shown in Fig.16.

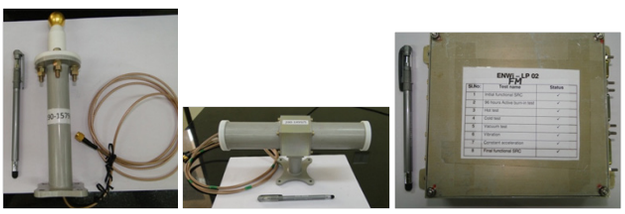

Figure 16: LP, ENWi and electronics hardware for SOUREX.

Technology Development

Development of laboratory model radio sounder

As part of the in-house development of digital sounder, a programmable transmitter for burst mode operation has been developed using an evaluation board, which is

programmed using a PIC microcontroller. The processing electronics for the receiver is simulated for different point FFTs to identify the optimal one for this application and the same has been simulated in VHDL environment. The simulation also includes ADC and RAM for data analysis and UART for final data interface to PC.

Development of reconfigurable beacon receiver

A reconfigurable coherent beacon receiver has been developed in-house with NI-USRP boards and LabVIEW software for acquisition of coherent beacon signals from (LEO) Low Earth Orbiting satellites. This receiver is integrated with the existing antennae and has been field tested. The system automatically tracks the incoming signals and saves the data for both amplitude and phase information. This is then pre-processed to obtain the STEC information and the results are compared with those obtained from a standard receiver. It is seen that this receiver is able to track the signals for a longer duration than the existing standard receiver. Detailed test and evaluation are being carried out.

Ground-based Radar Systems

HF Radar

As the HF Radar system is getting aged, the antenna and the transmitter and receiver systems require very frequent inspection, testing and maintenance. The system has been maintained to provide optimum signal from the ionosphere in its existing configuration. A new transceiver (TR) switch was developed for the radar. This switch is designed to be compact while retaining the ability to handle the 50 kW peak power with average power levels up to 600 W. The TR switch is a conventional TR/ATR design with equivalent lambda/4 transmission line sections comprising of RG213 cables. Three TR sections are placed in series to achieve adequate receiver protection. The switch is set into the transmit mode by forward biasing the 4 PIN diodes while the receive mode is achieved by reverse biasing the diodes to -15 V. The PIN diode driver has been used to switch the PIN diodes between the two impedance states required: a forward biased low impedance state and a reverse biased high impedance state.

18.1 MHz Double Tuned LC Bandpass Filter for HF and PR Radar Receivers

A double tuned LC bandpassfilter (bandwidth of 400 kHz) with resonance frequency at 18.1 MHz has been designed, developed, tested and interfaced for the HF Radar digital receiver (Fig. 17).It employs inductors wound with 17 SWG and 19 SWG laminated copper wire and ceramic multi-layer type capacitors and enables very low insertion loss at the resonant frequency. The received signals from the phased array antenna are passed through T/R switch, RF limiter and the double tuned LC bandpassfilter. This filter optimizes the signal-to-noise ratio and sensitivity of the receiver.

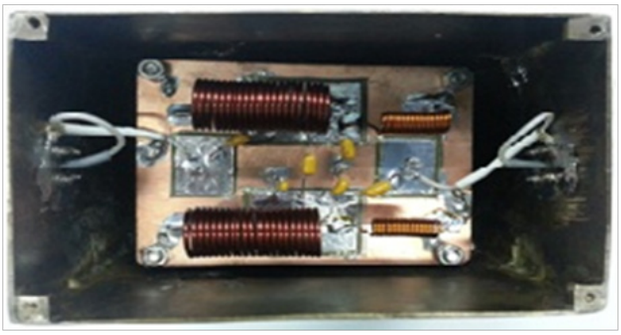

Figure 17: Double tuned LC bandpass filter for HF Radar digital receiver.

Three numbers of double tuned LC bandpassfilters (band width of 100 KHz) with resonance frequency at 2.5 MHz has been designed, developed, tested and interfaced for three identical channel digital receivers of Partial Reflection Radar system (Fig. 18).

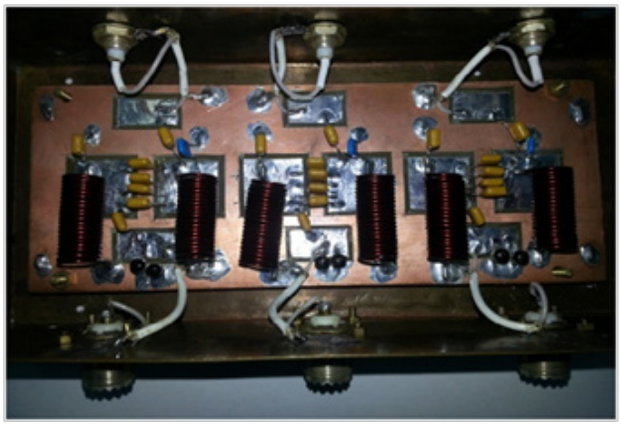

Figure 18: Double tuned LC bandpass filter for PR Radar system.

ARFI Technical Activities

Subsystem Development for Aerosol Humidograph Instrument (AHI)

Aerosol Humidograph Instrument (AHI) has been conceptualized at SPL (ARFS) to provide an experimental facility for investigating hygroscopic properties of aerosols. The different subsystems and the control and data acquisition software are being developed.

10-channel data acquisition system for Temperature & RH probes

Monitoring the relative humidity (RH) and temperature (T) of the air stream at different points is very critical for the operation of the AHI.The RH and T probes communicate the data to PC using RS-232 port. In order to save the hardware as well as software resources, a data multiplexer has been introduced. The main part of the multiplexer is the Microcontroller (MCU) with built-in multi-channel high resolution ADCs, which acquire the analog RH and T data from the probes and send them to PC in digital format

(RS-232). The MCU contains 10 channels of ADC so that 5 numbers of RH and T probes can be interfaced. These 5 sets of data, upon acquisition, are sent sequentially to the PC as a single channel. The software then reads the whole data from a single RS-232 port and split them for individual processing. Each set of the data is acquired based on the command query from the PC.

Programmable Temperature Controller (PTC)

The PTC is used for real time monitoring and active control of RH levels in the humidifier module of the AHI by precisely controlling the heater temperature programmed remotely via PC. The block diagram of the PTC is shown in Fig.19. The hardware have been developed and implemented using a Microcontroller (MCu). The temperature required for the humidifier can be set using the AHI software on PC. The high power heater (50 W) is switched using a solid state relay (SSR). The heater temperature is sensed by a thermo-couple type (Type-K) heat sensor, which has a response of ~0.04mV/°C. The signal is amplified and fedback to the MCU and compared the same with the set temperature value to estimate the error temperature. Logic is developed and implemented in the MCU to vary the switching rate (pulse width modulated signal) of the heater using the SSR in accordance with the error temperature. The heater temperature is sent periodically to the PC through RS232 interface for online monitoring. The PTC module developed can be operated over a range of 0-100°C with accuracy better than ±1°C.

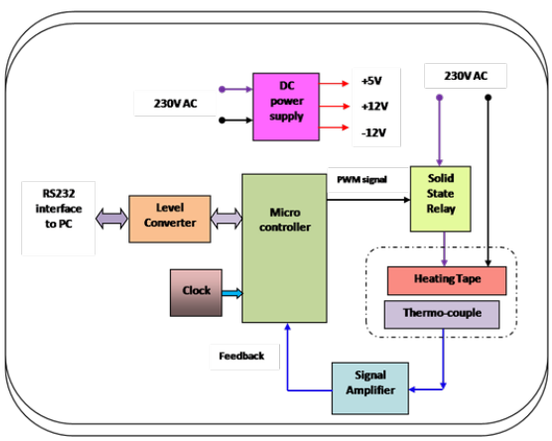

Figure 19: Block Diagram of Programmable Temperature Controller (PTC).

ARFINET

As part of ARFINET expansion, two MWR units have been assembled and tested for installation at KL University-Vijayawada and IIT-Bhuvaneshwar.Under ARFINET maintenance, MWR stations at IIRS-Dehradun, ARIES-Nainital, Goa University-GOA, IIA-Hanle and Culcutta University-Kolkata have been refurbished. At present, 27 MWR observatories are operational under ARFINET.

NOBLE Activities

A 32-m micrometeorological tower with 7 levels of instrumentation (5 slow response and 2 fast response) has been commissioned at TERLS on 05 January 2017 (Fig.20). The sensors were tested in the lab, and mounted and aligned in the tower-arms as per requirements. Intermittent data loss was noted for the fast-response systems as the cable length between the sensors and the data acquisition system exceeded 50 m. This was rectified using two interfacing modules with RS422 toRS232 converters. Data from all the sensors are being acquired continuously.

Figure 20: 32 m micrometeorological tower installed at TERLS.

Renovation of the Phased Array SODAR system

Signal level from the phase-array SODAR system (over 10 years old) has substantially reduced in the recent period. The system is being renovated by identifying and replacing the faulty sub-systems using. All 52 transducers were found good. Out of the eight audio amplifiers, six were found to be faulty and were replaced. The interior foams (noise reducers) are being replaced.

Data acquisition and control system for Multi-Wavelength Day-glow Photometer

A new hybrid stepper motor controlled receiver and USB based data acquisition software were developed for the Multiwavelength Day-glow Photometer (MWDPM), which replaced the obsolete Pascal-based DAQ unit (Fig.21). The new DAQ unit uses a LabVIEW based user-friendly control and display software. The stepper motor movement and the delay and timing pulses are generated using the same LabVIEW program and the data is processed online for subtracting the background from the signal.

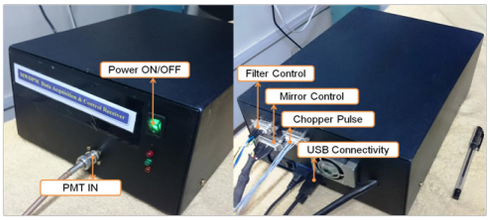

Figure 21: The hybrid stepper motor controlled receiver for Multiwavelength Day-glow Photometer (MWDPM).

UV Radiometer data acquisition and transmission software

Fully-automatic data acquisition and processing software were developed using an NI DAQ unit and LabVIEW GUI software for the UV radiometer, which is being used for the precise measurements of atmospheric ultraviolet radiation in three spectral ranges. The acquisition delay is programmable and the GUI software is capable of converting the voltage levels to the actual irradiance and record the data. Windows based software was also developed to access this data remotely through VSSC intranet.

Setting up of Clean Room

Development of spaceborne payloads require dust-free environment (Clean room). This is especially essential for the development of payload sensors involving optical front-end and sensitive detectors, mass spectrometers, and payload electronics. For this purpose, Class 10000 and Class 100000 Clean Rooms having areas of 23 m^2 and 43 m^2 were setup at SPL. The rooms are also equipped with work benches of Class 100 and Class 1000 Laminar Flow Tables (LFT). HEPA filters remove up to 0.3 micron particles at an efficiency of >99.97% and maintains Class 100 conditions. The work benches can withstand up to 350 kg load and are made of SS304 material and are provided with fume exhaust hoods.Temperature and relative humidity of the rooms are maintained at 23±1°C and <60% respectively. Double door interlocked enclosures (Dynamic Pass Boxes) are provided for movement of material in and out of the Clean Room and between the Clean Rooms. When the door is opened the blower switches on and HEPA filtered air flushes the enclosure and the material being transferred. The air handling unit has a total capacity of 10520 CMH. State-of-the-art HEPA filters are installed in specially designed Terminal Plenum with protective grille in the false ceiling.2-Stage Air showers in the Entry as Enclosure with interlocked doors. Building Management System (BMS) controls the Clean Room conditions and stores all the environmental parameters. The BMS also switches on and off the system automatically.

Scientific Results

Upper limit of He-4 in the Sunlit Lunar Exosphere from CHACE/MIP/Chandrayaan-1 observations

Alpha particles from the solar wind get neutralized upon incidence on the lunar surface and constitute a majority of the lunar neutral Helium inventory. The Chandra's Altitudinal Composition Explorer (CHACE), a quadrupole mass spectrometer based payload aboard the Moon Impact Probe (MIP) in the Chandrayaan-1 mission in 2008, is the first instrument to investigate the latitudinal and altitudinal distribution and composition of the lunar daytime neutral exosphere. The in-situ observations by CHACE were carried out in the lunar dayside, covering a broad range of lunar latitudes, when the Moon was on the verge of exiting the Earth's magnetotail. A combination of daytime He depletion and decrease during the magnetotail passage of the Moon, along with low flux of alpha particles in the solar wind at the time of CHACE observations present a case when the He abundance in the Moon was in its minimum. Since the signal level due to the He-4 atoms was poor, a new algorithm was developed in order to detect the He-4 signal from the system noise, based on pattern recognition. The pattern recognition based Peak Detection Algorithm (PDA) has a false alarm probability of ~2 $x10^{-4}$. Out of the 340 mass spectra acquired from 20°S to 89°S lunar latitudes, 16 spectra passed the PDA-test. Figure 22 shows the PDA-positive detections at different lunar latitudes. Surface densities were derived from the PDA-positive spectra for He-4, which were observed to be very close to the detection threshold of the instrument. Based on these observations, this study shows that the upper limit of surface density of lunar He-4 in the sunlit hemisphere is ~8.0 x 10^2 cm-3. Using the night-side observations by NMS/LADEE, normalized to the conditions prevailing during the MIP mission and the dayside observations by CHACE-1, a nightside-to-dayside He surface density ratio of ~12 is suggested, which imply that lunar He undergoes on an average of 4 or more hops in the lunar surface. This is an important observation towards the understanding of the dynamics of the He atoms in the lunar exosphere.

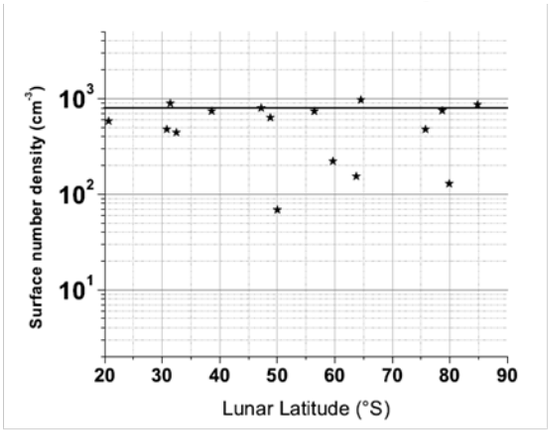

Figure 22: Inferred surface density of He-4 from the PDA-positive spectra, detected based on pattern recognition. The dark horizontal line represents the detection threshold of the instrument, limited by the system noise. (Icarus, 297, 189-194, 2017, DOI: 10.1016/j.icarus.2017.07.001).

Future Projections

- Realization and delivery of QM and FM of CHACE-2 – Chandrayaan-2 orbiter
- Investigations on the lunar atmosphere using CHACE-2
- Realization and delivery of QM and FM of ChaSTE – Chandrayaan-2 lander

- Realization and delivery of QM and FM of RAMBHA – Chandrayaan-2 lander
- Experimental exploration of Venus using orbiter and balloonborne experiments
- Experimental exploration of the composition of Mars using future Mars mission
- Development, testing and qualification of ENWi and EACE payloads for SOUREX program
- Design and development of checkout system for PAPA payload
- Design and development of a tri-band beacon system for TEC studies
- Indigenization of mass spectrometer electronics system
- Aerosol Humidograph Instrument: Development of Electronics systems, system integration, and testing.
- Solar occultation experiment: Development of Control systems and data acquisition
- Development of experimental systems for near-surface studies
- Regular operation and maintenance of the existing experimental systems including radars

Publications in Peer-Reviewed Journals

1. Tirtha Pratim Das, Smitha V. Thampi, M.B. Dhanya, Anil Bhardwaj, S.M. Ahmed, R. Sridharan, Upper limit of Helium-4 in the sunlit lunar exosphere during magnetotail passage under low solar wind condition: Result from CHACE aboard MIP in Chandrayaan-1, Icarus, 297, 189-194, doi: 10.1016/j.icarus.2017.07.001 (2017).
2. Anil Bhardwaj, Smitha V. Thampi, Tirtha Pratim Das, M. B. Dhanya, NehaNaik, Dinakar Prasad Vajja, P. Pradeepkumar, P. Sreelatha, J. K. Abhishek, R. SatheeshThampi, Vipin K. Yadav, B. Sundar, Amarnath Nandi, G. Padma Padmanabhan and A.V. Aliyas, Observation of suprathermal argon in the exosphere of Mars, Geophysical Research Letters, vol. 44 (5), 2088-2095,doi:10.1002/2016GL072001 (2017).

Publications in Proceedings

1. Reshma, C, B. Ramesh, P. Pradeepkumar, An FPGA based Low Cost Receiver for Ultrasonic Anemometer, Proceedings of 2016 IEEE International Conference on Control, Instrumentation, Communication and Computational Technologies (ICCICCT), pages 729-733, 978-1-5090-5240-0/16 (2016).
2. Pooja, C., B. Ramesh, P. Pradeep Kumar, Time of Flight Measurement System for an Ultrasonic Anemometer, 2016 IEEE International Conference on Control, Instrumentation, Communication and Computational Technologies (ICCICCT), pages 734-737 (2016).

Technical Reports

1. Ajeeshkumar PS, AdityaVaishya and Sobhan Kumar Kompalli, "Development of an experimental facility for the study of aerosol hygroscopic properties (Electrical integration and software development)", ISRO-VSSC-TR-0585-0-16, November 2016.
2. AdityaVaishya, Ajeeshkumar PS and Sobhan Kumar Kompalli, "Development of anexperimental facility for the study of aerosol hygroscopic properties (Design overview and technical details)", ISRO-VSSC-TR-0434-0-16, August 2016.

Payload Development - Technical/Review Documents

1. Baseline Configuration Control Document (CCD) of the CHACE-2 payload, document number TTCP-S-298
2. CHACE-2 Operation requirement document, version-0, document number CHACE2-ORD-01
3. CHACE-2 Ionizer Heater Shroud (CIHS) Thermal Test Report, document number CHACE2-TR-CIHS-01
4. Timing Analysis document for Qualification Model (QM) of CHACE-2 Payload, onboard Chandrayaan-2 (TR: SPL-CHACE-2-TA-01)
5. A report on effect of autozero parameter on the packet structure of the mass spectrometer data (TR: SPL-MS-01)
6. Technical Report on IDEA payload for PSLV-C38, SPL:TR:2017:IDEA:01
7. Electrical Interface Document of IDEA experiment for PSLV-C38, (Ver 1) SPL/IDEA/EID/2017/01
8. Electrical Interface Document of IDEA experiment for PSLV-C38, (Ver 1.2) SPL/IDEA/EID/2017/01
9. Checkout system for IDEA Electronics, SPL: Test Report: IDEA-06-201

10. Software Requirement Specifications (SRS) of Onboard Firmware of ChaSTE Payload on Chandrayaan-2 Lander, TR-SPL-CH2-ChaSTE-SRS, March 2017

11. Software Design Details Document (SDD) of ChaSTE Payload on Chandrayaan-2 Lander, TR-SPL-CH2-ChaSTE-SDD, May 22017

Invited Talks

Sreelatha P

1. "Indian Space Odyssey- A Glimpse", Rajadhani College of Engineering, Nagaroor, Feb 24, 2017.
2. "Challenges in scientific instrumentation for space applications", ICCS-2017, Mar 3-4, 2017, Sastra University, Tanjore.
3. "Satellite Interfaces and checkout systems for Scientific Payloads", Structural Training Programme (STP) on Challenges in Space Science and Exploration, SPL, VSSC, March 13-17, 2017.
4. RF Systems for Scientific Studies: An overview, Amrita College of Engineering & Technology, Amrithapuri Campus, Apr 29, 2017.

Tirtha Pratim Das

1. "Scientific payloads: from conceptualization to realization", Structural Training Programme (STP) on Challenges in Space Science and Exploration, SPL, VSSC, March 13-17, 2017.

Training Programme

1. Ajeeshkumar PS, "Training on QC and QA", 14-16 June, 2016 at VSSC.
2. AjeeshkumarPS , "Training on LabVIEW (Basic course)", 1-5 May, 2017 at VSSC.
3. P.T Lali, One week training at SAMEER, Mumbai for testing and maintenance of SODAR sub-systems.
4. Tirtha Pratim Das, First National Finite Element Developers/FEASTSMTUsers Meet, Organised by the STR entity, VSSC, on 12 December, 2016.

Office and Administrative Support

Team

Suseela P. R.
Geetha C.
Shajahan J.
Sisira R.
Salini M. S.
Shiji N. D.
Vijayan T. K.

SPL administration facilitates the administrative and secretariate requirements for a smooth and effective functioning of SPL by providing co-ordination, communication and logistics. Besides the general administration, office management and housekeeping of SPL, it caters to the necessary official assistance to different ISRO projects such as ARFI, ICARB, RAWEX and NOBLE. It co-ordinates and provides logistic support for different national observation campigns of SPL. Also SPL administration is responsible for coordinating activities within SPL, involving other Divisions, Facilities of VSSC and/or other ISRO centers and different Institutions/ Universities. It meets the administrative requirements of different payload such as MENCA, CHACE-2, ChaSTE, RAMBHA and PAPA development for different ISRO's space missions.

Research programme facilitated by ISRO fellowship program including research fellowship program and research associate program is a major activity of SPL. SPL administration provides the required assistance in terms of documentation, intervening between universities and organizing PhD Synopsis/Defence, Doctoral Committee meetings, student reviews, regular student/faculty seminars and Central Level Monitoring Committee meeting of VSSC. It also supports for arranging Seminar Talks/Invited Talks in SPL by leading scientists from India and abroad and arranges necessary logistics required during their visit and stay.

ACADEMIC PROJECTS

Well aware of societal commitments, SPL boasts a strong capacity building programme by imparting in-house training through M.Sc. & B.Tech. project work, and M.Phil. & M.Tech. dessertation supervision to young students of different colleges, institutes and universities. SPL also hosts Summer Research Fellows of Indian Academies and INSPIRE fellowship awardees for two months project works. During the academic year 2016-2017, a total of 32 students underwent the training under different disciplines of SPL.

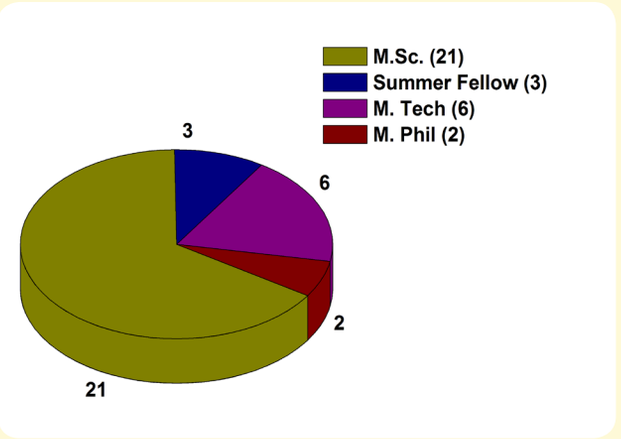

M.Tech.

1. Sreelakshmi T. M., National Institute of Technology, Warangal, Telangana; "Usage of Indian Satellite Data for Land Surface Parameters on Numerical Meoscale Model", August 2016-June 2017 [Supervisor: Radhika Ramachandran]
2. Raksha Janet Jathanna, Manipal Institute of Technology, Manipal, Karnataka; "Estimation of the Electric Potential Developed on a Spacecraft"; July, 2016-May 2017. [Supervisor: Vipin K. Yadav]
3. Tejas, Manipal Institute of Technology, Manipal, Karnataka; "Testing and calibration of Electrostatic analyser under high vacuum conditions"; July, 2016-May 2017. [Supervisor: R. Satheesh Thampi]
4. Catherine Augustine, National Institute of Technology, Warangal, Telangana; "Title of the M.Tech. Project"; August 2016-May 2017 [Supervisor: Suresh Raju C.]
5. Prakash Mishra, Shri Ramdeobaba College of Engineering & Management, Nagpur; "Development of receiver system for sounder applications"; January-June 2017. [Supervisor: Sreelatha P.]
6. Jitendra Y Turkar, Shri Ramdeobaba College of Engineering & Management, Nagpur; "Development of pulsed transmitter system for sounder applications"; January-June 2017 [Supervisor: Sreelatha P.]

M. Phil.

1. Ajithra V. S., Department of Physics, Nesamony Memorial Christian College, Tamil Nadu; "Light scattering by spherical particles", January-June 2017 [Supervisor: Mukunda M Gogoi]
2. Suji A., Neshamani Memorial Christian College, Marthandam, Kerala; "Study on the response of equatorial and low latitude ionosphere- thermosphere system to 3 strong geomagnetic storm events", February-May, 2017 [Supervisor: G. Manju]

M. Sc.

1. Sreedevi P and Resmi Mol M. C., Mahatma Gandhi University, Kottayam, Kerala; "Characterization of carbon and nitrogen aerosol species over Thumba region, Thiruvananthapuram, India", June-August 2016 [Supervisor: Prashant Hegde]
2. Anila K. and Vinitha R. B., D. B. Pampa College, Mannar, Kerala; "Dual frequency radar observations of three-dimensional structure of clouds using Global Precipitation Mission", July- August 2016 [Supervisor: Karanam Kishore Kumar]
3. Anjana T. P. & Revathy Anand A., School of Technology and Applied Sciences, Edappally, Kerala; "Estimation of soil moisture using satellite based microwave radiometric observations"; July-August 2016 [Supervisor: Manoj Kumar Mishra]
4. Neha G., JECRC University, Jaipur, Rajasthan; "Study of Solar Plasma Waves with Magnetic Field observations at L1 point"; July-November 2016 [Supervisor: Vipin K. Yadav]
5. Aparna C., Kannur University, Payyannur, Kerala; "Evaluation of Trapped Humidity in the Lower Atmosphere over the Coastal Station Trivandrum"; March-May 2017 [Supervisor: Nizy Mathew]
6. Reshma A. K., Govt. Victoria College Palakkad, Kerala, "Estimation of diurnal variation of Upper Tropospheric Humidity from Megha-Tropiques-SAPHIR data"; March-May 2017 [Supervisor: Nizy Mathew]
7. Jubie Raju, Christian College, Chengannur, Kerala, "Study on diurnal variability of temperature over India using INSAT-3DR satellite measurements", March-May 2017 [Supervisor: Siddarth Shankar Das]

8. Rosiya Fathima, Muhammed Abdurahman Memorial Orphanage College, Calicut, Kerala, "Diurnal Variability in the Upper Tropospheric Humidity during different seasons using Kalpana observations"; March-May, 2017 [Supervisor: K. N. Uma]
9. Savitha K., Ansar Womens College, Thrissur, Kerala, "Observations of convective precipitating cloud systems using C-band Polarimetric Doppler Weather Radar (DWR) at Thumba", April-May 2017 [Supervisor: Kandula V. Subrahmanyam]
10. Aiswarya K. K., N.S.S. College, Ottapalam, Kerala, "Climate Change and its effect on summer monsoon precipitation over the south Indian region"; April-May 2017 [Supervisor: Sijikumar S.]
11. Smruthi Gokul, N.S.S. College, Ottapalam, Kerala, "Climate Change and its effect on winter monsoon precipitation over the south Indian region"; April-May 2017 [Supervisor: Sijikumar S.]
12. Benzeera K. V., Asaabah Arts & Science College, Malappuram, Kerala, "Study of the vertical profile of atmospheric ozone using balloon-based ozonesonde over Trivandrum", April-May 2017 [Supervisor: Girach Imran Asatar]
13. Serene T. C and Aabidh Hussain H., St. Aloysius College, Elthuruth and St. Stephen's College, Pathanapuram, Kerala, "Study of the Martian Thermosphere and Ionosphere using MANEN/NGIMS Observations"; April-May, 2017 [Supervisor: Smitha V Thampi]
14. Jamsheena P. T., M. E. S. Kalladi Collage, Mannarkkad, Kerala, "'Evaluation of Trapped Humidity in the Lower Atmosphere over the Coastal Station Trivandrum"; April-May 2017 [Supervisor: Manoj Kumar Mishra]
15. Kavitha K., M. P. M. M. S. N. Trust College, Shoranur, Kerala, "Estimation of diurnal variation of Upper Tropospheric Humidity from Megha-Tropiques-SAPHIR data"; April-May 2017 [Supervisor: Manoj Kumar Mishra]
16. Anu Aprem, Al Ameen College, Aluva, Kerala, "Estimation of Ion Neutral Collision Frequency in Thermosphere-Ionosphere region over Thiruvananthapuram"; April-May 2017 [Supervisor: N. Mridula]
17. Nina. S. Darsan, Sree Narayana College, Cherthala, Kerala, "The Mercury: Magnetized and Atmosphereless Planet in our Solar System"; April-June 2017 [Supervisor: M. B. Dhanya]

IASc-NASI-INSA Summer Research Fellows

1. Rahul Kumar, Institute of Science, Banaras Hindu University, Varanasi, Uttar Pradesh; "Impact of Solar Flares on Mesospheric Neutral Winds"; June-July 2017 [Supervisor: C. Vineeth]
2. Veer Vikram Singh, Institute of Science, Banaras Hindu University, Varanasi, Uttar Pradesh; "Study of cloud condensation nuclei (CCN) properties over high altitude region, Ooty during pre-monsoon season", May-July 2017 [Supervisor: Vijayakumar S. Nair]
3. V.Sai Subba Rao, Indian Institute of Technology, Mandi,Himachal Pradesh, "Observations of Lunar Exosphere using Neutral Mass Spectrometer aboard LADEE mission", June-July 2017 [Supervisor: Smitha V Thampi].

VISITORS

1. **Dr. Amal Chandran,** Research Scientist, Laboratory for Atmospheric and Space Physics, University of Colorado, Boulder, USA, 14 February 2017.
2. **Dr. A Ajayaghosh,** Director, NIIST, Thiruvananthapuram, 25 May 2017.
3. **Dr. Shailesh Nayak,** Former Secretary, EOS, New Delhi, 26 May2017, delivered a talk on "*Societal benefits of Earth Observations*".
4. **Dr. K. J. Ramesh**, Director General, India Meteorological Department, 01 June 2017.
5. **Prof. A Jayaraman,** Director, NARL, Gadanki, Tirupathi, 16 June 2017, delivered talk on "*Beauty of doing Science; my personal experience*".

हिन्दी गतिविधियाँ

1. अनिल भारद्वाज, मुख्य अतिथि एवं मुख्य वक्ता "भारत के ग्रहीय अभियान" एवं "देशांश" पत्रिका का उदघाटन; विश्व हिन्दी दिवस कार्यक्रम; जनवरी 10, 2017; मुख्य नियंत्रण सुविधा (MCF), हासन, कर्नाटक

हिन्दी तकनीकी लेख

1. अनिल भारद्वाज, टी. पी. दास, विपिन कुमार यादव, स्मिता वी थंपी, धन्या एम बी, नेहा नाईक, दिनकर पी वज्जा, पी प्रदीपकुमार, पी श्रीलता, जी सुप्रिया, अभिषेक जे के, एस वी मोहनकुमार, आर. सतीश थंपी, बी सुंदर, अमरनाथ नंदी, जी पद्मा पद्मनाभन एवं ए वी एलियास; "मंगल कक्षित्र अभियान पर अवस्थित मेनका द्वारा मंगल के बहिर्मंडल का अध्ययन"; केंद्र स्तरीय तकनीकी हिन्दी संगोष्ठी: "अन्तरिक्ष विज्ञान एवं इसके उपयोग"; जुलाई 19 - 20, 2016; विक्रम साराभाई अन्तरिक्ष केंद्र, तिरुवनन्तपुरम, केरल. पृष्ठ: 1-6
2. श्रीलता पी, रोस्मी जॉन, मंजु जी, तरुण कुमार पंत, पी प्रदीप कुमार एवं एस वी मोहनकुमार; "साउंडिंग रॉकेट एक्सपेरिमेंट (सौरेक्स-SOUREX) में प्रयुक्त होने वाले आयनमंडलीय अन्वेषिकाएँ एवं उनकी प्रसंस्करण इलेक्ट्रॉनिक्स", जुलाई 19-20, 2016; विक्रम साराभाई अन्तरिक्ष केंद्र, तिरुवनन्तपुरम, केरल. पृष्ठ: 14-19
3. जी मंजु, तरुण कुमार पंत, राज कुमार चौधरी; "चंद्रयान-2 अभियान पर रेडियो एनैटॉमी ऑफ मून बाउंड हाइपर एट्मस्फीयर व आईओनोस्फेयर (RAMBHA) प्रदायभार: विज्ञान एवं विकास"; जुलाई 19-20, 2016; विक्रम साराभाई अन्तरिक्ष केंद्र, तिरुवनन्तपुरम, केरल. पृष्ठ: 25-31
4. आर. सतीश थंपी, विपिन कुमार यादव, अनिल भारद्वाज, धन्या एम बी एवं जी गोविंद एन; "सौर-पवन के अध्ययन के लिए अदित्य-L1 का प्लाज़्मा पैकेज (PAPA)"; तकनीकी सत्र, केंद्र स्तरीय तकनीकी हिन्दी संगोष्ठी: "अन्तरिक्ष विज्ञान एवं इसके उपयोग"; जुलाई 19-20, 2016; विक्रम साराभाई अन्तरिक्ष केंद्र, तिरुवनन्तपुरम, केरल. पृष्ठ: 42-49
5. डी बाला सुब्रहमण्यम, "अन्तरिक्ष विज्ञान में संख्यात्मक मौसम पूर्वानुमान के अनुप्रयोग: वर्तमान दशा और दिशा"; तकनीकी सत्र, केंद्र स्तरीय तकनीकी हिन्दी संगोष्ठी: "अन्तरिक्ष विज्ञान एवं इसके उपयोग"; जुलाई 19- 20, 2016; विक्रम साराभाई अन्तरिक्ष केंद्र, तिरुवनन्तपुरम, केरल. पृष्ठ: 58-63
6. तीर्थ प्रतिम दास, अनिल भारद्वाज, विपिन कुमार यादव, स्मिता वी थंपी, एस वी मोहनकुमार, पी प्रदीपकुमार, पी श्रीलता, अभिषेक जे के, बी सुंदर, अमरनाथ नंदी, दिनकर पी वज्जा, धन्या एम बी, नेहा नाईक, आर. सतीश थंपी, जी पद्मा पद्मनाभन एवं ए वी एलियास; "चंद्रयान-2 पर अवस्थित चेस-2 प्रयोग"; केंद्र स्तरीय तकनीकी हिन्दी संगोष्ठी: "अन्तरिक्ष विज्ञान एवं इसके उपयोग"; जुलाई 19-20, 2016; विक्रम साराभाई अन्तरिक्ष केंद्र, तिरुवनन्तपुरम, केरल. पृष्ठ: 76-82
7. विपिन कुमार यादव एवं अनिल भारद्वाज; "सूर्य से पृथ्वी के निकट का प्लाज़्मा वातावरण"; केंद्र स्तरीय तकनीकी हिन्दी संगोष्ठी: "अन्तरिक्ष विज्ञान एवं इसके उपयोग"; जुलाई 19-20, 2016; विक्रम साराभाई अन्तरिक्ष केंद्र, तिरुवनन्तपुरम, केरल. पृष्ठ: 98-104
8. सुरेश राजू सी, मनोज कुमार मिश्रा, अनिल भारद्वाज और चेस्ट दल; "रेगोलिथ के तापीय गुणों के प्रत्यक्ष मापन हेतु प्रायोगिक अन्वेषी का विकास"; तकनीकी सत्र, केंद्र स्तरीय तकनीकी हिन्दी संगोष्ठी: "अन्तरिक्ष विज्ञान एवं इसके उपयोग"; जुलाई 19-20, 2016; विक्रम साराभाई अन्तरिक्ष केंद्र, तिरुवनन्तपुरम, केरल. पृष्ठ: 120-126
9. सिद्धार्थ शंकर दास और के. वी. सुनीत; "समतापमंडल – क्षोभमंडल के बीच आदान-प्रदान: तिरुवनन्तपुरम में ओज़ोन का एक समान्य परिदृश्य"; तकनीकी सत्र, केंद्र स्तरीय तकनीकी हिन्दी संगोष्ठी: "अन्तरिक्ष विज्ञान एवं इसके उपयोग"; जुलाई 19-20, 2016; विक्रम साराभाई अन्तरिक्ष केंद्र, तिरुवनन्तपुरम, केरल. पृष्ठ: 132-138
10. गिराच इमरान और प्रभा आर नायर; "तटीय स्टेशन थुंबा पर विभिन्न परिवेशी अनुरेख गैसों का विचरण"; तकनीकी सत्र, केंद्र स्तरीय तकनीकी हिन्दी संगोष्ठी: "अन्तरिक्ष विज्ञान एवं इसके उपयोग"; जुलाई 19-20, 2016; विक्रम साराभाई अन्तरिक्ष केंद्र, तिरुवनन्तपुरम, केरल. पृष्ठ: 149-155

11. मनोज कुमार मिश्रा, "भारतीय-फ्रांस उपग्रह मेघा-ट्रोपिक्स के स्कराबी (ScaRaB) प्रदायभार के उपयोग से ऐरोसोल रेडिएटिव फोर्सिंग का अध्ययन"; तकनीकी सत्र, केंद्र स्तरीय तकनीकी हिन्दी संगोष्ठी: "अन्तरिक्ष विज्ञान एवं इसके उपयोग"; जुलाई 19-20, 2016; विक्रम साराभाई अन्तरिक्ष केंद्र, तिरुवनन्तपुरम, केरल. पृष्ठ:164-169
12. करणम किशोर कुमार और कंदुला वेंकटा सुब्रमण्यम; "पृथ्वी के भूमध्यरेखीय समतापमंडल के दीर्घ आवर्ती दोलन: आज की समझ और भविष्य की चुनौतियां"; तकनीकी सत्र, केंद्र स्तरीय तकनीकी हिन्दी संगोष्ठी: "अन्तरिक्ष विज्ञान एवं इसके उपयोग"; जुलाई 19-20, 2016; विक्रम साराभाई अन्तरिक्ष केंद्र, तिरुवनन्तपुरम, केरल. पृष्ठ: 183-189
13. के. एन. उमा; "सामान्य एवं सूखे मॉनसून के दौरान ऊपरी क्षोभमंडलीय आर्द्रता (UTH) की परिवर्तनशीलता"; तकनीकी सत्र, केंद्र स्तरीय तकनीकी हिन्दी संगोष्ठी: "अन्तरिक्ष विज्ञान एवं इसके उपयोग"; जुलाई 19-20, 2016; विक्रम साराभाई अन्तरिक्ष केंद्र, तिरुवनन्तपुरम, केरल. पृष्ठ: 196-201
14. शोभन कुमार कोंपल्ली; "भारत में वायुमंडलीय ऐरोसोल भार की प्रवृत्ति"; तकनीकी सत्र, केंद्र स्तरीय तकनीकी हिन्दी संगोष्ठी: "अन्तरिक्ष विज्ञान एवं इसके उपयोग"; जुलाई 19-20, 2016; विक्रम साराभाई अन्तरिक्ष केंद्र, तिरुवनन्तपुरम, केरल. पृष्ठ: 211-216

हिन्दी राजभाषा लेख

1. विपिन कुमार यादव एवं अनिल भारद्वाज; "हिन्दी वैज्ञानिक साहित्य का हिन्दी में अनुवाद: व्यावहारिक समस्याएँ तथा चुनौतियाँ"; राजभाषा सत्र; केंद्र स्तरीय तकनीकी हिन्दी संगोष्ठी: "अन्तरिक्ष विज्ञान एवं इसके उपयोग"; जुलाई 19-20, 2016; विक्रम साराभाई अन्तरिक्ष केंद्र, तिरुवनन्तपुरम, केरल. पृष्ठ: 339-344
2. विपिन कुमार यादव एवं अनिल भारद्वाज; "भारत में राजभाषा हिन्दी को सरल बनाने के उपाय"; राजभाषा सत्र; केंद्र स्तरीय तकनीकी हिन्दी संगोष्ठी - 2016; अगस्त 5, 2016; भारतीय दूर-संवेदी संस्थान, देहरादून, उत्तराखंड. पृष्ठ: 260-265
3. विपिन कुमार यादव; "राजभाषा हिन्दी हिन्दी में तकनीकी अनुवाद"; अंतर-केंद्र हिन्दी तकनीकी सेमिनार"; अप्रैल 20-21, 2017; भौतिक अनुसंधान प्रयोगशाला, अहमदाबाद, गुजरात. पृष्ठ: 241-244

हिन्दी गतिविधियों में पुरस्कार

1. नेहा नाईक, प्रथम पुरस्कार (हिंदीभाषी), लेख "चंद्रयान-2 पर अवस्थित चेस-2 प्रयोग" के लिए, तकनीकी सत्र, केंद्र स्तरीय तकनीकी हिन्दी संगोष्ठी: "अन्तरिक्ष विज्ञान एवं इसके उपयोग"; जुलाई 19-20, 2016; विक्रम साराभाई अन्तरिक्ष केंद्र, तिरुवनन्तपुरम, केरल.
2. सिद्धार्थ शंकर दास, प्रथम पुरस्कार (अहिंदीभाषी), लेख "समतापमंडल – क्षोभमंडल के बीच आदान-प्रदान: तिरुवनन्तपुरम में ओज़ोन का एक समान्य परिदृश्य" के लिए, तकनीकी सत्र, केंद्र स्तरीय तकनीकी हिन्दी संगोष्ठी: "अन्तरिक्ष विज्ञान एवं इसके उपयोग"; जुलाई 19-20, 2016; विक्रम साराभाई अन्तरिक्ष केंद्र, तिरुवनन्तपुरम, केरल
3. डी. बाला सुब्रहमण्यम, प्रथम पुरस्कार, विक्रम साराभाई अन्तरिक्ष केंद्र की हिन्दी गृह पत्रिका "गगन-43" अप्रैल-सितंबर 2016 अंक में लेख "डी पी सी का भूत" के लिए.
4. विपिन कुमार यादव, सांत्वना पुरस्कार, विक्रम साराभाई अन्तरिक्ष केंद्र की हिन्दी गृह पत्रिका "गगन-43" अप्रैल-सितंबर 2016 अंक में लेख "मेरी कलम से" के लिए.

हिन्दी गतिविधियों में सम्मान

1. विपिन कुमार यादव, सदस्य, संपादकीय एवं प्रकाशन समिति, केंद्र स्तरीय तकनीकी हिन्दी संगोष्ठी-2017 "तकनीकी उपलब्धियाँ एवं स्पिन-ऑफ", विक्रम साराभाई अन्तरिक्ष केंद्र, तिरुवनन्तपुरम, केरल, सितंबर 2017

SPL DAY LECTURE

Delivered by Prof. Shashikumar M. Chitre

To celebrate the decades of excellence in scientific research, SPL has been organising the SPL Day Lecture since 2014, wherein Indian academicians of international repute are invited to SPL for a lecture. This year, distinguished professor and Padma Bhushan awardee, Prof. Shashikumar M. Chitre, Centre for Excellence in Basic Sciences, University of Mumbai, delivered the lecture on the topic "How well do we know our Sun" on March 17, 2017 at SPL.

Dr. K. Sivan, Director, VSSC delivered the presidential address. Shri T. Mookiah, Associate Director (R & D) and Dr. Biju Jacob, Chief Controller, VSSC addressed the gathering. Dr. Anil Bhardwaj, Director, PRL, Ahmedabad introduced the speaker. Prof. Chitre started his lecture with an overview of studies on the origin of the Sun and what makes Sun shine. The lecture enlightened the audience about the internal structure of the Sun, solar neutrino problem, differential rotation of sun as well as internal rotation, magnetic field and magnetic loops. The lecture was followed by an interactions with Prof. Chitre.

Dr. K. Rajeev welcomed the gathering and Dr. Prabha R. Nair proposed the vote of thanks. A gathering of scientists, research scholars and participants of the Structure Training Programme on 'Challenges in Space Science and Exploration' attended the lecture.

Structured Training Programme on Challenges in Space Science and Exploration

Eleventh batch of five days residential ISRO level Structured Training Programme on 'Challenges in Space Science and Exploration' was organized by SPL, VSSC from March 13 – 17, 2017. A total of 35 Scientist/ Engineers from various ISRO Centres attended the training programme. Dr. Radhika Ramachandran, Director, SPL welcomed the gathering. Dr. K. Sivan, Director, VSSC inaugurated the programme. In his address, Dr. Sivan highlighted the importance of Space science in ISRO's upcoming missions. Shri T. Mookiah, Associate Director (R & D) offered felicitations and Dr. Tarun Kumar Pant proposed the vote of thanks.

Eminent faculty from within ISRO and other external agencies delivered 17 lectures giving a wider perspective on the major challenges in Space science and exploration. Facility visits were organised to Space Museum, Control Centre and major laboratory visits at TERLS as part of the training program.